Topoisomerase-II mediated biochemical mapping of centromeres and nitroreductase mediated drug metabolism in Trypanosomatids

Thesis submitted to the University of London

for the degree of PhD

Christopher Bot

Queen Mary University of London

Declaration by Candidate

I declare that the work presented in this thesis is my own and that the thesis presented is the one upon which I expect to be examined.

Signed (Candidate):..... Date.....

Full name:.....

Signed (Supervisor):..... Date.....

Full name:.....

Abstract

The protozoan parasites *Trypanosoma cruzi* and *Trypanosoma brucei* are the causative agents of Chagas disease and Human African sleeping sickness respectively. Existing therapies are toxic and ineffective against the later stages of the two diseases, consequently safer, improved therapies are urgently required. Here, two areas of trypanosome biology are explored. In the first section, the process of cell division is approached from a fundamental biology perspective. Centromeres are the region of DNA where kinetochore structures form, allowing the attachment of microtubules to facilitate chromosome segregation. In *T. brucei* we have characterized the nature and location of centromeres by exploiting the localized activity of topoisomerase-II, a cancer chemotherapy target, at the centromere. Etoposide mediated DNA cleavage mapping revealed the presence of signature AT-rich repeat regions coupled with adjacent retrotransposons at the centromere. Further experiments demonstrate that of the two nuclear *T. brucei* topoisomerase-II isoforms, only topoisomerase-IIα is essential and active at the centromere. The second section centres on pro-drug development against a trypanosome type I nitroreductase. This enzyme has previously been implicated in activation of nifurtimox and benznidazole, the two therapies in clinical use against Chagas disease. Initially we have developed a luciferase based drug assay system in the clinically relevant intracellular *T. cruzi* stage and rapidly screened a range of nitroaromatic based compounds for trypanocidal activity. A series of derived nitrofuryl compounds previously developed against Chagas disease were also screened against *T. brucei*, where most demonstrate trypanocidal activities of less than 1 μM. Further we show that these compounds are active substrates of nitroreductase, and act as pro-drugs within the parasite by specific activation of nitroreductase to generate cytotoxic moieties.

Acknowledgments

I would like to thank John Kelly and Shane Wilkinson for the opportunity to study for a PhD, and without their continuing support this thesis would not have been possible. I am also greatly indebted to Sam Obado and Martin Taylor for their countless pub based tutorials and discussions on all things involving trypanosomes. Less than grateful about the possible accompanying liver damage though. I would also like to show my gratitude to Flora Logan for keeping me on the right side of sane, and Sam Alsford, Belinda Hall, Michael Lewis, and Andrew Voak for all of their constructive help and advice.

Publications

Longqin Hu, Xinghua Wu, Jiye Han, Lin Chen, Simon Vass, Patrick Browne, Belinda Hall, **Christopher Bot**, Vithurshaa Gobalakrishnapilla, Peter Searle, Richard Knox, Shane Wilkinson. Synthesis and structure-activity relationships of nitrobenzyl phosphoramide mustards as nitroreductase-activated prodrugs. *Bioorganic & Medicinal Chemistry Letters* 2011, **21** (13): 3986-91.

Belinda Hall, **Christopher Bot,** Shane Wilkinson. Nifurtimox activation by trypanosomal type I nitroreductases generates cytotoxic nitrile metabolites. *Journal of Biological Chemistry* 2011, **286** (15): 13088-95.

Samson Obado, **Christopher Bot**, Maria Echeverry, Julio Bayona, Vanina Alvarez, Martin Taylor, John Kelly. Centromere-associated topoisomerase activity in bloodstream form *Trypanosoma brucei. Nucleic Acids Research* 2011, **39** (3): 1023-33.

Christopher Bot, Belinda Hall, Noosheen Bashir, Martin Taylor, Nuala Helsby, Shane Wilkinson. Trypanocidal activity of aziridinyl nitrobenzamide prodrugs. *Antimicrobial Agents and Chemotherapy* 2010, **54** (10): 4246-52.

Samson Obado, **Christopher Bot**, Daniel Nilsson, Bjorn Andersson, John Kelly. Repetitive DNA is associated with centromeric domains in *Trypanosoma brucei* but not *Trypanosoma cruzi. Genome Biology* 2007, **8** (3).

Contents

Figures

Tables

1 General Introduction to Trypanosomatids

1.1 The Trypanosomatid Diseases

Trypanosomatidae are a family of parasitic protozoa in the Order Kinetoplastida. As a grouping, this family of pathogens can infect an array of hosts ranging from plants through to higher mammals. In humans they are responsible for several major infections including Chagas disease, African sleeping sickness (also known as human African Trypanosomiasis) and Leishmaniasis which are caused by *Trypanosoma cruzi*, *Trypanosoma brucei* and *Leishmania* species respectively. These diseases are reported to afflict more than 20 million people worldwide leading to an estimated 110,000 deaths, with 500 million individuals living in areas deemed at risk (WHO, 2004). They are often considered neglected diseases since they attract relatively little research interest. Of the total amount of money spent worldwide on research, US$ 2.5 billion for 2007, less than 5% was directed towards these three diseases combined (Moran et al., 2009). This thesis will focus on the trypanosomes: *T. brucei* and *T. cruzi*, but will also feature *Leishmania major*.

1.1.1 African sleeping sickness

The first medical reports of African sleeping sickness were described by the physician Thomas Winterbottom. In 1734 he noted an infection whose early stage was characterized by swollen lymph glands at the back of the neck, a symptom apparently used by Arabian slave traders when discriminating between healthy and unfit slaves (Steverding, 2008). The next significant step in recognizing African sleeping sickness was made by the explorer David Livingstone who observed that cattle bitten by the Tsetse fly (Figure 1.1.1) went on to develop Nagana, an infection now known to be the cattle disease equivalent to African sleeping sickness. However, it took the microbiologist David Bruce to discover that a trypanosome infection was responsible for Nagana, and later to make the connection that the trypanosome was transmitted by the Tsetse fly vector. At the end of the 19th century, this trypanosome was observed in human blood by Joseph Everett Dutton, and later in human spinal fluid by Aldo Castellani, prompting the first suggestions that African sleeping sickness was also

caused by the trypanosome. David Bruce further demonstrated that African sleeping sickness was spread by the Tsetse fly, the same way as Nagana (Steverding, 2008). The trypanosome species responsible for African sleeping sickness and Nagana was named *Trypanosoma brucei*, in honour of the scientific contribution made by David Bruce.

Figure 1.1.1. ***African sleeping sickness insect vector: the Tsetse fly***
Image from The Science Photo Library Ltd.

The Tsetse fly (*Glossina* spp.) vector is critical to the epidemiology of African sleeping sickness. The Tsetse are restricted to the African continent, ranging from south of the Sahara to north of the Kalahari desert (Barrett et al., 2003). This in turn confines the transmission of *T. brucei*, and hence the regional distribution of the disease. Historically, the level of disease prevalence has fluctuated greatly. During the 1920s a major epidemic was recorded in the region of what is now the Democratic Republic of Congo, with up to 60,000 cases reported per year (WHO, 2000). The response of the governing colonial powers was to introduce new medical services, coupled with a significant improvement in living standards. This resulted in a dramatic reduction in the numbers of infected cases over a period up until the 1960s (Steverding, 2008). Unfortunately the social upheaval and political instability that followed the independence of many African countries resulted in a significant reduction in public health services and control

programmes. This led to the last major epidemic of African sleeping sickness which peaked in the late 1990s, with at its height in 1997 over 37,000 new cases reported (WHO, 2000). Since then, the number of new cases reported has steadily been declining, with the latest statistics showing that 9,689 new cases of African sleeping sickness were diagnosed in 2009, in the context of a significant improvement in passive screening for the disease (Simarro et al., 2011). The late 20th century epidemic prompted a 1997 WHO resolution to raise international awareness of the disease. It is believed that following this resolution, the intensified political cooperation between African nations towards improved surveillance and control, combined with the successful distribution of drugs made available through benevolent agreements with pharmaceutical companies, is predominantly responsible for the decline in reported cases of African sleeping sickness.

The important lesson here, emphasized by a World Health Organization report (WHO, 2006), is that the development of safer, more effective, orally administered drug therapies should be coupled with the continuation of the socio and political collaboration between African States against African sleeping sickness.

The African trypanosome responsible for African sleeping sickness, *T. brucei*, has two human infectious sub-species, each with distinct disease pathologies. *T. brucei gambiense* occurs within the western and central regions of the Tsetse fly's habitat of Africa, while *T. brucei rhodesiense* is endemic to east Africa (Brun et al., 2010). Although this discreet divide has often been referred to in the literature, there now appears to be an emerging overlap of endemic areas within Uganda between the *T. brucei* sub-species, potentially as the animal reservoirs of *T. brucei rhodesiense* move into the predominantly non-zoonotic *T. brucei gambiense* endemic region (Picozzi et al., 2005). The third sub-species of *T. brucei*, named *T. brucei brucei*, is non-pathogenic to humans and only infects cattle, causing the disease Nagana.

Infection by *T. b. gambiense* results in a slow chronic disease, estimated to last on average around 3 years (Checchi et al., 2008). Conversely *T. b. rhodesiense* results in a rapid onset acute disease lasting from only weeks to a couple of months. Both types of disease progress in two distinct stages. In the first haemolymphatic stage, the parasites begin to replicate around the site of infection and gradually spread to the lymph and

blood system, resulting in general symptoms such as headaches and fever, as well as potentially swollen lymph glands at the back of the neck (Winterbottom's sign). The second encephalitic stage develops as parasites enter the central nervous system, by what appears to be an active migration process (Masocha et al., 2007; Nikolskaia et al., 2006), as opposed to an opportunistic exploitation of any breakdown in the blood-brain barrier. During this stage, patients exhibit disrupted sleep patterns as the circadian rhythm becomes disrupted (Lundkvist et al., 2004), the clear symptom that gives this disease its name. The various symptoms of the two separate stages are significant, as while the first stage is much easier to treat, the general symptoms are easily mis-diagnosed or ignored by the patient. Symptoms of the disease's second stage are much more obvious, although the treatment is less effective, and with a greater risk of adverse side-effects (see Section 1.2.1). If this disease remains untreated it will be fatal (Barrett et al., 2003).

This thesis will focus solely on *T. brucei brucei* as a representative model of the two human pathogenic sub-species, due to the ease of culturing the physiologically relevant lifecycle stage, the number of reliable genetic tools available for the functional dissection of the parasite, together with a completed genome sequencing project (Berriman et al., 2005). Therefore the implications of any observations reported here should be considered in the wider context of applicable disease research.

1.1.2 Chagas Disease

Evidence of Chagas disease, also known as American trypanosomiasis, appears to date back 9 millennia, as indicated by samples taken from preserved 9000 year old mummies excavated from coastal regions of South America testing positive for DNA remnants of the disease causing *T. cruzi* parasite (Aufderheide et al., 2004). It has also been suggested Charles Darwin may have suffered from the disease, given his diary account of an encounter with the parasite's insect vector, alongside the pattern and nature of the symptoms he displayed for many years before his death (Bernstein, 1984). The first recorded case of Chagas disease was made by Dr. Carlos Chagas in a 2-year old girl, in 1909 (Chagas, 1909). Dr. Chagas was also first to describe the *T. cruzi* parasite, which he named after his mentor, Oswaldo Cruz, and first to identify the insect vector and the

transmission life-cycle of the parasite. Surprisingly, despite being nominated twice, Chagas never won the Nobel Prize.

Figure 1.1.2. ***Chagas disease insect vector: Rhodnius prolixus.***
Image from The Science Photo Library Ltd.

A significant animal reservoir exists for *T. cruzi* in wild animals, for example in rodents, bats, and armadillos, as well as domesticated animals such as cats and dogs. The *T. cruzi* parasite is predominantly transmitted by blood-sucking bugs from the Reduviidae family, with *Triatoma infestans*, *Rhodnius prolixus* (Figure 1.1.2), and *Triatoma dimidiata* considered 3 of the most important vector species to man (Rassi et al., 2010). Chagas disease is endemic to Latin America, reflecting the distribution of the various insect vectors. *T. infestans* is found mainly in sub-Amazonian regions, while *R. prolixus* and *T. dimidiata* occur further north beyond the Amazon basin, through Central America, reaching Mexico (WHO, 2002). Alternative mechanisms of transmission are also worth noting. Vertical transmission of the parasite between a mother and her baby is a risk (Azogue et al., 1985), as well as blood transfusions from *T. cruzi* contaminated samples (Dias, 1984).

In 2004 it was estimated that in Latin America, 7.7 million people were infected with Chagas disease (PAHO/WHO, 2007) with a resulting 11,000 deaths per year (WHO, 2004). This is a significant decrease in the incidence reported for 1985 where 17.4 million people were estimated to be infected with Chagas disease (WHO, 2002). A major factor in the reduction of cases was the initiation of the 'Southern Cone Initiative' vector control programme in Argentina, Bolivia, Brazil, Chile, Paraguay, Peru and Uruguay. This political collaboration introduced a widespread insect control programme designed around extensive use of insecticides to clear the insect vector from infested rural and urban dwellings, coupled with co-ordinated blood screening to prevent any medically derived transmission (Moncayo, 1999). Following its inception, Chile and Uruguay, with parts of Argentina, Paraguay and Brazil, are now classed as free of vectorial transmission (Miles et al., 2003; Moncayo and Silveira, 2009). In contrast, arguably complacency and a lack of co-ordination in some regions such as Peru has led to a resurgence of the disease (Delgado et al., 2011), as investment towards control projects is diverted. Chagas disease is also an emerging problem in non-endemic regions as increased globalization leads to mass worldwide migration. For example, estimates in the United States indicate that approximately 300,000 people suffer from Chagas disease (Bern and Montgomery, 2009), with numerous cases reported in regions ranging from Canada and Japan to Australia and Europe (Rassi et al., 2010).

The pathologies associated with Chagas disease can be divided into three phases. The initial, acute stage develops over a 4-8 week period and is often asymptomatic (Rassi et al., 2010). Possible signs of the disease can arise after 1-2 weeks for an infection originating from a bug bite, or after a couple of months from infection via a blood transfusion. These potential symptoms can include a swelling at the site of infection and/or a rapid onset fever, either of which can be easily missed or mis-diagnosed. Approximately 10% of acute cases results in death from either myocarditis (inflammation of the heart) or meningoencephalitis (inflammation of the brain) (Barrett et al., 2003). Beyond the acute stage, the disease progresses into an indeterminate stage, a pathology that can last the rest of the patient's natural life. Here, the disease remains latent and no obvious signs of infection are felt or observed by the patient. In 15-30% of patients, the so-called chronic form of the disease can occur. This is characterized by

premature heart disease and enlargement of the oesophagus and colon (mega syndromes) often resulting in heart failure and sudden death. The length of time a patient is in the indeterminate stage varies, with some individuals not entering the chronic disease state decades after the initial infection (Barrett et al., 2003). While drug treatment (see Section 1.2.2) for the acute stage is usually successful (Bahia-Oliveira et al., 2000), chemotherapy for the chronic stage remains ineffective (Cancado, 2002), placing an even greater emphasis on the importance of early diagnosis.

Although there is only a single defined species of *T. cruzi*, a significant degree of variation between strains exists, amounting to greater intra-species diversity than even that observed between some classified species of *Leishmania* (Tibayrenc, 1998). The current classification system describes the sub-division of *T. cruzi* strains into six discrete groups: TcI - TcVI (Zingales et al., 2009). It has been reported that *T. cruzi* TcII, TcV, and TcVI strains are predominantly the cause of Chagas disease (Di Noia et al., 2002; Freitas et al., 2005), however *T. cruzi* Type I strains appear in patients in northern South America (Anez et al., 2004). It has been shown that clonal *T. cruzi* populations can undergo genetic exchange (Gaunt et al., 2003; Ocana-Mayorga et al., 2010). This makes it difficult to interpret the full implications of genetic diversity between *T. cruzi* strains towards its epidemiology and human pathogenicity.

1.1.3 Leishmaniasis

The earliest medical reports of Leishmaniasis date back to 1903 where two military doctors, Dr. William Boog Leishman and Dr. Charles Donovan, independently identified a species, subsequently named *Leishmania donovani*, in spleen samples taken from patients in India (Herwaldt, 1999). Recent estimates indicate that there are nearly 2 million new cases of Leishmaniasis each year (WHO, 2010) resulting in approximately 50,000 deaths per year (WHO, 2004). Leishmaniasis is endemic at multiple geographic locations, encompassing 88 countries, ranging from South America, to southern Europe, northern Africa and across much of Asia (WHO, 2010). Given that 72 of these 88 endemic countries are in the developing world, this infection represents yet another neglected parasitic disease associated with poverty.

Figure 1.1.3. ***Leishmaniasis insect vector: the Sand fly.***
Image from The Science Photo Library Ltd.

Transmission of *Leishmania* parasites from animal reservoirs to human hosts occurs via the bite of various species of the Sand fly (Figure 1.1.3), commonly of either the *Phlebotomus* (Old World) or *Lutzomyia* (New World) genus (Murray et al., 2005). There are numerous defined species of the *Leishmania* parasite responsible for the human disease (Desjeux, 1996), which creates a complex and diverse variety of disease pathologies. Reminiscent of Chagas disease, many cases of *Leishmania* infection remain asymptomatic, however this disease may manifest itself in a variety of forms depending on the infective species. For instance *L. donovani* and *L. infantum* are two examples of species that cause visceral Leishmaniasis, the most dangerous form of the disease. If symptoms are presented by a patient and remain untreated, this disease is often fatal (Desjeux, 1996). Symptoms of this form of disease may show as part of the acute phase weeks post infection, and can be severe such as developing splenomegaly, hepatomegaly, immunosuppression, anaemia and fever (Herwaldt, 1999). The cutaneous form of Leishmaniasis represents a milder form of disease and is often the result of infection by *L. major* (Old World) or *L. mexicana* (New World) species. Skin lesions may appear weeks after infection, which may further develop into scarring, or potentially self-cure over the long-term. Occasionally (less than 5% of cases) the cutaneous form can resurge as a form termed Mucocutaneous Leishmaniasis, possibly years after the initial cutaneous infection has cleared. An example of a species

associated with this type of disease progression is the New World *L. braziliensis*, where infection can result in significant damage to the larynx, nasal cavities, and other parts of the face through the formation of major destructive inflammatory lesions (Murray et al., 2005). This thesis will feature *L. major* as a model species for Leishmaniasis, due to the availability of its completed genome project (Ivens et al., 2005).

A vaccine against either African sleeping sickness and Chagas disease appears unlikely anytime soon (Barrett et al., 2003; Rassi et al., 2010), while a Leishmaniasis vaccine based on live *L. major* once existed, but was discontinued in the 1990's. This was due to the development of serious lesions on a number of recipients. The development of a vaccine for Leishmaniasis is still considered possible (Handman, 2001), however for the foreseeable future tackling African sleeping sickness and Chagas disease will rely on accurate and effective diagnosis, vector control and chemotherapy.

1.2 Current Diagnostics and Therapies

1.2.1 Treating African sleeping sickness

The standard detection method for *T. brucei* is the card agglutination test for Trypanosomiasis (CATT) (MSF, 2010), which was developed in the 1970's and detects the presence of anti- parasite antibodies in the host's blood. It is both a simple and fast test to perform, with a ~95% degree of sensitivity and specificity towards the parasite (Truc et al., 2002), and is widely used for mass population screening (Lutumba et al., 2005). The drawback of this high-throughput diagnostic is that it is only reliable in detecting *T. b. gambiense* (Brun et al., 2010); consequently diagnosing *T. b. rhodesiense* infection relies on the identification of symptoms presented by patients. Confirmatory detection of the parasite is strongly recommended before the administration of chemotherapy due to the associated toxicity.

Two effective chemotherapies are available for the treatment of early stage African sleeping sickness: pentamidine and suramin. The sub-species *T. b. gambiense* is treated with pentamidine, which is administered either by injection into muscle over a week or intravenously as a saline solution for 2 hours. The side-effects of pentamidine are often

mild relative to alternative trypanosomatid chemotherapy, and include diarrhoea, nausea, and pain at the site of injection (Barrett et al., 2007). Also preventative measures are taken to reduce the potential of induced hypoglycaemia (MSF, 2010). Suramin is used to treat *T. b. rhodesiense*, and is administered through a slow intravenous injection, as a course of 6 injections over 31 days (MSF, 2010). Although pentamidine is easier to administer, the increased possibility of severe allergic reactions to pentamidine as a consequence of more frequent parallel infection by *Onchocerca* species in *T. b. rhodesiense* endemic regions (Brun et al., 2010) precludes its use against this sub-species. Additional side-effects include rash, fatigue, anaemia, peripheral neuropathy, and bone marrow toxicity, plus the possibility of acute and severe anaphylactic shock (Brun et al., 2010). Neither drug is particularly effective against the second stage of the disease, as the charged nature of the compounds means they do not easily traverse the blood-brain barrier (Barrett et al., 2007)

For the last 60 years second-stage encephalitic African sleeping sickness was treated with melarsoprol, an arsenical compound. However it is no longer the standard drug of choice (but does present a cheaper option) for second stage *T. b. gambiense*, although it still remains in clinical use for second-stage *T. b. rhodesiense* infection and for *T. b. gambiense* relapse cases. Its administration is complex, comprising a course of 3-4 slow intravenous injections given on consecutive days, with 3-4 repeats of this course separated by 7-10 day intervals; though for *T. b. gambiense* relapse patients a shorter 10 day course is prescribed (MSF, 2010). Melarsoprol generates significant side-effects including an encephalopathic syndrome that affects 5-10% of treated patients, with ~50% of those affected dying as a result (Barrett et al., 2007). Evidence is also emerging of possible melarsoprol resistance in the field. Melarsoprol uptake by *T. brucei* has previously been shown to occur via an adenosine transporter (TbAT1) (Carter and Fairlamb, 1993; Maser et al., 1999). Genetic mutations in this transporter have been observed in clinical parasite isolates taken from a region where patients are refractory to melarsoprol treatment (Matovu et al., 2001). Re-sampling this region years later, after melarsoprol treatment had been discontinued, revealed that all clinical isolates possessed the wild-type transporter allele, losing the acquired genetic mutations, and suggesting the occurrence of drug pressure drives selection of melarsoprol resistant *T. brucei*

(Kazibwe et al., 2009). The preferred alternative to melarsoprol treatment for *T. b. gambiense* is nifurtimox-eflornithine co-therapy (NECT). While sole treatment with eflornithine is possible and has been used previously (Burri and Brun, 2003), this strategy has now been superseded by the co-therapy regime. This requires a 10 day course of the orally administered nifurtimox and intravenously dosed eflornithine (MSF, 2010). Nifurtimox originated as a chemotherapy to Chagas disease (see later), while eflornithine was developed as an anti-cancer treatment and first trialled against African sleeping sickness in the 1980's (Van Nieuwenhove et al., 1985). While the side-effects of eflornithine are not as severe as melarsoprol, its use may still result in convulsions, gastrointestinal symptoms such as nausea, vomiting and diarrhoea, and bone marrow toxicity (Burri and Brun, 2003). However, by combining its use with nifurtimox, the number of injections and side-effects have been reduced (as well as cost) with no loss to efficacy (Yun et al., 2010). Recently, an eflornithine uptake transporter has been identified in *T. brucei* (TbAAT6), which during *in vitro* selection with eflornithine can easily be lost, leading to induced drug resistance (Vincent et al., 2010). It will be interesting to see if this observation is reflected in the field.

In summary, early stage African sleeping sickness chemotherapy is effective though limited, while significant side-effects are associated with late stage disease treatments. All of the current therapies are difficult to administer and require professional medical supervision. This, together with the potential of emerging resistance, emphasizes the need for safer, preferably orally administered drugs, particularly for the late stage of African sleeping sickness.

1.2.2 Treating Chagas disease

Diagnosis of Chagas disease in the acute stage is performed by the straightforward detection of parasites in a patient's blood sample (WHO, 2002). Difficulty arises in diagnosing chronic stage Chagas disease due to the very low abundance of parasites in the peripheral blood. Diagnosis relies on detecting specific antibodies in the blood instead, which only has around a 20-50% sensitivity for indicating the presence of the parasite (Gomes et al., 2009).

Only two drugs are available to treat Chagas disease: nifurtimox and benznidazole. Both are nitroheterocyclic compounds and are only effective at treating the early acute stage of the disease. Neither is ideal. A nifurtimox treatment regime lasts for 30-60 days and is administered orally 2-3 times a day (MSF, 2010). Side-effects of nifurtimox are common and include nausea, gastric pain, sleeping disorders and seizures (Jackson et al., 2010). Benznidazole treatment is also delivered orally over a period of 30-60 days (MSF, 2010), with side-effects occurring in up to 50% of patients, ranging from nausea and skin rash to fever and peripheral polyneuritis (Pinazo et al., 2010). Both drugs are based on a nitroheterocyclic chemical structure, and function as pro-drugs through activation by a type I nitroreductase enzyme (see Section 6.1). Parasites cross-resistant against nifurtimox and benznidazole can be generated through *in vitro* drug pressure, resulting from the selected loss of the type I nitroreductase gene (Wilkinson et al., 2008). Therefore, resistance to either drug usually equates to resistance to both (all) drugs available to treat Chagas disease, and would be gravely significant if observed in the clinic. With an absence of chemotherapies available towards the chronic stage of Chagas disease and the potential for resistance to the existing remedies, new treatments are again urgently required.

1.2.3 Treating Leishmaniasis

Diagnosis of Leishmaniasis is achieved by the microscopic identification of parasites from tissue biopsies or skin scrapings taken from the site of infection (MSF, 2010). Further identification of the *Leishmania* specific species can be made with a PCR based assay. This process is considered 100% sensitive and specific (Vega-Lopez, 2003), and is important as different medications are prescribed for different species. The visceral form caused by *L. donovani* and *L. infantum*, and the mucocutaneous form of *L. braziliensis* is treated with either daily intravenous or intramuscular injections of meglumine antimoniate or sodium stibugluconate for 30 days (MSF, 2010). As the cutaneous form of Leishmaniasis can self-cure, the intervention with treatment is made only if the lesions are severe. Suitable chemotherapies include: meglumine antimoniate or sodium stibogluconate (1-2 week intravenous treatment), fluconazole (6 week oral treatment) or paromomycin (2 week topical treatment). Only then, if these therapies fail

the treatment of Leishmaniasis may resort to pentamidine (5-25 weeks, intramuscular injections) (MSF, 2010).

1.3 The Trypanosomatid Life-Cycles

Trypanosomatids are well adapted to live in the different environments of their mammalian host and insect vector, and possess a variety of life-cycle stages to thrive in their diverse surroundings. From the perspective of drug development it is clear that focusing research towards the disease causing human host stages is imperative, whether exploring potential drug targets or developing improved chemotherapies. Unsurprisingly, notable differences have been observed between the insect and mammalian parasite stages. In *T. brucei* for example, 6% of genes appear to be life-cycle regulated (Siegel et al., 2010), while 9% of genes are stage regulated in *L. major* (Rochette et al., 2008). For *T. cruzi*, proteomic studies have highlighted many differences in protein abundance between life-cycle stages (Atwood et al., 2005). Much of the work discussed here concentrates on the clinical parasite forms. Often however, utilizing the insect stages provides technical advantages, which may be useful when studying particular parasite features conserved across all life-cycle stages.

1.3.1 The *T. brucei* life-cycle

In the mammalian host *T. brucei* lives free within the bloodstream and replicates as morphologically slender trypomastigote forms (Figure 1.3.1a). Then as parasite numbers increase, these shift into non-replicative morphologically stumpy forms. This is believed to prevent parasite numbers reaching a critical mass that would be fatal for the host, therefore prolonging the host lifespan and increasing the probability of transmission to the insect vector (Matthews et al., 2004). To shield the mammalian parasite stages from the host adaptive immune response, the pathogen's cell surface is covered with a single antigen, the variant surface glycoprotein (VSG) coat, which acts to thwart consistent antibody recognition of the foreign invasive organism. This dense masking of the accompanying invariant proteins on the cell surface membrane prevents recognition of the parasite by host specific antibodies. A parasite infection consists of a dominant population of a single variant surface glycoprotein structure (Cross, 1975). However, a

random genetic switching event facilitates the formation of tiny sub-populations of *T. brucei* equipped with alternative variant surface glycoproteins (Stockdale et al., 2008). Once the original dominant population of the infection has been eradicated by the acquired host immune response, this minor sub-population establishes itself as the new dominant population, evading the current antibody response (McCulloch, 2004; Pays et al., 2004). It is this feature of *T. b gambiense* and *T. b. rhodesiense* pathogenesis that makes the development of a vaccine against these organisms particularly unlikely.

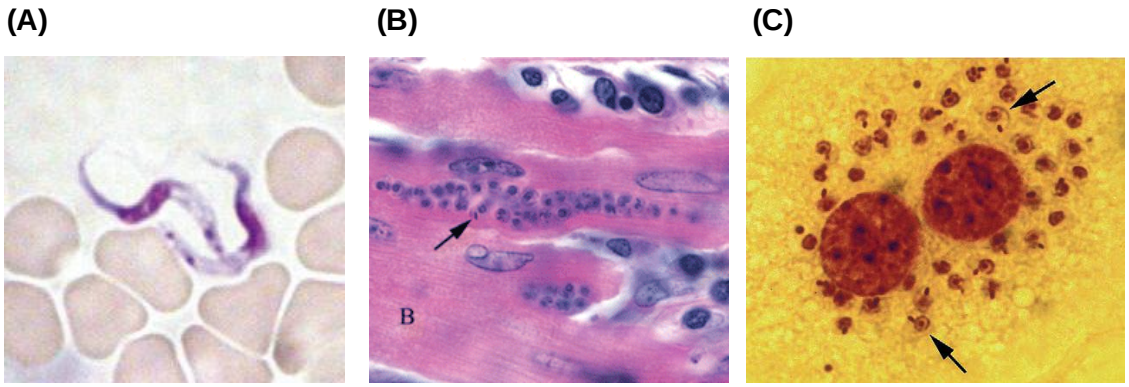

Figure 1.3.1. ***Images of the trypanosomatid clinical parasite forms.***
(**A**) A blood film showing the human bloodstream form of *T. brucei* (Barrett et al., 2003). (**B**) A heart biopsy specimen containing the intracellular *T. cruzi* parasites (Kun et al., 2009). (**C**) A mouse macrophage isolate infected with the intracellular form of *L. donovani* (Murray et al., 2005).

Even though *T. b. brucei* could evade the adaptive immune response, this sub-species remains non-pathogenic to humans due to the additional protective properties of the immune system. Standard human serum contains an effective trypanolytic factor, apolipoprotein L-I that, in tandem with a haptoglobin-related (Hbr) protein, (Rifkin, 1978; Shiflett et al., 2007; Vanhamme et al., 2003) lyses the parasite via the formation of destructive pores in lysosomal membranes (Perez-Morga et al., 2005). Both *T. b. gambiense* and *T. b rhodesiense* sub-species are resistant to this trypanosome lytic factor by different mechanisms. In *T. b rhodesiense*, a Serum Resistance Associated (SRA) protein appears to reduce the level of the trypanolytic complex successfully targeting the

lysosome, inhibiting the parasite lysis mechanism (Hager and Hajduk, 1997; Oli et al., 2006). In *T. b. gambiense* SRA is absent and another mechanism is employed. It has been suggested that in this sub-species, the conserved haptoglobin-related protein receptor is down-regulated and altered in amino acid sequence, thus inhibiting the internalization of the trypanolytic complex (Kieft et al., 2010). This highlights the fact that although *T. b. gambiense* and *T. b rhodesiense* are of the same species, they are not equivalent in basic biology, implying that from the perspective of research and drug development, African sleeping sickness should not necessarily be considered a single disease. It is also worth noting the *T. b. brucei* strain used in many laboratory experiments (Section 3.1.3) have lost the ability to differentiate into the stumpy forms, and remain monomorphic in culture as the slender forms (Hendriks et al., 2000). A small proportion of these can differentiate directly into the insect forms though (Matthews and Gull, 1994).

Once a Tsetse fly feeds on a host infected with *T. brucei*, short stumpy form parasites residing in the blood meal become deposited in the fly mid-gut. Here, they differentiates into the replicative procyclic forms, shedding the variant surface glycoprotein coat and replacing it with a less dense covering of procyclin proteins (Roditi et al., 1987). These procyclic parasites later migrate to the salivary gland and differentiate into replicative epimastigotes, which then mature into the metacyclic infectious forms, now equipped with a variant surface glycoprotein coat (Fenn and Matthews, 2007; Lenardo et al., 1984) in preparation for re-infection into the mammalian host, completing the life-cycle (Figure 1.3.2). It is believed that at the epimastigote stage, genetic exchange between parasites is possible (Peacock et al., 2011).

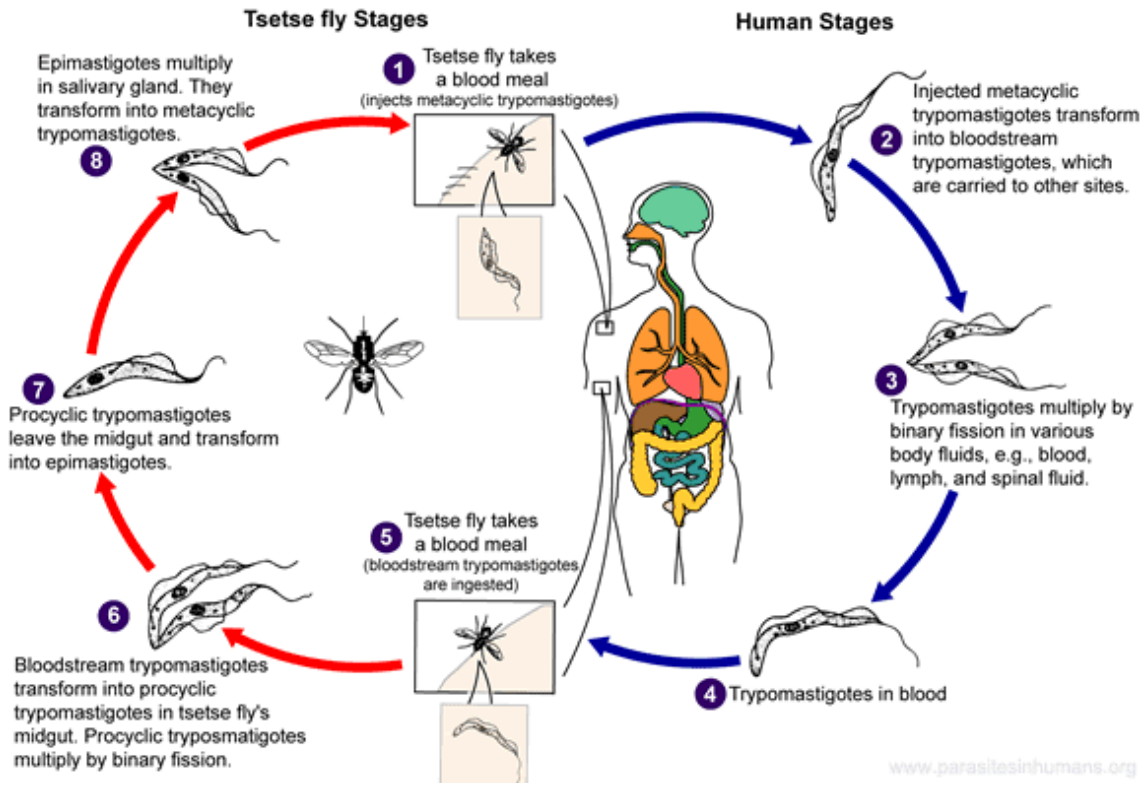

Figure 1.3.2. ***A diagram of the life-cycle stages of T. brucei.***
Image from the Centre for Disease Control and Prevention.

1.3.2 The *T. cruzi* life-cycle

T. cruzi enters the human host as an infectious metacyclic trypomastigote through skin wounds or mucosal membranes of the eyes and mouth. This parasite stage is covered in various mucin glycoproteins (Di Noia et al., 1995). Some mucins are involved in protecting the parasite from digestion by host proteases (Mortara et al., 1992), while others are important in host cell invasion (Yoshida et al., 1989) through interactions with host cell molecules (Ruiz et al., 1993). *T. cruzi* metacyclic forms are capable of invading both phagocytic and non-phagocytic cells through a subversive cell signalling mechanism. The full repertoire of molecular interactions between parasite and host that triggers this mechanism is varied and complex, and also depends on the particular *T. cruzi* strain and tissue cell-type (de Souza et al., 2010). These interactions consequently result in the activation of a Ca^{2+} signalling cascade (Ruiz et al., 1998) that leads to internalization of the metacyclic trypomastigotes within a lysosome (Rodriguez et al.,

1997). Once inside, the metacyclic trypomastigotes are temporarily contained within a vacuole compartment, which they then disrupt by secreting a porin-like molecule (Tc-TOX) (Andrews et al., 1990). Upon release into the cytoplasm the parasites differentiate into the smaller rounded amastigotes (Figure 1.3.1b), which replicate by binary fission. It is this stage that genetic exchange between parasites appears to occur (Gaunt et al., 2003). Once these amastigotes reach a high density they differentiate into bloodstream trypomastigotes and rupture the host cell plasma membrane, releasing them to infect neighbouring cells (Tyler and Engman, 2001).

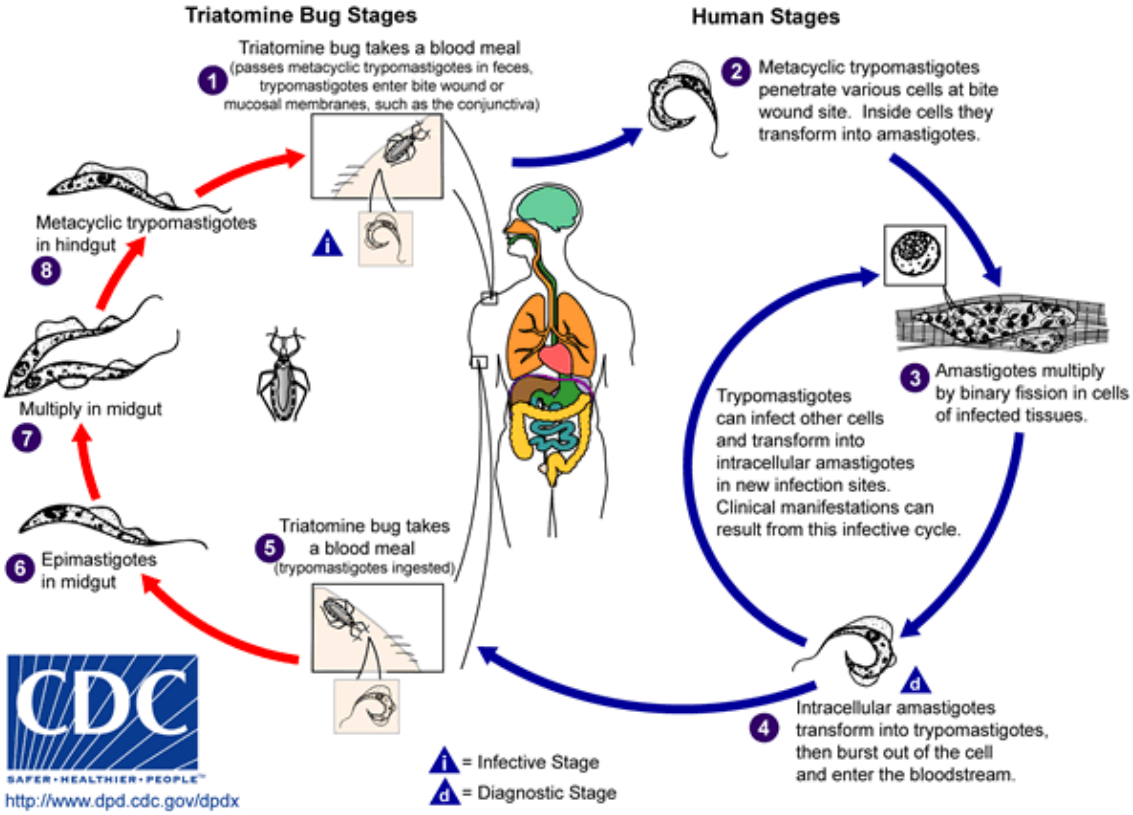

Figure 1.3.3. ***A diagram of the life-cycle stages of T. cruzi.***
Image from the Centre for Disease Control and Prevention.

Some free *T. cruzi* bloodstream trypomastigotes are taken up by the invertebrate vector during a blood meal. As these parasites traverse the insect's gut, the trypomastigotes differentiate into the epimastigote stage that then adheres to gut epithelial cells. This form begins to replicate by binary fission, occasionally releasing parasites into the lumen of the digestive tract gut. These then pass through into the hind-gut, eventually differentiating into the metacyclic trypomastigotes ready to be excreted in the invertebrate's faeces (Figure 1.3.3) (Kollien and Schaub, 2000).

1.3.3 The *Leishmania* life-cycle

Infectious metacyclic promastigote *Leishmania* enter the human host through the bite of the sand fly. The metacyclic promastigotes are capable of residing within a selection of phagocytic cell types, with the macrophage being the most common. Once in the bloodstream they covertly invade macrophages to prevent activation of the full immune response. However, unlike *T. cruzi*, which manipulates host cells to internalise the parasite via lysosomes, *Leishmania* rely on the active phagocytic uptake of the target macrophages. The metacyclic promastigotes express a variety of surface molecules to purposefully induce phagocytic uptake by macrophages, without specifically activating the macrophage's respiratory burst response (Alexander et al., 1999). When inside the macrophage vacuole, *Leishmania* also suppress specific cytokine signals, preventing the immune system from being alerted to their presence (Sacks and Sher, 2002). It is within the macrophage vacuole that the metacyclic promastigotes differentiate into the replicative amastigotes (Figure 1.3.1c). These increase in number inside the vacuole (in contrast to *T. cruzi*) until they are released from the macrophage, and further invade new phagocytic cells.

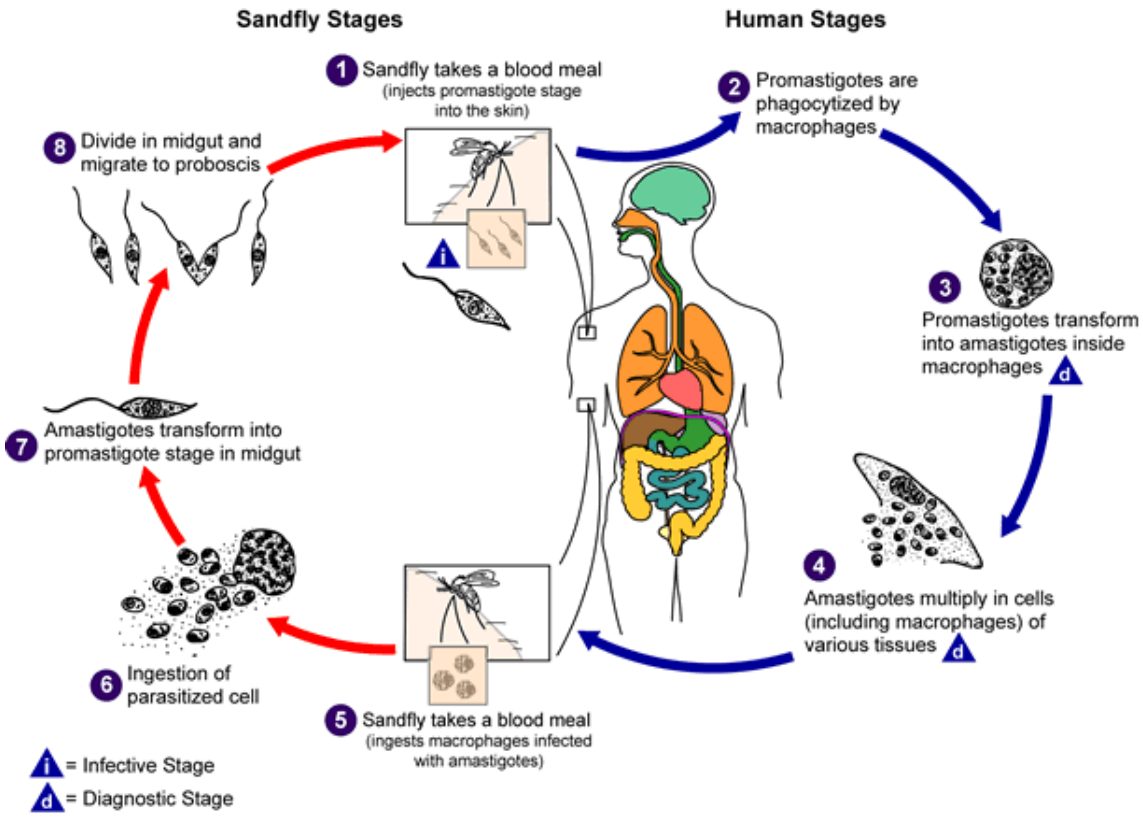

Figure 1.3.4. ***A diagram of the life-cycle stages of Leishmania.***
Image from the Centre for Disease Control and Prevention.

When a sand fly then feeds on a *Leishmania* host, a few infected macrophages may be taken up as part of the blood meal. As the meal passes down into the gut, the sand fly internally forms a peritrophic matrix made of proteins and glycoproteins, held together by microfibrils. This generates a protective sac that is designed to protect the sand fly gut from abrasive food particles and other infectious microbes. However, since the transitory differentiation stages are susceptible to destruction by digestive proteases, it also provides the time window required for the amastigotes once contained within the macrophage to fully differentiate into the promastigotes, (Pimenta et al., 1997). Eventually this sac is degraded by both the host and the parasite (Kamhawi, 2006) releasing the parasites to the gut. To prevent the free promastigote parasites being excreted by the fly, the parasites attach themselves through lipophosphoglycan molecules present on the pathogen's flagella to the epithelium lining of the gut (Sacks

and Kamhawi, 2001). These free promastigotes replicate intensely and by the 7th day begin to differentiate into the short and slender infectious metacyclic promastigotes. These are believed to be regurgitated by the fly into the new host next time it takes a blood meal (Rogers et al., 2004), establishing a new human infection (Figure 1.3.4).

1.4 Cell Biology

Trypanosomatids possess many cellular features common in eukaryotic cells, containing for example a membrane bound nucleus, an endoplasmic reticulum and Golgi apparatus. In addition, they also have less typical structures, some of which are unique to this group of organisms. A few notable features are summarized below.

One of the most striking features of trypansomatid parasites is their single flagellum. This is comprised of the classical axoneme of nine peripheral microtubule doublets circling a central pair of single microtubules, coupled with a large paraflagellar rod that runs the full length of the axoneme (Bastin et al., 1996). This rod appears to be involved in increased flagellar motility (Portman and Gull, 2010). Beyond its role in motility, the flagellum also has a role in attachment such as for *Leishmania* promastigote attachment to the fly gut wall, as well as being implicated in several other processes including cell division and immune evasion (Ralston & Hill 2008). At the base of the flagellum lies the flagellar pocket, which acts as the focal point of vesicular trafficking in trypanosomatids (Field and Carrington, 2009).

Trypanosomatids possess a single mitochondrion which varies in size, structure and function during the parasite's life-cycle. The mitochondrial genome (kDNA) is composed of thousands of circular, inter-linked DNA molecules that form a network referred to as the kinetoplast. This structure is characteristic of all organisms in the Order Kinetoplastida. The kinetoplast is located within the mitochondrial matrix, and for most life-cycle stages of *T. brucei*, *T. cruzi* and *Leishmania* spp. appears as a rounded bar, although in *T. cruzi* trypomastigotes this takes on a more circular morphology (de Souza et al., 2009). The DNA network consists of two types of DNA molecule, the large (~20 kb) maxi-circles, which are few in number (copy number between 20-45) and encode for certain mitochondrial proteins, and the more numerous (up to 5,000), smaller

mini-circles (0.1-10 kb), which encode for various RNA molecules (Lukes et al., 2005; Stuart, 1979). Bizarrely, the genes encoded in the maxi-circle DNA are flawed and in a process known as RNA editing, require post-transcriptional modification by addition or removal of uridine nucleotides to the mRNA in order to generate the functional coding sequences (Benne et al., 1986; Simpson et al., 2003). This process is catalyzed by the editosome protein complex, and directed by guide RNAs, which are encoded on both the DNA maxi- and mini- circles (Stuart et al., 2005). Another unusual mitochondrial property of bloodstream form *T. brucei* is their ability to effectively shutdown ATP production by this organelle by down-regulating the expression of cytochrome-dependent respiratory electron chains. In this situation the parasites become reliant on glycolysis for energy needs (Tielens and Van Hellemond, 1998).

To facilitate the above need for energy production via glycolysis, trypanosomatids have compartmentalized this system within the glycosome, a dedicated membrane bound organelle unique to the kinetoplastids. This organelle, related to peroxisomes found in many other eukaryotic cells, was first identified in *T. brucei* and contains the first nine enzymes involved in glycolysis (Michels et al., 2006). The reasons for localizing this pathway in a specialised organelle are unclear but could be an adaptation event that allows the cellular energy demands of certain life cycle forms to be met solely via substrate level phosphorylation. In addition to glycolysis, glycosomes also contain a number of other enzymes involved in processes as diverse as sterol biosynthesis (Urbina et al., 2002), β-oxidation of fatty acids and purine salvage (Michels et al., 2006) plus ancillary systems involved in detoxification of unwanted by-products (Wilkinson et al., 2005).

1.5 Trypanosomatid Genome Architecture

In 2005 an important landmark was reached with publication of the *T. brucei*, *T. cruzi* and *L. major* genome sequences (Berriman et al., 2005; El-Sayed et al., 2005a; Ivens et al., 2005). With ~50% of the genes identified as hypothetical and having no known function, this has provided an unparalleled opportunity in terms of drug discovery and represents a fantastic tool allowing scientists to understand the cellular processes of these pathogens at a greater detail than before. For the genome sequencing project, reference laboratory cultured strains were chosen of each parasite that were believed to best reflect the natural life-cycle and disease pathology processes specific to each species, whilst also being amenable to everyday research.

1.5.1 The *T. brucei* genome

Arguably the most common *T. brucei* strain used in research is *T. b. brucei* Lister 427 MITat 1.2 clone 221a, however *T. b. brucei* TREU 927/4 is able to fulfil the complete life-cycle, and so was chosen for sequencing (van Deursen et al., 2001). Analysis revealed that *T. brucei* has a diploid genome with a haploid content of ~35 Mb. This is divided into three distinct classes of chromosome, which based on size are referred to as megabase chromosomes, intermediate chromosomes and mini-chromosomes.

Both *T. brucei* strains contain 11 megabase chromosomes which range in size from 1 to 5.2 Mb for *T. brucei* TREU 927/4, and 1 to ~6 Mb for *T. brucei* Lister 427 MITat 1.2 clone 221a (Melville et al., 1998; Melville et al., 2000). An unusually large size variation between some individual chromosome homologues within a single clone is observed. Chromosome 1 of the *T. brucei* Lister 427 MITat 1.2 clone 221a is a prime example, where homologue Ib (3.6 Mb) is twice the size of the Ia homologue (1.85 Mb) (Melville et al., 2000). Sequencing has shown that the *T. brucei* TREU 927/4 megabase chromosomes contain 9,068 protein coding genes in addition to 904 pseudogenes (Berriman et al., 2005). Of the full protein coding gene complement on the megabase chromosomes, around 800 of these encode for alternative VSGs, which are deployed to evade the mammalian host immune response (Section 1.3.1). These are found in large arrays on the megabase chromosomes at sub-telomeric sites, and it is currently thought that a large proportion of the intra-homologue size difference is due to varying lengths

of these sub-telomeric regions (Callejas et al., 2006). Most of the remaining genes are contained within the core central body of the megabase chromosomes in large directional gene clusters (Berriman et al., 2005). This type of gene arrangement for the standard "housekeeping" genes is common in all the trypanosomatids.

In addition to the 11 megabase chromosomes, *T. brucei* 927 also appears to contain 2 intermediate chromosomes around 350 kb in size (Melville et al., 1998). The function of this chromosome type is unclear but they may act as a dedicated reservoir of gene expression sites required for transcription of specific VSGs (Hertz-Fowler et al., 2008). Besides the presence of these sequences, the only other feature of note present on many of the intermediate chromosomes is a distinct 177 bp repeat unit (Wickstead et al., 2004).

Mini-chromosomes represent the third class of chromosome present in *T. brucei*. These are between 50–150 kb in size with a copy number estimated to be around 100 per cell (Van der Ploeg et al., 1984). This represents approximately 10% of the *T. brucei* total genome DNA content. The central core of the mini-chromosomes consists of the 177 bp repeat found on the intermediate chromosomes. This repeat is organized as a palindrome with the switch point at the chromosomal centre (Wickstead et al., 2004). Towards the edges of the chromosome are additional variant surface glycoproteins genes, further increasing the reservoir pool of these genes (Van der Ploeg et al., 1984).

1.5.2 The *T. cruzi* genome

T. cruzi CL Brener was selected for genome sequencing mainly because of its highly infectious nature (Zingales et al., 1997). However, assembly of its genome has been complicated as over 50% of its nuclear DNA content is composed of highly repetitive DNA sequences (El-Sayed et al., 2005a) and even today closure of the genome into large contiguous regions is problematic. A further challenge to accurate assembly is that *T. cruzi* CL Brener (group TcVI) is a genetic hybrid between two different strains from groups TcII and TcIII (El-Sayed et al., 2005a; Machado and Ayala, 2001). This has lead to a high level of allelic variation (~2%), and even trisomy (Obado et al., 2005). Together, this has made accurate sizing of chromosomes and the determination of chromosome copy number difficult, although estimates indicate that the haploid genome

size is around 67 Mb split across ~28 chromosomes (El-Sayed et al., 2005b). It is predicted that this haploid genome contains around 12,570 genes, with around 900 mucin genes and an estimated 219 ribosomal RNA genes. The molecular dissection of particular genes is made challenging by the nature of the *T. cruzi* CL Brener hybrid genome and the consequential unknown gene copy number. Recently, the DNA 'shotgun' sequence of the *T. cruzi* X10/1 strain (group TcI) has been released, which should help combat this issue, as the TcI group genome appears less corrupted by hybridizations (Franzen et al., 2011).

1.5.3 The *L. major* genome

The genome of *L. major* MHOM/IL/80/Friedlin is diploid, with the haploid genome containing 36 chromosomes ranging from 0.3 to 2.5 Mb in size (Ivens et al., 1998). These encode a predicted number of 8,272 protein-coding genes, with only 39 additional pseudogenes (Ivens et al., 2005). In contrast to *T. cruzi*, there is little allelic variation between homologues (~0.1%). Intriguingly, of the 36 chromosomes in the *L. major* genome, 20 of these are almost completely syntenic (conserved gene order) with the much larger *T. brucei* chromosomes. Around half of the breakpoints in synteny between *L. major* and *T. brucei* are observed at "strand-switch" regions, *i.e.* where there is a change in transcriptional orientation of the polycistronic gene arrays (El-Sayed et al., 2005b). This suggests much of the chromosomal arrangement has been conserved since these species diverged, over 200 million years ago (Douzery et al., 2004).

1.5.4 Gene expression

Many trypanosomatid genes are arranged in large directional gene arrays. These are transcribed as long polycistronic units that are post-transcriptionally modified to generate individual mature mRNAs. The genes within an array generally have unrelated functions and thus do not constitute the operon arrangement observed in bacteria (Clayton, 2002). Unlike many eukaryotes, trypanosomal genes do not generally have an exon/intron structure, being solely made up of coding sequence: to date only two *T. brucei* genes have been shown to contain introns (Mair et al., 2000). Transcription of the large polycistrons is RNA polymerase II dependent, but surprisingly no RNA polymerase II promoters have been found. Instead, it seems that transcription initiation

is regulated at the chromatin level, a proposal made after it was noted that certain histone variants were enriched at the start of polycistronic arrays in *T. brucei* (Siegel et al., 2009). To generate mature mRNAs, each gene of the polycistronic unit is trans-spliced with a standard 5' splice leader mRNA cap, and also cleaved and polyadenylated at the 3' end. These processes appear to be linked, and guided by the presence of a polypyrimidine tract marker within the intergenic regions (Matthews et al., 1994). Expression of the ribosomal RNA arrays is promoter driven and mediated by RNA polymerase I, as are some protein coding genes in *T. brucei* such as the variant surface glycoproteins (Kooter and Borst, 1984).

1.5.5 Genetic manipulation

Artificial DNA molecules can be successfully delivered into trypanosomes by electroporation, facilitating a range of reverse genetic techniques. Parasite populations that have taken up exogenous DNA can be selected through exerting drug pressure against parasites lacking the accompanying drug markers. To effectively express drug maker genes, plus any other additionally introduced genes, the transcript must be correctly processed by the parasite. To generate mature mRNA from the initial transcription product, accessory flanks commonly derived from 'housekeeping' genes such as α- and β- tubulin, or glyceraldehyde 3-phosphate dehydrogenase (GAPDH), are included in DNA constructs to provide the necessary signals to guide RNA processing.

Arguably the most straightforward form of transgenic gene expression is through a non-integrative replicative circular episome. For reasons that have yet to be fully elucidated, this does not require inclusion of a promoter and is effective in *T. cruzi* and *Leishmania*, but not in *T. brucei*. The first trypanosomal episomal expression plasmid was pTEX, which contained a neomycin phosphotransferase (Neo) gene flanked with GAPDH untranslated sequences (a drug cassette), plus a multiple cloning site featuring an array of restriction endonuclease sites to facilitate the insertion of the desired gene (Kelly et al., 1992). Additional GAPDH untranslated sequences facilitate elevated expression of the desired gene. This basic vector has subsequently been modified to allow even higher levels of gene expression (e.g. pRIBO-TEX) (Martinez-Calvillo et al., 1997), epitope tagging of a given protein (e.g. pTEX-9E10) (Tibbetts et al., 1995) or fluorescent

localization (e.g. pTEX-eGFP and pTEX-RED) (Wilkinson et al., 2002). The major drawback of this system however, is that gene expression may not be stable or consistent, as episomes are not faithfully segregated during mitosis, instead relying on the random distribution between dividing cells, and transcription is stochastic rather than promoter driven.

An alternative strategy, which provides greater stability of gene expression, is to integrate directly into the nuclear genome by homologous recombination. Linear DNA molecules can be inserted into a chromosome by using flanking regions composed of matching target DNA sequences, combined with a central drug marker cassette. This can be used to replace existing DNA (Rudenko et al., 1994), for example to effect a gene knockout, or to replace non-coding intergenic DNA with an exogenous gene. If these two targeting flanks are located adjacent to one another on the chromosome, no native DNA is deleted and instead the transgenic DNA sequence is looped into a single locus, effectively extending the chromosome marginally with an additional DNA sequence, such as an epitope tag (Schimanski et al., 2005). Unless an additional promoter is included in the transgenic sequence, constitutive expression of the drug marker and any accompanying genes depends on the native RNA polymerase II transcription.

The next level of sophistication in transgenic gene expression is the development of an on-demand inducible gene expression system. This commonly involves using the tetracycline (Tet) repressor system from *E. coli*, which consists of a tetracycline repressor and a tetracycline operator sequence, combined with a RNA polymerase promoter. The presence of a powerful promoter effectively generates over-expression of the desired downstream target gene. An early example of this was developed for *T. brucei*, where a procyclic acidic repetitive protein (PARP) promoter becomes de-repressed under tetracycline treatment conditions, facilitating expression of the luciferase reporter gene (Wirtz and Clayton, 1995). Other systems have been developed such as the inducible bacterial T7 promoter based system in *T. cruzi* (Taylor and Kelly, 2006; Wen et al., 2001) and the designated ribosomal expression locus coupled to RNA polymerase I in *T. brucei* (Alsford and Horn, 2008).

A significant exploitable feature of *T. brucei* is that it is able to perform RNA interference (RNAi), an ability that is absent from *T. cruzi* and *L. major* (DaRocha et al., 2004; Ngo et al., 1998; Robinson and Beverley, 2003). RNAi represents a form of post-transcriptional gene silencing mediated by the production of double stranded RNA (dsRNA). This double stranded RNA molecule is cleaved into 21 – 26 nucleotide long RNA fragments by an RNase III endonuclease termed DICER (Shi et al., 2006). These small double stranded fragments become bound to an RNA induced silencing complex (RISC) by a direct interaction with an Argonaute protein (Shi et al., 2004), which induces the degradation of the target RNA template by site-directed cleavage. By generating double stranded RNA molecules through an inducible expression system, which are unique to a specific gene, it is possible to induce 'knockdown' of the corresponding transcript, thus depleting the corresponding protein levels. Generally, this genetic approach is considered simpler than creating gene null mutants, although it can generate off-target effects and in many cases the desired protein may not be fully depleted. The double stranded RNA required for RNAi can be artificially generated by orientating two inverted copies of target DNA sequence downstream of a single RNA polymerase promoter so once transcribed the corresponding transcript folds to form a hairpin loop structure (Bastin et al., 2000), or by placing two inverted promoters at either side of the target DNA sequence to form a 'head to head' arrangement (Wang et al., 2000). Recently, the 'head to head' approach has been applied to generating a *T. brucei* RNAi library where RNAi inducing DNA fragments representative of the whole genome can be used in an unbiased approach to identify new metabolic pathways and processes to open up new areas for drug discovery (Alsford et al., 2011; Baker et al., 2010).

Many of the aforementioned strategies are employed in the work presented here, to investigate a variety of hypotheses on a range of gene targets.

1.6 Research Aims

This thesis is split into two sections, with each section comprised of a separate research project. This is as a result of discontinuous funding for the initial project. In the first section of this thesis, the genetic nature and location of centromeres on *T. brucei* and *L. major* chromosomes is explored. The second section investigates pro-drug compound candidates functioning through a nitroreductase dependant activation mechanism in *T. cruzi* and *T. brucei*.

SECTION I:

Topoisomerase-II mediated biochemical mapping of centromeres

2 Introduction to Centromeres

The faithful segregation of replicated chromosomes is essential to the process of cell division for all eukaryotic cells. This area of biology has experienced much general interest, as a failure to control the process of cell division is thought to be a cause of many human cancers (Jallepalli and Lengauer, 2001; Kops et al., 2005). Central to the process of mitosis, is the mechanical separation of replicated sister chromatid DNA, which requires microtubules from opposing poles of the nucleus attaching to the chromosomes, and on the appropriate cellular trigger, physically pulling the sister chromatids apart in preparation for cytokinesis. These microtubules attach to the chromosomes through the kinetochore protein super-structure, and the chromosomal base upon which the kinetochore anchors to the DNA, is termed the centromere.

Little is known about the participating components and cellular regulation involved this aspect of mitosis in trypanosomatids, beyond the observation that many of the genes encoding core mitosis proteins identified in a range of other organisms appear absent in the trypanosomatid genomes (Berriman et al., 2005). These essential proteins may either be highly divergent from their other eukaryote orthologues, or alternatively the whole process may proceed via a different mechanism requiring different protein protagonists. Any major differences between the human and trypanosomatid systems would create the potential to identify novel therapeutic targets, in an area of disease biology already established as viable for chemotherapy intervention (Weaver and Cleveland, 2005). An important first step in identifying novel or highly divergent proteins is to identify the centromeric DNA regions on the chromosomes, because the centromere lies at the heart of the chromosome segregation process of cell division. Understanding the centromere would facilitate the addressing of further important biological questions including what makes these DNA regions unique to a chromosome, and are there associated epigenetic features of a centromere in terms of constitutive chromatin structure and the components of the kinetochore?

2.1 Cell Division

Cell division is a highly dynamic aspect of cell biology as every feature of the cell must be accurately duplicated and separated into daughter cells. The faithful segregation of the genomes is no exception to this, being critical in generating viable daughter cells. Aneuploidy occurs when aberrations in the chromosome segregation mechanism leads to cells with either a fewer or greater number of chromosome homologues than normal. In developing human embryos for example, this proves almost always fatal except for certain arrangements of sex chromosomes (Kops et al., 2005), and a few rare cases such as a triploid chromosome 21, which causes Down's syndrome. In general, the approach to cell division in trypanosomatids is similar to most other eukaryotes, although there appears to be some differences in components such as for mitosis, as well as variations in the cell-cycle regulation process between the life-cycle stages (Hammarton, 2007).

2.1.1 The cell-cycle: Interphase

Of the trypanosomatids, probably *T. brucei* is the best studied in respect to the cell-cycle and so will be the reference here. The eukaryotic cell-cycle can be considered in two main stages: interphase and mitosis. These represent the period when a cell makes the preparations for cell division (interphase), and the actual process of cell division (mitosis). Interphase itself can be sub-divided into 4 phases (Figure 2.1.1): Gap 0 (G_0), Gap 1 (G_1), DNA Synthesis (S), and Gap 2 (G_2). The G_0 stage represents a resting quiescent period in the cell-cycle where the process of cell division is effectively suspended, and is reflected by specific trypanosomatid life-cycle stages such as the *T. brucei* bloodstream non-dividing stumpy forms, and the infectious metacyclic forms (Section 1.3.1) (Seed and Wenck, 2003). This relationship illustrates the complexity for trypanosomatids in co-ordinating their cell-cycle processes with the various life-cycle stages of parasitic infection. The first active period of a dividing life-cycle stage cell, such as the *T. brucei* long slender bloodstream form or procyclic form, is the G_1 phase. As for most other eukaryotes, this is the point when the cell prepares for the replication of the nuclear genome. At this time, trypanosomatids must also prepare to replicate the single concatenated network of the kinetoplast DNA. Physically associated with the trypanosome kinetoplast is the basal body of the characteristic flagellum. This cellular

component appears to be the first feature to replicate during S phase, allowing for the further development of a duplicate flagellum (McKean et al., 2003). This is soon followed by the DNA replication of a two-part trypanosome S phase, where first the kinetoplast DNA (S_K phase), and then the nuclear DNA (S_N phase), is replicated sequentially (Woodward and Gull, 1990). Microscopy of DNA stained procyclic *T. brucei* cells suggests that while the cell proceeds to replicate the nuclear DNA, the segregation of the previously duplicated kinetoplast DNA is performed (Siegel et al., 2008). Coinciding with the separation of the kinetoplast DNA, is the coupled segregation of the duplicated flagellar basal bodies (Robinson and Gull, 1991). Once this is completed and the nuclear genome has been replicated, the cell exits S phase. Now in the G_2 phase, preparations are made for mitosis, where the complex task of separating sister chromatids, that can be megabases of DNA in length, is enacted.

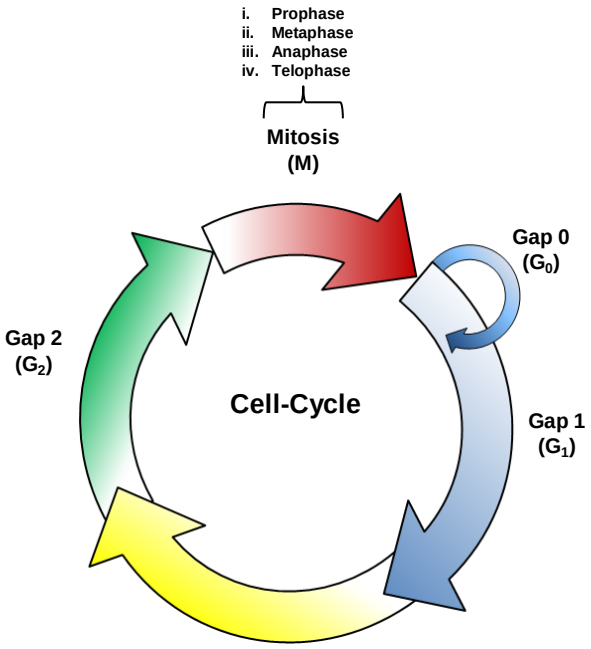

Figure 2.1.1. ***A scheme showing the basic phases of the cell-cycle.***
Eukaryotic cells may either reside in the G_0 phase, or progress through the cell-cycle: first preparing to replicate the genomes (G_1), and then duplicating the DNA (S), before preparing to segregate the DNA (G_2). Collectively these phases are referred to as interphase. Mitosis follows interphase, and can be sub-divided into four stages: prophase, metaphase, anaphase, and telophase. Once mitosis completes, the separate process of cytokinesis is performed, generating two daughter cells. Arrows are for illustration only and do not reflect the duration of individual phases.

2.1.2 The cell-cycle: Mitosis

The period of segregating the replicated chromosomes is mitosis. For general eukaryotes, this can be sub-divided into four stages: prophase, metaphase, anaphase, and telophase (Figure 2.1.1). The timings and specific processes varies between organisms, however the themes mostly remain constant, and are outlined below.

In prophase, the sister chromatids that were replicated previously in S phase remain held together by a protein complex called cohesin. The number of components varies, but at least four common core components have been identified: two Structural Maintenance of Chromosome proteins (Smc) – Smc1 and Smc3, plus Sister Chromatid Cohesion proteins (Scc) - Scc1 and Scc3 (Haering and Nasmyth, 2003). The protein complex of Smc1 and Smc3 forms a 'V' structure, and is assembled on chromatids during S phase. This binds with the Scc1 protein, forming a conjoined ring structure around both sister chromatids, binding them together (Haering et al., 2008). In yeast, this enclosing ring structure is maintained through prophase and metaphase, until the chromosomes are prepared for segregation. In vertebrates though, much of the cohesin complexes are lost during prophase (Darwiche et al., 1999), and only a concentration at the centromeres remain, along with a small amount along the chromosomal arms (Waizenegger et al., 2000). The signal that makes the vertebrate cohesin complexes of the chromosome arms dissociate is unknown, although a shugoshin protein has been shown to block the dissociation of the concentrated cohesins specifically at the centromere (LeBlanc et al., 1999; Tang et al., 2004).

Ordinarily, the characteristic feature of eukaryotic prophase is the condensing of chromosomes, where they become easily visible under the microscope. This process appears to be driven by a condensin complex containing further Smc proteins: Smc2 and Smc4, along with three other proteins: CAP-D2, CAP-G and CAP-H (Losada and Hirano, 2001). The details and the mechanism of this process remains a mystery (Hudson et al., 2009), however recently it has been shown in *Saccharomyces cerevisiae* that condensin is heavily enriched at the centromere, for as yet unknown reasons (D'Ambrosio et al., 2008). In regard to trypanosomatids, putative orthologues of the Smc1, Smc3, Scc1 and Scc3 proteins of the cohesin complex have been identified in the

T. brucei genome (Gluenz et al., 2008), along with potential orthologues for Smc2, Smc4 and CAP-D2 of the condensin complex (Hammarton, 2007). The apparent presence of components of the condensin complex in the trypanosome genome is surprising, as trypanosomatid chromosomes appear not to condense during mitosis (Galanti et al., 1998), although it is worth noting condensin complexes also appear to have roles outside of mitosis (Wood et al., 2010).

During the prophase of higher eukaryotes, the nuclear envelope breaks down, and mitosis is performed in the open (De Souza and Osmani, 2007), however for trypanosomatids and many other protists the nuclear envelope remains intact, and mitosis is performed within a closed nuclear environment (Vickerman and Preston, 1970). The assembly of the large kinetochore structures at the centromeres of the individual chromosomes is finalized during prophase, in preparation for attachment to the microtubules (Chan et al., 2005). Commonly these microtubules are propagated from two opposing microtubule organizing centres, which are part of specialized bodies dedicated for mitosis, termed centrosomes (Bornens, 2002). Normally a single constitutive centrosome, or equivalent body, is present throughout the cell-cycle, which then duplicates in S phase in readiness for mitosis (Lim et al., 2009). No centrosome or similar feature has been identified in *T. brucei*, although during mitosis it appears that microtubules are still seeded from two opposing points near the intact nuclear envelope, suggesting the existence of some form of microtubule organizing centre that can form the mitotic spindle and attach microtubules to kinetochores (Ogbadoyi et al., 2000). Another unresolved question in *T. brucei* is that so far only eight kinetochore-like plaques have been identified by using electron microscopy (Ogbadoyi et al., 2000), which doesn't correlate with the 22 megabase chromosomes of the duplicated genome that requires segregation. This however, assumes that *T. brucei* follows the classical segregation mechanism of each chromosome attaching separately to microtubules through their own kinetochore. It also raises the further question of how do the approximately 100 mini-chromosomes of *T. brucei* also become faithfully segregated, given the limited number of kinetochores (Gull et al., 1998). These issues are not restricted to *T. brucei*, as there appears to be a shortfall in the number of kinetochore-like plaques observed in *T. cruzi* and also *L. major* (Solari, 1980; Urena, 1988).

The metaphase procedure whereby microtubules propagate from centrosomes seeking out the kinetochores assembled on centromeric DNA is thought to be random (Haering and Nasmyth, 2003). For many eukaryotes, after a chromosome has been successfully connected to mitotic microtubules from both of the opposing sides of the nucleus in a bi-polar attachment, the resulting physical tension leads to the chromosome being drawn to the middle of the nucleus. As this migration is repeated across the full complement of chromosomes, they begin to line up spanning the nucleus equator (Figure 2.1.2). Cells are held in metaphase by the mitotic spindle checkpoint until all kinetochores have successfully attached to mitotic microtubules, ensuring that all sister chromatids can be faithfully segregated (Yu, 2002). It remains controversial what the actual signal is for reporting when a chromosome is correctly associated with mitotic microtubules. Whether the trigger is simply the tethering of the kinetochore to a number of microtubules, or alternatively the microtubule tension produced by pulling apart sister chromatids still bound together, is debated (Bloom and Yeh, 2010).

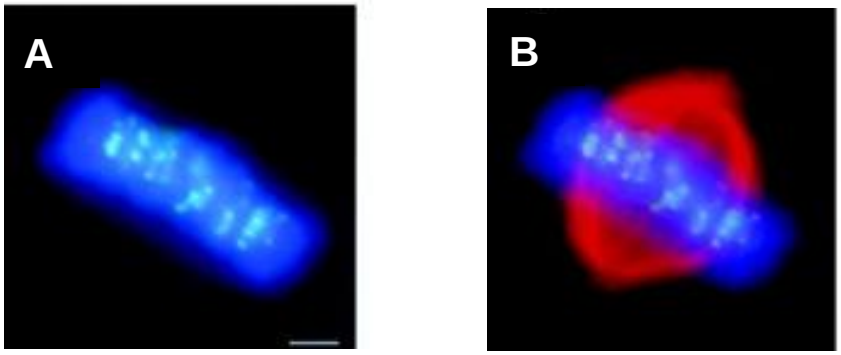

Figure 2.1.2. ***Immunofluorescence images of human chromosomes at metaphase.***
(**A**) Chromosomes of a HeLa cell stained with DAPI (blue) have condensed and aligned across the nuclear equator (Dynek and Smith, 2004). The centromeres have been labelled with a specific antibody (green). (**B**) A further antibody against α-tubulin (red) highlights the microtubules emanating from the centrosomes towards the kinetochores assembled on the centromeres. Images reproduced from Dynek and Smith, 2004.

While the sensor mechanism detecting the kinetochore attachment to microtubules remains unknown, more is known about the sophisticated signalling system. Mitotic-arrest deficient (MAD) proteins MAD1, MAD2, and MAD3, plus budding uninhibited by benzimidazole (BUB) proteins BUB1 and BUB3 were first identified in *S. cerevisiae* as key components of a complex signalling pathway that inhibits the start of the chromosome segregation process while any chromosomes remain unattached to the microtubules (Hoyt et al., 1991). These key proteins have since been identified in a range of eukaryotes and appear to localize at the kinetochore (Yu, 2002), although of these, only MAD2 has been identified so far in *T. brucei* (Berriman et al., 2005). Collectively, they represent the spindle assembly checkpoint (Figure 2.1.3). It has been observed in *S. cerevisiae* that mutating centromeric DNA leads to a delay in mitosis, which is believed to be mediated by the spindle assembly checkpoint, despite the kinetochore correctly assembling on the mutated centromere (Spencer and Hieter, 1992). Once all of the chromosomes are ready for segregation, this inhibition pathway is retracted via the spindle assembly checkpoint proteins no longer binding to another protein, CDC20 (Hwang et al., 1998). The CDC20 protein is a co-factor of the anaphase promoting complex (APC), and a wealth of research has shown that when CDC20 is freed of the spindle assembly checkpoint proteins, it no longer represses the activity of the anaphase promoting complex (reviewed in Musacchio and Salmon, 2007). As the anaphase promoting complex becomes active, it begins the process of chromosome segregation, the period of anaphase.

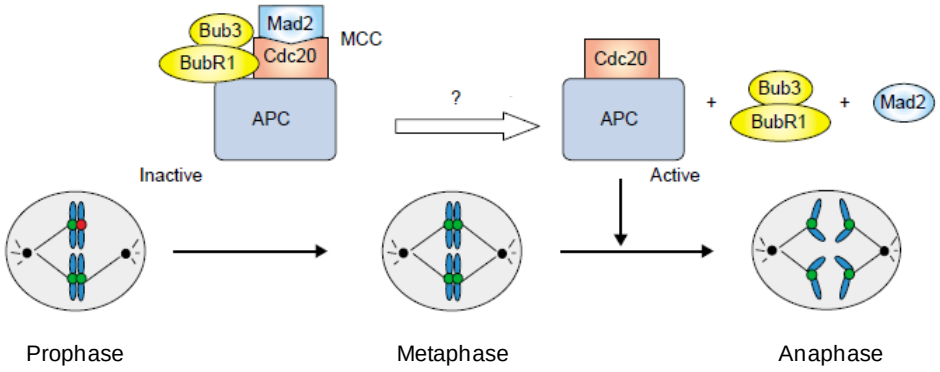

Figure 2.1.3. ***Diagram showing key protein interactions of the mitotic control checkpoint.***
During the transition from prophase to metaphase the spindle assembly checkpoint proteins MAD2, BUB3, and BubR1 (MAD3) inhibit the activation of the chromosome segregation pathway by binding the anaphase promoting complex (APC) via the protein CDC20. Once all kinetochores have attached to the mitotic microtubules at metaphase, an unknown trigger releases the spindle assembly checkpoint proteins from CDC20, which activates the APC and promotes chromosome segregation and anaphase. Diagram reproduced from Yu, 2002.

The anaphase promoting complex is an E3 ligase, part of the ubiquitination system (King et al., 1995; Sudakin et al., 1995). It ubiquitinates a range of mitosis related proteins, targeting them for proteasome mediated degradation (Peters, 1999). One important protein is securin (Funabiki et al., 1996; Yamamoto et al., 1996), which acts as an inhibitory chaperone of the protein separase (Ciosk et al., 1998). Upon the degradation of securin, separase is free to sever the cohesin ring complex through cleavage of the Scc1 sub-unit (Uhlmann et al., 1999). In yeast, this frees both the chromosome arms and centromeres of their restrictive ties, while in vertebrates the remaining cohesin still located at the centromeres is finally removed. For all studied eukaryotes this separase activity triggers the segregation of the nuclear chromosomes, anaphase.

Last in mitosis is telophase, during which the kinetochores disassemble as the cell tidies up from the segregation process. In organisms where chromosomes have condensed during prophase, these now de-condense, and for organisms that perform an open

mitosis, new nuclear envelopes are constructed around the two daughter nuclei (Walczak et al., 2010).

Cytokinesis, or mitotic exit, represents the final stage of the cell-cycle, and is a separate process from mitosis, involving the cell physically splitting into two daughter cells. While many genes involved in the exit from mitosis have been identified in model organisms, it has proved difficult to unravel the complex and often overlapping signalling systems (Bosl and Li, 2005). Even less is known in trypanosomes, where many potential candidates have been identified, but little experimental research has been performed (Hammarton, 2007). The various life-cycle stages of trypanosomes look set to complicate matters further, as it has been shown that a mitotic exit checkpoint present in the bloodstream form *T. brucei* appears absent in the procyclic form (Hammarton et al., 2003).

2.2 Centromere structure

2.2.1 Centromeric DNA

As described previously, the centromere has a vital role in segregating the nuclear chromosomes, in both providing the kinetochore assembly site facilitating the tethering to mitotic microtubules, and binding sister chromatids together until the cell is ready for anaphase. Despite the conservation of the basic mechanism of mitosis in eukaryotes, the composition of centromeric DNA in both length and sequence varies considerably.

The first centromere to be identified was in the budding yeast *S. cerevisiae* (Clarke and Carbon, 1980), and was shown to consist of a minimal 'point' entity of only 125 bp of DNA, which was conserved across chromosomes (Cottarel et al., 1989). This small centromeric region is comprised of three conserved DNA elements: CDEI (14 bp), CDEII (~90 bp), and CDEIII (11 bp), notably with the DNA of element CDEII being 90% AT-rich (Figure 2.2.1) (Fitzgerald-Hayes et al., 1982). Even at this early stage, experiments had shown that simply inserting this DNA sequence on a foreign piece of DNA was insufficient to generate an effective budding yeast centromere, suggesting a

role for chromatin in establishing a centromere, and the potential for epigenetic inheritance of centromeres (Bloom and Carbon, 1982).

The 'point' centromere of *S. cerevisiae* is far from mainstream, for instance the fission yeast *Schizosaccharomyces pombe* possesses a much larger, regional centromere spanning 40-100 kb in length (Chikashige et al., 1989; Fishel et al., 1988). At the centre of these centromeres is a non-repetitive 4-7 kb central core region, flanked by innermost repeats, and then outermost repeats (Figure 2.2.1). The central core region is not identical between chromosomes, but does share a high level of homology, with approximately a 70% AT codon bias (Wood et al., 2002). The innermost repeat region consists of divergent inverted repeat sequences, while the outermost repeats actually contain 3 separate types of repeat sequences. Different protein compositions were observed at the central core and innermost repeat region, compared with the outermost repeats (Partridge et al., 2000), for example the histone H3 variant, CENP-A was only found at the central core (Kniola et al., 2001), which is suggestive of multiple functional chromatin domains in the region. In *S. pombe* a centromeric enhancer DNA sequence, dispensable for native chromosomes, is required to establish a new centromere on artificial chromosomes (Marschall and Clarke, 1995). Further, as two completely different DNA sequences derived from centromeres have been used in conjunction with this enhancer to generate a new active fission yeast centromere on an artificial chromosome (Ngan and Clarke, 1997), it seems that specific DNA sequence does not define a fission yeast centromere. Instead it is suggested that only certain classes of DNA elements are required to form an active centromere, and once established the epigenetic features of an active centromere are inherited (Ngan and Clarke, 1997).

Much larger regional centromeres than those of *S. pombe* were later found in *Drosophila melanogaster*. Here, the central centromeric core occurs in a region spanning 200 kb, flanked either side by a further 200 kb of repeat sequence (Figure 2.2.1) (Murphy and Karpen, 1995). Unlike the model yeast systems, the *Drosophila* centromeric region is contained within heterochromatin blocks. The flanking satellite repeats consist of only two types of 5 bp repeat sequence (Sun et al., 1997), which are heavily AT codon biased (AATAT & TTCTC). These satellite repeats are not unique to the centromeric regions,

suggesting they do not represent a centromere in themselves (Sun et al., 2003). At the centromere the 200 kb central core features multiple intact retrotransposons, interspersed with the AATAT satellite repeat, plus a single 16.2 kb island containing a single AT-rich sequence. This single sequence is not identical between centromeres of different chromosomes (Sun et al., 2003), fuelling the notion that DNA sequence itself does not define a centromere. The idea of epigenetic marking of centromeres is further supported in *Drosophila* where experiments showed that by first inserting a non-centromeric test DNA sequence next to an existing centromere, then liberating the new test sequence by irradiation, a viable centromere on the test sequence was could be generated (Maggert and Karpen, 2001). The observation supported the concept of a protein based centromeric defining marker spreading to neighbouring DNA regions to establish a neocentromere.

Human centromeric regions are larger still, spanning megabases of heterochromatin along a chromosome (Figure 2.2.1). They are made predominantly of 171 bp uniformly directed α-satellite repeats (Heller et al., 1996), which are approxiamtely 70% rich in AT content (Koch et al., 1989), and interspersed with retroelements (Schueler et al., 2001). Since human centromeres span such large distances it has proved difficult to fully sequence these regions, meaning that it is possible that any small unique centromeric sequences could be easily missed (Murphy and Karpen, 1998). These α-satellite repeats are also not required for an active centromere, as neocentromers formed in alterative euchromatic regions of human chromosomes do not contain these sequences (Voullaire et al., 1993), again suggesting a role for epigenetic marking of centromeres. Plant centromeres also contain this satellite DNA, for example *Arabidopsis thaliana* centromeres contain a 180 bp satellite repeat, unrelated to the human sequence, but which is arranged in a similar fashion including the presence of intact retroelements (Copenhaver et al., 1999). These repeat regions range from around 1.4 to 4.4 Mb in size (Haupt et al., 2001), but unlike the human repeats, the AT/GC codon bias of the *Arabidopsis* centromeric repeats remains consistent with the genome average (~64% AT) (Copenhaver et al., 1999). The centromeres of rice chromosomes are again composed of retroelements and satellite repeats, this time of 155 bp units spanning between 65 kb to 2 Mb (Cheng et al., 2002).

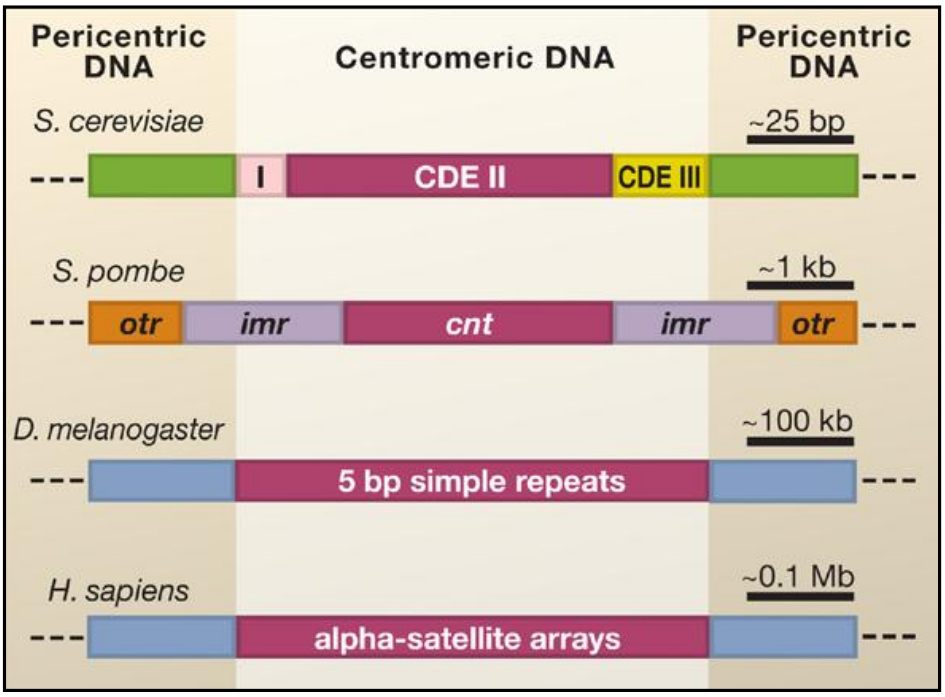

Figure 2.2.1. ***Structure of eukaryotic centromeres.***
The 'point' centromere of *S. cerevisiae* spans 125 bp and consists of 3 conserved DNA elements (CDE) that are identical between all chromosomes (Clarke and Carbon, 1980; Cottarel et al., 1989). The small regional centromere of *S. pombe* contains a non-repetitive 4-7 kb central core region (cnt), flanked by innermost repeats (imr), and outermost repeats (otr). Unlike *S. cerevisiae* the central core of *S. pombe* is not conserved in sequence between chromosomes (Chikashige et al., 1989; Fishel et al., 1988). *Drosophila* centromeres span much larger regions, and contain small satellite repeat sequences with a central core containing retroelements and a unique AT-rich sequence 'island'(Murphy and Karpen, 1995; Sun et al., 2003). The human centromere spans megabases of 171 bp α-satellite repeats, interspersed with retroelements (Heller et al., 1996; Schueler et al., 2001). Figure reproduced from Morris and Moazed, 2007.

Although the mainstream centromere of fission yeast, metazoans and plants appear to be single regional centromeres of various lengths and compositions, the point centromere of *S. cerevisiae* is not alone in being unusual. The site of kinetochore assembly of the worm, *Caenorhabditis elegans*, is not a single centromere entity, as for all the previously described organisms, but instead is a series of centromeres that extend the full length of the chromosomes (Albertson and Thomson, 1982). Each centromere contains a fully functional kinetochore capable of attaching to mitotic microtubules and facilitating chromosome segregation (Oegema et al., 2001). Given the potential for the

introduction of neocentromeres in some of the previously discussed organisms containing the more common regional centromeres, the holocentric nature of *C. elegans* raises the question of how only one functional regional centromere can be actively maintained on these chromosomes at a time?

2.2.2 Centromeric proteins

Since there seems no consensus DNA sequence that constitutes a centromere between organisms, or indeed a conserved centromeric DNA sequence between chromosomes of a single organism, the evidence supports a significant role for epigenetics. Although the typical kinetochore consists of over 80 proteins, most of these are transiently assembled at the centromere during mitosis (Cheeseman and Desai, 2008). The known major constitutive protein elements are the DNA binding proteins CENP-A, CENP-B, and CENP-C (the antigens of the ACA antibody in Figure 2.1.2), although the levels of CENP-B and CENP-C fluctuate during the cell-cycle (Hemmerich et al., 2008). Therefore the prime candidate for epigenetically establishing centromeres is the histone H3 variant, CENP-A. This was first identified in humans, where it shares approximately 60% sequence identity to that of the standard histone H3 at the C-terminal end (Palmer et al., 1987). The centromere specific CENP-A histone variant has now been found in almost all other studied eukaryotes including: *S. cerevisiae* (Meluh et al., 1998), *S. pombe* (Takahashi et al., 2000), *Drosophila* (Henikoff et al., 2000), *C. elegans* (Buchwitz et al., 1999), and *Arabidopsis* (Talbert et al., 2002), making it widely accepted as the key constituent of the centromere (Mellone et al., 2009). Further evidence for CENP-A regulating the centromere came from experiments analyzing neocentromeres on human chromosomes. These showed that only the new active centromere contained CENP-A, while the old inactive α-satellite repeat region now lacked CENP-A (Warburton et al., 1997). It is a surprise then, that a CENP-A orthologue has not yet been found in trypanosomatids (Berriman et al., 2005). Another constitutive candidate for regulating a centromere is the DNA binding protein, CENP-B, which was first identified as binding to short sequences of α-satellite repeats (Masumoto et al., 1989). CENP-B forms a complex with CENP-A and CENP-C, and also proteins of the inner kinetochore, suggesting that CENP-B has a role in connecting the kinetochore assembly to the centromere (Ando et al., 2002). While putative orthologues

of CENP-B have been identified in most model eukaryotes (Chan et al., 2005), it is not essential in establishing the kinetochore (Hudson et al., 1998), and is also not found at neocentromeres (Choo, 2001). As for CENP-A, no potential orthologues have been identified in trypanosomatids (Berriman et al., 2005). In fact this pattern continues, with the DNA binding protein CENP-C (Sugimoto et al., 1994) also apparently absent from the trypanosomatid genome.

With no obvious DNA sequence that defines a eukaryotic centromere in trypanosomatids, and the absence of any constituent centromeric proteins, locating the centromeric loci on chromosomes is not straightforward. Even many transient kinetochore proteins have yet to be identified in trypanosomatids, making the eventual task of discovering novel or divergent proteins involved in mitosis challenging but full of potential. These missing key proteins include the microtubule motor protein of the kinetochore CENP-E (Wood et al., 1997), the kinetochore matrix protein CENP-F (Liao et al., 1995), the Mis12 protein of the inner kinetochore (Takahashi et al., 1994), and the kinetochore-microtubule linker complex Ndc80 (McCleland et al., 2004). However, an enzyme that is present in the nucleus of trypanosomatids (Fragoso et al., 1998) and has been shown to locate to centromeres of mammalian cells (Rattner et al., 1996) is the DNA topological manipulation enzyme, topoisomerase-II.

2.3 Topoisomerase-II

Topoisomerases are enzymes that cut and anneal DNA strands to regulate the topological properties of DNA during transcription and replication such as DNA super-coiling and tangles. They can be separated into two types: topoisomerase-I enzymes cut only a single strand of DNA to aid the relaxation of super-coiled DNA by passing the intact strand through the gap in the cleaved strand and then re-sealing the single stranded break; topoisomerase-II cleaves both DNA strands allowing the passage of an intact DNA duplex through the gap, which is then re-annealed after the passage of the α-helix. Topoisomerase-II can either pass through a DNA duplex that is part of the same DNA molecule that has been cut by the enzyme to untangle a knot, or the cleaved DNA

duplex may be decatenated from a separate DNA molecule, such as sister chromatids following DNA replication.

The first topoisomerase-II (DNA gyrase) was discovered in bacteria where it was shown to be ATP and magnesium dependent (Gellert et al., 1976). Later in *Xenopus laevis* the first eukaryotic topoisomerase-II was identified, sharing the same dependencies as its bacterial counterpart (Baldi et al., 1980). The bacterial DNA gyrase was shown to stay covalently bound to the cleaved DNA molecule through 2 phosphodiester bonds located 4 bp apart on opposing strands (Morrison and Cozzarelli, 1979). This behaviour was found to be conserved in eukaryotic topoisomerase-II (Liu et al., 1983; Sander and Hsieh, 1983), with the interaction shown to be mediated via an N-terminal catalytic tyrosine residue (Horowitz and Wang, 1987). Based on a large body of biochemical data, a central mechanism of topoisomerase-II decatenation has been proposed. It begins with topoisomerase-II dimerizing, followed by the binding and cleavage of the first DNA molecule by the paired tyrosine residues of the dimerized N-terminal catalytic domains. Then the central ATPase domain of topoisomerase-II controls the passage of the second DNA molecule through the double stranded DNA break in an ATP dependent gate-regulated manner, before the double stranded DNA break is then re-ligated (Champoux, 2001). The C-terminus of topoisomerase-II appears unnecessary for enzyme activity, as deletions up to around 240 amino acids from the C-terminal end resulted in no loss of *in vitro* activity in *Drosophila* (Crenshaw and Hsieh, 1993) and budding yeast (Caron et al., 1994).

The lack of any obvious functional role for the C-terminus of topoisomerase-II has lead to much speculation that it may instead be involved in regulation of the enzyme. In *S. cerevisiae* topoisomerase-II is phosphorylated by casein kinase II *in vivo* at the C-terminus (Cardenas et al., 1992). A later study in *S. cerevisiae* using affinity purification techniques has showed that casein kinase II is stably associated with topoisomerase-II even after phosphorylation, and that topoisomerase-II becomes more active following its phosphorylation (Bojanowski et al., 1993). Human topoisomerase-II has also been shown to be phosphorylated at the C-terminus by casein kinase II (Daum and Gorbsky, 1998), as well as casein kinase I δ/ε (Grozav et al., 2009). The phosphorylation of

topoisomerase-II also appears to be cell-cycle dependent and up-regulated during G_2 phase and mitosis (Escargueil et al., 2000; Wells and Hickson, 1995), potentially because at this stage in the cell-cycle, chromosomes have now been replicated and therefore may require decatenation before the beginning of the segregation process. In fact phosphorylation of topoisomerase-II by polo-like kinase 1 has been shown to be essential for sister chromatid segregation (Li et al., 2008).

Topoisomerase-II has been shown to specifically accumulate at conventional centromeres and at neocentromeres during mitosis (Rattner et al., 1996; Saffery et al., 2000), suggesting its recruitment to the centromere may not be DNA sequence based. This is supported by the finding that on human chromosomes with multiple centromeres, only the single active centromere contains topoisomerase-II (Andersen et al., 2002). With an artificial chromosome, centromere adjacent truncations which introduces a neighbouring telomere, also shifts cleavage loci of topoisomerase-II at the centromere, again suggesting an epigenetic guidance of topoisomerase-II activity (Spence et al., 2002). This domain of topoisomerase-II activity also coincided with the presence of the centromeric proteins CENP-A, and CENP-C. It also seems that topoisomerase-II activity specifically at the centromere is important for mitosis, however not essential, as segregation of a small human artificial chromosome is perturbed by depletion of topoisomerase-II (Spence et al., 2007). Separation of *Drosophila* centromeres at anaphase is also inhibited by the depletion of topoisomerase-II, further supporting this observation (Coelho et al., 2008). It appears in human cells that centromeres are held together at anaphase by not only the cohesin ring complex, but also catenated DNA fibres that persist after the anaphase promoting complex mediated activity of separase, and which require the activity of topoisomerase-II to untangle (Baumann et al., 2007; Wang et al., 2008).

There is now increasing evidence that topoisomerase-II localization at the centromere is controlled by the small ubiquitin-like modifier protein (SUMO). The SUMO protein conjugates to a target protein in a similar fashion to ubiquitin, through an E3 ligase pathway. In *S. cerevisiae* there is evidence that SUMOylation of topoisomerase-II coincides with the cohesion between sister chromatid centromeres and chromosome

segregation defects (Bachant et al., 2002). Experiments in *Xenopus* suggest that SUMO conjugation of topoisomerase-II is responsible for the localization to the centromere during mitosis (Azuma et al., 2005), with a similar observation made in human cells (Dawlaty et al., 2008). Intriguingly, in procyclic *T. brucei* cells, SUMO deficiency leads to cell-cycle arrest between G_2/Mitosis. Therefore potentially, topoisomerase-II and SUMO may play an important role during chromosome segregation and centromeric specific activity in trypanosomatids.

2.3.1 Biochemical mapping of centromeres with topoisomerase-II

The anti-cancer drug etoposide was first licensed in the mid 1980s and targets topoisomerase-II. It has been used to treat Hodgkin's disease, non-Hodgkin's lymphoma, lung cancer, gastric cancer, breast cancer and ovarian cancer (Hande, 1998). It was shown to act as a poison by inhibiting only the DNA re-ligation step, once the DNA had been enzymatically cleaved, thus trapping the topoisomerase-II complex and generating permanent lesions in chromosomes (Chen et al., 1984). In etoposide treated mice, these DNA lesions were found concentrated in centromeric regions of chromosomes (Kallio and Lahdetie, 1996), which correlates with what is known about topoisomerase-II accumulation at centromeres. Following this observation, an experiment was performed in *Drosophila* where flies were treated with a topoisomerase-II poison (VM-26), and then their genomic DNA was isolated and separated by pulsed field gel electrophoresis. By resolving the DNA lesion fragment sizes, the positions of the lesions were found to localize towards centromeric regions, similar to the experiments in mice, and hence topoisomerase-II poisoning was proposed as a method for mapping centromeric chromatin regions on chromosomes (Borgnetto et al., 1999). This technique was first implemented to map the centromeric region of the human Y chromosome (Floridia et al., 2000) to the α-satellite repeats, then the X chromosome (Spence et al., 2002) and later chromosome 11 (Spence et al., 2005). It has since been used to map the centromeres on the malaria parasite *Plasmodium falciparum* (Kelly et al., 2006).

2.4 Research Objectives

The aim of investigating the nature and location of centromeres on trypanosomatid chromosomes can be defined by the following core objectives:

- To biochemically map the centromeric locations of *T. brucei* megabase chromosomes using topoisomerase-II and etoposide mediated DNA cleavage.
- To identify any signature DNA sequences or features indicative on a centromere between *T. brucei* chromosomes.
- To extend the biochemical mapping technique to investigate the activity on the *T. brucei* mini-chromosomes.
- To apply the biochemical mapping technique to *L. major* chromosomes.
- To investigate potential centromeric specific activity of topoisomerase-II in bloodstream form *T. brucei*.

3 Materials and Methods

3.1 Cell Culturing and Storage

3.1.1 Bacterial strains

The *E. coli* strains used in this project were DH5α (φ80d*lacZ*ΔM15, *recA*1, *endA*1, *gyr*AB, *thi*-1, *hsdR*17(r_K-, m_K+), *supE*44, *relA*1, *deo*R, Δ(*lacZYA-arg*F) U169, *pho*A), XL1-Blue (*rec*A1, *end*A1, *gyr*A96, *thi*-1, *hsd*R17(r_K-, m_K+), *sup*E44, *rel*A1, *lac*, [F', *proAB*, *lac*I^qZΔM15::Tn10(tet^r)]) and SCS110 (*rpsL* (Strr) *thr leu endA thi-1 lacY galK galT ara tonA tsx dam dcm supE44* Δ(*lac-proAB*) [F´ *traD36 proAB lacI*qZΔ*M15*]). They were grown in NZCYM broth (10 g l^{-1} enzymatic casein digest, 1 g l^{-1} Casamino acids, 5 g l^{-1} yeast extract, 5 g l^{-1} NaCl, 0.98 g l^{-1} $MgSO_4$: Sigma) or on plates supplemented with 1.5% (w/v) agar (Sigma), containing 50 µg ml^{-1} ampicillin, where appropriate.

3.1.2 Mammalian cells

African Green Monkey Kidney epithelial (Vero C1008) cells (ATCC CRL-1586) were cultured in RPMI-1640 medium (Sigma) supplemented with 5 g l^{-1} HEPES (4-(2-hydroxyethyl)-1-piperazineethanesulfonic acid), 0.34 g l^{-1} sodium glutamate, 0.22 g l^{-1} sodium pyruvate, 2500 U l^{-1} penicillin, 0.25 g l^{-1} streptomycin and 10% (v/v) foetal calf serum at 37°C with 5% CO_2. To passage cells, the existing growth medium was removed and replaced with 10 ml UV-irradiated trypsin containing EDTA (PAA). After 2 minutes at room temperature, the trypsin was removed, and the cells were incubated at 37°C for a further 10 minutes, with gentle agitation. Detached cells were collected in fresh medium and transferred to a new flask containing fresh medium. Cultures were passaged once every 3-4 days, with a single Vero cell line maintained in culture for no longer than 6 months. Fresh medium was prepared at least once a month.

The foetal calf serum used in all eukaryotic culturing was designated as tetracycline free by the manufacturer (Autogen Bioclear) and was heat treated (55^{o}C for 30 min) to inactivate components of the complement cascade prior to use.

3.1.3 *Trypanosoma brucei*

The procyclic form (PCF) of *T. brucei* TREU 927/4 was cultured in SDM-79 medium (Invitrogen) supplemented with 7.5 mg l^{-1} haemin and 10% (v/v) tetracycline-free foetal calf serum at 27°C (Brun and Schonenberger, 1979). In topoisomerase-II mediated DNA cleavage studies, *T. brucei* PCF cells (2 x 10^6 cells ml^{-1}) in the logarithmic phase of growth were treated with 500 µM etoposide (Sigma) dissolved in dimethyl sulfoxide (DMSO) for 1 hour.

The bloodstream form (BSF) of *T. brucei* Lister 427 MITat 1.2 clone 221a was grown in HMI-9 (Invitrogen) supplemented with 3 g l^{-1} sodium bicarbonate, 0.014% (v/v) β-mercaptoethanol and 10% (v/v) foetal calf serum at 37°C with 5% CO_2 (Hirumi and Hirumi, 1989). A derivative of this cell line (designated 2T1/TAG^{PURO}), that constitutively express the tetracycline repressor protein, was maintained in the above medium supplemented with 2 µg ml^{-1} phleomycin (Alsford and Horn, 2008). De-repression of the tagged locus via removal of the DNA bound tetracycline repressor protein was initiated with 1 µg ml^{-1} tetracycline. In topoisomerase-II mediated DNA cleavage studies, *T. brucei* BSF cells (2 x 10^6 cells ml^{-1}) in the logarithmic phase of growth were treated with 100 µM etoposide for 30 minutes.

3.1.4 *Trypanosoma cruzi*

All *T. cruzi* epimastigote cell-lines were cultured in RPMI-1640 medium (Sigma) supplemented with 5 g l^{-1} trypticase, 5 g l^{-1} HEPES pH 8.0, 20 mg l^{-1} haemin, 0.34 g l^{-1} sodium glutamate, 0.22 g l^{-1} sodium pyruvate, 2500 U l^{-1} penicillin, 0.25 g l^{-1} streptomycin and 10% (v/v) tetracycline-free foetal calf serum at 27°C (Kendall et al., 1990).

The amastigote form of *T. cruzi* (clones MHOM/BR/78/Sylvio-X10-6 and CL Brener) were cultured as follows. *T. cruzi* epimastigote cultures (1 ml) in the stationary phase of growth (8-10 day old cultures) were transferred to a freshly passaged Vero culture and allowed to infect the mammalian cells overnight at 37°C under a 5% CO_2 atmosphere. The following day, free parasites were removed by extensively washing the monolayer with fresh Vero cell growth medium. The infected Vero culture was maintained at 37°C

under a 5% CO_2 atmosphere, and every 4 days the growth medium changed. Ten to 14 days after the initial infection, bloodstream trypomastigotes were microscopically observed. These were collected and used to infect fresh Vero cell monolayers to propagate the infection. Amastigote cells were maintained in culture for no longer than 3 months before being discarded.

3.1.5 *Leishmania major*

The promastigote form of *L. major* MHOM/IL/80/Friedlin was cultured in SDM-79 medium supplemented with 3 g l^{-1} sodium bicarbonate, 7.5 mg l^{-1} haemin and 10% (v/v) foetal calf serum at 27°C.

3.1.6 Cell storage

For long term storage, bacterial strains and trypanosomatid lines were deposited as frozen stocks in liquid nitrogen (parasite lines) or at -80^{o}C (prokaryotic strains) in fresh growth medium containing 20% (v/v) glycerol. For BSF *T. brucei* each 1 ml stock contained approximately 1 x 10^6 parasites whereas for *T. cruzi* epimastigotes, *L. major* promastigotes and *T. brucei* PCF approximately 1 x 10^7 cells ml^{-1} were used. Bacterial strains were frozen directly at -80^{o}C in 1.2 ml cryogenic vials (Nunc). Trypanosomatid lines, in 1.2 ml cryogenic vials (Nunc), were frozen slowly (1-2 days) to -80^{o}C using a Cryo 1°C Freezing Container (Nalgene) containing isopropanol, then transferred to liquid nitrogen for long-term storage. Mammalian (Vero) cells were frozen in fresh growth medium containing 20% (v/v) DMSO at a density of 1 x 10^5 cells ml^{-1}. Frozen stocks were generated as described for trypanosomatid lines using the Cryo 1°C Freezing Container (Nalgene).

Eukaryotic cell lines were revived by quickly thawing the contents of the frozen vial. Thawed cells were washed in 10 ml of appropriate medium, pelleted by centrifugation for 5 minutes (parasites: 1640 g, Vero cells: 400 g), and the medium removed. Cells were then re-suspended in fresh medium as per normal culturing.

3.2 Nucleic Acid Extraction

3.2.1 Plasmid DNA

A tube of NZCYM (5 ml) containing 50 µg ml^{-1} ampicillin was inoculated with the desired *E. coli* strain and incubated overnight at 37^{o}C with vigorous aeration. Plasmid DNA was then extracted from the culture using an *Accu*Prep® Plasmid Mini extraction kit (Bioneer), in accordance to manufacturer's instructions. The basis of this approach involves the alkali lysis of the bacteria followed by neutralisation of the extract. Chromosomal DNA and cell debris was then removed following centrifugation and the cleared lysate is applied to a DNA binding column. Under the salt concentrations derived from the neutralisation buffer, any DNA molecules bind to the silica membrane within the column. Salts and precipitates were then removed by a series of centrifugation and ethanol-based wash steps, before eluting DNA from the column into a low salt buffer such as TE (10 mM Tris-HCl, 1 mM EDTA). Plasmid samples were then stored at -20°C.

3.2.2 Parasite genomic DNA

Parasites (5 x 10^{7}) in the logarithmic phase of growth were pelleted by centrifugation at 1640 g for 10 minutes at room temperature, washed in PBS (137 mM NaCl, 2.7 mM KCl, 10 mM Na_2HPO_4, 1.76 mM KH_2PO_4, pH 7.6), then harvested. The cell pellet was re-suspended in 2 ml lysis buffer (10 mM Tris-HCl pH 8.0, 1 mM EDTA, 100 mM NaCl, 1% (w/v) sodium dodecyl sulphate (SDS) containing 100 µg ml-1 proteinase K) and incubated at 37°C overnight. The lysis solution was then gently mixed with an equal volume of phenol. The aqueous/organic phases were partitioned by centrifugation at 3555 g for 10 minutes and the aqueous phase collected. This was then mixed with an equal volume of phenol/chloroform (1:1), partitioned as described above and the aqueous phase retained. If required, the phenol/chloroform step was repeated. The DNA containing aqueous phase was finally transferred to a fresh tube and the nucleic acid precipitated using an equal volume of isopropanol. The resultant fibrous material was collected, transferred to a fresh 1.5 ml centrifuge tube and briefly dried under vacuum. The nucleic acid was re-suspended in TE buffer containing RNase A (Sigma), added to

a final concentration of 1 µg ml^{-1}, and incubated for 1 hour at 37°C. Samples were stored at 4°C.

3.2.3 Intact trypanosomatid chromosomes

Parasites in the logarithmic phase of growth were pelleted by centrifugation at 1640 g for 10 minutes at room temperature, washed in PBS, and the cells harvested. The pellet was re-suspended at a density of 2 x 10^7 cells ml^{-1} in 1.4% Low Melting Point Agarose (BioRad) in PBS held at 42°C, and dispensed into a mould (BioRad)**: t**he cell density used equated to 5 x 10^7 parasites per agarose block. The agarose was allowed to solidify for 30 minutes on ice, before transferring the blocks to digestion buffer (3% sarkosyl, 0.5 M EDTA) supplemented with 100 µg ml^{-1} proteinase K (Van der Ploeg et al., 1984). Samples were then incubated at 56°C for 24 hours.

3.2.4 Total RNA extraction

Parasites (2 x 10^8) in the logarithmic phase of growth were pelleted by centrifugation at 1640 g for 10 minutes at room temperature and washed in PBS. The cells were harvested and RNA from the pellet extracted using the RNeasy kit (Qiagen), in accordance to manufacturer's instructions. Briefly, cells were lysed by re-suspension of the pellet in an RNA stabilization solution containing guanidine-thiocyanate: this inactivates endogenous RNases. The extract was then homogenized through a QIAshredder column (Qiagen), shearing the parasite genomic DNA. Ethanol was then added to the resultant, homogenised lysate and the material added to an RNeasy spin column: addition of ethanol promotes selective binding of RNA to a silica membrane within the centrifuge column. Following centrifugation, any contaminating residual genomic DNA was degraded using an RNAase-free DNase kit (Qiagen), applied directly to the silica membrane. Residual salts and precipitates were then removed by a series of centrifugation and ethanol-based wash steps, before eluting RNA off the column into RNase-free water. Samples were then stored at -20°C.

3.3 Restriction Endonuclease analysis

3.3.1 Restriction of DNA in solution

A typical restriction digestion was set up as follows. In a total volume of 50 µl, the DNA (5 µl) sample was mixed with x10 restriction buffer (5 µl), appropriate for the particular enzyme under study, and sterile distilled water (39 µl). Restriction enzyme (1 µl: 10-20 units, Table 3.3.1) was added and the tube contents consolidated by centrifugation. The tube was then placed at an appropriate incubation temperature, generally 37°C, for 2 hours. The reaction was halted by addition of a 1/10th volume (5 µl) of loading dye (10 mM Tris-HCl pH 7.6, 0.03% bromophenol blue, 0.03% xylene cyanol FF, 60% glycerol, 60 mM EDTA) to the mixture.

Enzyme	Sequence
*Age*I	A^CCGGT
*Apa*I	GGGCC^C
*Asc*I	GG^CGCGCC
*Bam*HI	G^GATCC
*Eco*RI	G^AATTC
*Hin*dIII	A^AGCTT
*Kpn*I	GGTAC^C
*Nco*I	C^CATGG
*Not*I	GC^GGCCGC
*Nru*I	TCG^CGA
*Sbf*I	CCTGCA^GG
*Stu*I	AGG^CCT
*Xba*I	T^CTAGA
*Xho*I	C^TCGAG
*Xma*I	C^CCGGG

Table 3.3.1. ***The restriction endonucleases and associated recognition sites.***
The ^ symbol corresponds to the specific site of DNA cleavage of the single strand shown. This site occurs in the same position of the palendromic sequence in the complementary strand.

3.3.2 Restriction of DNA in agarose embedded chromosomes

For the *in-situ* restriction digest of intact chromosomes, the agarose blocks were washed 3 times in 10 ml TE buffer containing 1 mM PMSF (phenylmethanesulphonylfluoride) at 25°C for 1 hour. Restriction digests on the entire block were performed overnight at a temperature appropriate for particular enzyme using excess enzyme (100-200 units) in 500 µl of appropriate 1x restriction buffer. Prior to analysis, the blocks were cooled on ice.

3.4 Nucleic acids separation

3.4.1 DNA by conventional gel electrophoresis

Conventional agarose gel electrophoresis was used to fractionate DNA molecules in the size range of 200 bp to 10 kbp. The agarose concentration, voltage and run times were altered to optimise separation in the desired range. A standard agarose gel was made by dissolving an appropriate amount of molecular grade agarose (Bioline) in 1x TAE buffer (40 mM Tris base, 40 mM acetic acid, 1 mM EDTA) containing ethidium bromide (0.1 mg l^{-1}). Generally, an agarose concentration of 0.6-1.0% (w/v) was used. Following casting, the solidified gel was placed in electrophoresis buffer (1x TAE containing ethidium bromide), samples loaded into the wells, including a GeneRuler™ 1 kb DNA ladder marker (Fermentas), and a constant voltage then applied across the gel for varying time periods. Generally, a run time of 1-2 hours was employed when using a constant voltage of between 3-5 V cm^{-1}. Migration of the sample through the agarose matrix was followed by monitoring the bromophenol blue/xylene cyanol dye fronts. When the DNA had migrated the desired distance, the gel was analysed on a UV transilluminator and documented (Syngene).

3.4.2 Contour clamped homogeneous electric field electrophoresis

Contour Clamped Homogeneous Electric Field Electrophoresis (CHEFE) was used to separate DNA molecules greater than 10 kb, with the CHEF Mapper II System (BioRad). The agarose concentration, voltage, electric field switching time, angle of the electric field, the run times, electrophoresis buffer and its temperature can all be altered

to optimise separation in the desired range. Agarose gels were prepared by dissolving an appropriate amount of High-Strength Megabase Agarose (BioRad) in 0.5x TBE (45 mM Tris-HCl, 45 mM boric acid, 1 mM EDTA). Following casting, DNA-containing agarose blocks were loaded into the wells of the gel and fixed into position using residual low melting point agarose. When solidified, the gel was placed in the electrophoresis chamber of the CHEF Mapper II and submerged in 2 l of 0.5x TBE, pre-cooled to the desired temperature.

To separate DNA molecules between 0.2–2.0 Mb (megabase chromosomes), a 0.8% strength gel was made with 0.5x TBE and electrophoresis carried out using a 0.5x TBE buffer maintained at 18°C. The CHEF Mapper II was programmed to give a linear pulse ramp from 90-300 s over a 36 hour time period using a constant voltage of 2.9 V cm^{-1}, followed by a second linear pulse ramp from 300-720 s over a 36 hour time period using a constant voltage of 2.6 V cm^{-1}. The angle between the 2 electric field, the switch angle, was set at 120° (-60° to + 60°) throughout the entire run. Samples were run along with *S. cerevisae* chromosomes (0.2–2.2 Mb) (Biorad).

To separate DNA molecules between 20 kb–1.6 Mb (intermediate and mini-chromosomes), a 1% strength gel was made with 0.5x TBE and electrophoresis carried out using a 0.5x TBE buffer maintained at 14°C. The CHEF Mapper II was programmed to give a linear pulse ramp from 3-136 s over a 27 hour time period using a constant voltage of 6 V cm^{-1} and a 120° switch angle. Phage lambda DNA concatemers (0.05–1.0 Mb) (Biorad) were used as DNA markers.

Restriction digested chromosomes were separated between 10 and 250 kb by an automated programmed size separation. This used the automated Field Inversion Gel Electrophoresis (FIGE) mode of the CHEF Mapper II system, with a 1% gel with running temperature maintained at 14°C. A constant forward voltage of 6 V cm^{-1} was programmed for 20 hours 18 minutes. Markers were 8.3–48.5 kb mixed digests of phage lambda DNA (Biorad).

Following electrophoresis, the gels were stained for 30 minutes in electrophoresis buffer containing ethidium bromide (1 mg l^{-1}), then de-stained in electrophoresis buffer for 45 minutes. Gels were then analysed on a UV transilluminator and documented (Syngene).

3.4.3 RNA

Prior to electrophoresis and gel/sample preparation, all glass and plastic ware was autoclaved and the electrophoresis tank treated with 3% H_2O_2 for 30 minutes. RNA samples were run on 1.2% agarose gels, prepared in 1x running buffer (5 mM sodium oxaloacetate, 20 mM MOPS (3-morpholinopropanesulfonic acid) pH 7.0, 1 mM EDTA) containing 2% (v/v) formaldehyde. Before loading the samples, the gel was subject to a constant voltage of 5 V cm^{-1} for 5 minutes in 1x running buffer. Prior to loading on the gel, 1 volume of RNA sample (10 µg in 10 µl) was mixed with 2 volumes of loading buffer (20 µl) (75% (v/v) formamide, 2.5% (v/v) formaldehyde, 1.5x running buffer, 7.5 mg ml^{-1} ethidium bromide) and incubated at 65°C for 5 minutes then cooled on ice. Sterile loading dye (0.03% bromophenol blue, 35% glycerol, 1x running buffer) was then added to the RNA mixture, the sample loaded on to the gel and a constant voltage applied across the gel for varying time periods. Generally, a run time of 3-4 hours was employed when using a constant voltage of between 3-5 V cm^{-1}. Migration of the sample through the matrix was followed by monitoring the bromophenol blue dye front. When the RNA had migrated the desired distance, the gel was washed twice in distilled water then once in 10X SSC (1.5 M NaCl, 0.15 M Sodium Citrate, pH 7.0), each wash was carried out for 15 minutes, and the gel was analysed on a UV transilluminator and documented (Syngene).

3.5 Nucleic Acid Manipulations

3.5.1 DNA purification

DNA products in solution were purified using an *Accu*Prep® PCR and Gel Purification Kit (Bioneer), in accordance to manufacturer's instructions. Briefly, DNA samples in a high salt buffer were applied to a DNA binding column. Under these conditions, the DNA binds to the silica membrane within the column. Salts and precipitates are then removed by a series of centrifugations and ethanol-based wash steps, before eluting

DNA off the column into a low salt buffer such as TE (10 mM Tris-HCl, 1 mM EDTA). Samples were then stored at -20°C.

To purify a DNA fragment fractionated on an ethidium bromide stained agarose gel, the gel was inspected on a UV transilluminator and the required DNA band excised with a scalpel. The DNA was extracted from the agarose slice using the *Accu*Prep® PCR and Gel Purification Kit (Bioneer), in accordance to manufacturer's instructions. The weight, hence volume, of the agarose slice was determined. This was then solubilised in 3 volumes of Gel Binding Buffer at 50°C until the agarose had completely dissolved. One volume of isopropanol was added to the solution to increase the purification yield and the mixture applied to a DNA binding column. The sample was then treated as described above when purifying DNA fragments in solution.

3.5.2 DNA amplification

A set of 2x stock buffers were prepared containing 2x polymerase chain reaction (PCR) buffer (40 mM Tris-HCl, 20 mM $(NH_4)_2SO_4$, 20 mM KCl, 0.2% Triton X-100 (New England Biolabs)), 200 µM deoxynucleoside triphosphates (dNTPs) (New England Biolabs), 10% DMSO and different magnesium concentrations (at either 2, 4, 6, 8 or 10 mM).

A typical DNA amplification reaction was set up as follows. In a reaction with a total volume of 20 µl, 2x stock buffer (10 µl) was mixed with the forward and reverse primer (both at 0.5 µM) and template DNA (approximately 0.2 µg). The volume of the reaction was adjusted to 19 µl with sterile distilled water to which 1 µl (2 units) of DNA polymerase was added. For low fidelity amplification, Taq DNA Polymerase (New England Biolabs) was used whereas Vent (New England Biolabs) DNA polymerase was employed when high fidelity was required.

Using a Techne TC-412 thermal cycler, a standard DNA amplification programme consisted of 1 cycle at 96°C for 1 minute (initial melting stage), then 30 cycles of the following: 96°C for 30 seconds (denaturing stage), 55°C for 30 seconds (annealing stage), 72°C for 1:30 minutes (extension stage). Based on the properties of the

oligonucleotide primers, the annealing temperature and extension times were varied as necessary.

3.5.3 A-tailing of DNA amplification products

DNA fragments generated by DNA amplification using high fidelity DNA polymerase were occasionally cloned into the pGEM-T Easy vector (Promega). To facilitate ligation into this vector, an additional adenosine residue was added to the 3' end of the DNA products. In a total reaction volume of 20 μl, Taq DNA Polymerase (New England Biolabs) (2 units), 200 μM dATP and 2x polymerase chain reaction (PCR) buffer (New England Biolabs) containing 2 mM $MgCl_2$ was mixed with the DNA sample. The sample was incubated at 70^{o}C for 15-30 minutes and the DNA purified.

3.5.4 DNA ligation

A typical DNA ligation reaction was set up as follows. In a total volume of 20 μl, varying amounts of vector and insert DNA were mixed with 2 μl x10 T4 DNA ligation buffer (500 mM Tris-HCl pH 7.5, 100 mM $MgCl_2$, 10 mM ATP and 100 mM dithiothreitol) (New England Biolabs) and the volume adjusted to 19 μl with sterile distilled water. T4 DNA ligase (1 μl: 400 units) (New England Biolabs) was then added to the mixture and the reaction consolidated by centrifugation. The reaction was then incubated at a room temperature for 2-4 hours, then placed at 4ºC overnight. The amount of vector and insert used in the ligation was judged by visualisation on an ethidium bromide-stained agarose gel and a ratio of 5-10:1 insert to vector molecules used in each reaction.

3.5.5 Bacterial DNA transformation

Competent bacteria were prepared the day of transformation. An overnight culture of *E. coli* was diluted 1:50 into NZCYM medium and grown for around 4-5 hours at 37ºC. The cells (5 ml culture) were pelleted at 3555 g for 5 minutes, re-suspended in 10 ml ice-cold 0.1 M $CaCl_2$ and then incubated on ice for 30 minutes. Cells were harvested and the pellet re-suspended in an appropriate amount of ice-cold 0.1 M $CaCl_2$. An aliquot (100 μl) of competent cells was taken, to which the DNA to be transformed was added. The bacteria/DNA mix was incubated on ice for 30 minutes, then heat shocked at

42ºC for 3 minutes, before being placed back on ice. Transformation mixes were then transferred on to NZCYM agar plates containing appropriate antibiotic selection. Agar plates were then incubated overnight at 37ºC to allow colonial growth. In certain instances, for example when using the T-easy vector (Promega), a blue/white selection was performed. Here, NZCYM agar was supplemented with 250 μM isopropyl β-D-1-thiogalactopyranoside (IPTG) and 60 mg l^{-1} bromo-chloro-indolyl-galactopyranoside (X-gal).

3.5.6 DNA sequencing

DNA was sequenced using either the BigDye® terminator cycle sequencing kit (Applied Biosystems) according to instructions, or by a custom DNA Service (Eurofins).

For the BigDye® terminator cycle sequencing (10 μl total volume), approximately DNA template (0.2 μg) was mixed with the appropriate primer (3.2 pMol), Terminator Ready Reaction Mix (1 μl) and 5x sequencing buffer (2 μl). Using a Techne TC-412 thermal cycler, the sample was subject to DNA amplification conditions consisting of 1 cycle at 96°C for 1 minute (initial melting stage) followed by 25 cycles of 96°C for 10 seconds, 50°C for 5 seconds, 60°C for 2 minutes. The DNA was ethanol precipitated by addition of 2 volumes of 100% ethanol and EDTA to a 25 mM final concentration, then incubated at room temperature for 15 minutes. The DNA was pelleted at 16,000 g for 10 minutes and residual supernatant removed with a pipette. The pellet was washed twice in 250 μl 70% ethanol, residual supernatant being removed with a pipette and dried by heating at 98ºC. Samples were stored at -20ºC and sequenced using an ABI3730 sequencer (Applied Biosystems).

For the Custom DNA Service (Eurofins), 0.75-1.5 μg of template DNA and 30 pmol of accompanying primer were used for sequencing by the supplier.

3.6 Plasmids

3.6.1 Probes for Southern blots of CHEFE gels

Individual probes were amplified from *T. brucei* 927 (Tb probes) or *L. major* Friedlin (Lmf probes) genomic DNA, using the appropriate pairs of primers (Appendix Table 10.2.1), and low fidelity Taq Polymerase. The resulting A-tailed PCR fragments were cloned into pGEM-T-easy (Promega), utilising the vector's incorporated T-overhangs. Cloned probes were excised from their vector by *Eco*RI digest, and gel purified.

3.6.2 Construction of pRPa^{iSL}-TopoIIβ

This vector facilitates the tetracycline-inducible RNAi mediated knockdown (Section 1.5.5) of topoisomerase-IIβ in *T. brucei*. It is used in conjunction with the hygromycin-tagged ribosomal spacer locus (2T1/TAG^{PURO}) cell-line (Alsford and Horn, 2008) discussed earlier (Section 3.1.3). A 626 bp fragment specific to topoisomerase-IIß (Genbank: DQ309463.1, nucleotide positions: 3743 – 4369) was amplified from *T. brucei* 427 genomic DNA with the TbTopo-IIß RNAi primers (Appendix Table 10.2.2) and low fidelity Taq polymerase. The forward and reverse primers both contained 2 restriction sites (*Xba*I/ *Bam*HI and *Xho*I/ *Kpn*I respectively) to facilitate the head-to-head cloning of the same PCR fragment into either of the multiple cloning sites of the pRPa^{iSL} stem-loop plasmid (Figure 5.1.2). The final construct: pRPa^{iSL}-TopoIIβ, was linearized with *Asc*I, and DNA purified, ready for transfection.

The plasmid pRPa^{iSL}-TopoIIβ was used in parallel with the plasmid pRPa^{iSL}-TopoIIα (Obado et al., 2007) to generate isoform specific RNAi of topoisomerase-II. The plasmid pRPa^{iSL}-TopoIIα had previously been developed by Dr Obado using a 657 bp fragment specific to topoisomerase-IIα (Genbank: DQ309462.1, nucleotide positions: 3629 – 4286). These cloned fragments were also used to probe Southern and northern blots to detect the specific isoforms.

3.6.3 Cloning the topoisomerase-II intergenic region

The intergenic DNA sequence between topoisomerase-IIα and topoisomerase-IIβ of *T. brucei* is not present in the genome database due to the 2 isoforms being mistakenly assembled as a single fusion protein of the 2 paralogues (Kulikowicz and Shapiro,

2006), so therefore the region was cloned for DNA sequencing. This sequence would allow the design of gene knock-out vectors. The TbTopoII Intergenic primers (Appendix Table 10.2.2) hybridize to the 3' end of the topoisomerase-IIα gene and the 5' end of the topoisomerase-IIβ gene. Using these primers, the intergenic DNA fragment was amplified from *T. brucei* 427 genomic DNA using high fidelity VENT polymerase. These PCR products were A-tailed using low fidelity Taq polymerase (Section 3.5.3) and cloned into the T-easy vector. This 1.5 kb fragment was sequenced using primers to the T7 and SP6 promoters (Promega) of the T-easy cloning vector.

3.6.4 Construction of pNAT$^{x12M\text{-}HYG}$-TopoIIα

This vector allows *in situ* tagging of a native allele with 12 c-myc tags in an array, for either immunofluorescence localization or immunoprecipitation experiments in *T. brucei*. The plasmid pNAT^{x12M} (Alsford and Horn, 2008), which features a blasticidin resistance gene, was modified by replacing the existing targeting fragment plus the 12 c-myc tag into pNAT$^{xG\text{-}HYG}$ (Alsford and Horn, 2008), to effectively replace the GFP tag with the 12 c-myc tag equivalent. This was achieved with a *Hind*III and *Bam*HI digest. Then a 1324 bp targeting sequence of the 3' end of topoisomerase-IIα (Genbank: DQ309462.1) featuring a unique *Age*I restriction site, and deleted stop codon (nucleotides: 3041-4365; removing the stop codon), was amplified from *T. brucei* 427 genomic DNA using high fidelity VENT polymerase with the TbTopo-IIα 12-Myc tag primers (Appendix Table 10.2.2). The products were cloned into the new pNAT$^{x12M\text{-}Hyg}$ with a *Hind*III and *Xba*I digest to generate pNAT$^{x12M\text{-}HYG}$-TopoIIα (Figure 5.1.5). The primers used for amplification were also used to confirm the correct protein sequence (Section 3.5.6). This plasmid was linearized with *Age*I and DNA purified, in preparation for transfection.

3.6.5 Construction of pKO^{BLA}-TopoIIα

A blasticidin resistance cassette with adjacent α/β tubulin intergenic regions, and flanking cloning sites (Rudenko et al., 1994), can be used to target the drug marker into a specific part of the *T. brucei* genome by double homologous recombination. Here, this vector is used for gene disruption of topoisomerase-IIα. A 317 bp fragment of the 5' end of topoisomerase-IIα (nucleotides: 25-342), and a 933 bp fragment of the 3' end

(nucleotides: 3361- 4294), was amplified from *T. brucei* 427 genomic DNA. The amplification used high fidelity VENT polymerase with the TbTopo-IIα 5' Disruption and TbTopo-IIα 3' Disruption primer pairs to generate the 2 PCR fragments (Appendix Table 10.2.2). The 317 bp fragment was cloned into the 5' end of a blasticidin resistance cassette with *Not*I and *Bam*HI, while the 933 bp fragment was cloned into the 3' end with *Apa*I and *Kpn*I forming pKO^{BLA}-TopoIIα (Figure 5.1.5). The flanks were sequenced using the PCR amplification primers. This construct was linearized with *Not*I and *Kpn*I, and DNA purified for transfection.

3.6.6 Construction of pKO^{HYG}-TopoIIα

To disrupt the second topoisomerase-IIα allele, a hygromycin version of pKO^{BLA}-TopoIIα was developed. The 2 gene disruption targeting fragments were directly cloned from pKO^{BLA}-TopoIIα (Figure 5.1.5b) to a hygromycin resistance cassette with *Not*I and *Bam*HI (the 5' fragment), plus *Apa*I and *Kpn*I (the 3' fragment). This generated the plasmid pKO^{HYG}-TopoIIα (Figure 5.2.4a). This construct was also linearized with *Not*I and *Kpn*I, and prepared as standard.

3.6.7 Construction of pTub-Ex^{BLA}-LmfTopoII

The purpose of this vector was to allow high levels of constitutive expression of a gene inserted into the α/β tubulin array of *T. brucei*. The original vector, pTub-EX^{PHLEO} (Cross et al., 2002) had been modified in our laboratory to possess a blasticidin drug resistance marker, forming pTub-EX^{BLA} (Obado et al., 2011). This allowed the vector to work in the 2T1/TAG^{PURO} cell-line (Alsford and Horn, 2008) without a conflict of drug markers. The full length *L. major* topoisomerase-II (Genbank: XM_001684460.1) was amplified from *L. major* Friedlin strain genomic DNA with high fidelity VENT polymerase and LmfTopo-II Complement primers (Appendix Table 10.2.2). The PCR fragment was cloned with *Sbf*I at the 5' end, and *Asc*I at the 3' end to construct pTub-Ex^{BLA}-LmfTopoII (Figure 5.2.1). The plasmid was linearized with *Bam*HI and *Kpn*I, as before.

By performing a *Not*I and *Asc*I restriction digest of the pTub-Ex^{BLA}-LmfTopoII plasmid, an 855 bp fragment of the 3' end of *L. major* topoisomerase-II could be excised

(nucleotide positions: 3639 – 4494) for the generation of specific radio-labelled DNA probes. These could be used for analysis of Southern and northern blots.

3.6.8 Construction of pTub-Ex^{PURO}-LmfTopoII

This vector was developed to allow constitutive expression of *L. major* topoisomerase-II in a null mutant *T. brucei* topoisomerase-IIα background, which would be generated under blasticidin and hygromycin selection. Therefore *L. major* topoisomerase-II was cloned from the blasticidin based pTub-Ex^{BLA}-LmfTopoII, and inserted into pTub-Ex^{PURO} developed by Dr Obado (unpublished), with *Sbf*I at the 5' end and *Asc*I at the 3' end, forming pTub-Ex^{PURO}-LmfTopoII (Figure 5.2.4b). The plasmid was linearized with *Bam*HI and *Kpn*I, and prepared as standard.

3.6.9 Construction of pTub-Ex^{PURO}-TcTopoII

This vector allows the constitutive expression of the *T. cruzi* topoisomerase-II for experiments as per section 3.6.8. Full length *T. cruzi* CL Brener topoisomerase-II was cloned from pTub-Ex^{BLA}-TcTopoII (Obado et al., 2011) into pTub-Ex^{PURO} with *Sbf*I (5' end) and *Asc*I (3' end). The plasmid pTub-Ex^{PURO}-TcTopoII (Figure 5.2.4c) was linearized with *Bam*HI and *Kpn*I, and prepared as before.

A specific radio-labelled DNA probe for use with Southern and northern blots was provided, which was derived from pTub-Ex^{BLA}-TcTopoII (Obado et al., 2011), and encompassed the *T. cruzi* topoisomerase-II nucleotides 3678 to 4452.

3.6.10 Construction of pC-PTP^{NEO}-TopoIIα

The purpose of this vector is to facilitate a high yield of tandem affinity purified topoisomerase-IIα by tagging the native allele with a tandem epitope tag. The plasmid pC-PTP^{NEO} (a gift from the Günzl laboratory) contains a variant of the traditional TAP-tag (Rigaut et al., 1999), where the calmodulin-binding peptide of the original is replaced with a protein C epitope (ProtC), leaving the remaining protein A epitope (ProtA) unchanged (Figure 5.3.1a). This vector also contains the necessary DNA processing sequences for gene expression in *T. brucei* (Schimanski et al., 2005).

A 1602 bp targeting sequence of the 3' end of topoisomerase-IIα featuring a unique *Stu*I restriction site, and deleted stop codon (nucleotides: 2763-4365; removing the stop codon), was amplified from *T. brucei* 927 genomic DNA using high fidelity VENT polymerase and the TbTopo-IIα PTP tag primer pair (Appendix Table 10.2.2). Two additional nucleotides were incorporated into the reverse primers between the 3' end of the gene and the restriction site, which placed the PTP tag in frame with the gene targeting sequence. The fragment was cloned into pC-PTP^{NEO} with *Apa*I and *Not*I to generate pC-PTP^{NEO}-TopoIIα (Figure 5.3.1b). The primers used for amplification were also used to confirm the correct protein sequence (Section 3.5.6). The plasmid was linearized with *Stu*I, and prepared for transfection as normal.

3.6.11 Construction of pC-PTP^{NEO}-TcTopoII

As an alternative to topoisomerase-IIα purification in *T. brucei*, this vector was developed to allow the purification of *T. cruzi* topoisomerase-II (Genbank: XM_805629.1) from *T. cruzi*. A 978 bp targeting fragment (nucleotides: 3514-4492; removing the stop codon) amplified with VENT polymerase from *T. cruzi* CL Brener genomic DNA, was cloned into pC-PTP^{NEO} with *Apa*I and *Not*I. Both the DNA amplification and sequencing was performed with the TcTopo-II PTP tag primers. The resulting pC-PTP^{NEO}-TcTopoII (Figure 5.3.1c) was linearized with *Stu*I, and gel purified to remove the plasmid backbone, ready for transfection into *T. cruzi*.

3.6.12 Construction of pGAP-Luciferase

This vector was designed to generate high levels of luciferase expression from the GAPDH locus in *T. cruzi*. To generate pGAP-Luciferase, the GAPDH intergenic region of the tandem repeat, the upstream neomycin drug resistance gene, and the β/α intergenic region of the tubulin array was excised as 1 fragment from pKS-FKN-Neo, (Figure 7.1.1a, provided by Dr. Wilkinson, unpublished) with *Xho*I and *Eco*RI, and cloned into pBlueScript II KS (Stratagene). Firefly luciferase was amplified from pGEM-luciferase (Promega) with high fidelity VENT polymerase and Luciferase primers (Appendix Table 10.2.3), and cloned downstream of the β/α intergenic region with *Xma*I and *Bam*HI. Then, the 3' UTR of GAPDH was amplified from pTEX (Kelly et al., 1992) with appropriate primers (Appendix Table 10.2.3) and cloned downstream

of the luciferase gene with *Sac*II and *Sac*I. This final plasmid (Figure 7.1.1b) could be linearized with a *Kpn*I and *Sac*I double digest, and gel purified to remove the plasmid backbone which prevents the formation of episomes within the parasite. The primers used for the PCR amplification were also used to confirm the correct sequences of the amplified products once they were cloned.

3.6.13 Construction of pTRIX

The vector pTRIX was developed as a general high level expression vector designed specifically for *T. cruzi*, targeting the ribosomal array. First, the 3' ribosomal spacer region was amplified with high fidelity VENT polymerase using the 3' rDNA Spacer primers (Appendix Table 10.2.3) from *T. cruzi* CL Brener genomic DNA, and cloned into pTEX (Kelly et al., 1992) with *Kpn*I. The inclusion of an additional *Asc*I site at the 3' end of the PCR fragment allowed the confirmation that the fragment was inserted in the correct orientation. The 5' GAPDH intergenic region and multiple cloning site of pTEX, was then replaced with the 5' ribosomal region (including a ribosomal promoter) and multiple cloning site of pRiboTEX (Martinez-Calvillo et al., 1997), via a *Sac*I and *Xho*I digest and cloning procedure. This generated the plasmid pTRIX (Figure 7.1.3a).

3.6.14 Construction of pTRIX-Luciferase

To create the luciferase reporter plasmid the firefly luciferase gene was excised from pGEM-Luc (Promega) and cloned into the multiple cloning site of pTRIX with *Bam*HI and *Xho*I. Before transfection, pTRIX-Luciferase (Figure 7.1.3b) was linearized with *Sac*I and *Asc*I and gel purified to remove the plasmid backbone to prevent the formation of episomes post transfection.

3.6.15 Construction of pRPa^{MYC}-SQE

This vector allowed high expression of squalene epoxidase fused with a 3' c-myc tag, from the ribosomal array of the tagged cell-line 2T1/TAG^{PURO} (Section 3.1.3). To form pRPa^{MYC}-SQE (Figure 8.1.6), full length squalene epoxidase (minus the stop codon, GenBank: XP_828409.1) was amplified from *T. brucei* 427 genomic DNA using high fidelity VENT polymerase and TbSQE-Full primers (Appendix Table 10.2.4). The PCR fragment was cloned into pRPa^{MYC}-NTR (Wilkinson et al., 2008) with *Hin*dIII and *Xba*I

(Figure 8.1.3a), replacing the nitroreductase gene with squalene epoxidase. The 1.7 kb squalene epoxidase gene was sequenced using 6 primers for total gene coverage (Appendix Table 10.2.4), to confirm the correct translated protein sequence. The plasmid was linearized with a *Not*I and *Sac*II digest, and prepared for transfection into *T. brucei* as standard.

3.7 Bioinformatics

3.7.1 Genome analysis

Assembled genome sequencing data of *T. brucei*, *T. cruzi*, and *L. major* (Berriman et al., 2005; El-Sayed et al., 2005a; Ivens et al., 2005) was accessed though GeneDB (Hertz-Fowler et al., 2004), and analysed using Artemis software (Berriman and Rutherford, 2003). Artemis was also used to identify and extract DNA sequences of the AT-rich repeat regions of *T. brucei* chromosomes. Repeats of the centromeric AT-rich regions were identified with Tandem Repeat Finder (Benson, 1999). Specific genes were identified using the BLAST standard algorithm (Altschul et al., 1990) implemented at GeneDB or NCBI, against the respective host databases.

3.7.2 Sequence analysis

Restriction analysis of DNA fragments, plus translation and reverse complementation of DNA sequences was performed with the Colorado State Molecular Toolkit. DNA and protein alignments were made with ClustalW (Thompson et al., 1994) using the algorithm parameters: Gap Opening Penalty (10) and Gap Extension (0.2). The output alignments were scaled and shaded for figure presentation with BioEdit (Ibis Therapeutics).

3.8 Nucleic Acid Detection

3.8.1 DNA and RNA blotting

Agarose gels (both conventional and pulse field) were depurinated for 20 minutes in 0.25 M HCl, washed in distilled water, and then soaked in denaturation buffer (0.5 M NaOH, 1.5 M NaCl) for 1 hour. The gel was then washed in distilled water, and soaked in neutralisation buffer (0.5 M Tris-HCl, 1.5 M NaCl, pH 7.2). For RNA gels, these steps were omitted and the gel was washed twice in sterile water, then in 10x SSC prior to blotting.

Nucleic acids were transferred to a 0.22 µm MAGNA, nylon membrane (GE Water & Process Technologies) by capillary action (Southern, 1975) using a 20x SSC solution (3 M NaCl, 0.3 M Sodium Citrate, pH 7.0) drawn by layers of paper towels for 16-24 hours. The gel was placed on a 3 MM filter paper 'wick' (Whatman), wetted with 20x SSC, with the wicks base submerged in a bath of 20x SSC. The nylon membrane was cut to gel size and placed on top of the gel, then 3 layers of 3 MM filter paper of gel size were placed on top. A pile of paper towels were placed on top of this construct and weighted down to compress the sandwich. The gel was lined with Clingfilm to prevent short-circuit of the capillary action. Following transfer, the nucleic acid was cross-linked to the membrane using a UV cross-linker (Stratagene), using an auto-algorithm, with the DNA or RNA side of the membrane facing the UV bulbs. Membranes were stored at room temperature in polythene bags.

3.8.2 Radio-labelling DNA probes

DNA probes were generated with α-^{32}P CTP (GE Healthcare) using the Rediprime II DNA Labelling System (GE Healthcare). Approximately 2 µg DNA, diluted with sterile distilled water to a volume of 40 µl, was incubated at 95°C for 5 minutes. The denatured DNA was used to re-suspend the components of a Rediprime Premixed Random-Prime Reaction mixture to which 30 µCi α-^{32}P CTP was added. The reaction was incubated at 37°C for 10 minutes to facilitate DNA labelling. Unincorporated radio-label was removed with a sephadex G50 column equilibrated in H_2O with the labelled, flow-through DNA collected in a fresh 1.5 ml microcentrifuge tube.

3.8.3 Nucleic acid hybridization

Nylon membranes containing immobilised, single stranded DNA were pre-hybridised at 65°C for 6 hours with 5x SSC buffer containing 0.5% (w/v) SDS**,** 1x Denhardt's solution (200 mg l^{-1} Ficoll® 400, 200 mg l^{-1} Polyvinylpyrrolidone, 200 mg l^{-1} Bovine Serum Albumin) and 0.2 mg ml^{-1} denatured, sheared salmon sperm. The radio-labelled DNA probe was denatured (95°C for 5 minutes), added immediately to pre-hybridisation solution and incubated at 65°C overnight. The following morning, the membrane was washed twice in 0.2x SSC, 0.2% SDS at 65°C, 30 minutes per wash, to remove non-specifically bound probe.

Nylon membranes containing immobilised RNA were treated similarly to those containing DNA except the pre-hybridization solution consisted of 5x SSC buffer containing 0.1% (w/v) SDS, 1x Denhardts solution, 50% (v/v) formamide, and 0.2 mg ml^{-1} denatured, sheared salmon sperm. The pre-hybridization and hybridization steps for RNA blots were carried out at 42°C.

Radio-labelled probes were detected by exposure to X-ray film (GE Healthcare) within an intensifier cassette at -80°C for the required duration. The X-Ray film was developed using a Mini-Medical Series X-Ray Film Processor (AFP Imaging), in accordance with the manufacturer's instructions.

3.8.4 Removal of radio-labelled DNA probes from nylon membranes.

Nylon membranes containing immobilised, single stranded DNA were used several times. To strip a probe, the membrane was washed twice in stripping solution (0.2 M NaOH, 0.1% (w/v) SDS) at 42°C, 30 minutes per wash. The membrane was then dried between 2 sheets of 3MM paper and checked for residual radioactive signal.

3.9 Protein Analysis

3.9.1 Parasite extracts

Parasites (1×10^8) in the logarithmic phase of growth were pelleted by centrifugation at 1640 g for 5 minutes, washed in PBS then harvested. The cell pellet was re-suspended in 1 ml sterile PBS and transferred to a 1.5 ml microcentrifuge tube. The cells were pelleted (16,000 g for 1 minute), the supernatant removed and the parasites re-suspended in 500 µl sample buffer (40 mM Tris-HCl pH 6.8, 2% (w/v) SDS, 2 mM β-mercaptoethanol, 4% (v/v) glycerol, 0.01% (w/v) bromophenol blue). Aliquots (15-20 µl) were taken and denatured (96ºC for 10 minutes) prior to loading onto SDS-PAGE analysis.

3.9.2 Parasite extracts for protein co-immunoprecipitation

Parasite cultures containing 5×10^9 cells were pelleted at 1640 g for 10 minutes at 4°C. Pellets were combined in a series of wash steps in 25 ml and then in 10 ml ice-cold wash buffer (20 mM Tris-HCl pH 7.4, 100 mM NaCl, 3 mM $MgCl_2$, 1 mM EDTA). The resultant pellet was washed twice in the cell pellet storage buffer (150 mM sucrose, 20 mM potassium glutamate, 3 mM $MgCl_2$, 20 mM HEPES-KOH pH 7.7, 2mM dithiothreitol) containing 10 µg ml^{-1} protease inhibitors (Roche): the first wash step was carried out in 10 ml storage buffer, the last wash step in a volume 1.5x that of the pellet volume. The washed pellet was then freeze-thawed 3 times in liquid nitrogen then at 37°C to lyse the cells. Aliquoted samples were then flash frozen in liquid nitrogen and stored at -80°C.

3.9.3 SDS Polyacrylamide Gel Electrophoresis (SDS-PAGE)

Pre-cast gels (Biorad) were used for protein electrophoresis with a Mini-Protean III system (Biorad). Denatured protein samples were separated on 10% polyacrylamide gels (5% gels for experiments involving topoisomerase II) with 1x SDS-PAGE running buffer (25 mM Tris-HCl, 200 mM glycine, 0.1% (w/v) SDS) using a constant voltage 150 volts for 60-90 minutes. Gels were either stained for 2 hours in Coomassie Blue solution (0.2% Coomassie brilliant blue, 7.5% acetic acid, and 50% ethanol) followed by de-staining in boiling distilled water, or transferred to 0.2 µm nitrocellulose

membrane. Samples were run alongside a PageRuler Prestained Protein ladder (Fermentas) as a marker.

3.9.4 Protein blotting and immunodetection

Protein blotting was carried out using a Trans-Blot Semi-Dry Transfer Cell (BioRad), in accordance with the manufacturer's instructions. A piece of Protran BA83 nitrocellulose membrane (Whatman) and 2 pieces of 3MM paper (Whatman), all cut to the size of the SDS-PAGE gel, and the SDS-PAGE gel itself were soaked in transfer buffer (25 mM Tris, 192 mM glycine, 0.5% SDS) for 10 minutes. One piece of 3MM paper was laid on the anode of the transfer cell on to which was placed the nitrocellulose membrane. The SDS-PAGE gel was then sandwiched between the membrane and a second piece of 3MM paper, with the cathode plate placed on top of the second sheet of 3MM paper, completing the transfer cell. A constant voltage of 10-15 volts for 1 hour was then applied to the apparatus and protein transfer confirmed by observing the presence of prestained markers on the membrane.

A chemilluminscent system was used in protein detection. Protein containing nylon membranes were washed in blocking buffer (10% marvel powdered milk, 1 x PBS, 0.1% (v/v) Tween 20) overnight at 4ºC, then washed twice in western wash buffer (1x PBS, 0.1% (v/v) Tween 20). The membrane was sealed in a polythene bag and challenged with primary antibody diluted in blocking buffer for 1 hour at room temperature with gentle shaking. Following copious washes in western wash buffer, the membrane was then challenged with the secondary horseradish peroxidase conjugate antibody, diluted in blocking buffer, for 1 hour at room temperature with gentle shaking. After further washes in western wash buffer, chemilluminscent detection was carried out using the ECL system (GE Healthcare) and the membrane exposed to X-Ray film (GE Healthcare) for different lengths of time. The X-Ray film was developed as described in section 3.8.3.

The primary antibodies used during this project were: the anti-Myc tag clone 4A6 (Millipore), a mouse monoclonal antibody raised against the 9E10 epitope on the c-Myc protein; and the C-tag antibody (ab18591) (AbCam), a rabbit polyclonal primary

antibody raised against an epitope (amino acids 206-216) on the human protein C. Both antibodies were used at a dilution of 1:1000.

The secondary antibodies used were a goat anti-mouse conjugated with the horseradish peroxidase enzyme (BioRad), diluted 1:2500, and a goat anti-rabbit conjugated with the horseradish peroxidase enzyme (BioRad), diluted 1:1500.

3.10 Parasite Transfection

3.10.1 *T. brucei* bloodstream form

T. brucei BSF parasites in the exponential phase of growth were pelleted by centrifugation at 1640 g for 5 minutes at room temperature, washed in 10 ml PBS then harvested as described above. The pellet was then re-suspended in cytomix (2 mM EGTA pH 7.6, 120 mM KCl, 0.15 mM $CaCl_2$, 10 mM K_2HPO_4/KH_2PO_4 pH 7.6, 25 mM HEPES pH 7.6, 5 mM $MgCl_2.6H_2O$, 0.5 % (w/v) glucose, 100 µg ml^{-1} bovine serum albumin, 1 mM hypoxanthine dissolved in 0.1 M NaOH) chilled to 4^oC at a density of 6 x 10^7 cells ml^{-1}. A 500 µl aliquot of parasite suspension was transferred to a sterile 2 mm gap electroporation cuvette (BioRad) then mixed with approximately 10 µg purified DNA: the DNA had been pre-treated at 65^oC for 30 minutes to minimise contamination and the volume used by transfection was no greater than 50 µl. Parasites were electroporated with a single pulse at 1.4 kV with a 25 µF capacitance using the BioRad Gene Pulser II apparatus and the transformation mixture was added to 36 ml pre-warmed HMI-9 medium. Following incubation at 37^oC under a 5% CO_2 atmosphere for 6 hours, the appropriate drug selection was carried out and 3 ml aliquots dispensed into the wells of a 12-well plate. The drug concentrations used were: G418 at 2 µg ml^{-1}; phleomycin at 2 µg ml^{-1}; hygromycin at 2.5 µg ml^{-1}; blasticidin at 10 µg ml^{-1}; puromycin at 2 µg ml^{-1}. Drug-resistant cultures were observed 5 to 7 days post transfection.

3.10.2 *T. cruzi* epimastigote form

T. cruzi epimastigotes in the exponential phase of growth were prepared as described in section 3.10.1**,** except the parasites were suspended at a density of 1 x 10^8 cells ml^{-1} in chilled cytomix. A 500 µl aliquot of parasite suspension was transferred to a sterile 2 mm gap electroporation cuvette (BioRad) then mixed with approximately 10 µg purified DNA. The parasite/DNA mix was electroporated with 2 pulses at 1.6 kV with a 25 uF capacitance (BioRad Gene Pulser II) and the cells transferred to 48 ml pre-warmed growth medium and incubated at 27°C for 24 hours. The selective drug (G418 at 100 µg ml^{-1}) was added to the culture and aliquots (2 ml) dispensed into the wells of a 24-well plate. Plates were sealed with surgical tape (VWR). Live and dividing parasites could be observed 2-4 weeks post transfection. In all *T. cruzi* transfections, an electroporation without DNA was carried out in parallel to confirm the effective positive selection by drug pressure.

3.11 Cell Imaging

T. brucei bloodstream form in the logarithmic phase of growth were pelleted at 1640 g for 5 minutes, washed twice in PBS before re-suspending in 0.5 ml PBS at a density of 1 x 10^7 cells ml^{-1}. An equal volume of fixative (4% (w/v) paraformaldehyde in PBS) was added slowly to the parasites and then incubated for 20 minutes at room temperature; all proceeding steps were carried out at this temperature. An aliquot (20 µl) of the parasite suspension (~1 x 10^5 cells) was then air dried on to a single well of a 12-well printed microscope slide. The slides were subject to a series of washes, firstly washed twice in PBS, 5 minutes per wash, then in 0.2 µM filtered 50 mM NH_4Cl**,** PBS (20 µl per well) for 10 minutes and finally in PBS for 5 minutes, before blocking in 50% (v/v) horse serum/50% (v/v) wash buffer (PBS, 0.1% (w/v) saponin) for 20 minutes. Following further wash steps in PBS (twice) and wash buffer (once), the sample was incubated for 45 minutes with the primary antibody. The slides were then washed 3 times in wash buffer then incubated for 30 minutes with the second antibody. Following further wash steps in wash buffer (twice) and PBS (twice), the slide was dried before mounting in a 1:1 mix of PBS/glycerol containing 200 pM 4',6-diamidino-2-phenylindole stain (DAPI). A seal (clear nail varnish) was applied around the edge of the coverslip that was

allowed to harden overnight at room temperature in the dark. Slides were stored at 4°C until use. All blocking steps and antibody incubations were carried out in a humid atmosphere (sealed sandwich box containing a wetted sheet of 3MM paper).

The primary antibodies used were c-Myc sc-40 (Santa Cruz), a mouse monoclonal antibody raised against the 9E10 epitope on the c-Myc protein, or a polyclonal antisera raised against the topoisomerase-IIα in rabbits (a gift from T. Shapiro, John Hopkins). Antibodies were diluted 1:50 for c-Myc (9E10) or 1:500 for anti-topoisomerase-IIα in 2% (v/v) horse serum, PBS, 0.1% (w/v) saponin. The AlexaFluor 488-conjugated goat anti-mouse or Alexa-Fluor 546 goat anti-rabbit (both Molecular Probes) were used as secondary antibodies. These were diluted 1:400 in 2% (v/v) horse serum, PBS, 0.1% (w/v) saponin. Images were taken on a Zeiss LSM 510 Axioplan microscope.

3.12 Drug Screening

3.12.1 *T. brucei* bloodstream form proliferation assays

Bloodstream form *T. brucei* were seeded at 1 x 10^3 cells ml^{-1} in growth medium containing different concentrations of drug: when appropriate, tetracycline (1 µg ml^{-1}) was added to cultures to induce gene expression. 200 µl aliquots were then dispensed into the chambers of a clear 96-well plate. Following incubation at 37°C for 3 days in a 5% CO_2 atmosphere, 20 µl alamarBlue® (Invitrogen) was added to each well. Plates were incubated for a further 16 hours before measuring fluorescence using a Gemini Fluorescent Plate Reader (Molecular Devices) set at 530 nm excitation wavelength, 585 nm emission wavelength, and cut-off at 550 nm. IC_{50} values were calculated from linear regression based data plots with Excel (Microsoft).

3.12.2 *T. cruzi* amastigote proliferation assays

Vero cells were seeded at 1.5 x 10^4 ml^{-1} in 100 µl growth medium and allowed to adhere to the base of each well of a clear 96-well plate at 37°C for 6 hours in a 5% CO_2 atmosphere. *T. cruzi* trypomastigotes (10,000 in 100 µl mammalian growth medium) derived from previous Vero cell infections and lacking free amastigotes, were added to the chambers containing mammalian cells resulting in a parasite:Vero cell ratio of ~7:1.

Following infection overnight at 37°C with 5% CO_2, the cultures were washed twice in mammalian growth medium to remove non-internalized parasites, and the supernatant replaced with 200 µl fresh mammalian growth medium containing drug. Drug-treated infections were incubated for a further 3 days at 37°C under a 5% CO_2 atmosphere. To assay infections, the growth medium was removed and the cells washed twice in fresh medium to remove extra-cellular parasites. The cells were then lysed using 50 µl cell culture lysis buffer (Promega) and 20 µl aliquots transferred to a white 96-well plate. Luciferase activity was measured by adding 100 µl enzyme substrate reagent (Promega) to the lysed 20 µl aliquots and light emission measured on a β-plate counter (Wallac). IC_{50} values were again calculated from linear regression based data plots.

3.12.3 Mammalian cells proliferation assays

Vero cells were seeded at 1.5 x 10^4 ml^{-1} in 100 µl growth medium and allowed to adhere to the base of each well of a clear 96-well plate at 37°C for 6 hours in a 5% CO_2 atmosphere. An equal volume (100 µl) of growth medium containing drug was then added to the chambers containing mammalian cells. Following incubation at 37^{o}C for 4 days in a 5% CO_2 atmosphere, 20 µl alamarBlue® (Invitrogen) was added to each well. Plates were incubated for a further 4 hours before measuring fluorescence using a Gemini Fluorescent Plate Reader (Molecular Devices).

3.13 Compounds

Nifurtimox and benznidazole were supplied from stocks held by Prof. Simon Croft, London School of Hygiene and Tropical Medicine (Figure 3.13.1). All other compounds used for drug screening were synthesized by collaborators. The aziridinyl nitrobenzamide compounds were purchased from Sigma (CB1954) or synthesized and supplied, and provided to us by Dr. Nuala Helsby, University of Aukland (Table 3.13.1) (Helsby et al., 2004a). The nitrobenzyl phosphoramide mustard series were synthesized by Prof. Lonqin Hu, Rutgers, University of New Jersey to a purity shown by LC-MS of greater than 90% (Table 3.13.2 and Table 3.13.3) (Hu et al., 2003; Jiang et al., 2006; Jiang and Hu, 2008). The nitrofuryl compounds were synthesized and provided to us by Hugo Cerecetto, Universidad de la República, Montevideo (Table 3.13.4) (Aguirre et al., 2004a; Aguirre et al., 2004b; Gerpe et al., 2008).

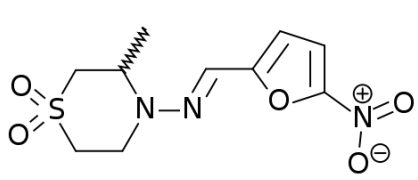

Nifurtimox

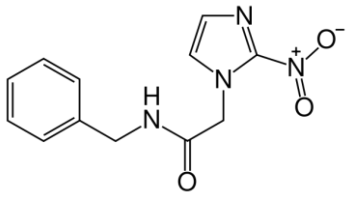

Benznidazole

Figure 3.13.1. ***The chemical structures of nifurtimox and benznidazole.***

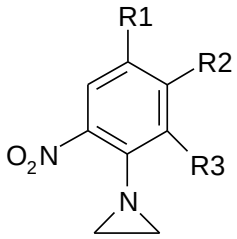

Compound	Structure
Type Ia:	
CB1954	R1=NO_2; R2=$CONH_2$; R3=H
NH1	R1=NO_2; R2=$CONH(CH_2)_2$Nmorpholide; R3=H
NH2	R1=NO_2; R2=$CONH(CH_2)_2CO_2Me$; R3=H
Type Ib:	
NH3	R1=H; R2=$CONH_2$; R3=H
NH4	R1= SO_2Me; R2=$CONH_2$; R3=H
NH5	R1=SO_2Me; R2=$NHCH_2CH(OH)CH_2OH$; R3=H
Type II	
NH6	R1= NO_2; R2=H; R3=$CONH_2$
NH7	R1= NO_2; R2=H; R3=$NHCH_2CH(OH)CH_2OH$
NH8	R1= NO_2; R2=H; R3=$CONH(CH_2)_2$Nmorpholide

Table 3.13.1. ***Chemical structures of the aziridinyl nitrobenzamides.***

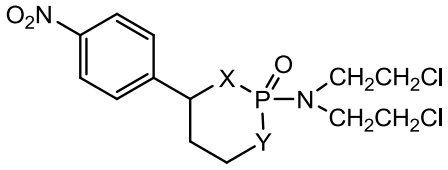

Compound	Structure
LH3	X=O; Y=NH; (cis)
LH4	X=O; Y=NH; (trans)
LH5	X=NH; Y=O; (cis)
LH6	X=NH; Y=O; (trans)
LH12	X=NH; Y=NH; (cis)
LH13	X=NH;Y=NH; (trans)

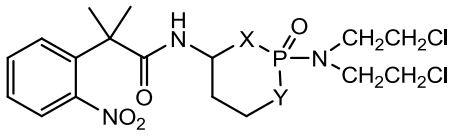

Compound	Structure
LH8	X=O; Y=NH; (cis)
LH9	X=O; Y=NH; (trans)

Table 3.13.2. ***Chemical structures of the cyclic nitrobenzyl phosphoramides.***

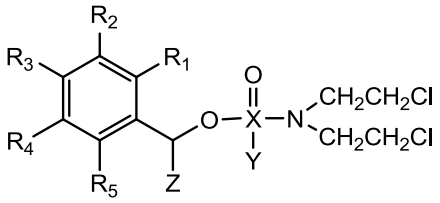

Compound	Structure
LH7	R_3=NO_2; X=P; Y=NH_2; R_1=R_2=R_4=R_5=Z=H
LH14	R_3=NO_2; X=P; Y=NH_2; Z=CH_3; R_1=R_2=R_4=R_5=H
LH15	R_5=NO_2; X=P; Y=NH_2; R_1=R_2=R_3=R_4=Z=H
LH16	R_4=NO_2; X=P; Y=NH_2; R_1=R_2=R_3=R_5=Z=H
LH17	R_3=NO_2; R_5=OCH_3; X=P; Y=NH_2; R_1=R_2=R_4=Z=H
LH18	R_3=NO_2; R_4=OCH_3; X=P; Y=NH_2; R_1=R_2=R_5=Z=H
LH19	R_3=NO_2; R_4=CH_3; X=P; Y=NH_2; R_1=R_2=R_5=Z=H
LH24	R_3=NO_2; X=P; Y=NH_2; Z=CH_3; R_1=R_2= R_4=R_5=H
LH27	R_3=NO_2; X-Y=C; R_1=R_2= R_4=R_5=Z=H
LH31	R_2=F; R_3=NO_2; X=P; Y=NH_2; R_1=R_4=R_5=Z=H
LH32	R_1=F; R_3=NO_2; X=P; Y=NH_2; R_2= R_4=R_5=Z=H
LH33	R_1=CF_3; R_3=NO_2; X=P; Y=NH_2; R_2= R_4=R_5=Z=H
LH34	R_1=Cl; R_3=NO_2; X=P; Y=NH_2; R_2= R_4=R_5=Z=H
LH37	R_1=R_5=F; X=P; R_3=NO_2; Y=NH_2; R_2= R_4=Z=H
LH47	R_1=R_2= R_4=R_5=F; R_3=NO_2; X=P; Y=NH_2; Z=H
LH48	R_1=R_4=R_5=F; R_3=NO_2; X=P; R_2=Y=NH_2; Z=H

Table 3.13.3. ***Chemical structures of the acyclic nitrobenzyl phosphoramides.***

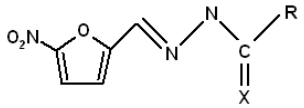

Compound a	X	R
HC-1	S	NH_2
HC-2	S	$NHCH_3$
HC-3	S	$NHCH_2CH_3$
HC-4	S	$NHCH_2CHCH_2$
HC-5	S	NHPh
HC-6	O	$OCHCH_2$
HC-7	O	OCH_3
HC-8	O	$O(CH_2)_3CH_3$
HC-9	O	$O(CH_2)_5CH_3$
HC-10	O	$O(CH_2)_6CH_3$
HC-11	O	$O(CH_2)_7CH_3$
HC-12	O	OPh
nitrofurazone	O	NH_2
HC-13	O	$NH(CH_2)_3CH_3$
HC-14	O	$NHCH_2CH_2OCH_3$

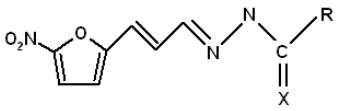

Compound b	X	R
HC-2b	S	$NHCH_3$
HC-4b	S	$NHCH_2CHCH_2$
HC-12b	O	OPh

Table 3.13.4. ***Chemical structures of the 5' nitrofuryl compounds.***

3.14 Spectrometry

3.14.1 Sample preparation

Drug metabolites were generated by reducing 100 µM nitrofuryl substrate with 40 µg ml^{-1} *T. brucei* nitroreductase in the presence of 200 µM NADH in 50 mM $NaHPO_4$ at 37ºC for 10 minutes. Recombinant parasite enzyme was removed from this mixture by the addition of Ni-NTA resin (Qiagen), followed by a centrifugation at 16,000 g for 10 minutes. The supernatant (900 µl) was transferred to a fresh 1.5 ml microcentrifuge tube for analysis. Non-reduced nitrofuryl substrate (100 µM) in 50 mM $NaHPO_4$ was examined in parallel.

3.14.2 Liquid Chromatography - Mass Spectrometry (LC-MS)

LC-MS of selected compounds and metabolites were analysed using an Agilant 1100 Series LC/MSD. An aliquot (20 µl) was injected into a 5 µm Hypurity Elite 15 x 2.1mm C18 column (Thermo Scientific), pre-equilibrated with 10% acetonitrile. Separation was carried out using a 10-30% acetonitrile gradient at a flow rate of 0.2 ml min^{-1}. Metabolites were detected using a diode array with absorption at 250, 300, 340 and 450 nm. Ions were generated by positive electrospray ionization with a capillary voltage of 4 kV, a nebulising gas flow of 25 psi, a dry temperature of 325ºC, and dry gas flow at 10 litres min^{-1}. Further settings were auto-optimised based on a target mass to charge ratio (*m/z*) of 200, with a maximum detected *m/z* value of 350.

Tandem mass spectrometry was used to identify the presence of a nitrile group on selected metabolites. Chromatography conditions remained the same, while ionization was performed with negative mode electrospray using the previous ionization conditions, with the generated precursor ions fragmented with a collision energy of 1.5 V.

4 Biochemical Mapping of Centromeres

This chapter sets out to identify the chromosomal regions that represent centromeric domains in trypanosomes. The chapter will focus on determining the locations of centromeres on *T. brucei* chromosomes, and will also attempt to identify centromeres on *L. major* chromosomes.

4.1 Biochemical Mapping of *T. brucei* Centromeres

Analysis of the trypanosome genomes reveal they appear to lack many of the core components involved in chromosome segregation, including the centromeric variant of histone H3. The absence of many proteins considered to be essential for faithful chromosome segregation in other eukaryotes poses the question of whether trypanosomes simply possess highly divergent homologues, or alternatively, is the segregation of chromosomes in trypanosomes mediated via a different mechanism. The first stage in addressing this question is to identify the chromosomal regions that comprise a centromere and which facilitate the formation of the kinetochore. With a lack of a DNA sequence or a constitutive protein based marker, the less direct approach of biochemical mapping with topoisomerase-II, a protein active transiently at the centromere, was used to map the centromeric regions of the megabase chromosomes of *T. brucei*. This mapping approach (see Section 2.3.1) was first used in a human cell-line, where topoisomerase II activity was shown to coincide with centromeric α-satellite DNA repeats (Floridia et al., 2000). Further studies in the malaria parasite have employed this technique to map the locations of the centromeric regions on *P. falciparum* chromosomes (Kelly et al., 2006).

4.1.1 Long-range *T. brucei* centromere mapping

Purification of whole chromosomes from procyclic stage *T. brucei* proved advantageous, as this lifecycle stage grows denser than the bloodstream forms, allowing for an efficient high yield of chromosomal DNA (Section 3.2.3). Initial chromosome separations allowed the validation of our laboratory isolate as the correct genome strain

T. brucei TREU 927/4, based on reference to the resolution of the mini-, intermediate-, and megabase sized chromosomes (Melville et al., 1998).

Chromosome 1 of *T. brucei* TREU 927/4 is the smallest of the 11 megabase sized chromosomes with homologues estimated at 1.15 Mb and 1.20 Mb, and is therefore the easiest to separate by CHEFE. Preliminary experiments demonstrated that etoposide is an effective poison of *T. brucei* topoisomerase-II. In these experiments, *T. brucei* cultures were treated with between 250 µM and 2000 µM etoposide for 1 hour before the parasites were embedded in agarose blocks, and then lysed in a mild detergent to release the intact chromosomes (Section 3.2.3). Chromosomes from treated parasites were then separated by CHEFE alongside chromosomes from untreated cultures under conditions designed to resolve chromosome 1 and any derivative breakdown products. Probing a Southern blot of the CHEFE gel with a radio-labelled probe specific to chromosome 1 detected a discrete band of around 1.2 Mb that corresponded to the predicted size of chromosome 1 (Figure 4.1.1). The probe was the α-tubulin gene (Tb1), selected due to the multi-copy nature of the gene which is located in a discreet tandem array alongside ß-tubulin on chromosome 1. This would therefore generate a strong signal from the Southern blots to reveal any cleavage product bands. All probes used with Southern blots were designed to be specific for their designated target, and cloned from PCR products to minimise background that might be caused by non-specific hybridization (Section 3.6.1). In lanes containing DNA from etoposide treated parasites, a second band was observed at around 0.8 Mb. This second band was observed for all etoposide concentrations. However as drug concentrations increased, the intact chromosomal bands diminished, accompanied with an increase in smearing in the lanes. The occurrence of this etoposide mediated cleavage product showed that etoposide was an effective poison of *T. brucei* topoisomerase-II, and prevents the re-ligation step following DNA scission (Section 2.3.1). It also demonstrated that the activity of topoisomerase-II is concentrated to a specific region of the chromosome. Using etoposide at 500 µM for 1 hour was considered the optimum treatment conditions for generating cleavage products to map the centromeric regions of chromosomes. A previous attempt using 100 µM etoposide for 30 minutes, 1 hour, and 2 hours generated no observable DNA cleavage products with procyclic *T. brucei* (data not shown).

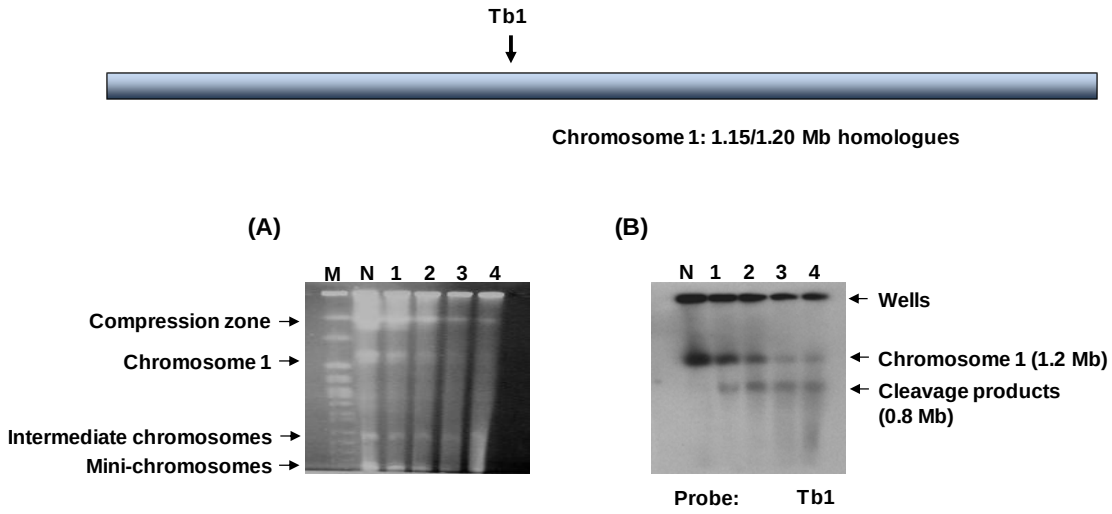

Figure 4.1.1. ***Topoisomerase-II mediated DNA cleavage in T. brucei.***
Chromosomes of *T. brucei* are separated by CHEFE using an auto algorithm that optimises separation up to 1.6 Mb (CHEF Mapper, Biorad; section 3.4.2). An ethidium bromide stained gel **(A)** shows the mini-chromosomes at the bottom (~ 100 kb), with the intermediate chromosomes above (~ 400 kb), and the major chromosome 1 further up. Many of the larger chromosomes get trapped in the gel compression zone under the separation conditions used. For size estimations *S. cerevisiae* chromosomal ladder markers (Bio-Rad) were run (M) next to un-treated parasites (N), with 250 µM (lane 1), 500 µM (lane 2), 1000 µM (lane 3), and 2000 µM (lane 4) etoposide treatment for 1 hour. A Southern blot **(B)** probed with Tb1 shows chromosome 1 and the etoposide mediated cleavage products. At higher etoposide concentrations the lane smearing intensifies and the chromosome 1 band fades. Given the relative position of the Tb1 probe (at ~ 570 kb), and the size of the cleavage product (approximately 800 kb), on a 1.2 Mb chromosome, it is not possible to determine at which end of the 1.2 Mb chromosome the centromere is located from this single experiment.

This experiment showed that DNA cleavage products generated by topoisomerase-II poisoning were stable and specific enough to be detected through Southern blotting of CHEFE gels, and identified the optimum conditions. The next step was to more accurately locate the site of topoisomerase-II activity. Multiple sets of chromosomal DNA isolated from etoposide treated procyclics were run in parallel with non-treated samples on CHEFE gels. This allowed simultaneous probing of split Southern blots with different probes (see Appendix Table 10.2.1 for probe details). For the next experiment, another probe (Tb4) located at the opposite end of the chromosome to probe Tb1, was used. This demonstrated that *T. brucei* chromosome 1, with homologues around 1.2 Mb, was effectively split in two, with the 0.8 Mb fragment identified by probe Tb1 corroborated with fragments between 0.3 and 0.4 Mb identified by Tb4 (Figure 4.1.2).

The smear observed with probe Tb4 is probably due to the difference in homologue sizes, coupled with topoisomerase-II activity focussed over a small chromosomal region rather than a single specific locus.

With reference to the genome database (www.genedb.org), the area of topoisomerase-II activity appeared to be located around a divergent polycistron strand-switch region containing a ribosomal RNA array, two INGI retrotransposons and a degenerate INGI-like retrotransposon element (DIRE). Within this region was also a degenerate AT-rich (66%) repeat sequence spanning 5.5 kb (Figure 4.1.2). In chromosome 1, this type of repeat sequence was specific to this region only. An additional experiment using two new probes located closer to this region (Tb2 and Tb3) further demonstrated topoisomerase-II activity focused within a 100 kb region containing these features (Figure 1.1.2). The additional two probes were designed on the basis of their proximity to the repeat region, while providing a unique and specific DNA hybridization site.

The proposed centromeric region of *T. brucei* chromosome 1 coincided with previous experimental results with *T. cruzi*. Chromosome 3 of *T. cruzi* is syntenic with that of *T. brucei* chromosome 1. In *T. cruzi*, a 65 kb region of chromosome 3 was determined to be essential for mitotic stability through a series of chromosome truncations generated by telomere-associated chromosome fragmentation experiments (Obado et al., 2005). Reminiscent of the centromeric region of *T. brucei* chromosome 1, this region also contained degenerate retro-elements, and uniquely to *T. cruzi*, a 16 kb GC-rich non repeat based sequence. The observation that topoisomerase-II based etoposide mediated cleavages sites were also located at this locus reinforced the notion that this region of *T. cruzi* chromosome 3 represents a centromeric domain (Obado et al., 2007). Therefore, a domain proposed as a centromere in *T. cruzi* chromosome 3, based on two independent experimental approaches, is syntenic with a *T. brucei* chromosome 1 domain proposed as a centromere on the basis of the biochemical mapping data presented here.

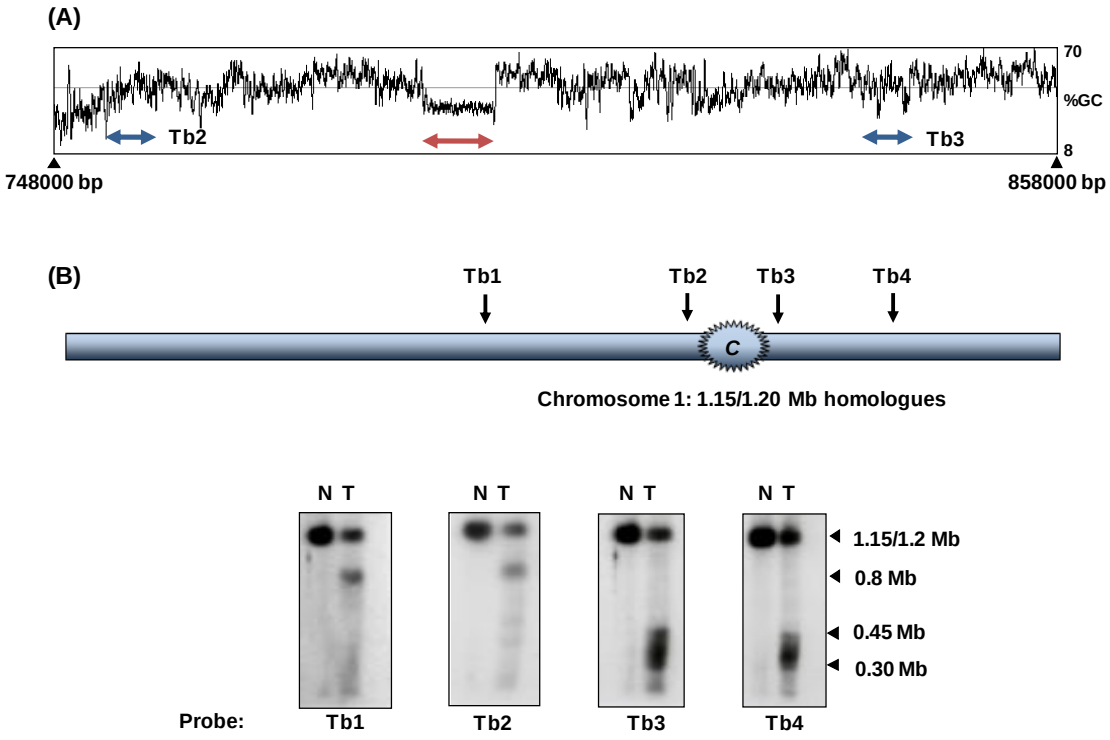

Figure 4.1.2. ***The centromeric region of T. brucei chromosome 1.***
A graphical display using Artemis software shows the %GC level of chromosome 1 between the labelled positions on a 110 kb region **(A)**. At each nucleotide position, the %GC composition is determined by the average composition of the surrounding 120 bp. The blue arrows show the location of the proximal DNA probes to the proposed centromeric locale, while the red arrow highlights a unique repeat region on chromosome 1 that is particularly AT rich. Southern blots of CHEFE separated chromosomes (0.2-3.5 Mb, section 3.4.2) demonstrate localized topoisomerase-II activity **(B)**. A schematic shows the location of the Southern blot probes labelled Tb1 – Tb4 on chromosome 1, and the location of the mapped centromere 'C'. Non-treated etoposide parasites (lane N) and parasites treated with etoposide (lane T) are run side by side for comparison. Predicted sizes of bands are shown as estimated from *S. cerevisiae* chromosomal ladder markers. The centromeric region is determined to be between probe Tb2 and Tb3, and within the region containing the AT-rich domain.

Analysis of the GeneDB database for chromosome 2 showed a similar AT-rich repeat region located at a single domain of the chromosome. It was hypothesized that this domain may be the location of the topoisomerase II cleavage foci on chromosome 2, and therefore specific probes were generated to this area, both proximal to the repeat region (Section 3.6.1). Concentrated DNA cleavage was observed in this region after etoposide treatment (Figure 4.1.3). Probes Tb5 and Tb6 both identified two cleavage product bands, possibly derived from the two chromosomal homologues of 1.25 Mb and 1.30 Mb. Probe Tb5 identified bands at 280 kb and 450 kb, whilst probe Tb6 identified bands of 900 kb and 1000 kb. When combined, these estimates fit closely with the predicted size of the intact chromosome.

Analysis of the putative centromeric region on chromosome 2 identified though etoposide mediated DNA cleavage displays similar features to that of chromosome 1. Accompanying the AT-rich (66%) repeat region are two INGI retrotransposons and two ribosomal RNA arrays, all sandwiched between a divergent polycistron strand-switch. Comparison of the 8 kb AT-rich region of chromosome 2 to its 5.5 kb chromosome 1 counterpart showed that while both regions are AT-rich and comprised of repeats, the actual sequences are not closely related.

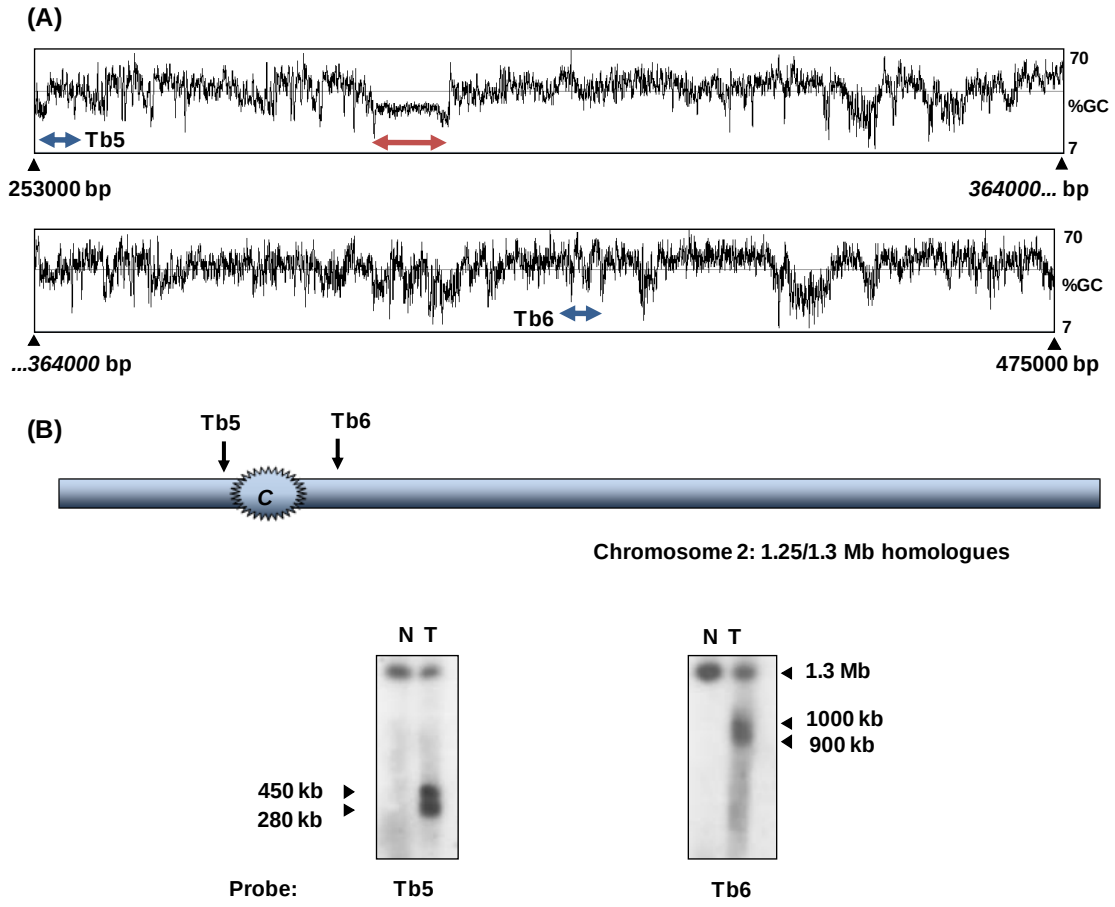

Figure 4.1.3. ***The centromeric region of T. brucei chromosome 2.***
A graphical display using Artemis software shows the %GC level of chromosome 2 between the labelled positions on a surrounding 222 kb region **(A)**. At each nucleotide position, the %GC composition is plotted (see Figure 4.1.2 for details). Blue arrows show the location of the two proximal centromeric DNA probes, the red arrow highlights a unique repeat region on chromosome 2 that is particularly AT rich. Southern blots of CHEFE separated chromosomes **(B)** with non-treated etoposide parasites (lane N) and parasites treated with etoposide (lane T). Specific cleavage is restricted to the region between probe Tb5 and Tb6.

Given that topoisomerase-II DNA cleavage appeared to be associated with a distinctive region of AT-rich repeats on both chromosomes, and that a domain of this nature could be readily identified on each of the 8 megabase sized chromosomes completely assembled by the genome project, further mapping experiments were performed. Putative centromeric domains of chromosomes 3 and 4 were mapped to these proposed domains by Dr Obado (Obado et al., 2007), with the data for chromosome 5 generated as part of this thesis. Chromosome 5 of *T. brucei* has 2 homologues of around 1.7 Mb.

Two probes were designed (Tb7 and Tb8), 1 either side of the single AT-rich repeat domain (Section 3.6.1). The Tb7 probe identified an intense band at 200 kb in lanes containing chromosomal DNA from etoposide treated parasites (Figure 4.1.4). Mapping with the Tb8 probe proved less clear. Although this probe did detect a strong band at 1.5 Mb, it also detected a smear including many smaller sized products. This could be as a result of non-centromere specific topoisomerase-II activity along the chromosome, which would become more apparent the larger the size of the centromere derived cleavage fragment generated.

The AT-rich (61%) repeat domain of chromosome 5 corresponded with the site of major etoposide mediated topoisomerase-II activity, as inferred from the data derived with probe Tb7 from the short arm of the chromosome. The GeneDB database shows the repeat region as 2.5 kb, adjacent to a single DIRE retro-element, and between divergent strand-switch polycistrons. Comparison of the repeat array with the sequences from chromosome 1 and 2 shows some similarity (Figure 4.1.5). Both the repeats of chromosome 2 and 5 appear to be consistent in sequence composition, albeit the chromosome 5 repeat is much longer. The repeats of chromosome 1 are highly degenerate however, and so a consensus sequence unit was used when generating the alignment.

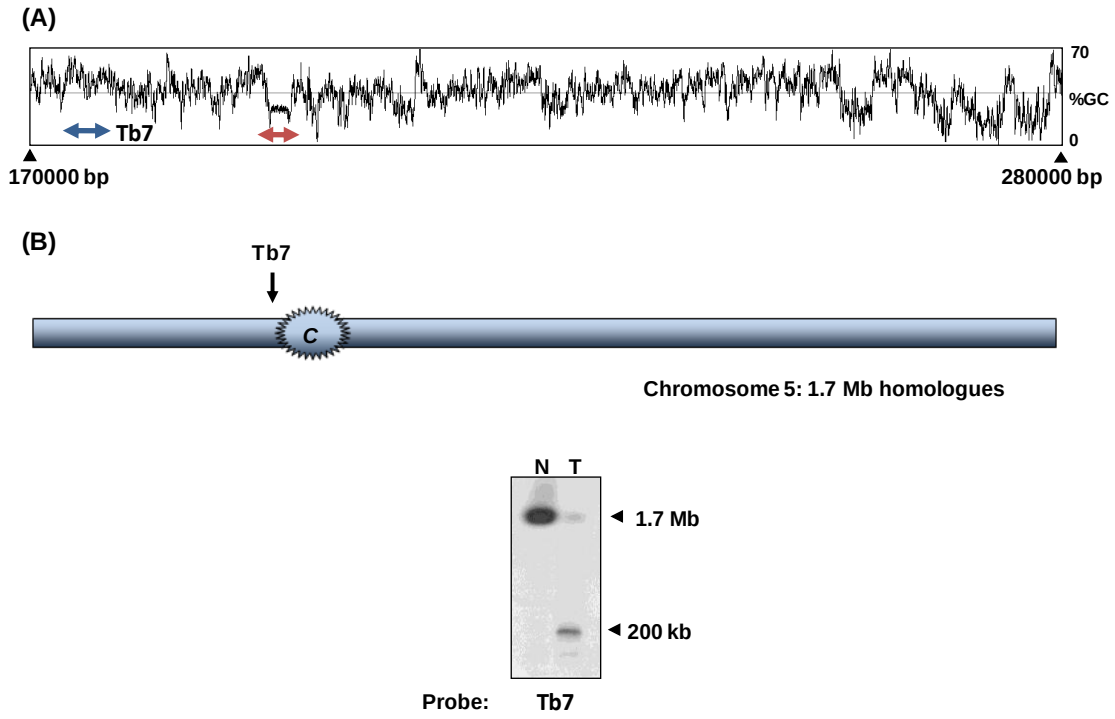

Figure 4.1.4. ***The centromeric region of T. brucei chromosome 5.***
Artemis shows the %GC level of chromosome 5 between the labelled positions on a surrounding 110 kb region **(A)**. A blue arrow shows the proximal centromeric DNA probe, and the red arrow highlights the characteristic AT rich unique repeat region on chromosome 5. A Southern blot of CHEFE separated chromosomes **(B)** from non-treated etoposide parasites (lane N) and parasites treated with etoposide (lane T). This shows intensive cleavage to be just beyond probe Tb7.

In each of the three examples above, topoisomerase-II activity is shown to be concentrated to specific loci along a given chromosome, as demonstrated though the mapping of etoposide mediated cleavage products. In each case, major topoisomerase-II activity is observed at domains unique on each chromosome that are comprised of an AT-rich repeat region accompanied by retro elements. For chromosome 1, this domain corresponds to the syntenic region of *T. cruzi* chromosome 3, which has been proposed as a centromeric domain, based on both topoisomerase-II based biochemical mapping and mitotic stability experiments. Although the centromere on chromosome 1 of *T. cruzi* has also been studied using biochemical mapping and mitotic stability experiments, with both converging on a domain comprising of a GC-rich region of DNA flanked by retrotransposons (Obado et al., 2007), this region cannot currently be related back to *T.*

brucei. This is because the syntenic region in *T. brucei* occurs in an unassembled contig of chromosome 11.

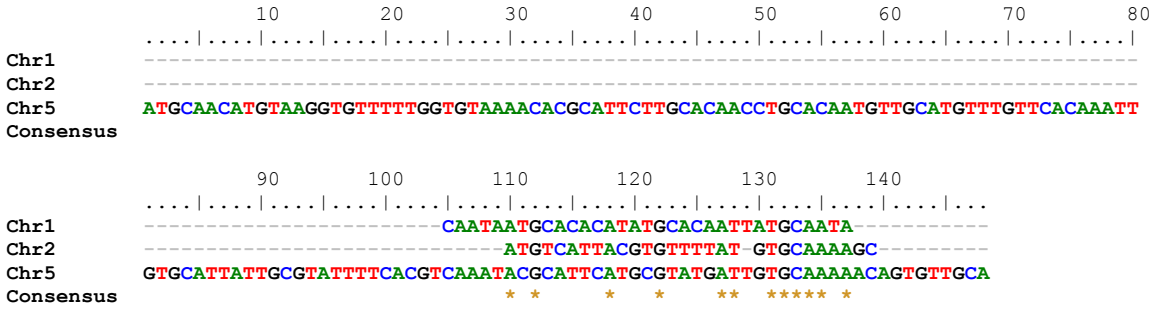

Figure 4.1.5. ***Alignment of AT-rich centromeric repeat sequences.***
Consensus repeat units within the AT-rich region for each chromosome were identified using Tandem Repeat Finder (Benson, 1999) on sequences derived from the genome database (Section 3.7.1). These were aligned with ClustalW (Thompson et al., 1994). Chromosomes 2 and 5 contained regions of consistent repeat sequence units of defined sequence and length. However, the repeat sequences of chromosome 1 were much more divergent throughout the AT-rich repeat region, so therefore the most abundant consensus sequence repeat identified by Tandem Repeat Finder is presented for chromosome 1. Some sequence similarity can be observed in an alignment of these three sequences.

Following successful biochemical mapping of the eight fully assembled chromosomes of *T. brucei* to the corresponding eight unique AT-rich repeat regions (Obado et al., 2007), a general analysis of these regions can be made. All of the ribosomal RNA arrays of the *T. brucei* megabase chromosomes are found within these regions (chromosomes 1, 2, 3, and 7), and DNA retro-elements are prevalent in these areas. Also, although some similarity in sequence was observed between the repeats of chromosomes 1, 2, and 5, as described here, a high degree of similarity can be found between the repeats of chromosomes 4, 5, 8, and the unassembled contigs of chromosomes 9, 10, 11. In addition the repeat sequence of chromosome 2 is very similar to the repeat of chromosome 7 (Figure 4.4.1). Whether any of these features represent a functional component of the centromere, or are merely acquired due to a relaxed regulation of DNA content at the centromere remains to be determined.

4.1.2 Fine mapping *T. brucei* chromosome 1

Since AT-rich repeat regions were common features of the domains that are major sites of topoisomerase-II DNA cleavage activity, these repeat domains were analysed in further detail to determine whether specific elements were the central focus of the activity. Although topoisomerase-II is active, to an extent, along the whole chromosome, there potentially could be unique structure or sequence features that mark out the transiently active zones in the centromeric domains. Each chromosome was analysed via *in silico* restriction mapping to identify potential endonuclease restriction fragments that would span the proposed centromeric domain, while containing a region that would allow specific hybridization of a radio-labelled probe to a single fragment. Chromosome 1 represented an ideal candidate for this strategy, using the enzyme *Not*I to generate the required restriction fragments.

To analyze the genome restriction fragments for etoposide mediated DNA cleavage on *T. brucei* chromosome 1, whole chromosomes from etoposide treated parasites were first embedded in agarose blocks as previously described (Section 3.2.3). These blocks were then washed repeatedly in a buffer containing a protease inhibitor, to remove the residual proteinase K remaining from the chromosome extraction process. This was required to prevent the downstream degradation of the restriction endonuclease used to generate the DNA fragments. The restriction digests were performed overnight on whole gel blocks using the enzyme *Not*I (Section 3.3.2). The next day the digested chromosome gel blocks were cooled to aid their loading into a CHEFE gel. The CHEFE separation conditions that allowed effective resolution of the full length restriction fragments of *Not*I digests on chromosome 1 were identified empirically using lambda digest and *S. cerevisiae* markers.

Unexpectedly, Southern blots of the resulting gel containing the separated DNA fragments showed two bands of 150 kb and 190 kb, when probed with Tb2. The *Not*I fragment size was predicted by GeneDB to be around 120 kb for this chromosome 1 probe (Figure 4.1.6). The genome sequencing project opted to sequence and assemble the smaller of the two homologues (Hall et al., 2003), therefore there is at least a 30 kb discrepancy between what we observe experimentally, and the genome database.

Significantly, this difference makes it difficult to map topoisomerase-II mediated DNA cleavage patterns directly back to specific loci on the chromosome. The difference suggests that this region of the chromosome may not be fully sequenced and/or assembled, most likely due to difficulties associated with the nature of AT-rich repeat regions. This observation could have important consequences in itself, as missing parts of the repeat region makes rigorous comparisons between repeats of limited value at this stage, and may mask any important downstream conclusions such as trying to relate any DNA sequence to a putative role within the centromere.

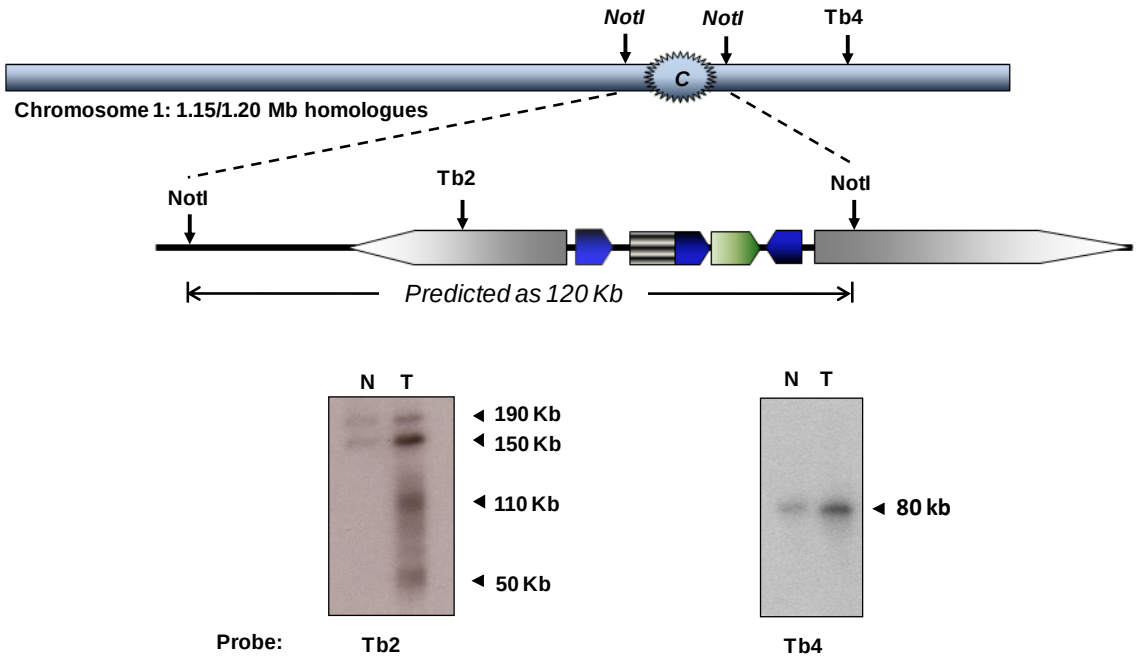

Figure 4.1.6. ***Fine-mapping topoisomerase-II mediated cleavage.***
Southern blot of *in-situ Not*I digested DNA embedded in agarose blocks, for both non-treated etoposide parasites (lane N) and parasites treated with 500 µM etoposide for 1 hour (lane T). The schematic shows the organization of the chromosome 1 centromeric region with directional gene arrays (shaded grey), retrotransposons (blue), a rRNA array (green) and the AT-rich repeat region (black/white striped box). Probe Tb2 is located within the mapped centromeric *Not*I "120 kb" restriction fragment and was used in an attempt to accurately map cleavage products. Tb4 is located away from the centromere and is shown as a control.

Despite the size variation, it is interesting that at the higher resolution achieved by fine-mapping, distinct topoisomerase-II cleavage products appear as bands within a smear (Figure 4.1.6). This suggests that topoisomerase-II can act on the DNA at discreet and prescribed sites, spread over a defined region. This potentially means there is some feature that very specifically guides topoisomerase-II localization and activity, which may be DNA or other epigenetic factors.

4.1.3 Mapping *T. brucei* mini-chromosomes

T. brucei have around 100 linear mini-chromosomes at around 100 kb in size (Section 1.5.1) (Van der Ploeg et al., 1984). These mini-chromosomes have been shown to be faithfully segregated during mitosis (Alsford et al., 2001; Zomerdijk et al., 1992). To investigate whether the mini-chromosomes possessed a centromere feature analogous to the megabase chromosomes, the etoposide mediated topoisomerase-II DNA cleavage technique was applied to these chromosomes. The principle was that any DNA or epigenetic marker of a megabase chromosomal centromere which guides the accumulation of topoisomerase-II could also apply similarly to potential centromeres on the abundant mini-chromosomes.

Procyclic *T. brucei* cultures were treated with etoposide (Section 3.1.3) and their chromosomes were embedded in agaraose blocks as before (Section 3.2.3). The chromosomal separation conditions by CHEFE were designed specifically for resolution of the much smaller mini-chromosomes, while preventing any lower molecular weight fragments from running beyond the end of the gel (Section 3.4.2). A single unit of the 177 bp inverted repeat region that constitutes over 80% of a mini-chromosome (Sloof et al., 1983) was cloned and used as a probe to detect the mini-chromosomes on a Southern blot of the CHEFE gel (TbMini, Section 3.6.1).

A Southern blot of the resulting CHEFE gel probed with TbMini, revealed that under these separation conditions many of the mini-chromosomes concentrate as a major band, although the probe also detected the intermediate chromosomes to a lesser extent. A comparison between the control gel lane containing chromosomes from an untreated *T. brucei* culture, with the experiment lane of chromosomes from etoposide treated parasites, displays no evidence of topoisomerase-II mediated DNA cleavage products

derived from the mini-chromosomes of etoposide treated parasites (Figure 4.1.7). To confirm the effectiveness of the etoposide treatment, this same Southern blot membrane was stripped of the TbMini probe (Section 3.8.4), and re-probed with Tb1 of the megabase chromosome 1. As expected, this displayed the same sized etoposide mediated cleavage product observed in a previous experiment (Section 4.1.1).

The lack of observable etoposide mediated DNA cleavage products demonstrates a lack of topoisomerase-II accumulation and activity on the mini-chromosomes. This in turn suggests that the characteristic centromeric domains of the megabase chromosomes that recruit topoisomerase-II are missing on the mini-chromosomes. Therefore it seems unlikely that the mechanism for segregating the mini-chromosomes is completely identical to that of the megabase sized chromosomes, at least in terms of centromere composition, and may even be centromere-independent.

A centromere-independent mechanism would be in agreement with a previous study. This showed that during mitosis an insufficient number of microtubules were observed to segregate the full complement of *T. brucei* chromosomes through the classical mechanism. Instead the authors propose that multiple mini-chromosomes are 'stacked' laterally on opposing microtubules potentially though chromatin interactions (Gull et al., 1998). This mechanism would not require the assembling of a kinetochore structure and would therefore not require a centromere.

It cannot be excluded however that tiny DNA cleavage fragments were lost, and any cleavage products detected with the TbMini probe were un-resolved from the whole mini-chromosomes, as a consequence of topoisomerase-II activity localized towards the telomeres of these chromosomes. In this instance, centromeres of the mini-chromosomes would be located at sub-telomeric loci and would be un-detectable with this experimental system.

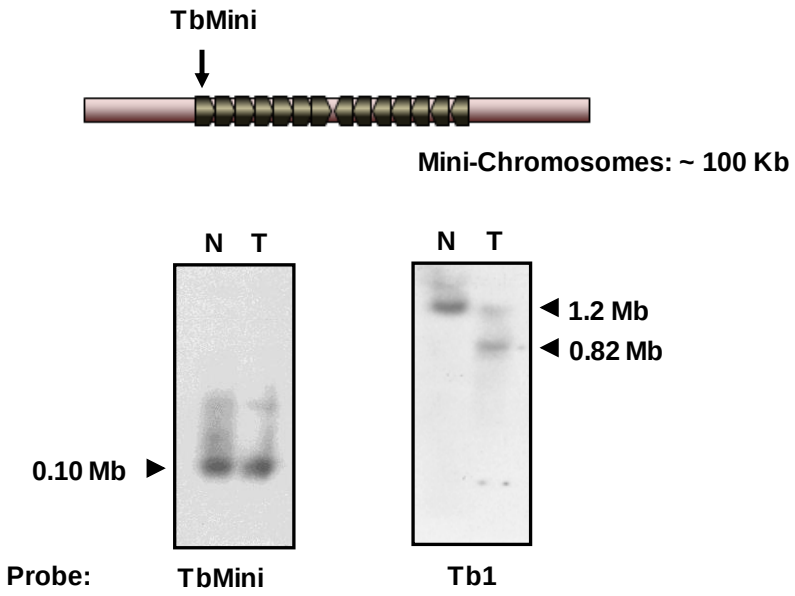

Figure 4.1.7. ***Topoisomerase-II activity at the mini-chromosomes.***
A Southern blot of CHEFE separated *T. brucei* chromosomes extracted from non-treated etoposide parasites (lane N) and parasites treated with 500 µM etoposide for 1 hour (lane T). The chromosomal separation was performed using conditions optimised for resolution of the mini-chromosomes (Section 3.4.2). The mini-chromosomes were probed with a cloned single unit of a repeat sequence common to all mini chromosomes (TbMini, marked brown; Section 3.6.1). This repeat is also found to a lesser extent on the slower migrating intermediate sized chromosomes, and is visible on the blot. Analysis of the Southern blot shows no apparent etoposide mediated topoisomerase-II activity on the mini-chromosomes, which would result in the generation of lower molecular weight cleavage products. To demonstrate the effective inhibition of topoisomerase-II by etoposide, this membrane was stripped of the TbMini probe (Section 3.8.4), and re-probed with Tb1. This revealed the corresponding chromosome 1 cleavage product of the expected size (see Figure 4.1.2).

4.2 Biochemical Mapping of *L. major* Centromeres

4.2.1 *L. major* chromosome 32 centromere mapping

Given the success of topoisomerase-II based biochemical mapping of centromeres in *T. brucei*, similar experiments were attempted in *L. major* Friedlin. Earlier research appeared to validate the strategy of applying etoposide to *Leishmania* to generate topoisomerase-II mediated DNA cleavage products. For example, experiments using *L. donovani* promastigotes treated with 100 µM etoposide resulted in the linearization of kDNA (Mittra et al., 2000), demonstrating that etoposide can successfully enter this parasite. Also, topoisomerase-II has been identified in *L. donovani*, where the recombinant enzyme was shown to decatenate kDNA *in vitro* (Sengupta et al., 2003).

Importantly, further experiments with this same topoisomerase-II showed etoposide was an effective inhibitor of topoisomerase-II ATPase activity within an *in vitro* assay, using both a recombinant truncated enzyme (Sengupta et al., 2005a), and full length topoisomerase-II (Sengupta et al., 2005b). This indicated that etoposide would mediate the formation of irreversible chromosomal DNA lesions within this parasite.

The preliminary experiments performed here focused on obtaining the optimum treatment conditions to detect etoposide mediated topoisomerase-II DNA cleavage products. *L. major* has 36 chromosomes ranging from 0.28 to 2.8 Mb (Section 1.5.3) (Ivens et al., 2005). Probes were cloned specific to chromosome 12 (syntenic with *T. brucei* chromosome 1 and *T. cruzi* chromosome 3) and chromosome 32 (syntenic with *T. brucei* chromosome 11 and *T. cruzi* chromosome 1). These 2 chromosomes were selected due to the available results of both biochemical mapping experiments in *T. brucei* and *T. cruzi,* alongside the mitotic stability data from *T. cruzi* (Obado et al., 2007; Obado et al., 2005). Treatments of parasites ranging from 100 µM etoposide for 30 minutes, to 1 mM etoposide for 1 hour resulted in no cleavage product bands (Figure 4.2.1b) with the chromosome 32 probe (Section 3.6.1). Indeed even low levels of smearing in treated lanes characteristic of previous experiments with high etoposide concentrations appeared absent. Similar results when probing for chromosome 12 were observed (data not shown).

Further experiments using amsacrine, another anti-cancer agent well characterised as a topoisomerase-II inhibitor (Zwelling et al., 1985), and chlorpromazine, implicated in inhibiting *E. coli* topoisomerase-I activity (Mizushima et al., 1992) were employed. Whereas etoposide inhibits topoisomerase-II facilitated DNA re-ligation, by directly binding to the active site of the enzyme (Chen et al., 1984), amsacrine intercalates within the DNA (Nelson et al., 1984) and appears to prevent the active site of topoisomerase-II from effectively interacting with the cleaved DNA by impeding the catalytic tyrosine residue from performing the re-ligation step (Rogojina and Nitiss, 2008). This alternative type of inhibition also results in the formation of topoisomerase-II mediated double stranded DNA breaks. Chlorpromazine is a less studied DNA intercalating compound, and is structurally related to amsacrine. It has been shown to

display greater cytotoxicity against *L. donovani* than either etoposide or amsacrine (Werbovetz et al., 1992), suggesting it may prove to be a more potent topoisomerase-II inhibitor within *Leishmania*.

Neither amsacrine nor chlorpromazine had any detectable effect in poisoning topoisomerase-II and generating DNA lesions in *L. major* using the established experimental system, even at concentrations of 500 µM for 4 hours (Figure 4.2.1c). This compares to previous experiments performed in the laboratory using these 2 drugs with *T. cruzi*, where intense, but non-specific lesions induced by drug treatment appeared to be easily generated.

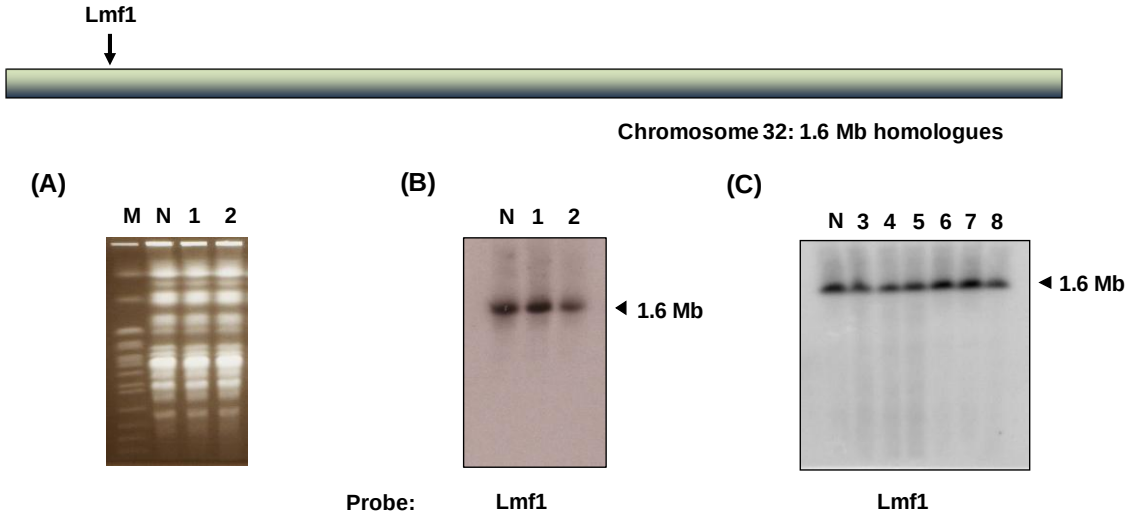

Figure 4.2.1. ***Attempts to generate topoisomerase-II mediated DNA cleavage in L. major.***
A Southern blot of CHEFE separated chromosomes from etoposide treated parasites **(A)** showed no cleavage products **(B)** from the standard 100 µM etoposide treatment for 30 minutes (lane 1) compared with untreated parasites (lane N). Increasing the etoposide treatment to 1 mM for 1 hour also generated no cleavage products (lane 2). Etoposide analogues that had previously resulted in indiscriminate chromosome cleavage in *T. cruzi* were used to treat *L. major* **(C)**. Amsacrine at concentrations 100 µM for 1 hour (lane 3), 500 µM for 1 hour (lane 4), and 500 µM for 4 hours (lane 5), as well as chlorpromazine at 100 µM for 1 hour (lane 6), 500 µM for 1 hour (lane 7), and 500 µM for 4 hours (lane 8) showed no evidence of either localized or general chromosome cleavage.

Taken together, the results of the preliminary drug treatments in *L. major* suggest that the *L. major* topoisomerase-II enzyme is refractory to poisoning by etoposide, amsacrine and chlorpromazine. This appears to contradict the earlier work which showed etoposide successfully inhibited *L. donovani* topoisomerase-II activity *in vitro* (Sengupta et al., 2005b). However, BLAST analysis of the *L. donovani* topoisomerase-II used by this group (GenBank ID: AF150876) against the annotated *L. major* genome database suggests they examined the mitochondrial topoisomerase-II isoform (95% amino acid identity; *L. major* GeneDB ID: LmjF.15.1290), and not the nuclear isoform (28% amino acid identity; *L. major* GeneDB ID: LmjF.28.2280). Although a detailed biochemical analysis has been performed with the *L. donovani* topoisomerase-II, no localization data has yet been presented in the literature to confirm the physiological activity of their topoisomerase-II isoform. If etoposide is only inhibiting the mitochondrial isoform, it would explain the resulting linearized DNA within the mitochondrion of etoposide treated *L. donovani* promastigotes (Mittra et al., 2000), and also the lack of nuclear DNA cleavage observed here in *L. major*. That nuclear *L. major* topoisomerase-II appears refractory to etoposide, may also occur in *L. donovani*, where IC_{50} values for etoposide and amsacrine could not be established at drug concentrations up to 100 µM (Werbovetz et al., 1992). If these compounds were successfully inhibiting nuclear topoisomerase-II, it could be expected that the resulting double stranded breaks in the genome would be fatal to the parasite. Although chlorpromazine is toxic to *L. donovani*, and has been shown to actively generate double stranded DNA breaks in mouse cells (Darkin et al., 1984), this compound has not been subjected to such a detailed analysis as etoposide and amsacrine, and may be generating cytotoxicity via alternative mechanisms.

Alternatively it could also be possible that the segregation of *L. major* occurs by a centromere-independent mechanism. Bioinformatic analysis of *L. major* chromosomes 12 and 32 with Artemis (Section 3.7.1) revealed no features that resembled either the AT-rich domain characteristic of a *T. brucei* centromere, or a GC-rich region observed in the *T. cruzi* centromeres. While these do not necessarily define a centromere in themselves, it is interesting that these very different DNA features are nonetheless

present in *T. brucei* and *T. cruzi*, while *L. major* appears to lack any noticeable features with respect to %GC skew.

Previous studies in *L. major* on chromosome 1, have shown that the only strand-switch region between the two polycistrons present on that chromosome, is not required for mitotic stability (Dubessay et al., 2002a). This contrasts with our findings on the strand-switch localized centromeric regions that are required for mitotic stability in *T. cruzi* (Obado et al., 2007; Obado et al., 2005). A further study by this group with a chromosome 1 derived, smaller artificial chromosome, supported this finding, and suggested that sub-telomeric regions possessing a relatively higher AT content may be involved in mitotic stability (Dubessay et al., 2002b), This was disputed by another group, who failed to identify these small sub-telomeric regions or similar domains, in a mitotic stability library screen of genome fragments incorporated into an artificial chromosome (Casagrande et al., 2005). Other attempts to identify characteristic centromeric domains in *L. donovani* have also proved elusive. Mitotic stability analysis through chromosome fragmentation yielded minimal sized chromosomes capable of faithful segregation, however analysis of either truncated native chromosomes (Tamar and Papadopoulou, 2001), or a truncated artificial chromosome (Dubessay et al., 2001), have so far failed to identify a definitive centromeric domain in *L. donovani*.

4.3 Chapter Summary

Biochemical mapping experiments using etoposide mediated topoisomerase-II DNA cleavage II have demonstrated:

- DNA cleavage foci are observed at unique AT-rich repeat domains in the 3 *T. brucei* chromosomes examined here (chromosomes 1, 2 and 5).
- The sites of etoposide-mediated DNA cleavage in *T. brucei* chromosome 1 and the biochemically mapped cleavage region of *T. cruzi* chromosome 3 are syntenic. This region of *T. cruzi* chromosome 3 also corresponds to a region required for mitotic stability (Obado et al., 2007).
- Topoisomerase-II based fine mapping using a restriction fragment encompassing the *T. brucei* chromosome 1 AT-rich domain, showed a discrete pattern of DNA cleavage bands. Also, the restriction fragments derived from this region are larger than predicted from the database.
- No etoposide-mediated DNA cleavage of the *T. brucei* mini-chromosomes was observed, consistent with the hypothesis that these may segregate through an alternative mechanism (Gull et al., 1998).
- Experiments in *L. major* yielded no detectable drug mediated DNA cleavage of any kind, suggesting either etoposide cannot interact with *L. major* topoisomerase-II, or that the nature of chromosome segregation, including the role of topoisomerase-II, is not conserved between trypanosomatids.

4.4 Discussion

In this chapter, three centromeric domains of *T. brucei* chromosomes have been biochemically mapped using etoposide mediated topoisomerase II cleavage experiments to AT-rich repeat regions. The AT-rich nature of the *T. brucei* centromeres is similar to those centromeres described for *S. cerevisiae*, *S. pombe*, *Drosophila*, *P. falciparum* (relative to the genome average) and human centromeres. An increase in AT-richness at the centromere appears fairly common in the various organisms studied to date, but by no means is it the rule. Plant centromeres such as those of *Arabidopsis* and rice contain no alteration in AT/GC content (Section 2.2.1), and *T. cruzi* display a GC-rich domain as opposed to an AT-rich region (Obado et al., 2007). Recently, the biochemical technique employed here was used to map the centromeric domains of *Toxoplasma gondii*, which revealed this organism also lacked any nucleotide bias in their centromere composition (Brooks et al., 2011). Therefore, although a nucleotide bias could potentially alter the DNA secondary structure at the centromere and contribute to a physical designation of a centromeric domain, it may alternatively be that these domains are simply susceptible to shifts in codon bias as they are non-gene coding regions. Susceptibility to a drift in nucleotide bias in this region due to an absence of selective pressure on genome maintenance may also explain the accumulation of retro-elements observed in *T. brucei* (Section 4.1.1), as well as in plants and metazoans (Section 2.2.1).

Consistent with the observations made in many of the model systems, the centromeric repeats in *T. brucei* vary in sequence across chromosomes, and therefore no single DNA sequence appears to define a centromere in this organism (Figure 4.4.1). It seems likely that centromeres in *T. brucei* are instead defined epigenetically by chromatin structure, despite the absence of the characteristic CENP-A histone variant (Section 2.2.2). This puzzle raises the question of what then is the defining marker, and is this marker for kinetochore assembly the same as that which guides topoisomerase-II accumulation? It is conceivable that the designation of a centromere could occur through the post-transcription modifications of canonical histones within the centromere, in a similar fashion to that of transcriptional start site markers (Siegel et al., 2009).

Another hypothesis would be that a novel DNA binding protein defines a centromere, and its location is maintained through epigenetic inheritance. Either result would support the founding hypothesis that the mechanism of chromosome segregation varies between *T. brucei* and the mammalian host.

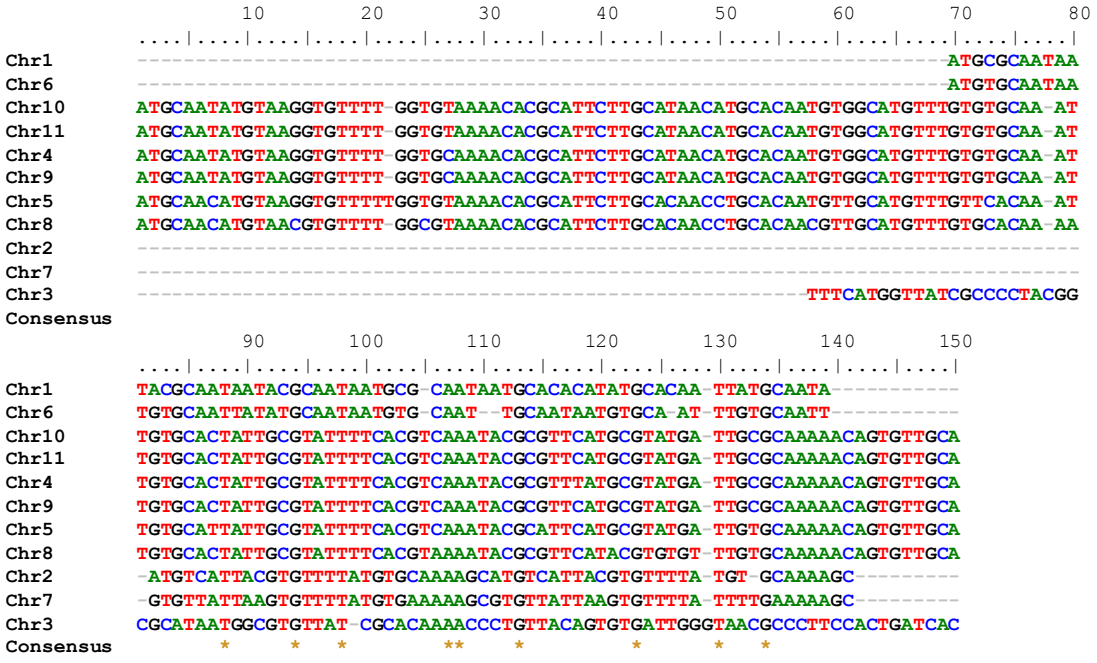

Figure 4.4.1. ***Complete alignment of AT-rich centromeric DNA repeat sequences.*** The software Tandem Repeat Finder (Benson, 1999) was used to identify consensus repeat units within the AT-rich region for each chromosome. These were aligned with ClustalW (Thompson et al., 1994). In generating this alignment, 2 units of the array were used for chromosomes 1, 2, 6 and 7. These units were much smaller (~30 bp), relative to the unit sizes of the other chromosomes (~150 bp). A high degree of similarity can be observed between the repeat units of chromosomes 4, 5, and 8-11, as well as clear similarity between chromosomes 2 and 7 (Obado et al., 2007).

The caveat remains that due to the repetitive nature and length of centromeric domains it is difficult to accurately sequence across the whole region and correctly assemble the resulting contigs, so it would be possible to miss a small *S. cerevisiae*-like 'point' centromere hidden amongst the repeats. This difficulty in assembly is highlighted by a restriction digest based fine-mapping experiment of *T. brucei* chromosome 1 (Section

4.1.2), which showed that the domain corresponding to a centromere is much larger than reported in the genome project. A difference between fragment sizes for the chromosome homologues of around 40 kb would also explain the difference in homologue sizes, as opposed to the previous proposal that size variations between sub-telomeric regions are the cause of these size variations (Callejas et al., 2006). A further experiment with chromosome 4 of *T. brucei* also identified larger than expected restriction digest fragments with a 10 kb difference between homologues (Obado et al., 2007). This secondary finding supports the original observation as genuine, rather than it being an experimental artefact as the result of an altered restriction site through a nucleotide polymorphism. It will be interesting to see if the nine yet to be analysed centromeres also contain longer than currently reported repeat regions, and whether the composition of these full length sequences are consistent in repeat formations, or if new embedded sequences are identified.

Once the mini-chromosomes have been duplicated, they seem to be faithfully segregated. While this process has been shown to be microtubule dependent (Ersfeld and Gull, 1997), the actual mechanism is still unknown. The biochemical evidence reported here supports the role for a non-classical kinetochore based mechanism, since there is no specific site attracting topoisomerase-II activity on the mini-chromosomes (Section 4.1.3), which is in agreement with the 'lateral stacking model' of mini-chromosomes on microtubules (Gull et al., 1998). During early anaphase, standard model kinetochores associate with the polar end of the microtubules, yet the lateral stacking model proposes that mini-chromosomes associate along the length of the microtubule polymer as it contracts during chromosome segregation. However, this leaves open the question of how do mini-chromosomes associate along the length of a tubulin polymer? This proposal is not as radical as it may first seem, as part of the general 'search and capture' mechanism of microtubules connecting to the assembled kinetochore begins with a lateral association of chromosomes to the microtubule polymer, followed by a migration towards the polar end (Tanaka et al., 2005). To achieve a kinetochore-microtubule attachment either an adapter complex must connect the DNA to tubulin, potentially through the existing chromatin, or alternatively DNA and microtubules could be tied together by a cohesin-like ring complex. A similarly

structured complex has been observed before in *S. cerevisiae*, when a 10 protein DASH complex formed an oligomer ring around microtubules *in vitro* (Miranda et al., 2005), which may potentially create a chromosomal tether *in vivo* (Buttrick and Millar, 2011). It is possible a similar structure may facilitate the lateral microtubule based segregation of the *T. brucei* mini-chromosomes.

While the biochemical technique of mapping the *T. brucei* megabase chromosomes proved successful, as well as the parallel mapping of *T. cruzi* chromosomes (Obado et al., 2007), this technique failed to identify any centromeres on *L. major* chromosomes. As discussed previously (Section 4.2.1), this could be due to the technical limitation of etoposide not being effective against *L. major* topoisomerase-II. Alternatively it may be that topoisomerase-II activity is not required at mitosis for *L. major*, perhaps due to the smaller nature or their chromosomes, or maybe chromosomes in this organism are segregated differently. If it is the latter, this raises the possibility that the mechanism used to segregate *L. major* chromosomes could be similar to the *T. brucei* mini-chromosomes, through a lateral stacking of chromosomes along microtubules. Investigating whether chromosome segregation in *L. major* is based on the classical microtubule spindle mechanism involving kinetochores assembled on centromeres remains a challenge.

5 Characterization of Topoisomerase-II

T. cruzi and *L. major* both possess one nuclear isoform of topoisomerase-II, however it has been shown that *T. brucei* has two isoforms of this enzyme (Kulikowicz and Shapiro, 2006) designated topoisomerase-IIα and topoisomerase-IIß. This chapter explores the roles of the two *T. brucei* topoisomerase-II isoforms at the centromere in bloodstream form *T. brucei*, and addresses the unknown mechanism in which centromere specific targeting is achieved.

5.1 The *T. brucei* Topoisomerase-II Nuclear Isoforms

The GeneDB database erroneously records only one entry for a nuclear topoisomerase-II (Tb11.01.3390) in *T. brucei*, which is a fusion between the N-terminus of the α-isoform and the C-terminus of the ß-isoform. Previously it has been demonstrated by RNAi experiments that in the insect procyclic stage, only the α-isoform is essential for growth (Kulikowicz and Shapiro, 2006). In addition, western blotting of cell extracts with a ß-isoform specific antibody showed that it appeared not to be expressed in the procyclic form. Also, the same authors found that recombinant topoisomerase-IIß appeared inactive by *in vitro* decatenation assays. The discovery that nuclear topoisomerase-II has two isoforms in *T. brucei*, raises the questions: which isoforms are essential, and responsible for the centromere specific DNA cleavage, in the clinically relevant bloodstream stage?

5.1.1 RNAi knockdown of topoisomerase-II in bloodstream form *T. brucei*

Topoisomerase-II contains four designated domains as shown in Figure 5.1.1. The ATPase, linker, and catalytic domains are highly conserved between trypanosomatids, however this conservation appears absent in regard to the variable domains (Appendix Figure 10.1.1). By taking advantage of the underlying variation in DNA sequence of the C-terminal variable domain of topoisomerase-II it is possible to distinguish between the α- and ß- isoforms, and indeed between these, and the *T. cruzi* and *L. major* homologues. This difference in the C-terminal variable domain can be exploited to clone specific sequences to generate RNAi mediated knockdown of either topoisomerase-II

isoform, or to produce isoform and species specific DNA probes for Southern and northern blotting.

Firstly to determine if either topoisomerase-II isoforms are essential for growth in the bloodstream form stage, RNAi mediated knockdown of both genes was performed independently. To generate effective RNAi mediated knockdown of *T. brucei* topoisomerase-IIβ, the *T. brucei* 427 strain featuring the hygromycin-tagged ribosomal spacer locus (2T1/TAG^{PURO} cell-line) was used in conjunction with the tetracycline regulated RNAi stem-loop plasmid pRPa^{iSL} (Alsford and Horn, 2008). A 600 bp DNA fragment specific to the variable domain of topoisomerase-IIß was amplified and cloned head-to-head into the stem-loop plasmid (Section 3.6.2) to generate pRPa^{iSL}-TopoIIβ (Figure 5.1.2). This plasmid was linearized with *Asc*I, purified, and used to transform the *T. brucei* 2T1/TAG^{PURO} cell-line.

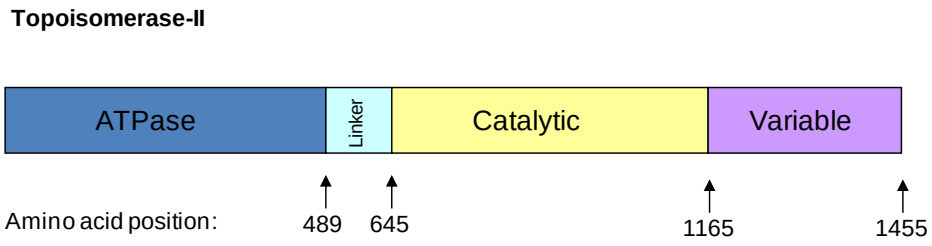

Figure 5.1.1. ***Illustration of the different topoisomerase-II domains.***
A typical topoisomerase-II enzyme contains four distinct domains. The ATPase domain is connected by a small linker domain to the catalytic DNA cleavage and re-ligation domain. The C-terminal variable domain's function is unknown. The sizes of each domain are based on *T. brucei* topoisomerase-IIα (Kulikowicz and Shapiro, 2006). Although around 85-90% amino acid sequence identity is observed between the first three domains of *T. brucei* topoisomerase-IIα and topoisomerase-IIβ, the identity between variable domains is reduced to only 23%. This identity between respective domains is maintained in further comparisons with the *T. cruzi* and *L. major* topoisomerase-II.

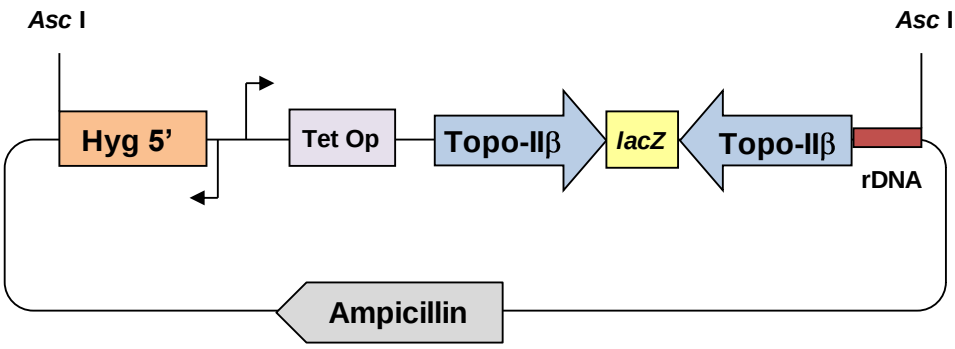

Figure 5.1.2. ***An RNAi construct for topoisomerase-IIβ.***
Two identical 600 bp DNA fragments of the unique 3' region of *T. brucei* topoisomerase-IIβ were cloned head to head to form a stem-loop RNAi fragment, separated by a lacZ stuffer into pRPa^{iSL} to facilitate tetracycline induced RNAi, driven by a rRNA promoter (Section 3.6.2). The resulting pRPa^{iSL}-TopoIIβ plasmid (linearized by *Asc*I digest) integrates into the tagged locus of the 2T1/TAG^{PURO} cell-line using the targeting 5' region of the hygromycin resistance gene to generate a complete resistance gene integrated into the chromosome (Alsford and Horn, 2008).

A drug-resistant topoisomerase-IIß RNAi clone selected on hygromycin was chosen for analysis, in parallel with a cell-line generated by Dr. Obado designed to knockdown the topoisomerase-IIα isoform (Obado et al., 2011). The effect of RNAi mediated knockdown of the 2 topoisomerase-II isoforms on parasite proliferation was studied first.

The two RNAi cell-lines representing the two topoisomerase-II isoforms were split into two cultures each. For a given cell-line, one of these cultures was supplemented with 1 μg ml^{-1} tetracycline to induce RNAi knockdown, while the other culture remained in standard growth medium as a negative control. Parasites of both cell-lines were seeded at 1 x 10^5 ml^{-1} and grown for 4 days in parallel and free of selective drug pressure. They were counted every 24 hours with a haemocytometer and then diluted back to 1 x 10^5 ml^{-1} at each daily time point. No change in growth rate of the topoisomerase-IIß RNAi cell-line was observed when RNAi was induced over a 4 day period, relative to the non-induced lineage. This contrasted with the topoisomerase-IIα experiment, where growth rate ceased within 24 hours of RNAi induction, followed by cell death (Figure 5.1.3a). Over 7 days, no phenotypic effect was observed as a result of topoisomerase-IIβ knockdown. After 5 days, outgrowth was observed in the cultures where topoisomerase-

IIα had been depleted, presumably as a consequence of the selection of revertants (data not shown). This phenomenon is common in RNAi experiments, especially when essential genes are targeted in the bloodstream form (Chen et al., 2003).

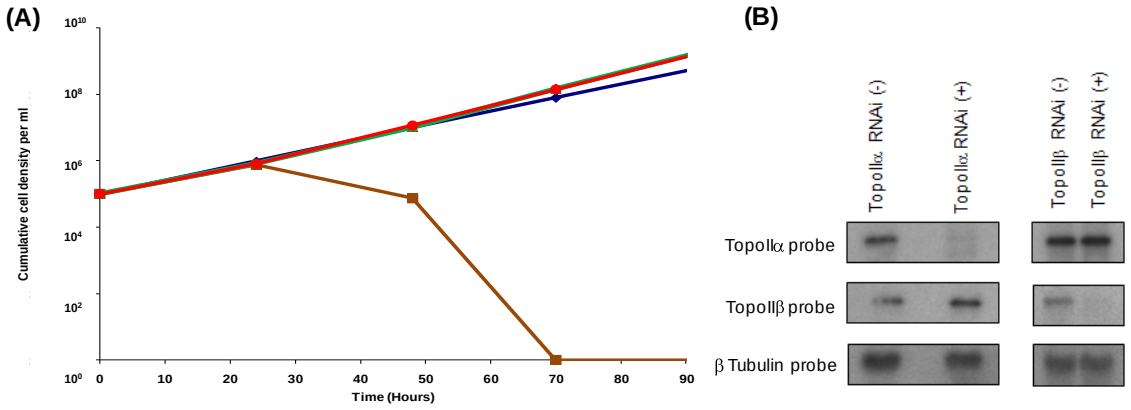

Figure 5.1.3. ***Topoisomerase-IIα, but not topoisomerase-IIβ, is essential for growth of bloodstream form T. brucei.***
(A) Cumulative growth plots of two *T. brucei* bloodstream form cell lines modified to facilitate specific inducible RNAi mediated knockdown of topoisomerase-IIα (Obado et al., 2011) and topoisomerase-IIβ by targeting their respective variable domains (Section 3.6.2). Cells were counted every 24 hours by haemocytometer then diluted back to 1 x 10^5 ml^{-1} with expression of the hairpin looped transcript initiated using 1 µg ml^{-1} tetracycline (Section 3.1.3). Only the topoisomerase-IIα isoform was found to be essential for growth of bloodstream forms, with cell death occurring after 24 hours (topoisomerase-IIα: blue line untreated, brown line tetracycline treated). Down-regulation of topoisomerase-IIβ appeared to have no effect on parasite growth (topoisomerase-IIβ: green line untreated, red line tetracycline treated). **(B)** Northern blots of RNA isolated 28 hours after RNAi induction were probed with isoform-specific fragments derived from the variable regions (Section 3.6.2), and with β tubulin as a loading control, to demonstrate appropriate RNAi knockdown respective to non-induced cell lines.

To demonstrate effective RNAi knockdown, RNA was isolated from both RNAi induced and un-induced cell-lines of the α- and ß- isoforms, separated by electrophoresis, and blotted. These northern blots were probed with the fragments specific to each isoform, which were isolated from the RNAi constructs (Section 3.6.2). The blots showed that both the α- and ß- isoform mRNA transcript levels were effectively reduced (Figure 5.1.3b). Both blots were probed with ß-tubulin to show equal loading of the gel. These results show that topoisomerase-IIα is essential for

growth in bloodstream from parasites, in addition to the procyclic stage (Kulikowicz and Shapiro, 2006).

Next, the two RNAi cell-lines were investigated using the etoposide mediated cleavage technique. This has the advantage that topoisomerase-II activity can be assessed under physiological conditions to provide an insight into the roles of the two isoforms at the centromere. Given that the tagged locus cell-line is of the *T. brucei* 427 strain, whose karyotype is different to that of the *T. brucei* 927 strain used for genome sequencing (Melville et al., 2000), cleavage products obtained after etoposide mediated cleavage will not necessarily be identical in size to previous centromere mapping experiments.

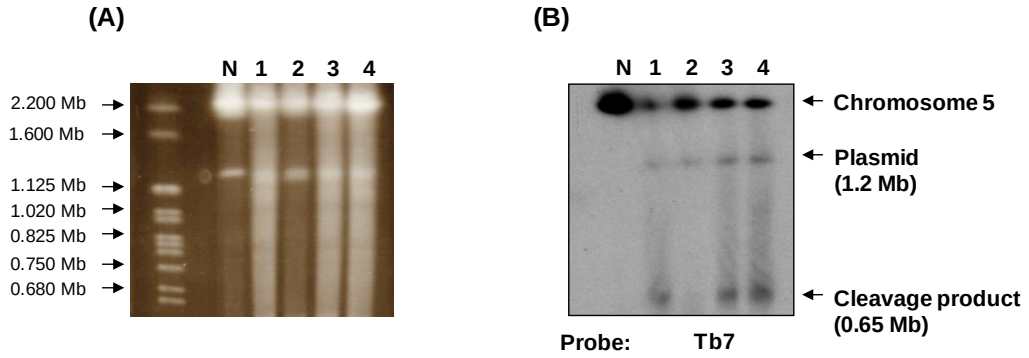

Figure 5.1.4. ***Topoisomerase-IIα, but not topoisomerase-IIβ generates chromosomal cleavage fragments.***
Etoposide mediated DNA cleavage experiments were performed on both the topoisomerase-IIα and topoisomerase-IIβ RNAi cell-lines, with a non-etoposide treated wild-type *T. brucei* 427 (lane N) as a control. Lanes 1 and 2 contain chromosomes extracted from etoposide treated cultures of the topoisomerase-IIα RNAi cell-line, while lanes 3 and 4 contain chromosomes extracted from etoposide treated cultures of the topoisomerase-IIβ RNAi cell-line (Section 3.1.3). Lanes 2 and 4 are from the stated cultures further supplemented with 1µg ml^{-1} tetracycline for 28 hrs to initiate the gene specific RNAi, before chromosome extraction (Section 3.2.3). The ethidium bromide stained gel (**A**) shows most of the chromosomes of this strain migrate in the non-resolved region of the gel under these separation conditions (0.2 - 2.0 Mb), within the gel compression zone. Sizes are interpolated from *S. cerevisiae* chromosomal markers (Section 3.4.2). The light coloured smearing observed in lanes 1, 3, and 4 are characteristic of lanes containing chromosomes derived from etoposide treated cultures. The Southern blot of the gel (**B**) demonstrates this more clearly, as the consequence of etoposide mediated cleavage results in a cleavage product of 0.65 Mb when probed with the Tb7 probe of chromosome 5. In this strain chromosome 5 is predicted to be 2.0 Mb in size (Melville et al., 2000). When topoisomerase-IIα transcript levels are reduced under tetracycline treatment, this cleavage product is no longer produced (lane 2 compared with lane 1). Conversely when topoisomerase-IIβ transcript levels are reduced, the cleavage product remains (lane 4 compared with lane 3). The 1.2 Mb band observed in the 4 lanes of the genetically modified cell-lines, and absent in the wild-type control lane, results from contaminating plasmid DNA hybridising to the tagged rDNA locus of chromosome 2a (Alsford and Horn, 2008).

Chromosomes from wild-type *T. brucei* 427 were embedded in agarose blocks, as well as chromosomes from the topoisomerase-IIα and topoisomerase-IIß RNAi cell-lines treated with 100 µM etoposide for 30 minutes. Another set of chromosome embedded blocks were prepared from both of these cell-lines following treatment with 1 µg ml^{-1} tetracycline induction for 28 hours, and then 100 µM etoposide for 30 minutes, just before chromosome extraction. These chromosomes were fractionated in parallel by CHEFE, blotted, and hybridised with the previously used Tb7 probe. Etoposide treatment of the un-induced topoisomerase-IIα RNAi cell-line generated a cleavage product of 0.65 Mb, however no cleavage was observed when topoisomerase-IIα had

been knocked down (Figure 5.1.4). In contrast, when the topoisomerase-IIß was depleted, the cleavage product remained. This shows that it is specifically the topoisomerase-IIα isoform that is responsible for cleavage at the centromere. In addition, given that knockdown of topoisomerase-IIα, but not topoisomerase-IIβ coincides with a loss of smearing in the ethidium bromide stained gel, it seems likely that only topoisomerase-IIα is active along the full length of chromosomes in this life-cycle stage. With the near identity of the protein sequence of the catalytic domain in the two isoforms (Appendix Figure 10.1.1), it is unlikely that etoposide inhibits only the α-isoform.

5.1.2 Localizing *T. brucei* topoisomerase-IIα

With the observation that only topoisomerase-IIα appears active at *T. brucei* centromeres the next experiment was to clearly demonstrate nuclear localization. This may appear superfluous, since if an enzyme is shown to be active on chromosomes within live cells, it is implicit it would be targeted to the nucleus. However, demonstrating this fact and establishing the system is an important first step into dissecting the mechanism by which topoisomerase-IIα is targeted to the nucleus, and more interestingly, focused towards the centromere in a cell-cycle specific manner.

A strategy was devised to knockout one topoisomerase-IIα allele, while *in-situ* tagging the remaining allele at the C-terminal end with a c-myc tag facilitating immunofluorescence based localization (see Methods for experimental details). As the two topoisomerase isoforms are found in tandem, despite the database erroneously showing a single fused gene, the first hurdle was to sequence the 3' un-translated region of topoisomerase-IIα to allow the cloning of flanking regions for incorporation into gene deletion constructs. Using two primers, one specific to the 3'-end of the topoisomerase-IIα gene, the other primer to the conserved 5'-end of topoisomerase-IIß, the intergenic region was amplified using high fidelity DNA polymerase (Section 3.6.3). However, this revealed that the sequence of the 3' un-translated region of topoisomerase-IIα is identical to the 3' un-translated region of topoisomerase-IIß, possibly as a consequence of gene duplication. Therefore a gene disruption, rather than a gene replacement approach was taken, where the majority of the catalytic region was removed and

replaced with a drug selectable marker (see below for details). This allowed the use of the 3' end of topoisomerase-IIα to facilitate specific targeted disruption to the intended isoform.

A gene disruption plasmid containing flanking regions of topoisomerase-IIα was developed based on the blasticidin resistance cassette p^{BLA} (Rudenko et al., 1994). A 800 bp fragment of the 5' end of topoisomerase-IIα, and a 1 kb fragment of the 3' end of topoisomerase-IIα were amplified and cloned into p^{BLA} (Section 3.6.5) to make pKO^{BLA}-TopoIIα (Figure 5.1.6). The gene tagging vector $pNAT^{x12M}$ (Alsford and Horn, 2008) was modified to incorporate a 1.7 kb targeting sequence derived from the 3' end of the gene to form $pNAT^{x12M\text{-}HYG}$-TopoIIα (Section 3.6.4 and Figure 5.1.5). A targeting fragment of this size should only allow *in situ* tagging of the allele that remains undisrupted.

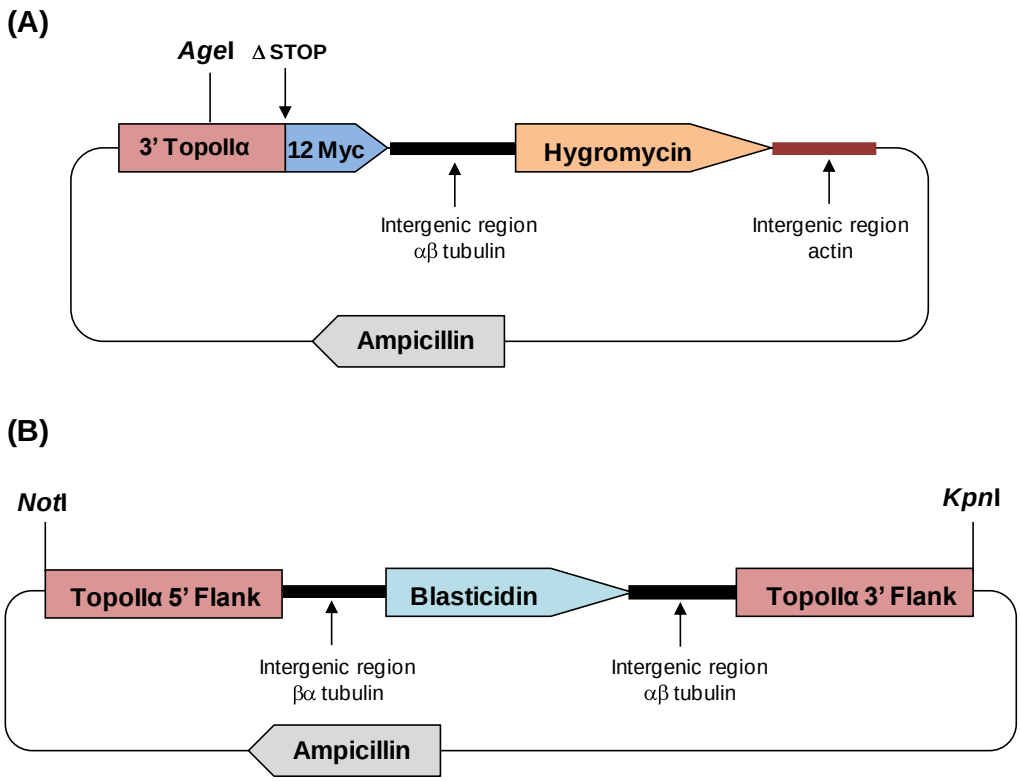

Figure 5.1.5. ***T. brucei topoisomerase-IIα localization constructs.***
Two constructs were generated to localize topoisomerase-IIα. **(A)** The plasmid pNATx^{TAG}, designed for tagging an *in-situ* gene locus with a C-terminal tag consisting of 12 consecutive c-myc epitopes (Alsford and Horn, 2008), was adapted for use here by replacing the existing drug selectable marker. Next a 1.6 kb specific 3' region of topoisomerase-IIα was cloned into this modified plasmid (Section 3.6.4), to generate pNAT$^{x12M\text{-}HYG}$-TopoIIα. The plasmid could be linearized with a unique *Age*I restriction site. **(B)** The second plasmid was designed to disrupt the second topoisomerase-IIα allele by truncating the gene, and removing the active site. An 800 bp region of the 5' end of topoisomerase-IIα and a 1 kb region of the 3' end of topoisomerase-IIα was amplified and cloned into p^{BLA} to form pKO^{BLA}-TopoIIα (Section 3.6.5). This plasmid was linearized with *Not*I and *Kpn*I restriction digests.

To generate the required cell-line for localization experiments, first the linearized gene disruption construct pKO^{BLA}-TopoIIα was electroporated into wild-type *T. brucei* 427. Blasticidin based drug selection using culture plates allowed the generation of clones (Section 3.10.1). One such clone was then immediately transfected with the linearized topoisomerase-IIα c-myc tagging construct pNAT$^{x12M\text{-}HYG}$-TopoIIα, with parasites selected on hygromycin while maintained on blasticidin drug pressure. A resulting dual-drug resistant clone was selected for analysis. Genomic DNA was extracted from this

clone, along with DNA from the single gene disruption cell-line and wild-type *T. brucei* 427 (Section 3.2.2). Restriction analysis of the topoisomerase-II region of the assembled genome (Berriman et al., 2005) showed an *Xho*I restriction site that would generate different size bands on a Southern blot for a wild-type, disrupted and tagged allele. The gene disruption of the first allele and the tagging of the remaining allele both proved successful (Figure 5.1.6), with a 4 kb increase in fragment size as a result of gene disruption, and a 6 kb increase as a result of inserting the myc-tag topoisomerase-IIα plasmid, as predicted by *in silico* restriction mapping.

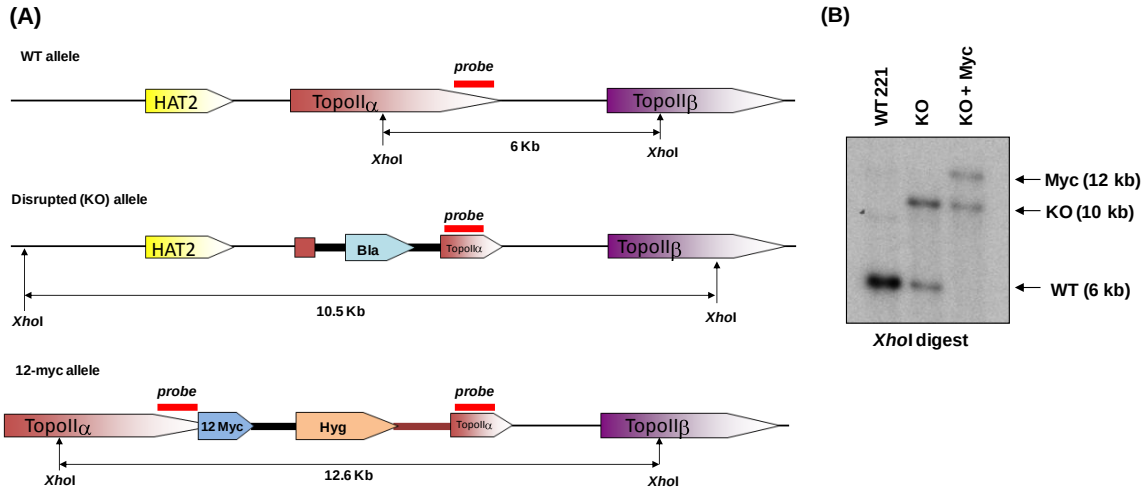

Figure 5.1.6. ***In-situ integration of tagged topoisomerase-IIα.***
Correct integration of localization plasmids was confirmed by a Southern blot probed by the specific 3' topoisomerase-IIα fragment (identified by red bar). Panel **(A)** shows the *Xho*I restriction sites affected, with the gene disruption of one allele removing the site within topoisomerase-IIα, and the locus tagging extending the region to the downstream *Xho*I site of topoisomerase-IIβ. This predicted increase in both allele fragment sizes are observed in the Southern blot **(B)**.

Localization of topoisomerase-IIα was performed by confocal immunofluorescence of bloodstream form parasites (Section 3.11). A mouse monoclonal antibody specific to the c-myc tag was incubated in conjunction with a rabbit polyclonal antibody raised against topoisomerase-IIα (a gift from the Shapiro laboratory) within permeablized cells fixed in paraformaldehyde. The concentrations of each antibody were determined empirically (Section 3.11). Secondary goat antibodies were conjugated with a green AlexaFluor (targeting the c-myc primary antibody), and a red AlexaFluor (targeting the topoisomerase-IIα primary antibody). Cells were mounted in PBS/glycerol containing DAPI to label the DNA. The images taken with a confocal microscope demonstrate that both the c-myc tag and topoisomerase-IIα specific antibodies detect topoisomerase-IIα only within the nucleus (Figure 5.1.7a). Analysis of cells in various stages of the cell-cycle showed topoisomerase-IIα localized solely to the nucleus. An example of a cell undergoing mitosis, where the kinetoplast (which replicates first, Section 2.1.1) has already doubled can be seen in Figure 5.1.7b. The distribution of topoisomerase-IIα within the nucleus appeared general, although given the small size of the trypanosome nuclei (around 5 μm), observing any punctuate patterns on individual chromosomes within the nucleus would be limited by the effective resolution of light microscopy.

These results established that c-myc *in-situ* tagging of the only intact topoisomerase-IIα allele gave a strong immunofluorescence signal with very little background. Importantly, they also demonstrate that localization and activity of topoisomerase-IIα is unperturbed by the presence of the C-terminal tag. This observation will facilitate further downstream experiments studying topoisomerase-IIα centromeric signal targeting with C-terminally tagged constructs (Obado et al., 2011).

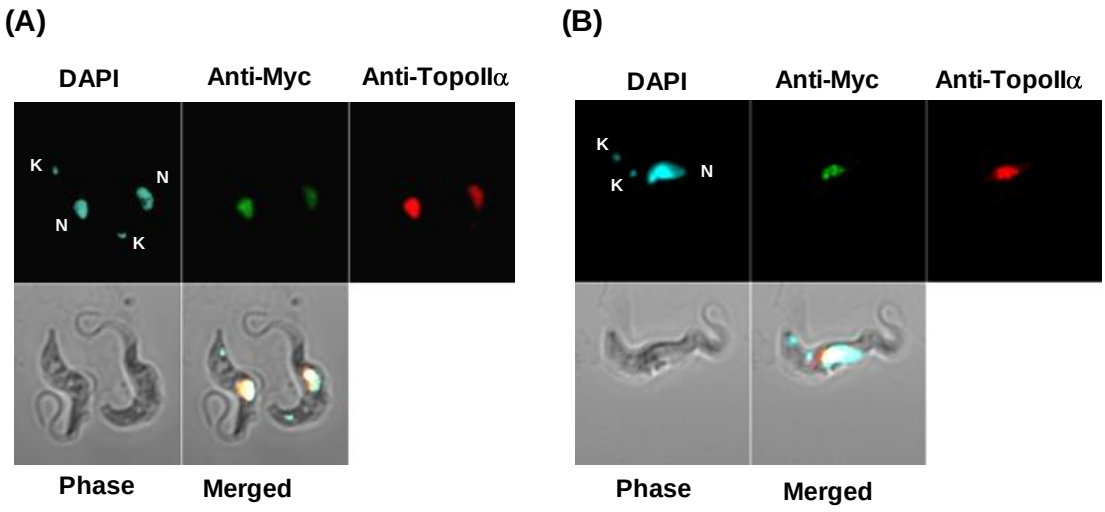

Figure 5.1.7. ***The nuclear localization of topoisomerase-IIα.***
DAPI (light blue) stains both the nucleus (N) and kinetoplast (K). Antibody labelled fluorescence to the c-myc tag (green) and native antibody labelling of topoisomerase-IIα (red) confirm localization (Section 3.11) of topoisomerase-IIα to the nucleus **(A)**. Since only the full length tagged allele is present this shows the tag does not perturb localization. Also pictured is a dividing cell **(B)** containing two kinetoplasts with topoisomerase-IIα remaining distributed around the nuclear region.

5.2 Functional Complementation of *T. brucei* Topoisomerase-IIα

While the N-terminal catalytic domain of topoisomerase-IIα appears highly conserved between trypanosomatids, there is great variation between the C-terminal sequences, a feature exploited previously to generate selective RNAi mediated knockdown. This feature could also prove advantageous in a search to identify essential regulatory regions of topoisomerase-II. By replacing the native topoisomerase-IIα in *T. brucei* with its *L. major* counterpart, and assessing if parasites are still viable, insight may be gained into the importance of the native C-terminal domain. Given that centromere identification in *L. major* by biochemical mapping proved elusive, replacing *T. brucei* topoisomerase-IIα with the *L. major* enzyme could also shed light on whether *L. major* topoisomerase-II is simply refractory to etoposide.

5.2.1 Complementing *T. brucei* with the *L. major* topoisomerase-II

To assess whether *L. major* topoisomerase-II can substitute for *T. brucei* topoisomerase-IIα, a complementation assay was performed featuring full length *L. major* topoisomerase-II expressed in the *T. brucei* topoisomerase-IIα RNAi cell-line. First, the

full length *L. major* topoisomerase-II was amplified from *L. major* Friedlin strain and cloned into the plasmid pTub-EX^{BLA} (Obado et al., 2011) to form the final plasmid (Section 3.6.7). The resulting pTub-Ex^{BLA}-LmfTopoII was linearized with *Bam*HI and *Kpn*I, and transfected into the topoisomerase-IIα RNAi cell-line, with clones generated under blasticidin drug selection (Section 3.10.1). The parasites were also maintained on hygromycin and phleomycin to select for retention of the RNAi machinery.

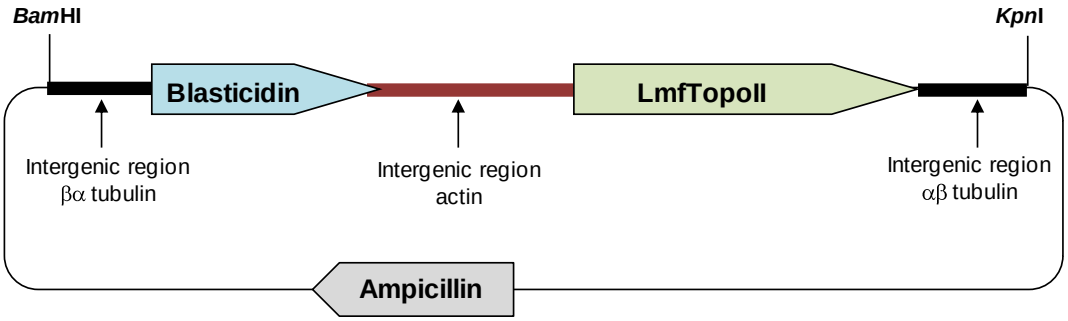

Figure 5.2.1. ***The L. major topoisomerase-II expression plasmid.***
Full length *L. major* topoisomerase-II (LmfTopoII) was amplified and cloned into pTub-Ex^{BLA} for constitutive expression from the tubulin array of *T. brucei* (Section 3.6.7). The resulting plasmid pTub-Ex^{BLA}-LmfTopoII was linearized with *Bam*HI and *Kpn*I restriction digests.

First, a growth assay was performed to assess whether *L. major* topoisomerase-II could complement the growth arrest phenotype of RNAi mediated knockdown of the *T. brucei* topoisomerase-IIα. The parent topoisomerase-IIα RNAi cell-line and the complemented cell-line were grown in parallel, with both tetracycline induction and non-induction. As observed previously, the non-complemented cell-line displayed growth arrest after 24 hours, whereas the cell-line complemented with *L. major* topoisomerase-II showed no evidence of a slowdown in growth, relative to the un-induced parasites (Figure 5.2.2a). This phenotype was observed for the 7 day duration of the assay. To establish that effective transcript knockdown had occurred, samples of RNA were purified for

northern blot analysis using specific probes generated from the 3' end of the gene (Section 3.6.2 and Section 3.6.7). Knockdown of *T. brucei* topoisomerase-IIα was observed in both the parental and complemented RNAi cell-lines under tetracycline induction, while the *L. major* topoisomerase-II was shown to be constitutively expressed in the complemented cell-line (Figure 5.2.2b).

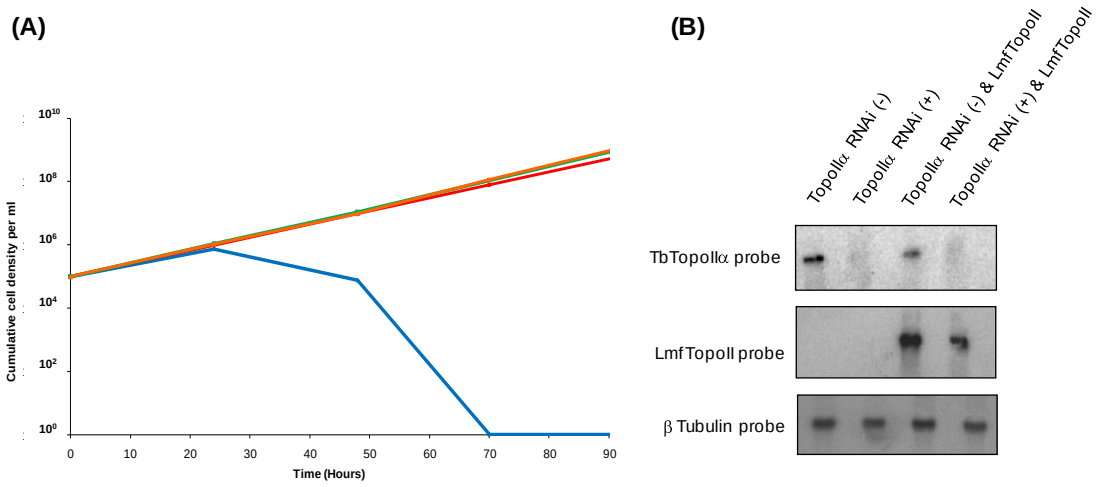

Figure 5.2.2. ***L. major topoisomerase-II complements RNAi mediated depletion of topoisomerase-IIα in bloodstream form T. brucei.***
Cumulative growth plots of the *T. brucei* topoisomerase-IIα RNAi and complemented cell-lines **(A)**. Cells were counted every 24 hours by haemocytometer then diluted back to 1 x 10^5 ml^{-1}. The topoisomerase-IIα RNAi cell-line untreated (red line), and tetracycline treated (blue line) displays the inducible lethal phenotype as before (Figure 5.1.3). Comparing the topoisomerase-IIα RNAi cell-line constitutively expressing *L. major* topoisomerase-IIα untreated (green line) with a tetracycline treated culture (orange line) to deplete native topoisomerase-IIα shows the growth inhibition phenotype of *T. brucei* topoisomerase-IIα RNAi is complemented by the expression of the *L. major* topoisomerase-II (Section 3.1.3). Northern blots of RNA extracted 28 hours after RNAi induction were probed with isoform-specific fragments (Section 3.6.2 and Section 3.6.7) from the variable regions **(B)**. This showed successful knockdown of *T. brucei* topoisomerase-IIα under tetracycline induction, and constitutive expression of *L. major* topoisomerase-II (LmfTopoII) in the complemented cell line.

Next, the biochemical activity of *L. major* topoisomerase-II at the centromere was examined using the etoposide mediated topoisomerase-II DNA cleavage assay. Cultures of both the original topoisomerase-IIα RNAi cell-line (Obado et al., 2011) and the topoisomerase-IIα RNAi cell-line constitutively expressing *L. major* topoisomerase-II, were induced for RNAi with tetracycline for 28 hours, and treated with etoposide for 30 minutes before being embedded in agarose blocks. Non-induced parasites were also treated with etoposide. As expected, both the non-induced cell-lines displayed etoposide mediated cleavage products, as a result of the activity of the native topoisomerase-IIα activity. As previously observed, the parent RNAi cell-line ceased to generate cleavage products when RNAi was induced, a phenotype concomitant with cell death. Interestingly the cell-line complemented with *L. major* topoisomerase-II also ceased to generate cleavage products (Figure 5.2.3), despite demonstrating that it could rescue the growth arrest phenotype. This could be a consequence of the *L. major* topoisomerase-II lacking the required recognition features of the *T. brucei* centromere to be successfully recruited, while still effectively complementing the general role of a nuclear topoisomerase-II enzyme. Alternatively etoposide may simply not inhibit the *L. major* orthologue. Indeed, analysis of the ethidium bromide stained gel supports the latter, given the lack of smearing in the lane corresponding to the complemented culture treated with etoposide. A smeared lane of a CHEFE gel appears characteristic of inhibited topoisomerase-II activity, and its absence here suggests that this etoposide mediated enzyme inhibition is not occurring in *T. brucei* parasites expressing only the *Leishmania* enzyme.

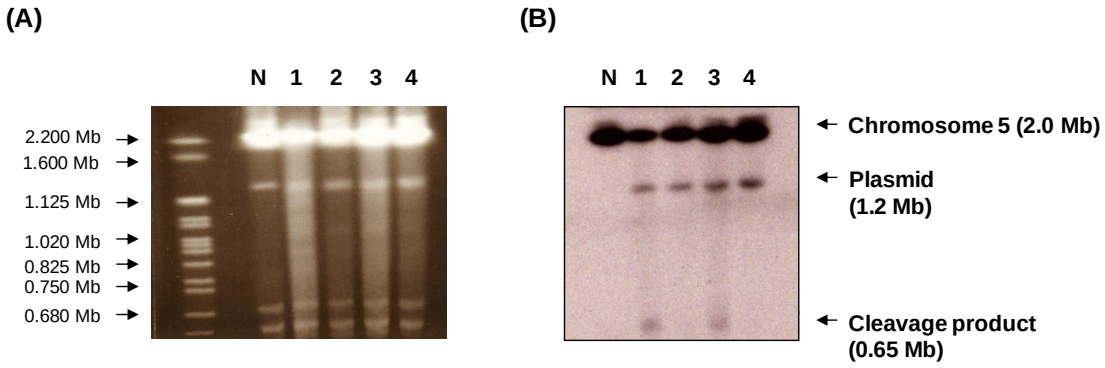

Figure 5.2.3. ***L. major topoisomerase-II does not generate etoposide mediated DNA cleavage products.***
Etoposide mediated DNA cleavage experiments were performed on the topoisomerase-IIα RNAi cell-line (Obado et al., 2011) and the topoisomerase-IIα RNAi cell-line constitutively expressing *L. major* topoisomerase-II. A non-etoposide treated wild-type *T. brucei* 427 (lane N) is shown as a control. Lanes 1 and 2 contain chromosomes extracted from etoposide treated cultures of the topoisomerase-IIα RNAi cell-line, while lanes 3 and 4 contain chromosomes extracted from etoposide treated cultures of the complemented cell-line (Section 3.2.3). Lanes 2 and 4 are from the stated cultures further supplemented with 1 µg ml^{-1} tetracycline for 28 hrs to initiate the gene specific RNAi (Section 3.1.3). The ethidium bromide stained gel (**A**) shows most of the megabase sized chromosomes within the compression zone of the CHEFE gel, with *S. cerevisiae* chromosomes used as size markers (Section 3.4.2). The Southern blot of the gel (**B**) shows etoposide mediated cleavage products of topoisomerase-IIα in lanes 1 and 3 (0.65 Mb) when probed for chromosome 5 using the Tb7 probe. In parasites depleted of topoisomerase-IIα, there is an absence of cleavage products (lane 2). With the added constitutive expression of *L. major* topoisomerase-II this absence of cleavage products remains (lane 4). A lack of cleavage product is again accompanied by a lack of smearing in the corresponding lane of the ethidium bromide stained gel (see also Figure 5.1.4). Plasmid contamination appears faintly in the RNAi cell-lines due to the presence of the tagged locus on chromosome 2a (Alsford and Horn, 2008).

As an alternative approach to the above question, we sought to express the *L major* topoisomerase-II in a null mutant background utilizing the single allele gene disruption cell-line already generated (Section 5.1.2, Figure 5.1.6) with the pKO^{BLA}-TopoIIα plasmid, which contained a blastacidin selection marker. To generate the second knockout vector for the remaining allele the two gene disruption targeting fragments were cloned from the blasticidin based vector (Figure 5.1.5b) to a hygromycin resistance cassette (Section 3.6.6) to form pKO^{HYG}-TopoIIα (Figure 5.2.4a). Then the *L. major* topoisomerase-II was transferred from pTub-EX^{BLA}-LmfTopoII to pTub-EX^{PURO} (Section 3.6.8) forming pTub-EX^{PURO}-LmfTopoII (Figure 5.2.4b). This prevented the complementation plasmid sharing the same drug selectable marker as the first gene disruption plasmid. In addition the *T. cruzi* topoisomerase-II orthologue was also transferred from the existing pTub-EX^{BLA}-TcTopoII (Obado et al., 2011), to create pTub-EX^{PURO}-TcTopoII (Section 3.6.9 and Figure 5.2.4c) for further analysis.

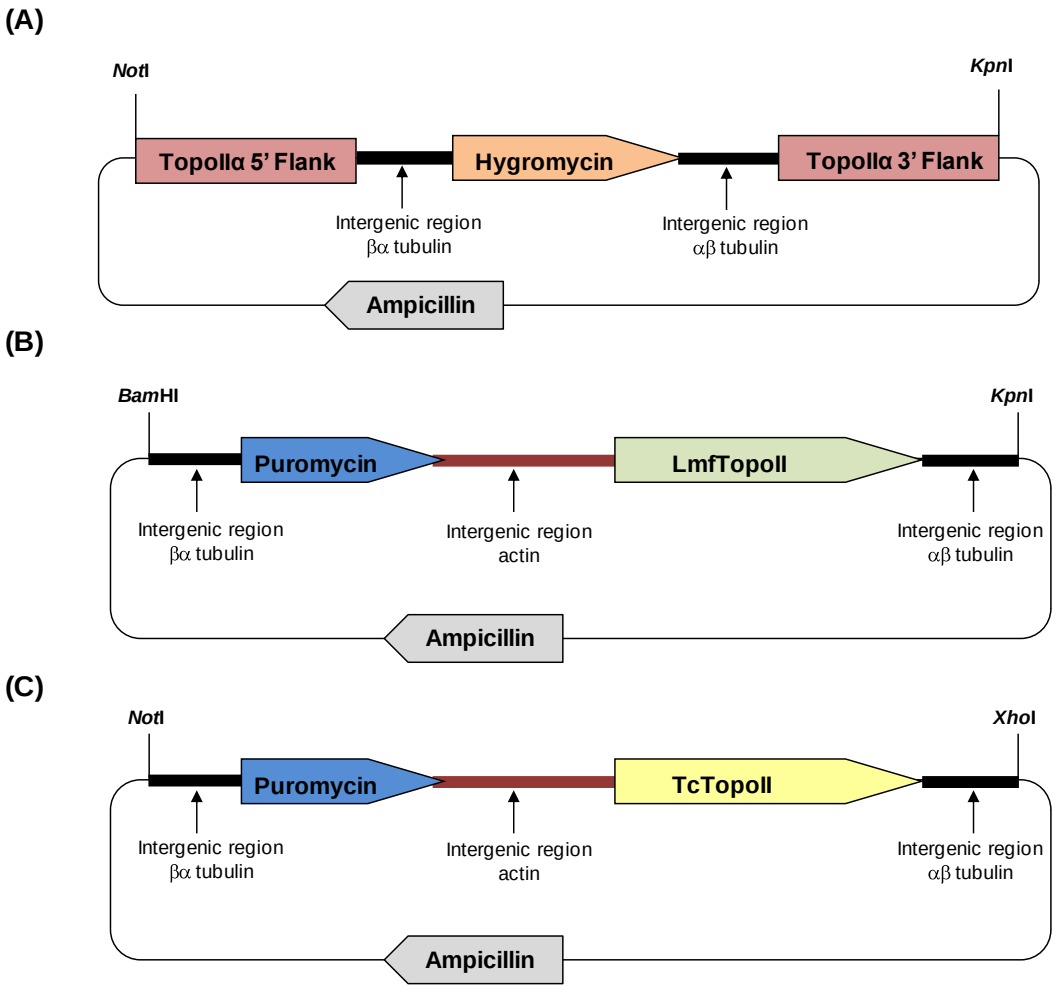

Figure 5.2.4. ***Plasmids for generating T. brucei topoisomerase-IIα null mutants with heterologous topoisomerase-II complementation.***
The targeting fragments of the gene disruption vector pKO^{BLA}-TopoIIα (Figure 5.1.5) were cloned into a hygromycin resistance cassette (Section 3.6.6) to produce the second gene disruption plasmid pKO^{HYG}-TopoIIα, required for the disruption of the remaining *T. brucei* topoisomerase-IIα allele (see Figure 5.1.6). The *L. major* topoisomerase-II gene was cloned from pTub-Ex^{BLA}-LmfTopoII (Figure 5.2.1) into pTub-Ex^{PURO}-LmfTopoII (Section 3.6.8) to prevent a conflict of drug markers. Also the *T. cruzi* topoisomerase-II was transferred from pTub-Ex^{BLA}-TcTopoII (Obado et al., 2011) to pTub-Ex^{PURO}-TcTopoII (Section 3.6.9). The latter two plasmids were used independently in attempts to generate *T. brucei* topoisomerase-IIα null mutants complemented with the constitutively expressed topoisomerase-II orthologue. The restriction sites used for the linearization of these plasmids are indicated.

With the first round of gene disruption previously genetically validated (Figure 5.1.6b), the next stage was to transform this cell-line with the *L. major* and *T. cruzi* pTub-EX^{PURO} based topoisomerase-II complementation vectors. After linearization of the complementation vectors using *Bam*HI and *Kpn*I (for *L. major*) or *Not*I and *Xho*I (for *T. cruzi*), the constructs were then independently used to transform the single knockout cell-line. Transformants were selected on puromycin drug pressure, while being maintained on blasticidin. The second *T. brucei* topoisomerase-IIα gene disruption vector (Figure 5.2.4a) was linearized with *Not*I and *Kpn*I before being immediately used to transfect one clone from each of the generated complementation cell-lines. Selection was performed with hygromycin, while parasites were maintained on both blasticidin and puromycin. Southern blots hybridised with *T. cruzi* and *L. major* specific probes (Section 3.6.7 and Section 3.6.9) demonstrated correct integration of the respective complementing genes in the tubulin array (Figure 5.2.5a and Figure 5.2.5b)

Analysis of nine clones complemented with the *T. cruzi* gene and six clones complemented with the *L. major* gene derived from two independent transfection experiments showed no loss of the remaining *T. brucei* topoisomerase-IIα allele, by either Southern blot of the target loci (Figure 5.2.5d) or northern blot analysis of the native transcript (Figure 5.2.5e), for any clones. The northern blot shows the clearest indication of the full length topoisomerase-IIα transcript remaining in triple drug resistant clones complemented with either topoisomerase-II orthologue. This is because the topoisomerase-IIα mRNA band is still present, and remains the same size as the wild-type transcript in the complemented null mutant cell-lines.

The resulting Southern blot of DNA from three triple drug resistant clones expressing the *T. cruzi* gene appears peculiar. The restriction fragment pattern does not match the single gene disruption pattern, suggesting there has been some form of second integration event, a notion supported by the fact that the clones are resistant to the three selection drugs. However this new pattern does not match the predicted sizes, in particular the appearance of a *Hind*III fragment at 3.5 kb, observed in three all cases. This is accompanied by an *Nru*I DNA digest showing all three clones producing restriction fragment bands larger than the predicted 8.2 kb fragment size.

Given the unexplainable Southern blot restriction patterns, combined with the topoisomerase-IIα transcripts remaining in a northern blot across a total of 14 clones, it can be concluded that topoisomerase-IIα null mutants cannot be readily generated in either a *L. major* or *T. cruzi* topoisomerase-II complemented background with this strategy.

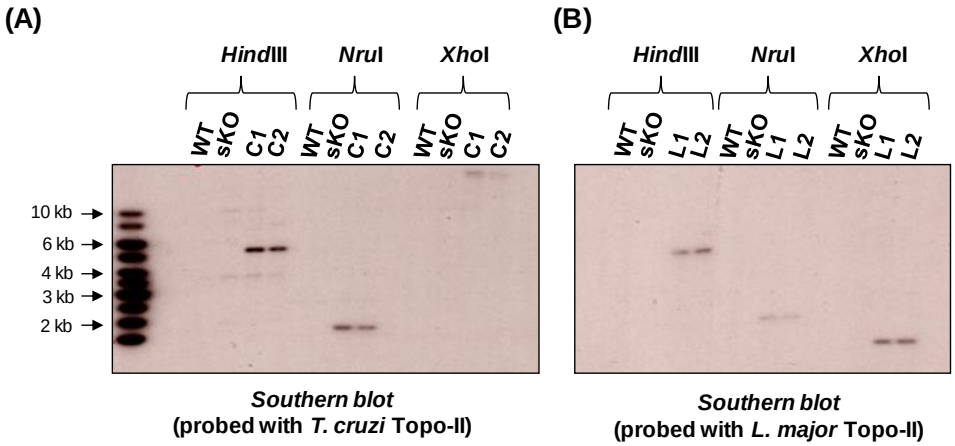
(A)
HindIII
NruI
XhoI
WT
sKO
C1
C2
10 kb
6 kb
4 kb
3 kb
2 kb
Southern blot
(probed with T. cruzi Topo-II)
(B)
HindIII
NruI
XhoI
WT
sKO
L1
L2
Southern blot
(probed with L. major Topo-II)

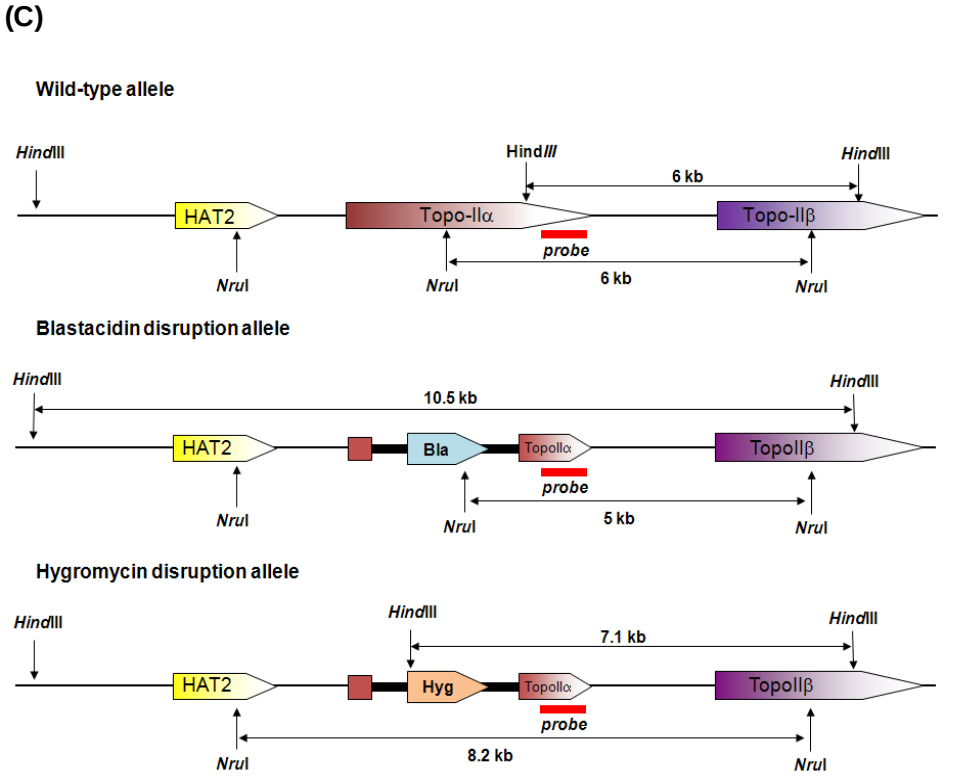
(C)
Wild-type allele
HindIII
HindIII
HindIII
6 kb
HAT2
Topo-IIα
Topo-IIβ
probe
NruI
NruI
6 kb
NruI
Blastacidin disruption allele
HindIII
10.5 kb
HindIII
HAT2
Bla
TopoIIα
TopoIIβ
probe
NruI
NruI
5 kb
NruI
Hygromycin disruption allele
HindIII
HindIII
7.1 kb
HindIII
HAT2
Hyg
TopoIIα
TopoIIβ
probe
NruI
8.2 kb
NruI

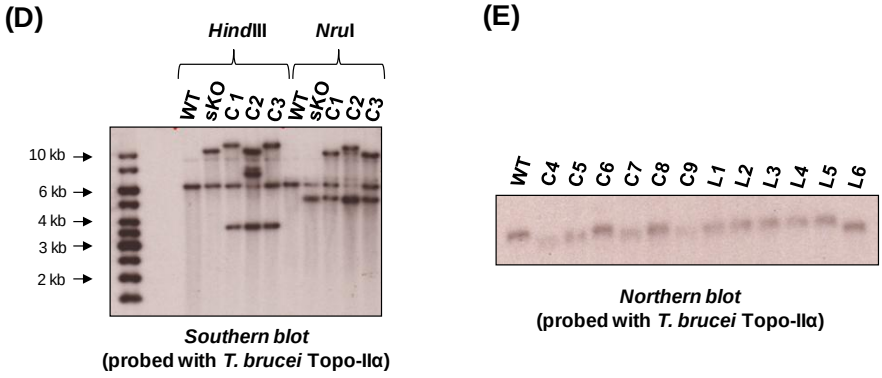
(D)
HindIII
NruI
WT
sKO
C1
C2
C3
10 kb
6 kb
4 kb
3 kb
2 kb
Southern blot
(probed with T. brucei Topo-IIα)
(E)
WT
C4
C5
C6
C7
C8
C9
L1
L2
L3
L4
L5
L6
Northern blot
(probed with T. brucei Topo-IIα)

Figure 5.2.5 (overleaf). ***T. brucei topoisomerase-IIα null mutants complemented with T. cruzi or L. major topoisomerase-II orthologues could not be created.***
T. cruzi topoisomerase-II or *L. major* topoisomerase-II were inserted into the tubulin array of the *T. brucei* 427 cell-line in which one copy of the topoisomerase-IIα gene had already been disrupted (sKO, see Figure 5.1.6). These two lines were then transfected with a second gene disruption fragment to target the remaining *T. brucei* topoisomerase-IIα allele. Southern blots of DNA extracted from triple drug resistant, potential null mutants complemented with either the *T. cruzi* or *L. major* topoisomerase-II were probed with gene specific probes (Section 3.6.7 and Section 3.6.9) to confirm the integration of the complementing topoisomerase-II orthologues into the tubulin array. This confirmed the presence of both the *T. cruzi* (**A**) and *L. major* (**B**) genes. To examine whether *T. brucei* topoisomerase-IIα null mutants had been generated in the *T. cruzi* complemented background a fresh Southern blot was probed with a fragment specific for the 3' end of topoisomerase-IIα (Section 3.6.2). (**C**) An *in silico* map outlines the predicted restriction fragment sizes from the 2 original wild-type *T. brucei* topoisomerase-IIα alleles, the first allele disrupted with the blasticidin resistance cassette, and the second allele generated with the hygromycin resistance cassette. The downstream topoisomerase-IIβ and the upstream histone acetyltransferase 2 (HAT2) genes are also shown. The results of the Southern blot (**D**) show the wild-type (WT) and first round gene disruption (sKO) fragment sizes match the *in silico* predicted pattern. However after the second round of gene disruption, the three clones analysed here show three new bands at 3.5 kb with a *Hind*III restriction digest, and in the case of clones 1 and 3, no loss of the native 6 kb restriction fragment. Even though clone 2 shows two bands at the predicted sizes, the origin of the additional 3.5 kb band remains unclear. An *Nru*I DNA digest shows a similar pattern with clones 1 and 3 maintaining the wild-type 6 kb band, while all three clones show bands larger than the predicted 8.2 kb fragment size. For a rapid screening approach of further potential null mutant clones, a northern blot analysis was performed **(E)**. This assessed the expression of *T. brucei* topoisomerase-IIα in parasite clones resistant to 3 drug selectable markers, and constitutively expressing either *T. cruzi* (C4-9) or *L. major* (L1-6) topoisomerase-II. The results indicated the native gene continued to be expressed in a further 12 independent clones.

5.3 Affinity Purification of Topoisomerase II Complexes

Affinity purification of topoisomerase-II from trypanosomes could allow the identification of regulator enzymes or any post-translational modifications of topoisomerase-II, which determine the regulatory mechanisms of topoisomerase-II activity and its accumulation at the centromere. Therefore a plasmid facilitating tandem affinity purification of proteins was obtained (a gift from the Günzl laboratory). There is both an N-terminal tag and C-terminal version of the PTP-tag plasmid available, termed pN-PTP^{NEO} and pC-PTP^{NEO} (Schimanski et al., 2005).

5.3.1 Co-immunoprecipitation of topoisomerase-II

To tag the C-terminus of *T. brucei* topoisomerase-IIα and *T. cruzi* topoisomerase-II, 3' targeting fragments (with the stop codon deleted) of each gene were cloned into pC-PTP^{NEO} to generate the plasmids pC-PTP^{NEO}-TopoIIα and pC-PTP^{NEO}-TcTopoII (Sections 3.6.10 and 3.6.11 respectively). The resulting plasmids were then sequenced to confirm the correct translated protein sequence, and that the tag was in frame with the gene. Both of the final plasmids (Figure 5.3.1) could be linearized by a unique *Stu*I restriction site and inserted into the native gene locus by double homologous recombination for stable integration.

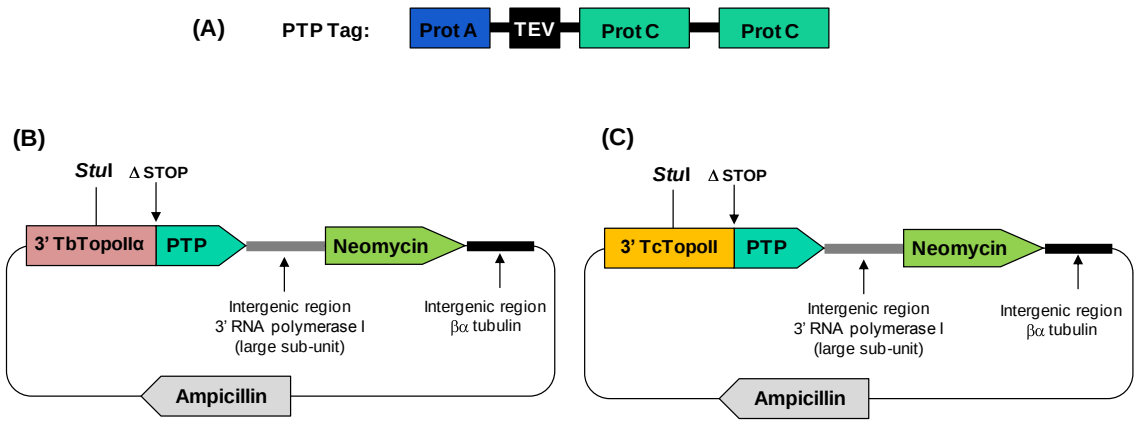

Figure 5.3.1. A*ffinity purification constructs for topoisomerase-II.*
The PTP tag **(A)** consists of a Prot A epitope separated by a TEV protease site and two parallel ProtC epitopes, which facilitates tandem affinity purification of the tagged protein from the native allele (Schimanski et al., 2005). A 3' targeting fragment from *T. brucei* topoisomerase-IIα and *T. cruzi* topoisomerase-II were cloned individually into pC-PTP-NEO (sections 3.6.10 and 3.6.11). The resulting plasmids pC-PTP^{NEO}-TopoIIα (**B**) and pC-PTP^{NEO}-TcTopoII (**C**) were linearized by a unique *Stu*I restriction site within the targeting fragment, and transfected into *T. brucei* 927 procyclic forms and *T. cruzi* CL Brener epimastigotes respectively.

Since *T. cruzi* epimastigotes grow to far higher densities than that of even the procyclic stage of *T. brucei*, the system was developed first in *T. cruzi*. This would facilitate the production of higher yields of tagged protein. Therefore linearized pC-PTP^{NEO}-TcTopoII was transfected into epimastigote *T. cruzi* CL Brener wild-type strain, and selected on G418 drug pressure. Multiple clones were generated. Genomic DNA was purified from 1 clone and subjected to restriction digest and Southern blot analysis to confirm the topoisomerase-II locus had been successfully targeted. Although *T. cruzi* CL Brener has been successfully sequenced (El-Sayed et al., 2005a), it has yet to be fully assembled. This often makes the generation of *in silico* restriction maps difficult. Figure 5.3.2a shows the predicted restriction map generated by independent *Eco*RI and *Nco*I digests of the allele possessing the largest shotgun sequence fragment (GeneDB Accession: Tc00.1047053508699.10). Results from the Southern blot demonstrate correct integration of the tag (Figure 5.3.2). The restriction digest of wild-type genomic DNA with *Eco*RI revealed the predicted 7.2 kb band, but also an additional band at 8.8 kb. This presumably is simply the consequence of allelic variation, which is extensive in the CL Brener genome (El-Sayed et al., 2005a). This band remains in the PTP-tagged cell-line, and therefore represents the untagged allele. The 7.2 kb band is replaced by

two bands at 3.7 kb and 9.4 kb. This is because insertion of the full pC-PTP^{NEO}-TcTopoII plasmid introduces a new *Eco*RI site (3.7 kb) and also extends the distance to the downstream native *Eco*RI site (9.4 kb). The former is detected by the probe to the newly introduced 3' gene fragment tagged with the PTP epitopes. The latter is the replaced native 3' gene fragment looped downstream by the recombination event. The *Nco*I digest is simpler to interpret, with both wild-type alleles generating a fragment at 3.5 kb. The tagged allele of the selected cell-line again produces two bands due to an *Nco*I site within pC-PTP^{NEO}-TcTopoII producing a 3.9 kb band and a 5.5 kb band.

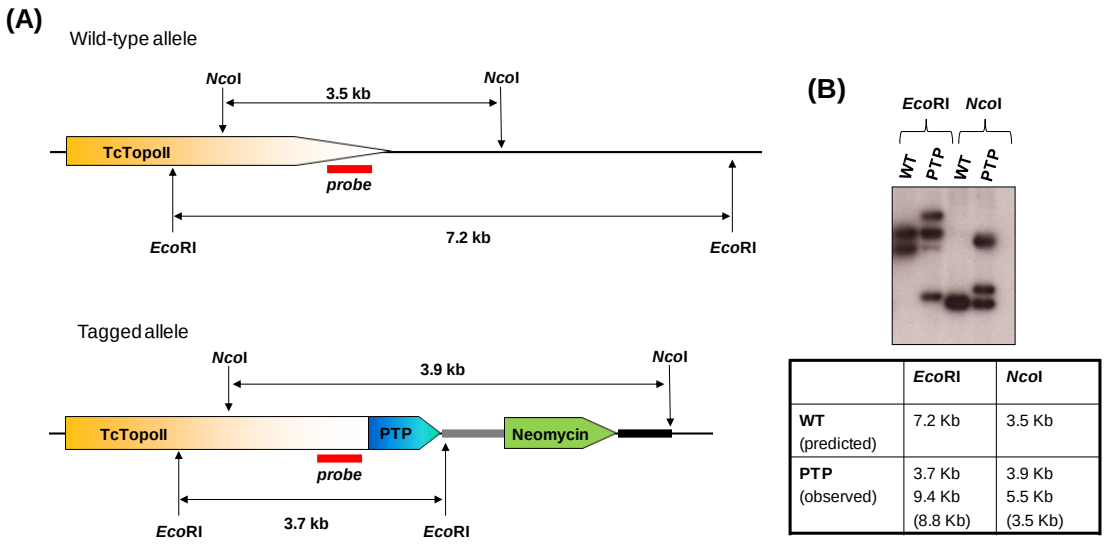

	*Eco*RI	*Nco*I
WT (predicted)	7.2 Kb	3.5 Kb
PTP (observed)	3.7 Kb 9.4 Kb (8.8 Kb)	3.9 Kb 5.5 Kb (3.5 Kb)

Figure 5.3.2. ***Integrating PTP tagged topoisomerase-II in T. cruzi.***
An *in silico* predicted map shows restriction site fragment sizes for two enzymes at the topoisomerase II locus of *T. cruzi* **(A)**. The Southern blot and accompanying table **(B)** demonstrates correct integration of the plasmid. The restriction fragment sizes from the wild-type (WT) is shown in the top row of the table, with the observed fragment sizes from the Southern blot described below. One modified allele generates two bands due to the mechanism of plasmid integration, whereby the probe detects both the *in situ* tagged allele and remaining native 3' end of topoisomerase-IIα now located further downstream (not shown on map). The *Eco*RI Southern blot results in two separate wild-type bands from a polymorphism between homologues. The remaining native allele is shown in parenthesis.

Whole cell lysate preparations were made from a total of 5 x 10^9 epimastigotes (Section 3.9.2), of either exponential growth phase wild-type *T. cruzi* cultures, or transformed *T. cruzi* cultures possessing the epitope tagged topoisomerase-II. A further culture which possessed the tagged topoisomerase-II was grown to stationary phase, before cell lysates were prepared. A 10 µl aliquot of each lysate sample was separated by SDS-PAGE on two 5% gels in parallel. The first gel was coomassie stained to demonstrate equal loading, the second was subjected to western blotting, and probed with a ProtC antibody (Figure 5.3.3). This revealed that topoisomerase-II tagged with PTP was cleanly recognised by the ProtC antibody and full length topoisomerase-II was successfully expressed, within the lysate. This preliminary result also suggests that topoisomerase-II may be present at higher concentrations in actively dividing cells, although further experiments would be required to confirm this.

This tagged system was designed and developed to analyse the nature of any post-translational modifications to topoisomerase-II, and identify any other proteins bound to topoisomerase-II in a complex, and is the subject of downstream work.

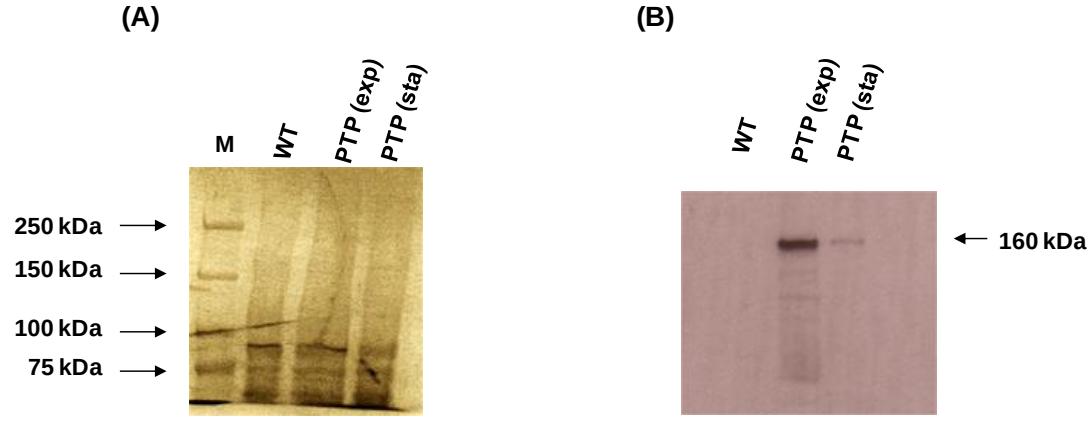

Figure 5.3.3. ***T. cruzi express PTP tagged topoisomerase-II.***
Protein lysates from *T. cruzi* epimastigotes were run on a 5% denaturing gel with PTP tagged topoisomerase II lines grown in exponential phase (exp) and to stationary phase (sta), and compared with the wild type. A coomassie stain **(A)** shows protein loading, with the western blot **(B)** probed with a ProtC antibody to the tag (Sections 3.9.3 and 3.9.4), showing *T. cruzi* topoisomerase II tagged protein expression.

5.4 Chapter Summary

The study of the nuclear topoisomerase-II isoforms in the *T. brucei* bloodstream form parasites is summarized below:

- RNAi experiments demonstrate that only the topoisomerase-IIα isoform is essential for parasite growth of bloodstream form parasites. The topoisomerase-IIβ isoform appears non-essential. This echoes what was observed previously in the procyclic parasite form (Kulikowicz and Shapiro, 2006).
- The RNAi studies further show that only the topoisomerase-IIα isoform generates centromere specific etoposide mediated DNA cleavage.
- Immunofluorescence localization demonstrates that topoisomerase-IIα resides within the nucleus. Also the *in situ* addition of a C-terminal c-myc epitope tag to topoisomerase-IIα does not perturb enzyme function.
- The heterologous expression of *L. major* topoisomerase-II rescues the cell death phenotype generated by the RNAi mediated depletion of topoisomerase-IIα.
- The expression of *L. major* topoisomerase-II does not however restore centromere specific etoposide mediated DNA cleavage. This suggests *L. major* topoisomerase-II may be refractory to etoposide poisoning.
- Since centromeric cleavage was not generated by heterologous *L. major* topoisomerase-II expression with etoposide treatment, no examination of the C-terminal function in respect to centromere targeting was possible.
- Generating topoisomerase-IIα null mutants with a gene disruption strategy, in a background of either *L. major* or *T. cruzi* topoisomerase-II constitutive expression, proved elusive.
- A *T. cruzi* cell-line was developed allowing the tandem affinity purification of native topoisomerase-II. In future this could facilitate the study of topoisomerase-II in terms of examining post-translational modification or associated bound proteins. The system would also be readily applicable to procylic form *T. brucei*.

5.5 Discussion

Since topoisomerase-II has been shown to accumulate at *T. brucei* centromeres, and yet no single primary DNA sequence appeared to define this region (Section 4.4) the question arises as to what guides this enzyme specifically towards the centromere? Unlike *L. major* and *T. cruzi*, there are two nuclear isoforms of topoisomerase-II in *T. brucei* (Kulikowicz and Shapiro, 2006). The first step in analyzing the targeting mechanism of *T. brucei* topoisomerase-II to the centromere was to establish which isoforms would be active at the centromere. Using isoform-specific RNAi mediated knockdown, it was shown that only the topoisomerase-IIα isoform was active at the centromere (Section 5.1.1). In fact the topoisomerase-IIβ isoform appeared dispensable, which is perhaps unsurprising as it appeared catalytically inactive during an *in vitro* DNA de-catenation assay (Kulikowicz and Shapiro, 2006). The reason for its inactivity *in vitro* is not clear, as the catalytic N-terminal shares a very high level of sequence homology to the topoisomerase-IIα isoform (Figure 10.1.1). It therefore seems that topoisomerase-IIβ could be a pseudogene, albeit with the catalytic and ATPase domains remaining highly conserved. Pseudogenes are fairly abundant in the *T. brucei* genome with approximately 10% of open reading frames designated as pseudogenes (Berriman et al., 2005). Recently it has been proposed that RNAi fragments derived from duplicated pseudogenes may have a regulatory role on their functional gene counterparts, however so far this has only been demonstrated for 9 proteins of unknown function (Wen et al., 2011). Notably, topoisomerase-IIβ is absent in *T. cruzi* and *L. major*, neither of which possess the RNAi machinery (Section 1.5.5). It may be that topoisomerase-IIβ plays some regulatory role on the –α isoform, which may warrant further investigation.

Given that in other model organisms, the C-terminal of topoisomerase-II is not required for *in vitro* activity, yet this domain contains *in vivo* cell-cycle dependent phosphorylation sites (Section 2.3), it is conceivable that the C-terminal of topoisomerase-IIα is involved in the cellular regulation of its activity and localization. An interesting experiment had shown that constitutive expression of the *T. cruzi* topoisomerase-II in an *T. brucei* topoisomerase-IIα RNAi mediated knockdown

background could rescue the growth inhibition phenotype and restore the withdrawal of centromeric activity (Obado et al., 2011). If the hypothesis of C-terminal based regulation is true, then despite a divergent C-terminus between topoisomerase-IIα and the *T. cruzi* orthologue, there must be shared features conferring the regulatory control and guidance towards a centromere. Here, using a similar approach to extend this hypothesis, it was shown that the constitutive expression of *L. major* topoisomerase-II could rescue the growth inhibition phenotype, but not restore the etoposide mediated centromeric cleavage activity (Section 5.2.1). This result strongly suggests that the *L. major* enzyme also shares at least some of these regulatory features, and that the reason behind the ineffective *L. major* centromere mapping experiments is that etoposide does not inhibit the nuclear *L. major* topoisomerase-II. An assessment of *in vitro* DNA cleavage activity with recombinant nuclear *L. major* topoisomerase-II and etoposide would aid confirmation. Although it appears likely that a technical limitation led to the failure to map centromeres of *L. major* chromosomes, the underlying question as to whether this organism segregates its chromosomes by a centromere dependent mechanism remains to be resolved. Since topoisomerase-II has received interest as a drug target in trypanosomatids (Das et al., 2004), noting differences in drug susceptibility between the *L. major* nuclear and kinetoplast isoforms could prove important in developing the appropriate drug screening strategies.

Experiments described in this chapter have shown that within the constitutive complementation background of either the *L. major or T. cruzi* topoisomerase-II, null mutants of *T. brucei* topoisomerase-IIα could not be generated (Section 5.2.1). Although failure to disrupt the remaining allele does not provide irrefutable proof that the native *T. brucei* topoisomerase-IIα is essential, it is noteworthy that the first allele proved routine to disrupt. Why it should be the case that the second allele could not be disrupted is unclear, given the success of its orthologues complementing the topoisomerase-IIα RNAi growth inhibition phenotype. Perhaps there is a requirement for a low level of native enzyme for a particular function that would remain from RNAi mediated knockdown. On the other hand it may be a technical problem due to the nature of the tandem repeat locus. In this region there is a high level of similarity in DNA sequences between the two isoforms, as well as between their surrounding un-translated regions.

While the single allele sequenced here contains notable similarities in the intergenic sequences for the two isoforms, any significant sequence differences across the two alleles would prevent the correct insertion of a second gene disruption plasmid, which was designed on the basis of the first allele. This may lead to unpredictable insertions using either topoisomerase-IIβ or downstream sequences as the template, and could explain the obscure Southern blot based restriction maps (Figure 5.2.5). Comprehensively sequencing the intergenic sequences of both alleles would help in answering these issues, especially given the current sequencing artefacts that still reside in the genome database.

Due to the inability of *L. major* topoisomerase-II to generate etoposide mediated DNA cleavage when expressed in *T. brucei*, it could not be exploited to dissect the centromere targeting mechanism. This is primarily because any experiment of this kind would be based on the unsupported assumption that the *L. major* enzyme locates to the centromere similarly to its *T. brucei* and *T. cruzi* counterparts. In addition, any experiments involving alterations to the enzyme's C-terminal that could affect its centromeric targeting behaviour would also be difficult to assess. Therefore it would not be possible to draw parallels between C-terminal protein sequence features of the native *T. brucei* topoisomerase-IIα to the *L. major* orthologue, or to the *T. cruzi* enzyme from other experiments. Consequently, a new experimental system was pursued where endogenous *T. brucei* topoisomerase-IIα was PTP tagged to facilitate native enzyme purification. As *T. cruzi* epimastigotes grow to higher cell densities in culture, this system was developed for the *T. cruzi* enzyme as well (Section 5.3.1). In future work this system could allow the study of any cell-cycle dependent phosphorylation of the enzyme, and also reveal whether other proteins relevant to mitosis are associated with topoisomerase-II.

The c-myc epitope tag system was originally designed as a positive control to assess the nuclear localization of the native topoisomerase-II for use in any future truncated or mutated enzyme experiments (Section 5.1.2). It has since been used to purify *T. brucei* topoisomerase-IIα. The purified protein was then analyzed for any associated SUMO conjugation using an antibody against the SUMO protein, which revealed that the

SUMO modifier could not be detected in the sample (Obado et al., 2011). In experiments with other organisms, SUMO modified topoisomerase-II can often be observed on a western blot as higher molecular weight bands above the native enzyme. In preliminary experiments with the PTP tagged *T. cruzi* enzyme, no such additional bands could be observed (Section 5.3.1). Together, these results tentatively suggest that unlike in some other systems (Section 2.3), SUMO does not play a role in targeting the enzyme towards the centromere.

Overall, the mechanism of centromere targeting of topoisomerase-II remains elusive. While it has now been shown that that *T. brucei* topoisomerase-IIα and *T. cruzi* topoisomerase-II enzymes are capable of locating *T. brucei* centromeres, the system that facilitates the specific target guidance remains unknown. The system is most likely sensitive to chromatin structure rather than pure DNA sequence, due to the differences observed between centromere sequences across chromosomes. Further analysis of the cell-cycle phosphorylation of topoisomerase-II, as well as any bound accessory proteins would help us to understand this process for topoisomerase-II. Many pieces of the centromere/kinetochore complex are yet to be identified. Although it was hoped that understanding topoisomerase-II in more detail would aid in the identification of other centromeric targeted proteins, other future experimental approaches will probably be required to begin to unravel the puzzle of chromosome segregation in trypanosomatids.

SECTION II:

Nitroreductase mediated drug metabolism

6 Introduction to Nitroreductase Based Drug Metabolism

Nitroaromatic compounds represent a large group of molecules characterised by a nitro group linked to a heterocyclic (e.g. furan, thiophene, imidazole, triazole etc) or cyclic (eg benzyl) ring (Raether and Hanel, 2003). They rarely occur in nature, with most generated synthetically during the production of plastics, dyes, solvents, pesticides, explosives and pharmaceuticals (Rieger et al., 2002; Roldan et al., 2008). Their medicinal uses were first recognised in the early 20th century with the 5' nitrofuryl, nitrofurazone emerging as a topical treatment for burns and wounds (Raether and Hanel, 2003). They have been used extensively to treat a variety of microbial urinary or gastrointestinal tract (GI) infections, but concern over their reported mutagenic properties has resulted in a decline in their use, particularly in Europe and the United States (McCalla, 1983). However, this scepticism about using nitro-based compounds is being questioned, as recent studies suggest that these compounds are not as toxic as initially thought (Trunz et al., 2011; Yamada et al., 1997). Such observations have led to renewed interest in this group of agents as potential anti-cancer therapies (Dachs et al., 2005; Denny, 2003) and anti-microbial agents (Stover et al., 2000; Wilkinson and Kelly, 2009).

This chapter will first discuss the initial key step involved in the mode of action of many nitroaromatics. It will then focus on the 5' nitrofuryl compounds using nitrofurazone, the best studied agent in terms of its activity, selectivity and host toxicity, as a lead example and explore how this can inform our knowledge relating to the trypanocidal activity of nifurtimox. Finally it will describe how the current knowledge of pro-drug activation has been exploited to develop anti-cancer therapies such as the azirindyl nitrobenzyl CB1954, and the nitrobenzyl mustards, which may be suitable as future trypanocidal agents.

6.1 Nitroreductase Mediated Drug Activation

Based on the nature of the ring structure and the position/number of nitro groups on the ring, nitroaromatics can be divided into several classes, with each sub-group having distinct chemical properties. One feature shared by the diverse medicinal compounds is that they function as pro-drugs and must be 'activated' before they mediate their cytotoxic effects. A key reaction to this activation process is catalyzed by a group of oxidoreductases called nitroreductases. Based on their sensitivity to oxygen, this group of enzymes can be separated into two distinct classes, the type I and type II nitroreductases, with members of each class often unrelated in their primary sequence and physiological substrate (Peterson et al., 1979; Roldan et al., 2008).

Type I nitroreductases are a group of flavin mononucleotide (FMN)-containing enzymes found in prokaryotes and absent from most eukaryotes, with a sub-set of protozoan parasites, including *Trypanosoma* and *Leishmania*, being major exceptions (Nixon et al., 2002; Wilkinson et al., 2008). They catalyse the reduction of the conserved nitro group present on the target substrate, through a nitroso intermediate, to a hydroxylamine derivative via a series of 2-electron transfers, utilizing NADPH and/or NADH as electron donors (Race et al., 2005). The hydroxylamine can then undergo further processing to generate a series of additional cytotoxic metabolites (Denny, 2003; Gavin et al., 1966; Streeter and Hoener, 1988). As this reaction does not involve oxygen and does not result in the production of reactive oxygen species, this activity is said to be "oxygen insensitive". Generally, bacteria have multiple type I nitroreductases. For example, *E. coli* expresses two major type I nitroreductases, designated as nfsA and nfsB, with 2 further minor activities also reported: azoR and nemA (Prosser et al., 2010; Zenno et al., 1996a; Zenno et al., 1996b). As with other type I nitroreductases, these *E. coli* enzymes can metabolize a wide variety of nitroaromatic compounds (Roldan et al., 2008), ranging from medicinally used pro-drugs such as nitrofurazone, to environmental pollutants including 2, 4, 6-trinitrotoluene (TNT). Intriguingly, the precise physiological role for any of these enzymes remains unknown.

A wide array of FMN or flavin adenine dinucleotide (FAD)-containing enzymes display a type II oxygen-sensitive nitroreductase activity. These mediate a 1-electron reduction of the conserved nitro group to produce an unstable nitro anion radical (Docampo and Stoppani, 1979; Mason and Holtzman, 1975; Peterson et al., 1979). In the presence of oxygen, this radical can undergo futile cycling, resulting in the production of superoxide anions and the regeneration of the parent nitro-compound. When oxygen is limited, the nitroso form can be produced by a further single electron reduction step, or by the interaction of two nitro anions, with the latter reaction also resulting in regeneration of the parent nitro-compound (Mason and Holtzman, 1975). The nitroso form is highly reactive and can promote cellular damage directly or through the formation of a hydroxylamine derivative (Leitsch et al., 2007). Examples of type II nitroreductases include the cytochrome P450 reductase and xanthine oxidoreductase. Most organisms express several cytochrome P450 reductases, with each enzyme containing FMN and FAD as co-factors, while using NADPH as a source of reducing equivalents (Iyanagi and Mason, 1973). They function to transfer a single electron to various physiological substrates including cytochrome P450, heme oxygenase, cytochrome b5 and squalene epoxidase (Murataliev et al., 2004). In mammals, the FAD-dependent xanthine oxidoreductases are iron-sulphur cluster enzymes that function to convert hypoxanthine to uric acid via a xanthine intermediate (Green, 1934). This activity was thought to be due to the concerted action of two distinct enzymes, xanthine oxidase and xanthine reductase, but it has been shown that a single enzyme can perform both reactions (Corte and Stirpe, 1972). Initially, this finding was believed to be an experimental artefact, however evidence is emerging that this behaviour may also occur *in vivo* (Nishino et al., 2008).

6.2 Anti-Microbial Activity of 5’ Nitrofuran Compounds

6.2.1 Nitrofurazone

The 5’ nitrofuryl class of compounds were one of the first nitroheterocyclics to be recognized as potential chemotherapies, and are characterized by a nitro group linked to a furan ring in the 5’ position (Figure 6.2.1). Screening programmes targeting different bacterial species using furyl derivatives revealed that the nitro group was key to cytotoxic activities (Dodd, 1944). From *in vitro* and mouse *in vivo* studies, nitrofurazone (5-nitro-2-furaldehyde semicarbazone, also called furacin) emerged as the lead structure, showing anti-microbial activity against bacteria species such as *Staphylococcus aureus* and *Salmonella spp.* (Dodd, 1946). These experiments were extended to other organisms, revealing that nitrofurazone was very effective against the trypanosomatid horse parasite *Trypanosoma equiperdum* (Dodd, 1946) and human parasite *T. b. gambiense* (Evens et al., 1957; Packchanian, 1955). However, due to adverse side-effects including severe joint pain and peripheral neuritis, the use of nitrofurazone became limited to a topical treatment of bacterial infections (Grunberg and Titsworth, 1973).

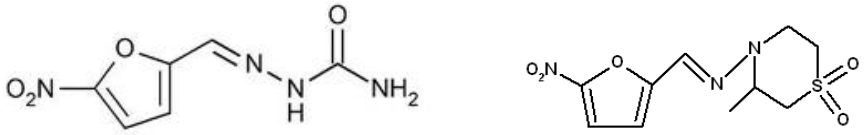

Nitrofurazone **Nifurtimox**

Figure 6.2.1. ***Chemical structures of nitrofurazone and nifurtimox.***

Early experiments exploring nitrofurazone's mode of action showed that bacterial strains lacking an unknown reductase activity displayed resistance to this nitrofuryl, relative to sensitive strains containing this activity (Asnis, 1957). This lead to the proposal that nitrofurazone functioned as a pro-drug and required 'activation' before it could mediate its bactericidal activity (Asnis, 1957). Further studies using *E. coli* strains selected on progressively higher concentrations of nitrofurazone revealed that resistance could be acquired in a stepwise fashion (McCalla et al., 1970). Firstly, a low (3-fold) level of resistance could be generated that coincided with the partial loss of the unknown reductase activity. Following prolonged drug exposure, strains exhibiting a higher (10-fold) level of resistance could be selected, with these cells now having a very low reductase capacity. Genetic analysis identified that this phenotype stemmed from the acquisition of mutations in 2 oxygen-insensitive (type I) nitroreductases called nfsA and nfsB (McCalla et al., 1978), resulting in the loss of enzymatic function. It was shown that the initial low level of nitrofurazone resistance was due to mutations in nfsA, while higher levels of resistance were caused by subsequent alterations in nfsB. These data provided the first direct link between nitroheterocyclic drug activity and bacterial oxygen-insensitive nitroreductases.

In addition to phenotypic selection, studies aimed at elucidating nitrofurazone's mechanism of action using biochemical approaches were also conducted. These studies centred on identifying the nature and toxicity of metabolites generated from pro-drug activation. Using the bacterial species *Aerobacter aerogenes* grown under hypoxic conditions, analysis of the nitrofurazone reduction products revealed that its nitro group underwent reduction to generate an aminofuran derivative (Beckett and Robinson, 1959). Prolonged storage of this product resulted in cleavage of the furan ring leading to an open chain nitrile structure (Beckett and Robinson, 1959). Studies on a nitrofurazone variant using *E. coli* indicated that in an aerobic environment the open chain nitrile form was the major end-product, without first going through an aminofuran intermediate (Figure 6.2.2) (Gavin et al., 1966). Following observations that production of the aminofuran under hypoxia was accompanied by production of free radical anion intermediates, it was proposed that formation of the aminofuran was due to the activity of a type II oxygen-sensitive nitroreductase, while the open-chain nitrile was generated

by an oxygen-insensitive type I nitroreductase (Peterson et al., 1979). The formation of an open chain nitrile by an oxygen-insensitive nitroreductase was later confirmed using a purified enzyme from *Enterobacter cloacae* (Bryant and DeLuca, 1991). This situation highlights that nitrofurazone can act as a substrate for more than one nitroreductase, creating the potential for a variety of reduction metabolites and a range of cytotoxic effects. Understanding these processes could prove vital in unravelling the mechanisms of parasite killing and host toxicity of nitrofurazone, nifurtimox, and for nitroaromatic compounds in general

Intriguingly, the open-chain nitrile product derived from nitrofurazone was shown to lack toxicity. This led to the hypothesis that intermediates generated by reduction of the nitrofuryl by a type I oxygen-insensitive nitroreductase were responsible for its antimicrobial properties (McCalla, 1983). A similar idea had already been proposed regarding the activity of mammalian oxygen-sensitive nitroreductases. Here, it was proposed that reduction of the nitro-group generated nitroso and hydroxylamine intermediates (Figure 6.2.2) that could then form adducts with proteins and DNA, leading to cytotoxicity (Swaminathan et al., 1982). This concept was supported by the observation that the addition of the thiol glutathione to mixtures containing intact *E. coli* and nitrofurazone resulted in a decrease in the level of the open chain nitrile product (McCalla, 1983). These findings all highlight that although prokaryotic and eukaryotic organisms activate nitroaromatic drugs by different mechanisms catalysed by type I or type II nitroreductases, the downstream cytotoxicity may be mediated in a common fashion (Figure 6.2.2). In most eukaryotic cells where oxygen is present, nitrofurazone reduction by type II nitroreductases leads to the establishment of a futile cycle resulting in formation of superoxide anions and nitro anion radicals (Figure 6.2.2) (Mason and Holtzman, 1975). Based on *in vitro* biochemical studies, cytochrome P450 reductase can catalyse this type of reaction (Orna and Mason, 1989). In an aerobic environment, this futile cycle may be the predominant metabolite pathway however the detection of open-chain nitrile end-metabolites in vertebrate tissue samples suggests the nitroso pathway also occurs to some degree (Tatsumi et al., 1984; Wang et al., 2010). In contrast, bacteria can readily form these reductive end products regardless of oxygen availability due to their expression of type I nitroreductases.

As several of the nitrofurazone derived reduction metabolites could potentially interact with DNA, worries over its genotoxic and carcinogenic properties have emerged. This issue has been complicated by different approaches in different model systems providing conflicting results. When nitrofurazone was analysed using the Ames test it was initially shown to be a strong mutagen (Gajewska et al., 1990; McCalla and Voutsinos, 1974). However, it soon became apparent that the 'classical' *S. typhimurium* strains used in these screens (designated TA98 and TA100) contained active type I nitroreductases. When the reversion assay tests were repeated using *Salmonella* strains lacking these activities, a significant reduction in the mutagenic effect was observed (Yamada et al., 1997). Experiments on mammalian toxicity using mice treated with nitrofurazone resulted in the identification of single stranded breaks in DNA that correlated with the reduction of nitrofurazone (Olive, 1978), whereas *in vivo* cytogenetic testing in rats and *Drosophila* failed to identify any DNA damaging activities (WHO, 1990). From these studies it was concluded at the time that there is inadequate evidence for the carcinogenicity of nitrofurazone in humans (WHO, 1990). Since stable nitrofurazone derived reduction intermediates have not been successfully isolated, it is difficult to allocate cytotoxicity to a particular intermediate. Yet, it appears clear that it is the reaction intermediates for both the type I oxygen-insensitive and type II oxygen-insensitive nitroreductases that cause cytotoxicity, not the final products.

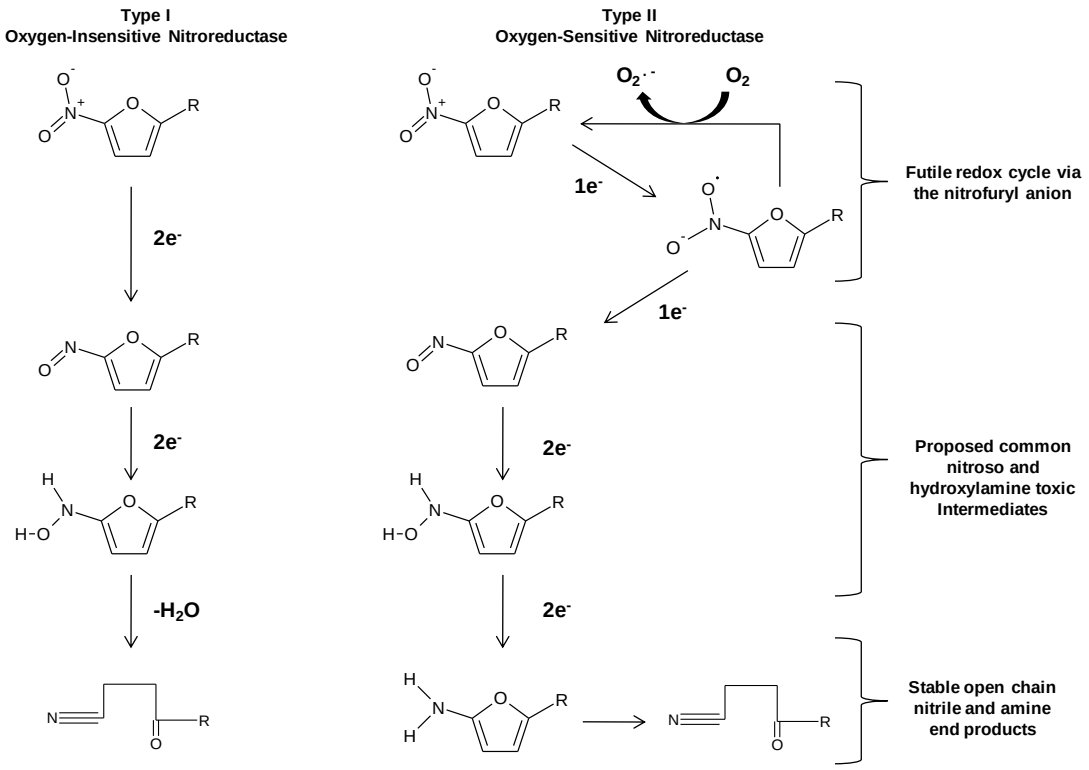

Figure 6.2.2. ***Summary scheme of type I & II nitroreductase mediated nitrofuran metabolites.***
Nitrofurans are metabolized by bacterial type I oxygen-insensitive nitroreductase via a 2-electron reduction to a non-toxic open chain nitrile end-product, implying cytotoxicity is derived from the proposed reaction intermediates (McCalla, 1983). Nitrofuryl adducts are found bound to DNA and protein (Hiraku et al., 2004; Samsonova et al., 2008), suggesting this is the mechanism of cytotoxic action. The ubiquitous type II oxygen-sensitive nitroreductases generates a nitrofuryl anion through a 1-electron reduction, which does not appear to easily react with proteins (Polnaszek et al., 1984). Therefore the nitroso and hydroxylamine intermediates formed by both pathways appear the likely protagonists in cell death.

6.2.2 Nifurtimox

The finding that trypanosomal infections could potentially be treated with nitrofurazone sparked a series of screening programmes to explore the parasite killing activities of other nitrofurans, with nifurtimox (Figure 6.2.1) showing particular promise against *T. cruzi* infections (Bock et al., 1969). Initial findings demonstrated that the addition of nifurtimox to *T. cruzi* mitochondrial fractions or rat liver microsomes stimulated production of superoxide anions (Docampo et al., 1981b; Docampo and Stoppani, 1979; Maya et al., 2003; Viode et al., 1999). This resulted in the widely accepted view that

nifurtimox induced oxidative stress within trypanosomes, and suggested that a type II nitroreductase mechanism was key to its trypanocidal activity. Several parasite enzymes such as trypanothione reductase, lipoamide dehydrogenase and cytochrome P450 reductase were shown to mediate this reaction *in vitro*, appearing to confirm these early findings (Blumenstiel et al., 1999; Henderson et al., 1988; Viode et al., 1999). This idea gained strength as reports had also shown that trypanosomes had a limited enzymatic capacity to metabolize reactive oxygen species (Boveris et al., 1980). Additional indirect evidence for this case arose following functional studies on a trypanosomal superoxide dismutase isoform, where parasites lacking this activity were more susceptible to nifurtimox than control lines (Prathalingham et al., 2007).

Another trypanosomal enzyme that has been implicated in the metabolism of nifurtimox is prostaglandin F2α synthase (also called the "old yellow enzyme"). *In vitro* studies using the *T. cruzi* enzyme revealed that it could catalyse the 2-electron reduction of the nitrofuran but only under anaerobic conditions. Immuno-precipitation of this activity in *T. cruzi* lysates drastically lowered the total extracts capacity to reduce nifurtimox, suggesting that this enzyme may have an important role in nifurtimox metabolism (Kubata et al., 2002).

Circumstantial evidence has shown that nifurtimox resistance between strains correlates with an increase in free glutathione levels (Moncada et al., 1989), and that *T. cruzi* life-cycle stages with the highest thiol levels display an increased resistance to nifurtimox (Maya et al., 1997). Additionally, treating *T. cruzi* with nifurtimox reduces the levels of detectable free glutathione and trypanothione (Repetto et al., 1996), an effect that appears to be independent of any superoxide production (Boiani et al., 2010). As in the case of nitrofurazone, the nitroso and/or hydroxylamine intermediates generated following nifurtimox reduction by a type I nitroreductase could result in the formation of thiol conjugates. Therefore, one possible mechanism that leads to nifurtimox resistance could stem from the parasite increasing its thiol synthesis capacity.

Any significant nifurtimox-glutathione conjugates formed in *T. cruzi* may be explained by the discovery that trypanosomatids contain a bacterial like type I oxygen-sensitive nitroreductase (Wilkinson et al., 2008). In the classical behaviour of a pro-drug activator, parasites with altered levels of the trypanosomal type I nitroreductase have been shown to posses differing susceptibility to nifurtimox such that null mutant/ heterozygous cells display resistance to the nitrofuran, while over-expression confers hypersensitivity. Additionally, *T. cruzi* parasites selected for resistance to nifurtimox undergo the loss of a chromosome containing the type I nitroreductase (Wilkinson et al., 2008). Also performing a nifurtimox drug resistance based selection with a *T. brucei* RNAi library singly identified the type I nitroreductase enzyme in a loss of function screen (Baker et al., 2010). Together, these data provide a clear link that this enzyme plays a key role in activating this drug within the parasite. The *T. cruzi* cell-lines selected for resistance to nifurtimox are also cross-resistant to other nitroheterocyclic compounds such as benznidazole and nitrofurazone (Wilkinson et al., 2008). This observation is re-affirmed by nifurtimox drug selection studies on *T. brucei*, where again the resulting cell-lines were found to display cross-resistance to nitrofurazone, the nitroheterocyclic drug candidate fexinidazole, and the anti-cancer nitroaromatic agent CB1954 (Sokolova et al., 2010). Although not established in these studies, the phenotype is reminiscent of observations made using the *T. cruzi* selected lines and *T. brucei*/ *T. cruzi* recombinant lines having lowered levels of the type I nitroreductase. Worryingly, this has significant repercussions for trypanosomal drug development, as investing in nitroheterocyclic monotherapies may have long term associated problems with clinical resistance.

As with nitrofurazone, nifurtimox has been shown to be mutagenic in *E. coli* assays (Ohnishi et al., 1980) and the Ames test using the 'classical' *S. typhimurium* strains TA98 and TA100 (Nagel and Nepomnaschy, 1983). Interestingly, the DNA mutagenicity observed in the Ames test was abolished when using bacterial mutants deficient in the oxygen-sensitive nitroreductase complement (Ferreira et al., 1988), suggesting this type I nitroreductase activity is the predominant activator of nifurtimox. Also, *E. coli* mutants deficient in their superoxide dismutase gene reportoire had no alteration on mutagenicity (Prieto-Alamo et al., 1993), implying that any superoxide

anions formed from a type II nitroreductase activity had no detectable role in causing DNA damage. The issue regarding the genotoxic properties of nifurtimox in eukaryotic systems is confusing. In *Drosophila*, nifurtimox appears to be mutagenic (Moraga and Graf, 1989), in contrast to what was reported when using nitrofurazone (this difference probably reflects the different approaches used), while a study in rats assessing nifurtimox's potential for inducing carcinogenicity found no evidence of cancer causing lesions over a 40 week period (Iatropoulos et al., 2006), despite its known genotoxicity in other systems (Buschini et al., 2009). Nevertheless, the carcinogenicity of this drug continues to remain controversial.

6.3 Nitroaromatic Pro-drugs as Anti-Cancer Agents

The nitroaromatic pro-drug CB1954 (5-aziridinyl-2, 4-dinitrobenzamide, also known as tretazicar) was first developed as an anti-cancer therapy in the 1970's and displayed promising pre-clinical results in a rat model (Cobb, 1970). Unfortunately, this success did not translate to human clinical trials, mainly as DT-diaphorase (also known as NADPH quinone oxidoreductase 1, or NQO1), the enzyme responsible for pro-drug activation, was far less active in human cells than its rodent orthologue (Boland et al., 1991; Knox et al., 1988). This lead to the concept of using *E. coli* type I nitroreductase nfsB, which had previously been shown to activate numerous nitroaromatic-based pro-drugs, to substitute as a mammalian CB1954 activator (Drabek et al., 1997). In a two-step process, known as gene-directed enzyme pro-drug therapy (GDEPT), firstly a gene encoding for a type I nitroreductase such as *E. coli* nfsB is targeted to, and expressed within the tumour cell. This is followed by administration of the CB1954 pro-drug which is then activated to cytotoxic moieties by the bacterial enzyme (McNeish et al., 1998). Although GDEPT requires the contentious implementation of trans-gene therapy, in which so far one trial participant has died (Lehrman, 1999) and two developed leukaemia (Kohn et al., 2003), clinical trials with nitroreductase and CB1954 are currently underway (Patel et al., 2009).

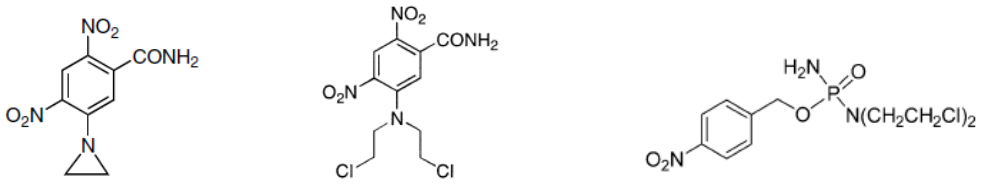

CB1954 | **Nitrobenzamide Mustard** | **4-Nitrobenzyl Phosphoramide Mustard**

Figure 6.3.1. ***Chemical structures of 3 anti-cancer compounds used with GDEPT.***

CB1954 possesses two nitro groups in the 2- and 4- positions on a benzyl ring, with an aziridinyl substituent found at the 5-position (Figure 6.3.1). Analysis of its mode of action indicates that following activation of either nitro groups by the type I nitroreductase, an equimolar mixture of 2- and 4- hydroxylamine metabolites are formed (Helsby et al., 2004b; Knox et al., 1991; Venitt and Crofton-Sleigh, 1987). Both of these intermediaries can then be processed further to form the corresponding 2- and 4- amine molecules, while the 4- hydroxylamine is also able to react with DNA. The interaction of the 4- hydroxylamine with DNA is not direct, but first requires it to react with a thioester such as acetyl coenzyme A to form the necessary reactive group (Figure 6.3.2) (Knox et al., 1991). All of these metabolites have cytotoxic activities in mammalian systems (Helsby et al., 2004b; Tang et al., 2005). Recently CB1954 has been shown to display good *in vitro* activity against bloodstream form *T. brucei* (Sokolova et al., 2010), raising the possibility that this clinical candidate represents a promising lead in developing new anti-trypanocidal agents.

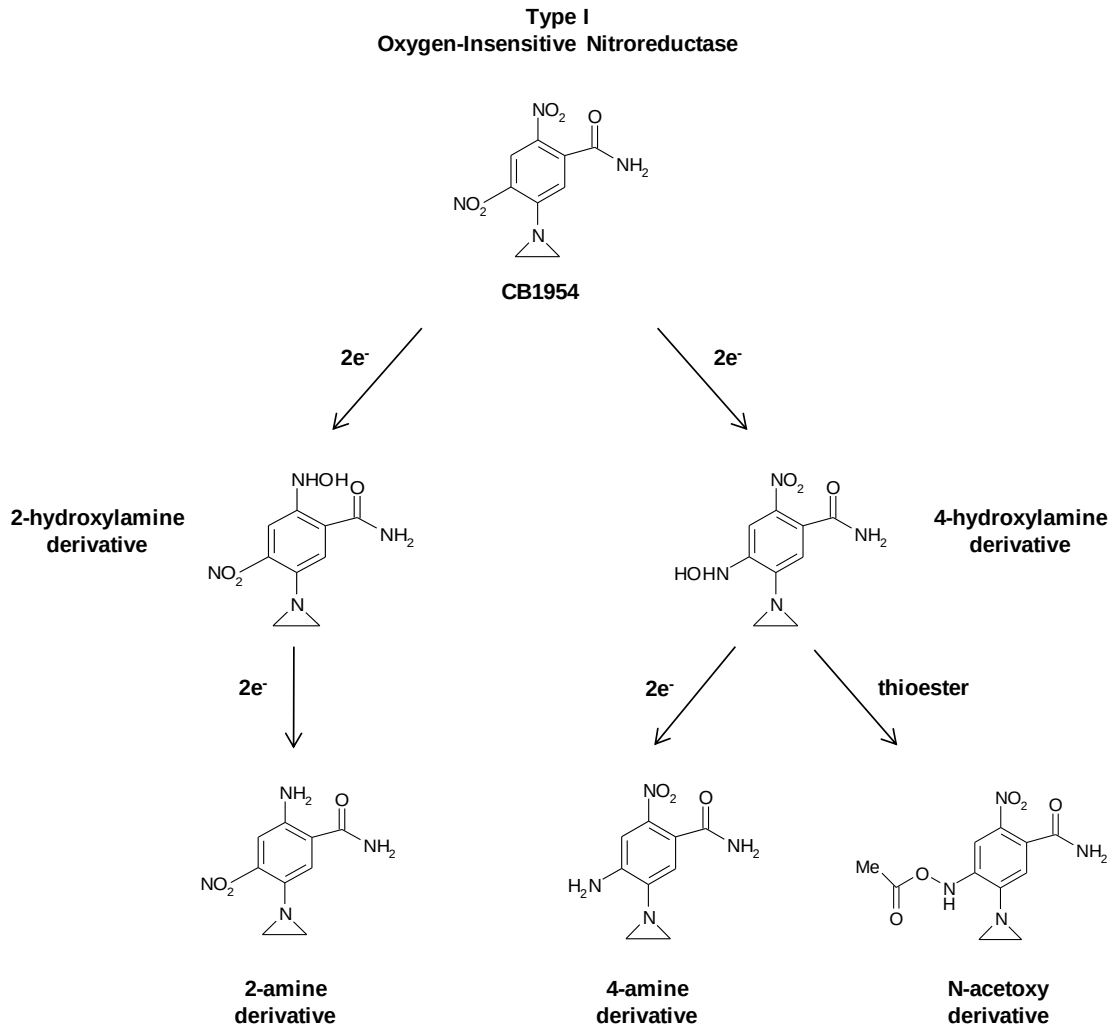

Figure 6.3.2. ***Summary scheme of nitroreductase mediated reduction of CB1954.*** Either nitro group of the benzyl ring may be reduced by nitroreductase. Reduction of the 2- nitro group first forms the 2-hydroxylamine, which can then be reduced further to form the 2-amine derivative. A similar pathway is observed for the 4- nitro group, however the 4-hydroxylamine is also able to react with thioesters such as acetyl coenzyme A. It has been shown that all of these metabolites have cytotoxic properties (Helsby et al., 2004b; Tang et al., 2005). Figure adapted from Wilkinson et al., 2011.

In an attempt to increase the potency of CB1954 against mammalian tumour cells, the aziridinyl group was replaced with a mustard group. This nitrobenzamide mustard (Figure 6.3.1) has an increased affinity for the nitroreductase enzyme, while its reactivity becomes limited to only reduction of the nitro group in the 2- position (Anlezark et al., 1995). Consequently, the benzene ring acts as an 'electronic switch', with the specific activation of the 2- position nitro group leading to the rearrangement of electrons throughout the molecule (Siim et al., 1997). This electronic rearrangement results in the opposite mustard group becoming highly reactive, now being able to directly react with DNA, without requiring an intermediate reaction step involving a stable hydroxylamine metabolite and thioester molecule (Helsby et al., 2003). It also improves the potency of the compound against human cell-lines featuring nfsB, relative to the original CB1954 (Helsby et al., 2004b).

Based on the studies with CB1954, another series of novel compounds for GDEPT were developed which combined a nitro-aromatic ring linked to a variety of phosphoramide mustards (Hu et al., 2003). These nitrobenzyl phosphoramides (Figure 6.3.1) expand upon the anti-cancer drug cyclophosphamide, which is used in co-therapies with drugs such as etoposide (El-Helw and Hancock, 2007). The cyclophosphamide itself acts as a pro-drug, and first requires activation via an interaction with cytochrome P450, which opens up the basic ring structure and forms a toxic linear alkylating mustard group (Borch and Millard, 1987). For the nitrobenzyl phosphoramides, activation of the nitro group on the benzene ring by nitroreductase triggers an electronic switch which replaces the need for cytochrome P450. Depending on the nature of the phosphoramide opposite the nitro group, the activation of this molecule can have one of two effects. If the nitrobenzyl component contains an associated cyclic phosphoramide, then nitroreductase mediated activation results in exposure of the mustard group, which is intended to cause direct cellular toxicity (Figure 6.3.3). However if a linear phosphoramide mustard is present opposite the electronic switch, then this group is designed to release from the nitrobenzyl, forming a separate linear alkylating mustard that generates cytotoxicity (Jiang et al., 2006). In assays with mammalian cells expressing nitroreductase, these compounds have been shown to generate strong growth inhibition, plus good selectivity towards these transgenic cells relative to their

unmodified parent lines (Jiang et al., 2006). It will be interesting to see if these compounds are active against trypanosomes, given the presence of a native nitroreductase.

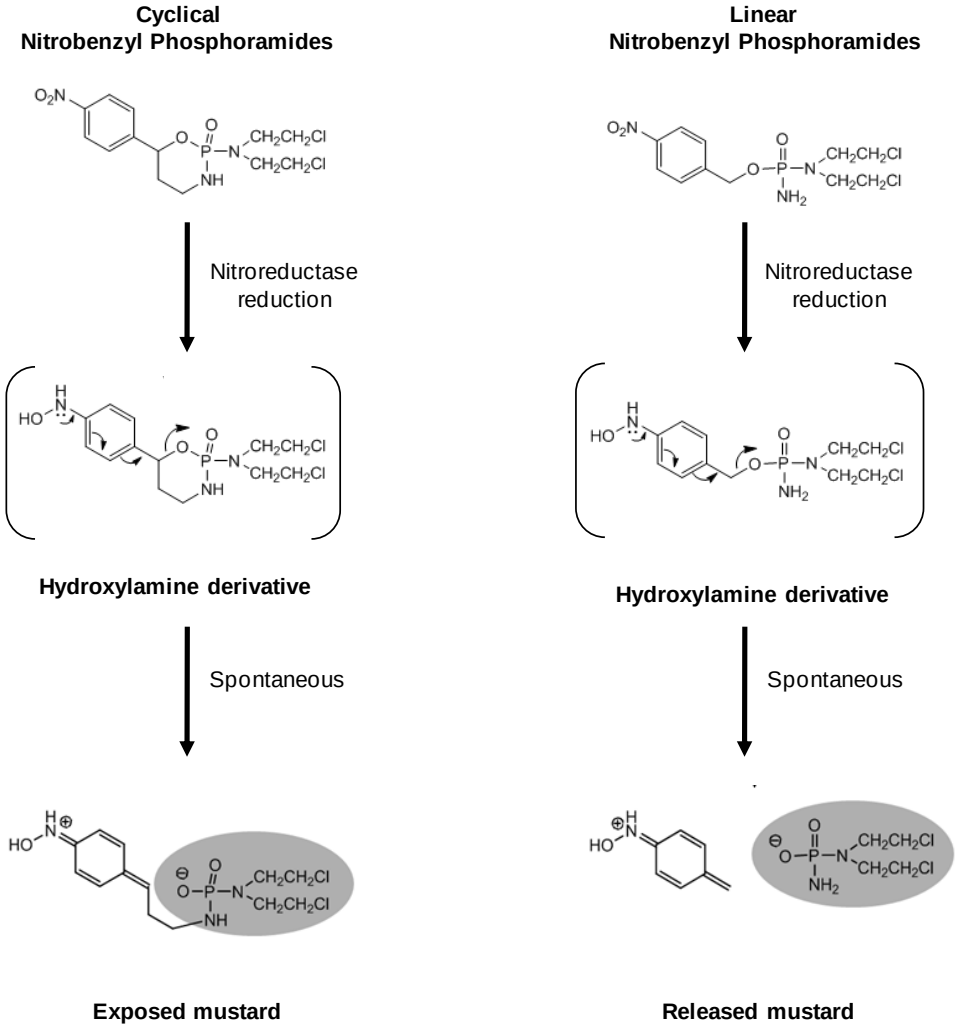

Figure 6.3.3. ***Summary scheme of nitroreductase mediated reduction of nitrobenzyl phosphoramides.***
For both cyclical and linear nitrobenzyl phosphoramides, reduction of the nitro group on the benzyl ring by nitroreductase leads to the formation of the hydroxylamine derivative. This leads to a rearrangement of electrons across the benzene ring. For cyclical nitrobenzyl phosphoramides, this movement of electrons results in exposure of the toxic mustard moiety, while for the linear nitrobenzyl phosphoramides the toxic mustard is released from the parent compound (Jiang et al., 2006). Figure adapted from Wilkinson et al., 2011.

6.4 Research Objectives

The aim of investigating novel type I nitroreductase activated nitroaromatic pro-drugs in trypanosomes can be defined by the following core objectives:

- Develop a high-throughput drug screening system for the medically relevant amastigote stage of *T. cruzi* to facilitate assaying nitroaromatic compounds.
- Screen novel nitroaromatic compounds for trypanocidal activity against *T. cruzi* using the high-throughput system.
- Utilize the *T .brucei* cell-lines with altered levels of nitroreductase expression to define the mechanism of action of nitroaromatic drugs in trypanosomes.

7 Nitroaromatic Compounds against *T. cruzi*

Nitroheterocyclic based pro-drugs such as nifurtimox and benznidazole have been used for more than forty years to treat trypanosomal infections (Wilkinson and Kelly, 2009). Recently, it has been demonstrated that such compounds undergo activation in a reaction catalysed by a type I nitroreductase (Wilkinson et al., 2008). This chapter describes the construction and validation of a luciferase-based *T. cruzi* reporter system, which is then used to evaluate the effectiveness of 39 nitroaromatic compounds from three distinct classes towards the medically relevant, intracellular amastigote form of the parasite.

7.1 The Luciferase Cell Reporter System

There is an urgent need for new drugs targeting the protozoan parasite *T. cruzi*. However, most research aimed at identifying trypanocidal compounds against this pathogen has focused on the insect epimastigote or the non-dividing, infectious trypomastigote stages instead of the medically important amastigote form. The main issues associated with analysing the epimastigote and trypomastigote lifecycle stages is that they do not accurately reflect the amastigote inside a mammalian cell where the abundance of protein drug targets, activators, and drug import/export complexes may vary considerably, as suggested by preliminary observations of the life-cycles differing relative proteomic profiles (Atwood et al., 2005). Therefore, promising trypanocidal compounds may be mistakenly overlooked while agents that show promise against the epimastigote or trypomastigote forms may not be effective against *T. cruzi* amastigotes.

The primarily reasons for focusing on *T. cruzi* epimastigote or trypomastigote forms for drug screening are that large quantities of these life-cycle stages can be cultured or obtained with relative ease, while high-throughput evaluation of parasite numbers can be carried out using colorimetric approaches with dyes such as MTT and AlamarBlue (Muelas-Serrano et al., 2000; Rolon et al., 2006). In contrast, maintaining *T. cruzi* amastigotes within a mammalian cell and evaluating parasite infectivity load is both time consuming and labour intensive. The construction of transgenic parasites

expressing β-galactosidase (Buckner et al., 1996) has greatly aided drug screening within the medically relevant lifecycle stages (Bettiol et al., 2009; Bressi et al., 2001; Buckner et al., 2003), but a major drawback with this strategy is that it does not work when testing coloured compounds (Buckner et al., 1996). Given that many of the nitroheterocyclic compounds in our library are coloured, it was decided that an alternative screening approach using a bioluminescence reporter should be developed. Luciferase-based cell reporter systems have been implemented for a range of organisms and applied in drug screening against various pathogens such as *Mycobacterium tuberculosis* (Jacobs et al., 1993), *Leishmania* species (Lang et al., 2005; Osorio et al., 2011; Roy et al., 2000), *T. brucei* (Claes et al., 2009) and *P. falciparum* (Lucumi et al., 2010). Here, a trypanosomal integrative expression vector facilitating the constitutive expression of a bioluminescence reporter gene is developed and used to evaluate whether three series of nitroaromatics have potential in treating *T. cruzi* intracellular form parasites.

7.1.1 Luciferase expression from the GAPDH locus

To develop a luciferase-based system that could be used in drug screens against *T. cruzi* amastigotes, a DNA vector was required that facilitated the constitutive expression of the bioluminescence reporter gene. Several episomal constructs such as pTEX (Kelly et al., 1992) and pRIBOTEX (Martinez-Calvillo et al., 1997) have been developed that meet this need. However, as culturing of *T. cruzi* amastigote within mammalian cells occurs in the absence of drug pressure, and recombinant parasites may readily lose plasmids in the absence of such selection, a more stable integrated expression system was required. Based on a previous finding that the 3' un-translated region (UTR) of glyceraldehyde 3-phosphate dehydrogenase (GAPDH) increased mRNA stability of episomal luciferase expression in *T. cruzi* (Nozaki and Cross, 1995), a DNA vector was designed that would integrate into the GAPDH loci of the parasite's genome. In *T. cruzi*, there are 4 GAPDH genes per diploid genome and these are arranged in tandem with two genes per array (Kendall et al., 1990). Using the *T. cruzi* GAPDH intergenic and 3' UTR sequences, an expression plasmid was developed to integrate into, and replace, the downstream copy of the GAPDH gene. To generate this plasmid, first the GAPDH intergenic region of the tandem repeat, the upstream neomycin drug resistance gene, and

the β/α intergenic region of the tubulin array was excised as 1 fragment from pKS-FKN-Neo, (Figure 7.1.1a) and cloned into pBlueScript II (Section 3.6.12). Next, the firefly luciferase gene and the 3' UTR of GAPDH were cloned adjacent to this fragment within pBlueScript II, to form the final plasmid, pGAP-Luciferase (Figure 7.1.1b). This was linearized with a *Kpn*I and *Sac*I double digest, and the 4.6 kb DNA fragment containing neomycin/luciferase cassette was gel purified.

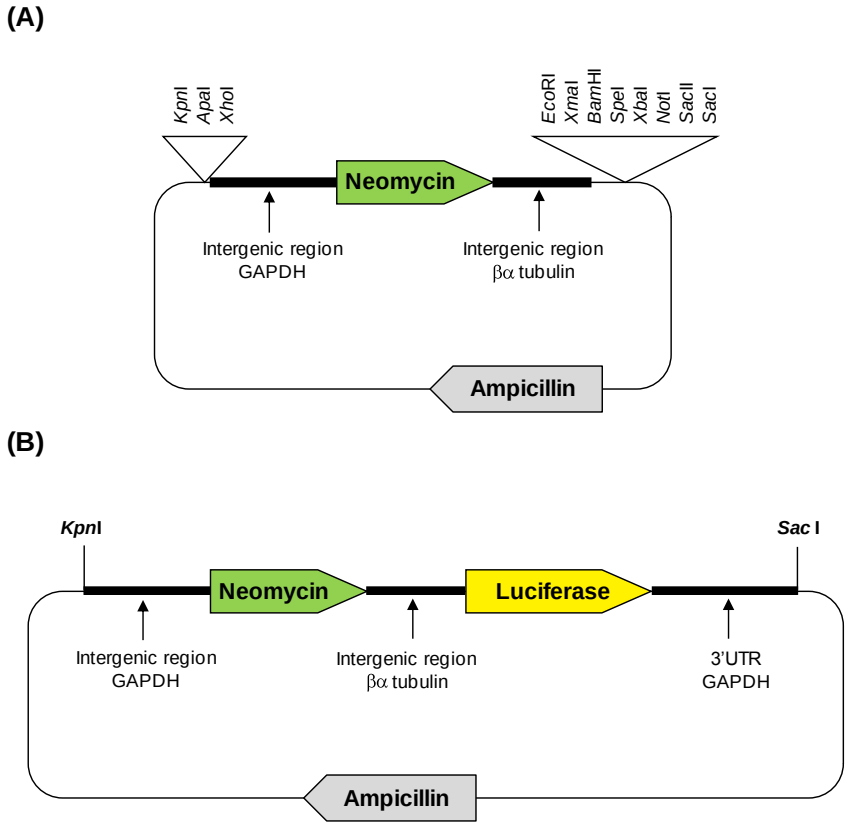

Figure 7.1.1. ***Map of pGAP-Luciferase, a GAPDH targeted expression construct.***
(**A**) Restriction map of pKS-FKN-Neo (provided by Dr. Wilkinson, unpublished). This construct contains a neomycin resistance gene flanked at its 5' end by the *T. cruzi* GAPDH intergenic region and at its 3' end by the *T. brucei* β/α tubulin intergenic repeat. The entire cassette is bordered by multiple cloning sites. (**B**) To form the bioluminescence expression vector, a DNA fragment containing the luciferase gene and *T. cruzi* GAPDH 3' untranslated region (UTR) was inserted into the downstream multiple cloning sites of pKS-FKN-Neo to generate the plasmid pGAP-Luciferase. The two intergenic sequences and the 3'UTR provide the genetic elements required for processing the neomycin and luciferase mRNAs. Restriction digestion of pGAP-Luciferase with *Kpn*I and *Sac*I releases the neomycin/luciferase expression cassette from the plasmid backbone (Section 3.6.12). Following introduction into *T. cruzi*, this cassette is designed to integrate into the GAPDH array, deleting the downstream GAPDH gene.

The purified DNA fragment was then introduced into wild-type *T. cruzi* X10/6 and a *T. cruzi* X10/6 $NTR^{+/-}$ heterozygous cell-line by electroporation, followed by drug selection using G418 (Section 3.10.2). The *T. cruzi* X10/6 $NTR^{+/-}$ heterozygous parasites were also grown in the presence of blasticidin to maintain selection of the nitroreductase gene deletion (Wilkinson et al 2008). From each transformation, drug resistant clones were selected. To rapidly assess whether the parasites were expressing luciferase, an aliquot of cells (20,000) was taken and their bioluminescence activity determined (Figure 7.1.2). The untransformed wild-type *T. cruzi* X10/6 control was analysed in parallel. For transgenic lines, designated as *T. cruzi* $X10/6^{Gap\text{-}Luc}$ and $X10/6^{Gap\text{-}Luc}$ $NTR^{+/-}$, a luminescence reading of more than 100,000- fold greater than the untransformed control was detected, indicating that the recombinant parasites had a high level of luciferase expression.

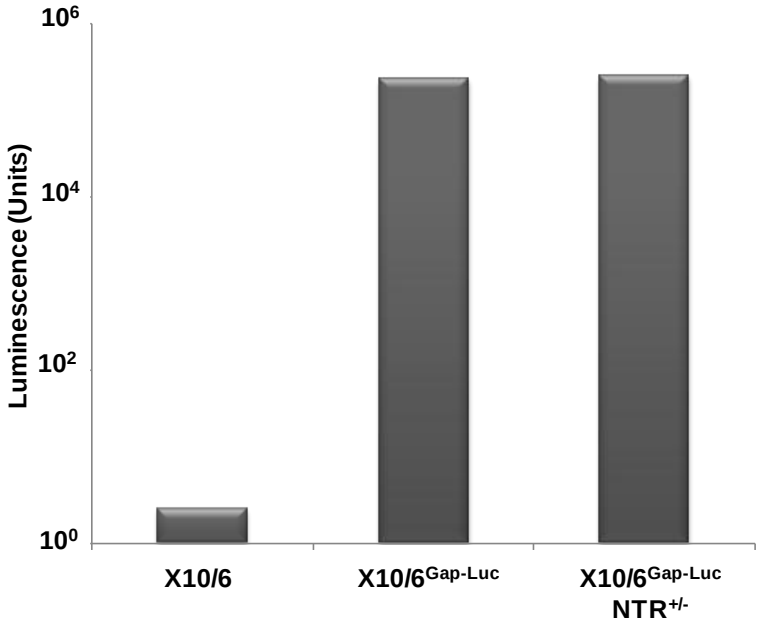

Figure 7.1.2. ***Luciferase expression by T. cruzi epimastigotes using a construct targeted to the GAPDH loci.***
The luciferase activity, as measured in light units, of extracts derived from 20,000 recombinant *T. cruzi* epimastigotes ($X10/6^{Gap\text{-}Luc}$ and $X10/6^{Gap\text{-}Luc}$ $NTR^{+/-}$) was determined and compared to that of the parental line (X10/6). Both luciferase expressing lines displayed a 100,000 fold increase in luminescence (measured in light units) relative to the wild-type, confirming expression of the luciferase gene.

The main reason for developing the luciferase reporter system was to facilitate a procedure for determining the intracellular amastigote loads within mammalian cells. Therefore, before analysing the bioluminescence activity of recombinant parasites any further, the infectivity of these lines was investigated. Cultures of wild-type *T. cruzi* X10/6 (control), X10/6$^{Gap\text{-}Luc}$ and X10/6$^{Gap\text{-}Luc}$ NTR$^{+/-}$ in the stationary phase of growth were used to infect African green monkey kidney (Vero) cells. For wild-type *T. cruzi* X10/6 controls, amastigotes were detected microscopically 2-4 weeks post-infection, with bloodstream trypomastigotes subsequently observed in the growth medium following mammalian cell lysis. For both luciferase expressing lines, amastigotes and bloodstream trypomastigotes were never seen, even 2-3 months post-infection. This strongly suggests that during *in vitro* infections, the luciferase expressing parasites were attenuated and were no longer infective. Interestingly, this non-infectious phenotype has been observed previously using a pTEX episomal plasmid that had inadvertently integrated adjacent to the GAPDH loci (Zacks, 2007). Combined, this data indicates that GAPDH activity is critical during the differentiation of epimastigotes to metacyclic trypomastigotes, or the establishment of the amastigote within the mammalian cell. This observation was not examined any further.

7.1.2 Construction of a ribosomal array-based luciferase expression system

As luciferase expression at the GAPDH locus resulted in the inability of *T. cruzi* to infect mammalian cells *in vitro*, an alternative strategy to integrate the bioluminescence reporter gene into another site of the parasite genome was required. In *T. brucei*, several DNA constructs have previously been targeted to ribosomal regions for functional genomics studies (Alsford and Horn, 2008; Obado et al., 2011). As there are numerous ribosomal gene arrays in trypanosomal genomes (Section 1.5.2) (Berriman et al., 2005; El-Sayed et al., 2005a), integration of constructs to these regions should not affect the overall expression levels of the encoded ribosomal proteins. Also, other protein coding regions of the genome would be unaffected, thus reducing any possible off-target effects such as loss of infectivity. The new cloning strategy involved using two episomal expression vectors pTEX (Kelly et al., 1992) and pRIBOTEX (Martinez-Calvillo et al., 1997) as the source of a neomycin expression cassette and ribosomal promoter, respectively.

The authors of pRIBOTEX have themselves shown that pRIBOTEX is already capable of genomic integration, although they only speculated as to the locus, suggesting GAPDH as the most likely. It has since been shown that pRIBOTEX integrates into the ribosomal array, although surprisingly not via targeting of the ribosomal spacer (Lorenzi et al., 2003), but by some currently unknown mechanism specifically involving the ribosomal promoter itself. The advantage of using pRIBOTEX as a template though, is that the ribosomal spacer contains a characterized ribosomal promoter (Martinez-Calvillo and Hernandez, 1994) to drive gene expression, and an apparent trans-splicing site (Martinez-Calvillo et al., 1997) to allow the required mRNA processing of the downstream expressed gene (Section 1.5.4). Since the actual mechanism of integration of pRIBOTEX is unknown, and gene expression in the amastigote stage would not be under drug pressure for extended periods of time, a new plasmid was designed to integrate through double homologous recombination, using twin rRNA flanking regions to ensure a stable integration.

To generate the integrative plasmid, a 3' ribosomal spacer region was amplified from *T. cruzi* CL Brener genomic DNA and cloned into a unique *Kpn*I site of pTEX located downstream of the neomycin expression cassette. This cassette contains the neomycin phosphotransferase gene flanked by intergenic (upstream) and 3' UTR (downstream) GAPDH sequences that provide the required trans-splicing/poly-A addition sites needed for processing the drug resistance mRNA. Next, the 5' ribosomal region of pRIBOTEX was inserted into pTEX, replacing a 5' UTR sequence of GAPDH. The cloning was done such that a multiple cloning site (MCS) was maintained between the 5' ribosomal region and neomycin expression cassette (Section 3.6.13). This resulted in the plasmid pTRIX (Figure 7.1.3a). Restriction digestion of pTRIX with *Sac*I and *Asc*I releases a 4.2 kb DNA fragment consisting of the neomycin expression cassette bordered by the 5' and 3' *T. cruzi* ribosomal spacer sequences. These flanking regions provide DNA sequences required for integration through double homologous recombination of this fragment into the *T. cruzi* ribosomal spacer loci. Additionally, several key features required for protein expression have been engineered into this vector, including: a multiple cloning site into which the gene of interest can be inserted, a characterized promoter in the 5' ribosomal region upstream of the multiple cloning site, and a trans-splicing and a poly-A addition

site (Martinez-Calvillo et al., 1997), found in the 5' ribosomal region and intergenic GAPDH sequence respectively. These provide the elements needed for processing the mRNA generated from a gene cloned into the multiple cloning site of the plasmid.

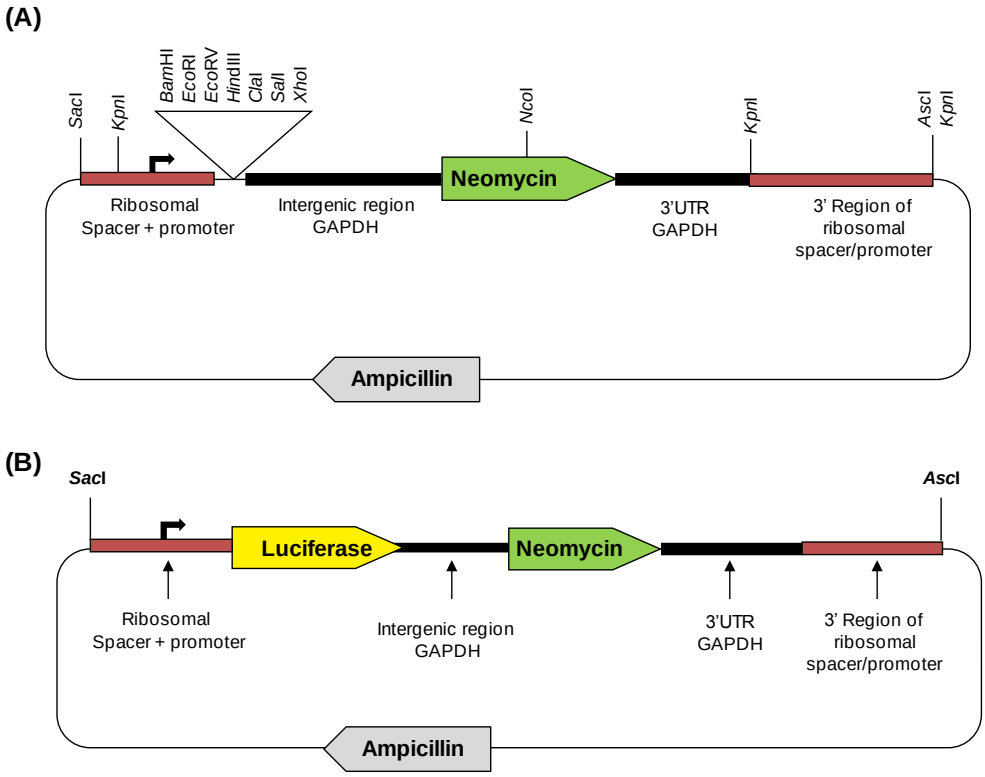

Figure 7.1.3. ***Map of pTRIX, a ribosomal promoter based expression construct.***
(**A**) The episomal expression plasmid pTEX (Kelly et al., 1992) was modified by inserting DNA sequences corresponding to the *T. cruzi* ribosomal spacer region either side of a neomycin expression cassette, generating the construct pTRIX. To facilitate high levels of gene expression, pTRIX contains a ribosomal promoter derived from pRIBO-TEX in the 5' ribosomal spacer sequence (Martinez-Calvillo et al., 1997). Immediately downstream is a multiple cloning site where the gene under study can be cloned. (**B**) The firefly luciferase gene was inserted into the multiple cloning site of pTRIX to form pTRIX-luciferase. Restriction digestion of pTRIX-luciferase with *Sac*I and *Asc*I releases the neomycin/luciferase expression cassette from the plasmid backbone. Following introduction into *T. cruzi*, this cassette is designed to integrate into the ribosomal array.

Following construction of the expression plasmid (Figure 7.1.3a), the firefly luciferase gene was cloned into the multiple cloning site of pTRIX (Section 3.6.14) to form pTRIX-luciferase (Figure 7.1.3b). Digestion of this plasmid with *Sac*I and *Asc*I liberated a 5.8 kb DNA fragment that was subsequently gel purified. The purified, linear DNA fragment was electroporated into wild-type *T. cruzi* (CL Brener and X10/6) and the X10/6 $NTR^{+/-}$ heterozygous cell-line. Selection was carried out using G418, with the heterozygous line maintained in the presence of blasticidin (Section 3.10.2). Drug resistant epimastigote clones were observed approximately 4 weeks post-electroporation. As previously described for the GADPH-based expression system, parasite extracts derived from 20,000 trypanosomes were assayed for luciferase activity. The luminescence readings were compared against untransformed wild-type *T. cruzi* (CL-Brener and X10/6) that were analysed in parallel. In total, 10 drug resistant *T. cruzi* cultures were examined including four clones from electroporations involving CL Brener and 3 each from the X10/6 and X10/6 $NTR^{+/-}$ lines. These cell-lines were designated as CL $Brener^{Ribo\text{-}Luc}$, $X10/6^{Ribo\text{-}Luc}$ and $X10/6^{Ribo\text{-}Luc}$ $NTR^{+/-}$. In all cases, the drug resistant clones displayed a higher luciferase activity than untransformed controls, exhibiting up to 10,000-fold increase in luminescence relative to the wild-type background (Figure 7.1.4).

Further comparisons revealed that luminescence data obtained from CL $Brener^{Ribo\text{-}Luc}$ clones was, on average, 10-fold higher than that of the X10/6 luciferase expressing lines. This result was consistent across all clones. One possible reason for this difference may be due to the origin of the ribosomal promoter, a sequence originally derived from the *T. cruzi* La Cruz cell-line. It is plausible that this ribosomal promoter may be able to initiate transcription more readily in CL Brener than in X10/6, resulting in a higher level of gene expression. Polymorphisms in *T. cruzi* ribosomal promoter sequences have been reported (Nunes et al., 1997), and shown to affect levels of gene expression (Floeter-Winter et al., 1997). Analysis of the luciferase activity levels from *T. cruzi* $X10/6^{Gap\text{-}Luc}$ and $X10/6^{Ribo\text{-}Luc}$ cells revealed that luminescence was approximately 10-fold higher in extracts derived from cells where the reporter was expressed at the GAPDH loci than from the ribosomal spacer region. Again, this difference may reflect transcription efficiencies, with the La Cruz ribosomal promoter not being as effective at initiating

transcription in *T. cruzi* X10/6 as compared to the endogenous RNA polymerase II machinery. However, it must be noted that this observation is based on a single luminescence value for the *T. cruzi* X10/6$^{Gap\text{-}Luc}$ cell-line. Additionally, although Southern hybridizations have not been carried out to map the sites of integration, it appears that using a 5' ribosomal targeting sequence from one *T. cruzi* strain (La Cruz), in combination with a 3' ribosomal targeting sequence from another strain (CL Brener), does not impede recombination of the expression vector into the *T. cruzi* CL Brener or X10/6 genomes.

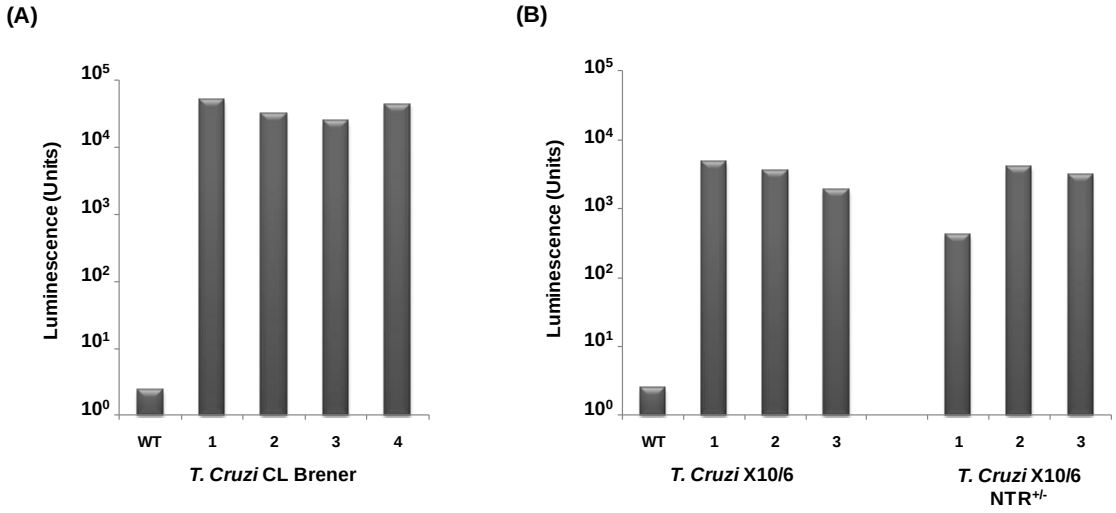

Figure 7.1.4. ***Luciferase expression by T. cruzi epimastigotes using a construct targeted to the ribosomal array.***
(**A**) The luciferase activity of 4 recombinant *T. cruzi* CL-Brener$^{Ribo\text{-}Luc}$ epimastigote clones (1-4) were determined and compared to the parental line (WT). (**B**) A similar analysis was carried out on 3 recombinant *T. cruzi* X10/6$^{Ribo\text{-}Luc}$ (1-3) and 3 X10/6$^{Ribo\text{-}Luc}$ NTR$^{+/-}$ (1-3) epimastigote clones. In both panels, 20,000 cells were used in each analysis. The luciferase activity, as measured in light units, was 1000 fold higher in recombinant *T. cruzi* X10/6 lines than wild-type background levels but was lower than that detected in recombinant CL-Brener extracts.

Since the *T. cruzi* CL Brener strains demonstrated the highest luciferase activity per sampled aliquot, consistently across clones, the *T. cruzi* CL Brener$^{Ribo\text{-}Luc}$ cell-line was selected to develop the first luciferase based drug screening system. Although high expression levels were observed in the epimastigote form of the parasite, it was unknown at this stage what the expression levels would be like when analyzing the amastigote stage in much fewer parasite numbers, and if luciferase activity would be high enough to detect in an infective replication stage based drug assay.

Initially, assays were performed to determine whether integration of the DNA construct into the *T. cruzi* genome and/or expression of the luminescence affected parasite growth (Figure 7.1.5). In these experiments, two CL Brener$^{Ribo\text{-}Luc}$ clones and a wild-type CL Brener cell-line, all grown without drug, were analysed in parallel. Starting from a density of 5 x 10^5 parasites ml^{-1}, the cumulative cell growth was determined over a 9 day period, with all cultures maintained in the exponential phase of growth. This was achieved by diluting cultures when they reached the late logarithmic phase of growth (1 x 10^7 parasites ml^{-1}; 96 hrs into the experiment). Over the 9 day time course, both CL Brener$^{Ribo\text{-}Luc}$ lines behaved similarly to the wild-type, with all 3 cell-lines demonstrating an approximate doubling time of 21 hours. This indicates that integration of pTRIX-luciferase into the CL Brener genome, and the resulting luciferase expression has no effect on epimastigote growth rates, demonstrating that pTRIX can be used as a general purpose integrative plasmid containing any required gene, without the plasmid components affecting parasite growth.

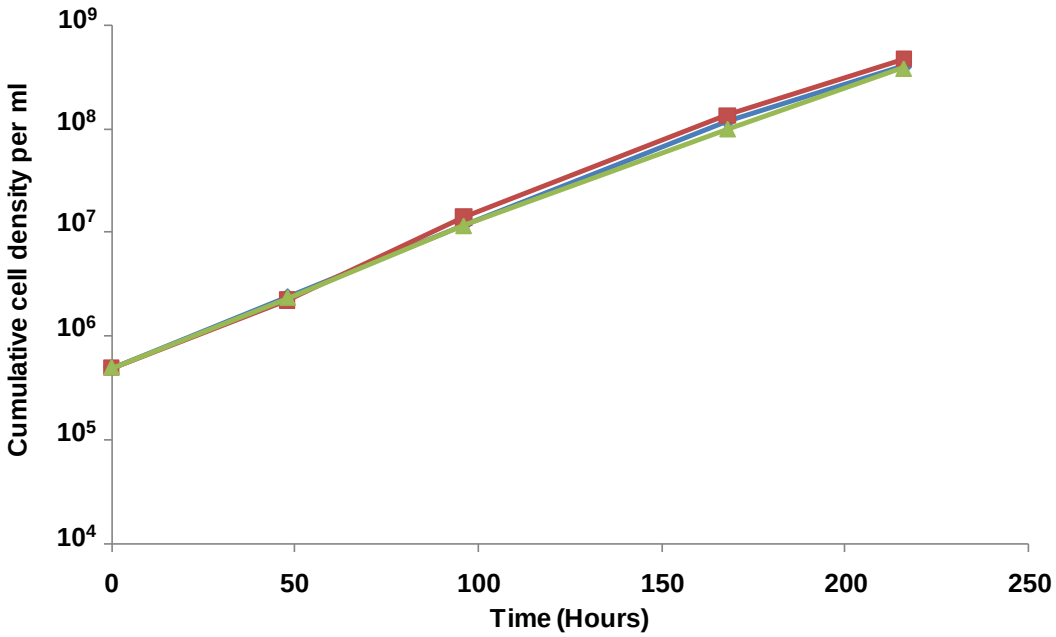

Figure 7.1.5. ***Growth of luciferase expressing T. cruzi CL Brener epimastigotes.*** The cumulative cell density of wild-type *T. cruzi* CL Brener epimastigotes (blue) and 2 CL Brener$^{Ribo\text{-}Luc}$ clones (clone 1: red, clone 2: green) was followed for 9 days. At day 0, all lines were seeded at 5 x 10^5 cells ml^{-1}. Parasite loads were determined every 2 days, and diluted back to 5 x 10^5 cells ml^{-1} when appropriate, to prevent the cultures from reaching the stationary phase of growth. Over the period examined here, all *T. cruzi* epimastigote lines grew at equivalent rates.

7.1.3 Characterizing *T. cruzi* CL Brener$^{Ribo\text{-}Luc}$ in mammalian lifecycle stages

After establishing that growth of *T. cruzi* epimastigotes is not affected by luciferase expression, the ability of CL Brener$^{Ribo\text{-}Luc}$ clones to infect mammalian cells was investigated. In these experiments, stationary growth phase epimastigote cultures of wild-type *T. cruzi* CL Brener and 2 CL Brener$^{Ribo\text{-}Luc}$ clones (those analyzed in Figure 7.1.5) were used to infect Vero cells. Under these stationary phase conditions, *T. cruzi* epimastigotes appear to undergo metacyclogenesis (Kollien and Schaub, 2000). Approximately 2-4 weeks post-infection, intracellular amastigotes were detected microscopically for all parasite lines, demonstrating that the recombinant *T. cruzi* CL Brener clones containing pTRIX-luciferase remained infectious. Maintenance of this infected Vero culture for approximately two months resulted in the near destruction of the mammalian cell monolayer and, based on morphology, high numbers of free amastigotes in the medium. Supernatants containing free amastigotes from the CL

Brener$^{Ribo\text{-}Luc}$ infections were collected and the parasites were washed in fresh culture medium. After evaluating the cell density using a haemocytometer, a series dilution was made and the relationship between luminescence activity and amastigote load determined (Figure 7.1.6). A direct linear correlation between cell number and luciferase levels was observed for both CL Brener$^{Ribo\text{-}Luc}$ clones, with as few as 10 amastigotes giving a luminescence reading above the negligible background signal. Together, this data indicates that for this *in vitro* model, the luciferase expressing parasites are infectious to mammalian cells, the amastigote parasites are able to express genes using the pTRIX system, and that luciferase expression by the mammalian form parasites is stable for up to 2 months.

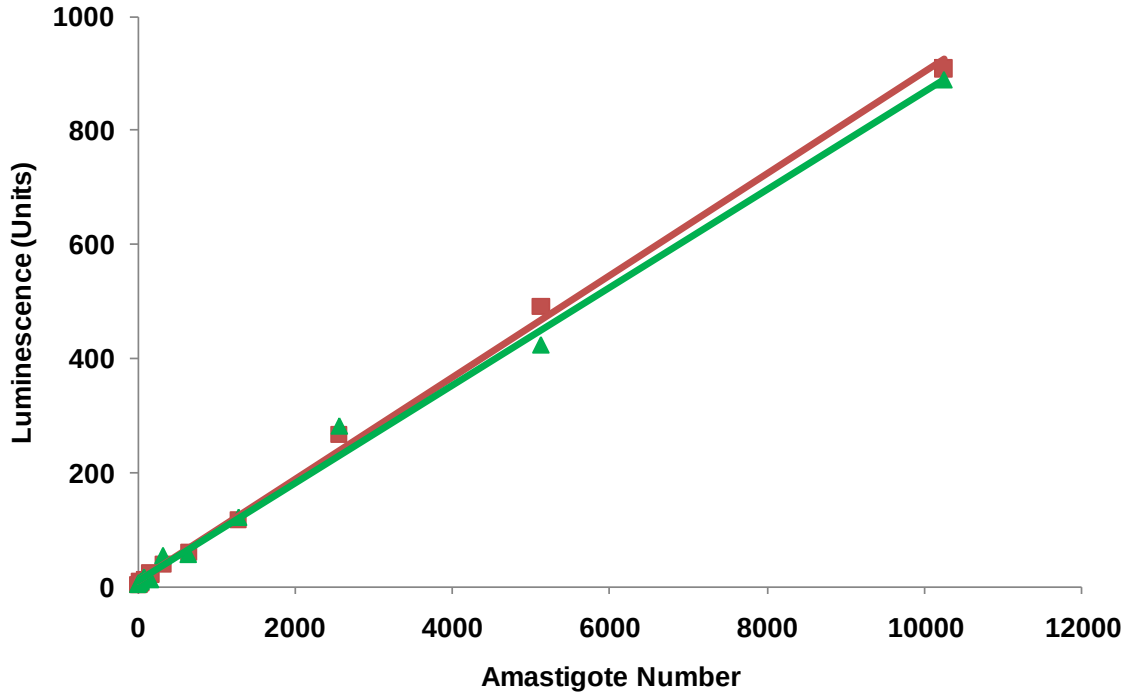

Figure 7.1.6. ***Correlation between T. cruzi amastigote load and luciferase activity.*** The luciferase activity, as measured in light units, of 10 to 10,000 recombinant *T. cruzi* CL Brener$^{Ribo\text{-}Luc}$ amastigotes, obtained from the supernatants of old Vero cell cultures infected with luciferase expressing parasites, was determined for two independent clones (clone 1: red squares, clone 2: green triangles). The "free" amastigote load was determined and a serial dilution performed before cell lysis.

To assess the ability of *T. cruzi* CL Brener$^{Ribo\text{-}Luc}$ amastigotes to differentiate into bloodstream form trypomastigotes and also indirectly measure amastigote growth, a defined number (7×10^4) of wild-type and transgenic trypomastigotes were used to infect Vero cells. The trypomastigotes were harvested from the supernatant of a previous Vero cell infection and multiple infections (in quadruplicate) were carried out for *T. cruzi* CL Brener and *T. cruzi* CL Brener$^{Ribo\text{-}Luc}$ lines. After an overnight incubation, non-internalised trypanosomes were removed through copious washing and the cultures were incubated for a further 10 days. The number of bloodstream form trypomastigotes present in the medium was then determined using a haemocytometer (Figure 7.1.7). The numbers of trypomastigotes observed in the luciferase expressing clone was similar to that of the wild-type, suggesting that the incorporated luciferase gene had no detectable affect on parasite infectivity or their intracellular growth rate.

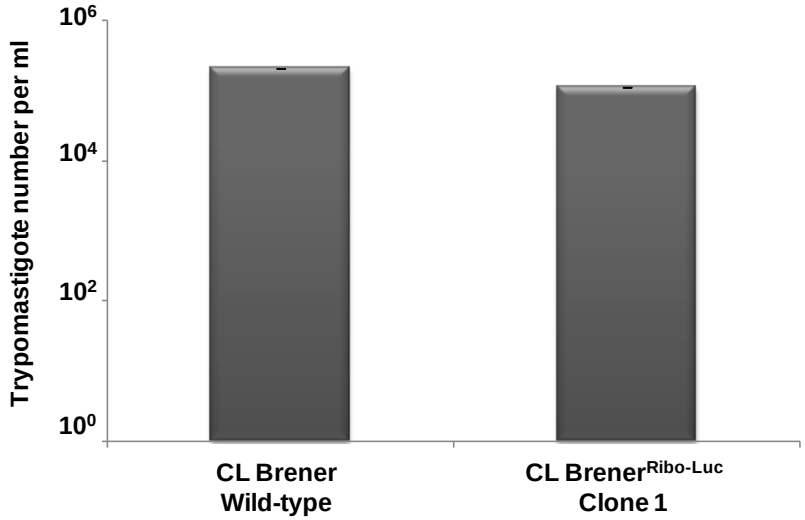

Figure 7.1.7. ***Luciferase expression by T. cruzi amastigotes does not affect growth rate.*** To assess the growth rate of *T. cruzi* amastigotes, Vero cells were infected with 7×10^4 metacyclic trypomastigote parasites (CL-Brener or CL Brener$^{Ribo\text{-}Luc}$ clone 1) overnight. The following morning, cultures were extensively washed to remove non-internalised cells and then incubated at 37°C under a 5% CO_2 atmosphere for 10 days. Equal aliquots of the medium were collected and the number of released bloodstream form trypomastigotes determined by haemocytometer. This count acts as an indirect measure of the amastigote growth rate and the ability of this parasite stage to differentiate into bloodstream form trypomastigotes. No observable difference in the number of released bloodstream form trypomastigotes was observed between the two cell-lines. The results are the mean of 4 parallel infections ± standard deviations.

All the above data shows that the expression of the reporter does not influence:

1. Growth of epimastigotes parasites.
2. The ability of epimastigotes cells to differentiate into infective metacyclic trypomastigotes.
3. Invasion of mammalian cells by metacyclic trypomastigotes.
4. Growth of intracellular amastigote parasites.
5. Differentiation of amastigote cells into infective bloodstream trypomastigotes.
6. The ability of bloodstream trypomastigotes to infect mammalian cells.

Therefore, it is implicit that luciferase has no effect on trypanosome growth, differentiation, and infectivity.

7.1.4 Development of the *T. cruzi* CL Brener$^{\text{Ribo-Luc}}$ drug assay

After showing that luciferase expression has no apparent adverse affects on parasite growth, differentiation, and infectivity, experiments were conducted to evaluate whether the transgenic parasites could be used in drug screening. The goal of this study was to develop a 5 day assay in a 96-well plate format. After considering the surface area of a flat bottomed single well in a standard 96-well plate and the growth rate of the Vero line, the average seeding density of mammalian cells required was calculated to be 1500 (1.5×10^4 cells ml^{-1}) per well; this value was designed to prevent the culture becoming too dense over the course of the assay. Next, a series of Vero cell infections were carried out using a range of bloodstream form trypomastigotes densities. From this, the 5 day end-point parasite infection levels were determined by evaluating the number of observed intracellular amastigotes. An optimised ratio of trypomastigote/mammalian cells was then estimated as 7:1 or 10,000 trypomastigotes to 1500 Vero cells for each well of a standard 96-well plate.

After establishing the above parameters, growth inhibition assays were performed using nifurtimox or benznidazole on Vero cells infected with the *T. cruzi* cells expressing luciferase (Section 3.12.2). After 5 days, all cultures were lysed and their luminescence activity determined. For both nitroheterocyclic compounds, a dose response curve was observed (Figure 7.1.8). From these plots, the concentration of each compound that inhibited parasite growth by 50% (IC_{50}) was calculated. All assays were conducted in triplicate and the mean IC_{50} values were determined ± the standard deviation between the replicates. In these assays, nifurtimox generated an IC_{50} value of 0.24 ± 0.04 µM while benznidazole produced a value of 2.88 µM ± 0.27. As a comparison, a previous assay with the β-galactosidase colorimetric assay system (Buckner et al., 1996) showed nifurtimox to generate an IC_{50} value of 0.52 µM using the modified Tulahuen C4 strain and Vero cells (Aponte et al., 2008).

A notable feature of these two validation assays is that luminescence values can vary. For example in Figure 7.1.8 the non-drug treated infection in the nifurtimox assay results in a luminescence reading of approximately 150 units while an equivalent untreated culture in the benznidazole assay gave around 600 units. Each set of assays were performed on separate occasions, and the observed difference probably reflects the initial level of infectivity of the bloodstream form trypomastigotes at that particular time. This should not greatly affect the final IC_{50} values, since the level of infectivity within a single assay should be equivalent. Also, in the benznidazole assay, it was apparent that sub-lethal levels of compound actually promote parasite growth. This phenomenon is often observed in drug assays with *T. cruzi* and *T. brucei*, both within our laboratory and in neighbouring laboratories, and could potentially be a form of parasite stress response. In conclusion, the pilot assays proved successful in generating dose dependant growth inhibition curves facilitating the calculation of replicable IC_{50} values.

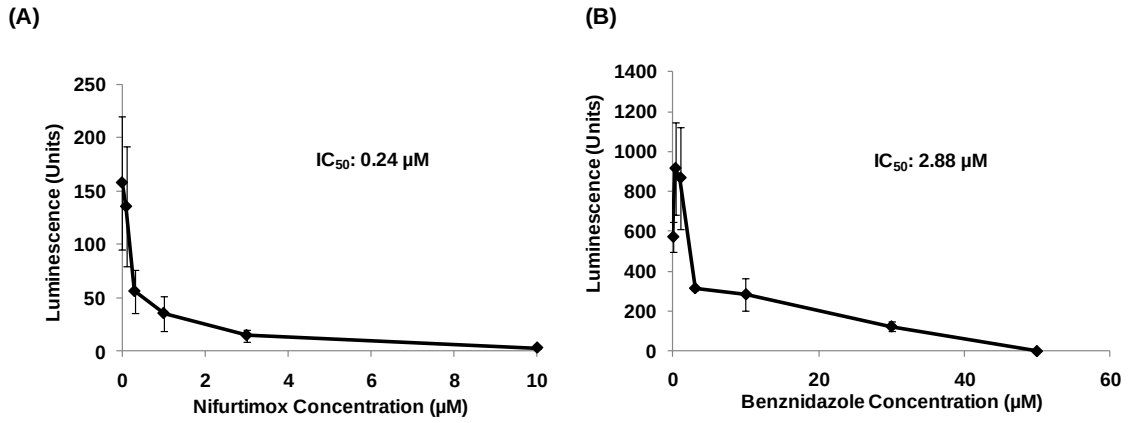

Figure 7.1.8. ***Susceptibility of luciferase expressing T. cruzi amastigotes to nifurtimox and benznidazole.***
In a 96-well plate format, mammalian Vero cells were infected overnight with luciferase expressing *T. cruzi* bloodstream form trypomastigotes. Non-internalised parasites were removed by extensive washing in culture medium. Amastigote parasites were grown for 3 days in the presence of different concentrations of nifurtimox or benznidazole and the luciferase activity, as measured in light units, determined for each infected mammalian culture. A dose response curve for nifurtimox and benznidazole was plotted from which the drug concentration that inhibited parasite growth by 50% (IC_{50}) was established. The data are the means from 3 experiments ± standard deviations.

7.2 Compound Screening with *T. cruzi* CL Brener$^{\text{Ribo-Luc}}$

Following the development and validation of the luciferase-based *T. cruzi* amastigotes screening system, a series of growth inhibition experiments were performed using three sets of nitroaromatic compounds. To facilitate throughput, all compounds were subject to an initial screen at a single concentration of 10 µM. Any agent that failed to display activity at this concentration was considered a poor candidate and not analyzed further. For the compounds displaying anti-parasitic properties, IC_{50} values were determined against the transgenic *T. cruzi* amastigote and the Vero cell-lines. Comparison of these values allowed a therapeutic index to be calculated, which acts as a crude measure of a compound's selectivity against the parasite.

The first series of compounds consisted of nine aziridinyl nitrobenzyl compounds (Helsby et al., 2004a) (Table 3.13.1). This included the lead compound CB1954 (Section 6.3), an agent originally developed as an anti-cancer agent designed to be used in a nitroreductase-based gene therapy approach called GDEPT (Gene Directed Enzyme

Pro-drug Therapy) (Knox et al., 2003). It also has promising activity against *T. brucei* (Sokolova et al., 2010). The second set of compounds comprised 24 nitrobenzyl mustards (Table 3.13.2 and Table 3.13.3). These compounds were originally designed as anti-cancer pro-drugs that undergo GDEPT activation via the same mechanism as CB1954 (Li et al., 2003). Again, some of these compounds have potent trypanocidal activity against bloodstream form *T. brucei* (Hall et al., 2010). The third class of compounds possess a common nitrofuran structure (Table 3.13.4) and were developed specifically as chemotherapeutic agents targeting *T. cruzi* (Aguirre et al., 2006). Currently these have mainly been screened against the epimastigote lifecycle stage, with a few progressing through into animal studies (Cabrera et al., 2009). For this reason, only a small sub-set of 6 compounds were tested here.

All of the compounds selected for screening against amastigote parasites are believed to function as pro-drugs that undergo activation through the activity of a parasite type I nitroreductase (Section 6.1).

7.2.1 Trypanocidal activity of aziridinyl nitrobenzamides

Based on the number and relative positions of nitro groups and the position of any additional substituents, the azirindyl nitrobenzyl compounds can be split into three classes, designated class Ia, Ib and II. When all nine compounds were screened against *T. cruzi* amastigotes, only three displayed any anti-parasitic effects at 10 μM. These (CB1954, NH1, and NH2) are all structurally related, and belong to the class Ia family of compounds. They all contain an amide (or related substituent) at position 1 on the benzyl ring, two nitro groups at positions 2 and 4, and an aziridinyl ring at position 5. The IC_{50} values for these trypanocides were determined using a range of drug concentrations (Table 7.2.1). Analysis of the data revealed that all had roughly similar growth inhibitory activities, generating IC_{50} values of around 1 μM. The IC_{50} value using nifurtimox was approximately 0.25 μM. CB1954 and NH1 were particularly potent, having values around 0.6 μM. When cytotoxicity studies were extended to mammalian cells, no growth inhibitory effects were observed at concentration up to 250 μM, while in contrast nifurtimox yielded an IC_{50} of 64 μM. Further analysis to determine cytotoxicity could not be performed as the DMSO solvent used to dissolve

the azirindyl nitrobenzyl compounds, proved toxic to the Vero cell-line. Therefore, to establish a therapeutic index between *T. cruzi* and mammalian cells (Table 7.2.1), the published cytotoxicity data against a Chinese hamster fibroblast (V79) cell-line was used (De Conti, 1998; Helsby et al., 2004a). This indicated that CB1954, NH1, and NH2 showed little toxicity towards V79 cells, generating IC_{50} values greater than 500 µM. In contrast, the nifurtimox IC_{50} was recorded at 35 µM. Evaluation of therapeutic index ratios clearly demonstrated that CB1954 and NH2 were >900-fold more effective at inhibiting parasite growth over the V79 cells, and approximately 6-fold more effective that nifurtimox.

Compound	IC_{50} (µM)			Therapeutic Index
	***T. cruzi* ± S.D**	**Vero**	**V79**	
Nifurtimox	0.24 ± 0.04	64.11 ± 0.57	35	146
CB1954	0.57 ± 0.04	> 250	543	953
NH1	1.59 ± 0.10	> 250	624	392
NH2	0.68 ± 0.11	> 250	634	919
NH3	>10	> 100	3838	-
NH4	>10	> 100	766	-
NH5	>10	> 100	122	-
NH6	>10	> 100	1038	-
NH7	>10	> 100	1269	-
NH8	>10	> 100	131	-

Table 7.2.1. ***Susceptibility of T. cruzi amastigotes to aziridinyl nitrobenzamides.***
The concentration of azirinidyl nitrobenzamide that inhibits parasite and Vero cell growth by 50% (IC_{50}) was determined. The lead compound (CB1954) and two derivatives (NH1, and NH2) displayed potent trypanocidal properties. The remaining compounds showed no anti-parasitic activity up to 10 µM. As a positive control, nifurtimox was analysed in parallel. The three trypanocidal azirinidyl compounds did not inhibit Vero cell growth at concentrations up to 250 µM. At higher drug concentrations, the solvent (DMSO) used to dissolve the azirinidyl nitrobenzamides began to affect mammalian cell growth. All growth inhibition assays were performed in quadruplicate and the values are means ± standard deviations. To obtain therapeutic indices, toxicity data for Chinese hamster fibroblast (V79) cells were taken from the work of Helsby et al. 2004 (CB1954, NH1, and NH2) or De Conti et al. 1998 (nifurtimox). The therapeutic index of each compound was calculated as a ratio of the V79 IC_{50} value to the parasite IC_{50} value.

7.2.2 Trypanocidal activity of nitrobenzyl mustards

The nitrobenzyl mustard class of nitroaromatics can be divided into two types. For the first type, a phosphoramide component is incorporated into a fixed cyclic structure allowing for the formation of stereoisomers (Table 3.13.2), while in the second type, the phosphoramide is part of a linear side chain (Table 3.13.3). Screening of all 24 mustard compounds against *T. cruzi* amastigotes at 10 µM identified 6 promising trypanocidal candidates. Out of the 18 compounds rejected, all the cyclic phosphoramide-based chemicals failed to display any cytotoxicity along with 10 agents possessing the linear phosphoramide configuration. Of the remaining compounds, all possessed some form of halogenation on the nitroaromatic ring. Further growth inhibition assays now using six drug concentrations ranging from 0 to 10 µM, with four replicates of each assay, were performed to determine IC_{50} values (Table 7.2.2). For 5 of these, the calculated values were between 8 and 10 µM. However, one compound, LH37, yielded an IC_{50} of just below 1 µM (Table 7.2.2). This compound possesses two fluorine substitutions at positions 2 and 6 of the benzene ring, a nitro substituent at position 4 and a linear phosphoramide mustard chain at position 1. As with the aziridinyl nitrobenzyl compounds, most nitrobenzyl mustards displayed no toxicity to Vero cells up to 100 µM with only two (LH47 and LH48) inhibiting growth below this value. For LH47, a therapeutic index value of approximately 1 was observed with a value of around 8 recorded for LH48. Intriguingly, the most promising trypanocidal compound, LH37, displayed no cytotoxicity up to 100 µM, suggesting that this compound may warrant further analysis, especially given that it displays potent activity against *T. brucei* (Hall et al., 2010).

Compound	*T. cruzi* IC_{50} (µM)	Vero IC_{50} (µM)
Nifurtimox	0.24 ± 0.04	64.11 ± 0.57
LH3 - LH9	>10	>100
LH12 - LH19	>10	>100
LH24	>10	>100
LH27	>10	>100
LH31	>10	>100
LH32	9.54 ± 0.27	>100
LH33	7.97 ± 1.13	>100
LH34	9.14 ± 0.54	>100
LH37	0.99 ± 0.01	>100
LH47	8.69 ± 0.76	6.98 ± 0.69
LH48	8.23 ± 0.30	64.38 ± 0.53

Table 7.2.2. ***Susceptibility of T. cruzi amastigotes to nitrobenzyl-based mustards.*** The concentration of nitrobenzyl-based mustards that inhibits parasite and Vero cell growth by 50% (IC_{50}) was determined. Out of the 24 compounds analysed, six displayed trypanocidal properties. The remaining compounds showed no anti-parasitic activity up to 10 µM. For four of the trypanocidal compounds (LH32-34 and LH37), no effect of Vero cell growth was observed. All growth inhibition assays were performed in quadruplicate and the values are means ± standard deviations.

7.2.3 Trypanocidal activity of nitrofuryls

As mentioned previously, only a sub-set of the 5' nitrofuryl compounds available were tested against *T. cruzi*. All of the six compounds examined displayed trypanocidal activity below the designated 10 µM cut-off point. Further growth inhibition assays against these compounds established an IC_{50} value for each agent. For four compounds, IC_{50} values of less than 1 µM were determined, with two compounds (HC-4 and HC-10) displaying an activity below 0.1 µM (Table 7.2.3). In contrast to the nitrobenzyl-based mustards or azirinidyl compounds, no relationship between the nitrofuryl structure and anti-parasitic activity was observed. However, the number of agents examined here is very small, and a more in depth investigation may be required to elucidate such associations.

Analysis of the six nitrofuryls toxicity against mammalian cells generated IC_{50} values similar, or lower than nifurtimox. This illustrates that a potential drawback of these compounds may lie in their toxicity towards the mammalian cells. However, when the

resulting therapeutic values are considered, they are equivalent to the clinically used trypanocidal agent nifurtimox. Based on their anti-parasitic activities, the nitrofuryls represent the most potent trypanocidal compounds screened here and display encouraging therapeutic index values.

The above screens against *T. cruzi* amastigotes using 39 nitroaromatic compounds identified seven promising trypanocidal compounds whose structures are shown in Figure 7.2.1. This represents a hit rate of just below 20%, and clearly demonstrates how understanding the mode of action for existing trypanocidal therapies can be exploited to identify new lead compounds, that warrant further evaluation to treat these neglected diseases.

Compound	*T. cruzi* IC_{50} (µM)	Vero IC_{50} (µM)	Therapeutic Index
Nifurtimox	0.24 ± 0.04	64.11 ± 0.57	267
HC-1	1.99 ± 0.04	23.80 ± 0.62	12
HC-2	0.72 ± 0.08	23.93 ± 0.25	33
HC-4	0.08 ± 0.03	20.34 ± 0.35	254
HC-10	0.06 ± 0.01	13.61 ± 1.10	227
HC-2b	0.20 ± 0.04	60.05 ± 1.31	300
HC-4b	4.35 ± 0.41	23.70 ± 0.63	5

Table 7.2.3. ***Susceptibility of T. cruzi amastigotes to 5' nitrofuryls.***
The concentration of 5' nitrofuryl that inhibits parasite and Vero cell growth by 50% (IC_{50}) was determined for compounds not previously screened against *T. cruzi* amastigotes. All proved potent trypanocidal agents, exhibiting IC_{50} values below 5 µM, with two giving values of less than 100 nM. For each compound, the therapeutic index was calculated as a ratio of the Vero IC_{50} value to the parasite IC_{50} value. All growth inhibition assays were performed in quadruplicate and the values are means ± standard deviations.

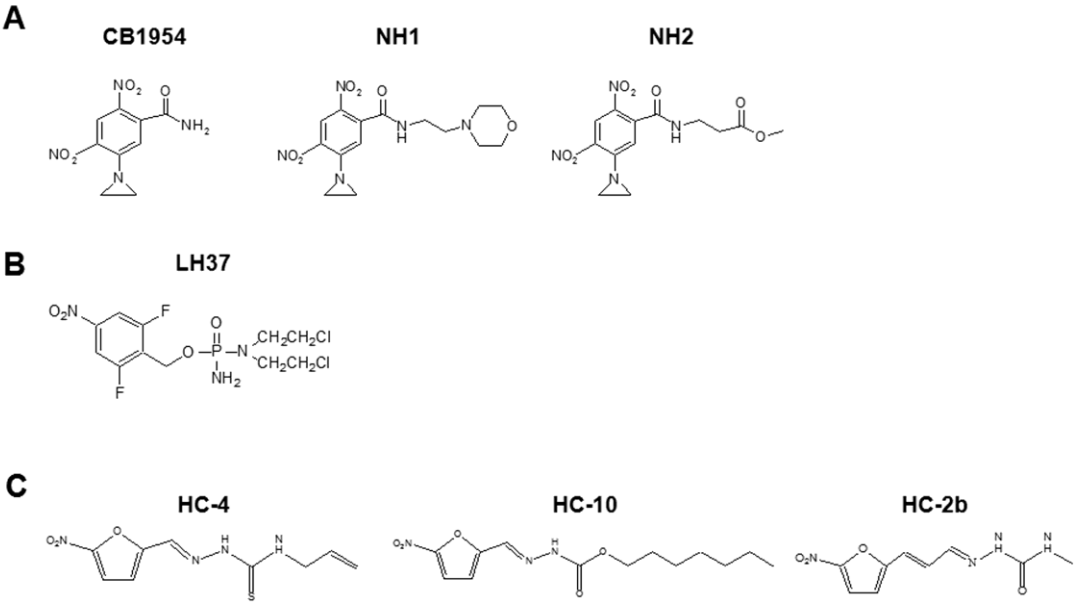

Figure 7.2.1. ***Structures of the most effective compounds identified in the T. cruzi amastigote screens.***
The compounds identified as potent trypanocidal agents with respectable therapeutic indices are derived from 3 classes of nitroaromatic compounds including: the azirindyl nitrobenzyls (**A**), nitrobenzyl mustards (**B**) and 5' nitrofuryls (**C**).

7.3 Chapter Summary

The development of a luciferase reporter system for the drug screening of intracellular *T. cruzi* has demonstrated:

- Integrating pGAP-Luciferase into the GAPDH region of *T. cruzi* X10/6 appears to impair parasite infectivity.
- Using the ribosomal targeting sequence of pTRIX to express luciferase, results in no apparent effect on epimastigote growth and infectivity, or amastigote growth and trypomastigote infectivity.
- Luciferase activity of lysed amastigotes is linearly proportional to cell number and sensitive down to 10 parasites per sample, so therefore the detected luminescence accurately represents parasite numbers.
- A 5 day growth inhibition assay provides a clear drug dose dependent growth response, facilitating the calculation of IC_{50} values with low variation.
- Three of the nine aziridinyl nitrobenzamides compounds displayed promising trypanocidal activities (~1 µM) and therapeutic indices (~900), and represent a class of potential drug candidates.
- Most of the nitrobenzyl phosphoramides proved ineffective against amastigote *T. cruzi*, with only compound LH37 displaying significant trypanocidal activity at ~1 µM.
- The 5' nitrofuryl compounds showed the most potent trypanocidal activities of the three classes of compounds tested, although the compounds also displayed levels of cytotoxicity below 100 µM against mammalian cells.

7.4 Discussion

Any drug development programme requires a reliable and high-throughput strategy for monitoring the growth or death of the target cell. Construction of the 96-well plate based luciferase drug screening system (Bot et al., 2010) has facilitated the rapid analysis of three series of nitroaromatic compounds for trypanocidal activity against the medically relevant amastigote life-cycle stage of *T. cruzi*.

When this project was initiated, the only reliable high-throughput assay available to monitor the growth of intracellular *T. cruzi* relied on a β-galactosidase based colorimetric reporter (Section 7.1) (Buckner et al., 1996). Although useful, a potential drawback of the β-galactosidase system is that it may not be well suited for screening strongly coloured chemicals. As many nitroaromatic compounds are coloured, an alternative reporter system based on luciferase was developed. Recently, two other screening strategies have been reported. These either rely on the heterologous expression of the red fluorescent protein (Canavaci et al., 2010), or exploit the size difference displayed by the mammalian nuclei versus the much smaller trypanosomal kinetoplast DNA (Engel et al., 2010). Each approach has its advantages and disadvantages. For example, both have been successfully used to analyze the growth of *in vitro* cultured intracellular *T. cruzi*, but neither can currently be employed to monitor parasite growth within an animal model. The DNA staining based assay is of particular interest, as although it is dependent on specialized image capture technology and detection algorithms, its major advantage over other systems, including the luciferase system developed here, is that no genetic modification of the parasite cell-line is required. Therefore, it could easily be used against a range of laboratory and clinical strains. The limitations of the red fluorescent protein system led its authors to develop another *T. cruzi* cell-line, this time engineered to express the firefly luciferase gene (Canavaci et al., 2010), in a system analogous to that described here (Bot et al., 2010). They attempted to use their luciferase expressing cell-line to monitor parasite numbers in a mouse model. However, this assay only measured infection levels within a mouse footpad, and so falls short of representing a true *in vivo* model. One explanation behind this limitation is that to produce an effective and accurate luciferase-based animal

model, an even distribution of the luciferase substrate fully dispersed within the host is required, followed by an efficient transmission of the luminescence signal. Evidence observed using a *T. brucei* based luciferase reporter mouse model implies this is not necessarily achieved, especially with intraperitoneal dosage of the luciferase substrate (Claes et al., 2009). Here, the distribution of luminescence signal levels detected from live animal based imaging did not always correlate with the signals detected from individually extracted organs immediately post-mortem, such as the brain. This suggests that luciferase systems may not be the best way forward in developing mouse infectivity models.

The first class of compounds screened with the luciferase reporter system was a series of aziridinyl nitrobenzamides based on the anti-cancer agent CB1954 (Section 6.3). These can be divided into 3 sub-classes, based on the number and positioning of nitro groups on the benzyl ring, coupled with the location of any substituent groupings (Section 7.2.1). Out of the aziridinyl nitrobenzamides tested, 3 showed trypanocidal activity against amastigote *T. cruzi* (Bot et al., 2010). These 3 compounds (CB1954, NH1 and NH2) all belong to a single sub-class, as they contain an amide containing substituent at the 1- position, 2 nitro groups located at the 2- and 4- positions, and an aziridinyl ring at 5- position on a benzyl ring. The other sub-classes either lack the 2- nitro group or contain a substituent (generally an amide) at the 6- position. A comparison of the trypanocidal activity and mammalian cytotoxicity data revealed that two of the three compounds (CB1954 and NH2) displayed high selectivity towards the parasites (Bot et al., 2010; Helsby et al., 2004a). Interestingly, biochemical screens using recombinant *T. brucei* type I nitroreductase revealed that these same three agents were the only compounds from this set that could be metabolized by the *T. brucei* enzyme. These were also the most effective at inhibiting bloodstream form *T. brucei* growth (Bot et al., 2010). Moreover, *T. brucei* with elevated levels of the type I nitroreductase had increased susceptibility (>10 fold) to these compounds, as compared to controls. Together, these findings demonstrate the importance of the type I nitroreductase in the *T. brucei* anti-parasitic activity of this aziridinyl nitrobenzamide sub-class. By implication it is assumed that a similar activation mechanism underpins their activity within *T. cruzi*. Overall, two aziridinyl nitrobenzamide compounds displayed excellent

trypanocidal activity against *T. cruzi* amastigotes through a characterized mechanism, with strong potencies (IC_{50} < 1 μM) and high therapeutic indices (> 900). These have real potential as future drug candidates, and warrant further studies with an *in vivo* model.

Many of the nitrobenzyl phosphoramides tested with the luciferase screening system were not effective trypanocidal agents against *T. cruzi* (Hu et al., 2011). This large series of chemicals contained 24 compounds that could be divided into those that possessed a cyclic phosphoramide component, and those containing a linear phosphoramide group (Section 7.2.2). None of the eight cyclic phosphoramides had an effect on the growth of *T. cruzi* amastigotes, a trait also observed in screens targeting bloodstream form *T. brucei* (Hall et al., 2010). One possible explanation for the lack of trypanocidal activity could relate to how they interact with the *T. brucei* type I nitroreductase, as many of the cyclical phosphoramide analogues do not function as substrates for the parasite enzyme, while the few that are turned over, do so at a low rate (Hall et al., 2010). This may reflect an electron withdrawing tendency displayed by the cyclic phosphoramide, limiting the vulnerability of the nitro group on the benzyl ring to type I nitroreductase-mediated reduction. For the remaining linear nitrobenzyl phosphoramides, 6 compounds (LH32-34, LH37, LH47 and LH48) demonstrated activity against *T. cruzi* amastigotes (IC_{50} < 10 μM) with LH37 having the highest potency (IC_{50} ~ 1 μM) (Hu et al., 2011). This mirrors what had previously been reported against bloodstream form *T. brucei*, although against this parasite the most potent compounds (LH34 and LH37) exhibited IC_{50} values of less than 10 nM (Hall et al., 2010). Biochemical studies using recombinant *T. brucei* type I nitroreductase demonstrated that out of all 16 linear nitrobenzyl phosphoramides, four generated very high specific activity values (LH32-34 and LH37) (Hall et al., 2010). The remaining compounds (LH47 and LH48) that displayed activity against *T. cruzi* have not been subject to biochemical analysis. When the biochemical studies were extended to the *T. cruzi* type I nitroreductase, the highest activities were also achieved with the same sub-set of compounds, although the specific activity values were generally between 5 to 10 fold lower for the *T. cruzi* enzyme as compared with that of the *T. brucei* protein (Hall and Wilkinson, unpublished data). This, in conjunction with susceptibility studies on *T. brucei* with altered levels of the

type I nitroreductase, shows that for this series of compounds, there is a direct relationship between parasite growth inhibition and enzyme activity. Structure-activity relationships for the linear nitrobenzyl phosphoramides show that the compounds displaying anti-*T. cruzi* properties contain either chlorine, fluorine or tri-fluoromethyl groups at the 2- position on the benzyl ring relative to the leaving phosphoramide. It is postulated that on a benzyl ring, the electron withdrawing substituents when coupled with the electronic properties displayed by the nitro group favour the reduction of the latter grouping by type I nitroreductases (Hall et al., 2010). Alternatively, such configurations could affect other biological properties displayed by these chemicals, such as drug uptake. In summary, although some of the nitrobenzyl phosphoramides display interesting trypanocidal effects on *T. cruzi*, their IC_{50} and therapeutic index values indicate that they would be better developed as African sleeping sickness pro-drugs.

The final series of compounds tested with the luciferase system were a sub-set of 5' nitrofuryls (Section 7.2.3). While some of the compounds had already been tested *in vivo* (Cabrera et al., 2009), it was interesting to see how some of the untested nitrofuryls would compare against the other chemical series tested here. Indeed, the nitrofuryls displayed the highest potencies of all compounds tested towards *T. cruzi* amastigotes, highlighting why this class has received so much attention in the past. Although these compounds also generated cytotoxicity when analyzed against mammalian cells, the therapeutic index values from *T. cruzi* and Vero cells were similar to that observed for nifurtimox. In addition, since the sampled set of nitrofuryls was so small, no meaningful structure-activity relationship can be inferred. As there is a greater understanding in how these nitroheterocyclic compounds function (Wilkinson et al., 2011), it is now worth revisiting this class against *T. brucei*.

8 Trypanocidal activity of 5' nitrofuryls against *T. brucei*

This chapter investigates the efficacy of a larger number of 5' nitrofuryl compounds against the bloodstream form of *T. brucei*. In addition, how these agents mediate their trypanocidal activity in relation to a range of bio-reductive enzymes, including a type I nitroreductase is explored.

8.1 Trypanocidal Activity of 5' Nitrofuryl Compounds

Interest in using nitrofuryls to treat African sleeping sickness and Chagas disease began in the 1950s after a trypanocidal screening programme identified nitrofurazone as a lead compound (Evens et al., 1957; Packchanian, 1955). The effectiveness of this agent in humans was demonstrated, but failure to totally eradicate parasitaemia, coupled with neuropathological toxicity resulted in these trials being suspended (Rodriques Coura and de Castro, 2002). However, these findings led to investigations into the activity of other nitroheterocyclic compounds, with nifurtimox emerging as a promising candidate.

Nifurtimox, marketed under the brand name Lampit™, was initially used as the front-line treatment against acute Chagas disease throughout Latin America. However, due to GI tract and CNS side effects, coupled with the refractory nature of some *T. cruzi* strains, its limited efficacy and genotoxicity, nifurtimox use has now been discontinued in Brazil, Argentina, Chile and Uruguay, and it is not available for use in the USA except via the CDC (Alejandre-Duran et al., 1988; Moraga and Graf, 1989; Rodriques Coura and de Castro, 2002). Despite these problems, nifurtimox, as part of nifurtimox-eflornithine combination therapy (NECT), has been successfully trialled as a treatment for late-stage West African sleeping sickness (Section 1.2.1) and has recently been added to the WHO Essential Medicines List (Priotto et al., 2009). Given the renewed interest in nitroheterocyclic compounds for the treatment of trypanosomal infections, a series of 5' nitrofuryl compounds is investigated here against bloodstream form *T. brucei*. Included in this set is nitrofurazone, the initial lead compound, and a series of other agents proposed to mediate their activity through the inhibition of sterol biosynthesis.

8.1.1 Trypanocidal activity of 5' nitrofuryls

The growth inhibitory properties of 18 nitrofuryl compounds (Table 3.13.4), including nitrofurazone, was tested against wild-type bloodstream form *T. brucei* 427 and compared against the potency of nifurtimox. For each compound, a total of 12 concentrations were analysed in quadruplicate and the parasite load in each culture determined using the alamarBlue® reporter system (Section 3.12.1). From each data set, dose response curves were drawn and the mean nitrofuryl concentration that inhibits parasite growth by 50% (IC_{50}) and 90% (IC_{90}) ± standard deviation was determined (Table 8.1.1).

This initial screen revealed that only one of the compounds (HC-5) did not affect growth of bloodstream form trypanosomes at concentrations up to 20 μM, so this was omitted from further tests. For the remaining 17 structures, all displayed a higher trypanocidal activity than nifurtimox, with 13 having IC_{50} values below 1 μM, and six yielding values lower than 250 nM: these were the thiosemicarbazones HC1, HC2 and HC4, the carbazonates HC10 and HC11, and the semicarbazone nitrofurazone. In contrast to other nitroaromatic compounds (Bot et al., 2010; Hall et al., 2010), no relationship between the nitrofuryl's anti-parasitic properties and chemical structure was observed. As the compounds used here were generally selected on the basis of their growth inhibitory properties against *T. cruzi*, less potent compounds that could have facilitated a meaningful structure activity relationship may have already been excluded from this analysis.

The six compounds displaying the highest trypanocidal activities against bloodstream form *T. brucei* were assayed for cytotoxicity against Vero cells (Table 8.1.1). The therapeutic selective index values (S.I), a ratio of the IC_{50} against the mammalian line versus the IC_{50} against the parasite, for each agent was then determined. In all cases, the 6 compounds displayed selective toxicity *in vitro* toward the parasite, having SI values between 3- and 11-fold greater than nifurtimox.

Compound	*T. brucei* IC_{50} (µM)	*T. brucei* IC_{90} (µM)	Vero IC_{50} (µM)	S.I
Nifurtimox	2.78 ± 0.20	3.86 ± 0.08	64.11 ± 0.57	23
HC-1	0.18 ± 0.00	0.30 ± 0.05	23.80 ± 0.62	133
HC-2	0.20 ± 0.01	0.38 ± 0.03	21.93 ± 0.25	110
HC-2b	0.67 ± 0.02	0.88 ± 0.04	-	-
HC-3	0.50 ± 0.05	0.85 ± 0.07	70.06 ± 1.35	140
HC-4	0.24 ± 0.03	0.38 ± 0.01	20.34 ± 0.35	83
HC-4b	0.79 ± 0.04	1.34 ± 0.01	-	-
HC-5	> 20	> 20	-	-
HC-6	0.54 ± 0.07	0.93 ± 0.01	-	-
HC-7	1.43 ± 0.09	2.31 ± 0.02	-	-
HC-8	2.52 ± 0.33	5.90 ± 0.09	-	-
HC-9	1.65 ± 0.06	4.10 ± 0.13	-	-
HC-10	0.12 ± 0.02	0.19 ± 0.00	13.61 ± 1.10	116
HC-11	0.17 ± 0.01	0.24 ± 0.01	44.83 ± 2.42	264
HC-12	0.38 ± 0.04	0.65 ± 0.08	-	-
HC-12b	0.43 ± 0.06	0.77 ± 0.01	-	-
Nitrofurazone	0.23 ± 0.01	0.29 ± 0.02	35.73 ± 3.02	157
HC-13	1.28 ± 0.06	2.31 ± 0.01	-	-
HC-14	0.57 ± 0.03	0.74 ± 0.00	-	-

Table 8.1.1. ***Susceptibility of bloodstream form T. brucei and mammalian cells to nitrofuryl compounds.***
The 50% growth inhibitory concentrations (IC_{50}) and 90% growth inhibitory concentrations (IC_{90}) of the 5' nitrofuryls (Table 3.13.4) are measured against *T. brucei* 427 (Section 3.12.1). Almost all compounds show a higher trypanocidal activity than nifurtimox. For select compounds, toxicity against Vero cells was also measured. The resulting IC_{50} values were compared to the respective *T. brucei* results to calculate the therapeutic selective index (S.I = Vero IC_{50}/*T. brucei* IC_{50}). All of the selected drugs displayed higher therapeutic index values compared to nifurtimox.

8.1.2 Trypanocidal activity of 5' nitrofuryls by a type I nitroreductase

A type I nitroreductase has been strongly implicated in the activation of nitroheterocyclic pro-drugs including nifurtimox (Bot et al., 2010; Hall et al., 2010; Wilkinson et al., 2008). Here, the question of whether this activation mechanism extends to other 5' nitrofuryls, including nitrofurazone was evaluated. Using a *T. brucei* type I nitroreductase heterozygous line (designated $TbNTR^{+/-}$) the question of whether cells with reduced levels of this reductase had altered susceptibility toward the 5' nitrofuryls, relative to the wild-type parasites was examined (Table 8.1.2; Figure 8.1.1). For most

compounds, trypanosomes containing a single copy of the type I nitroreductase gene displayed resistance to the nitroheterocycle under investigation as compared to wild-type cells. However, when examining the susceptible of TbNTR+/- line to HC-6 or HC-10, IC_{50} values similar to that observed for wild-type parasites were recorded. This may reflect a combination of contributory factors such as parasite permeability and their affinity for the nitroreductase enzyme. To demonstrate that the increase in drug resistance upon elevated nitroreductase levels is specific to the nitrofuryls, the non-nitroheterocyclic drug G418, which is a protein synthesis inhibitor, was used as a negative control.

Compound	***T. brucei* IC_{50} (nM)**	
	Wild-type	**$TbNTR^{+/-}$**
Nifurtimox	2800 ± 195	4200 ± 290
G418	580 ± 10	625 ± 25
HC-1	180 ± 5	320 ± 10
HC-2	200 ± 15	560 ± 35
HC-2b	665 ± 20	1080 ± 125
HC-3	500 ± 45	760 ± 5
HC-4	240 ± 35	1295 ± 30
HC-4b	790 ± 40	1350 ± 95
HC-5	-	-
HC-6	535 ± 70	620 ± 25
HC-7	1430 ± 90	2100 ± 135
HC-8	2520 ± 330	4595 ± 550
HC-9	1650 ± 65	2930 ± 250
HC-10	120 ± 15	140 ± 15
HC-11	170 ± 5	310 ± 55
HC-12	380 ± 40	700 ± 75
HC-12b	430 ± 60	765 ± 1250
Nitrofurazone	225 ± 10	540 ± 15
HC13	1275 ± 55	1720 ± 85
HC14	575 ± 25	905 ± 30

Table 8.1.2. ***Susceptibility of bloodstream form T. brucei with reduced nitroreductase gene copy number.***
Growth-inhibitory effects as indicated by IC_{50} values (in nM) of all nitrofuryl compounds on *T. brucei* wild-type parasites and the nitroreductase heterozygous line (designated $TbNTR^{+/-}$). Data are means from four experiments ± standard deviation. G418 and nifurtimox were used as drug controls.

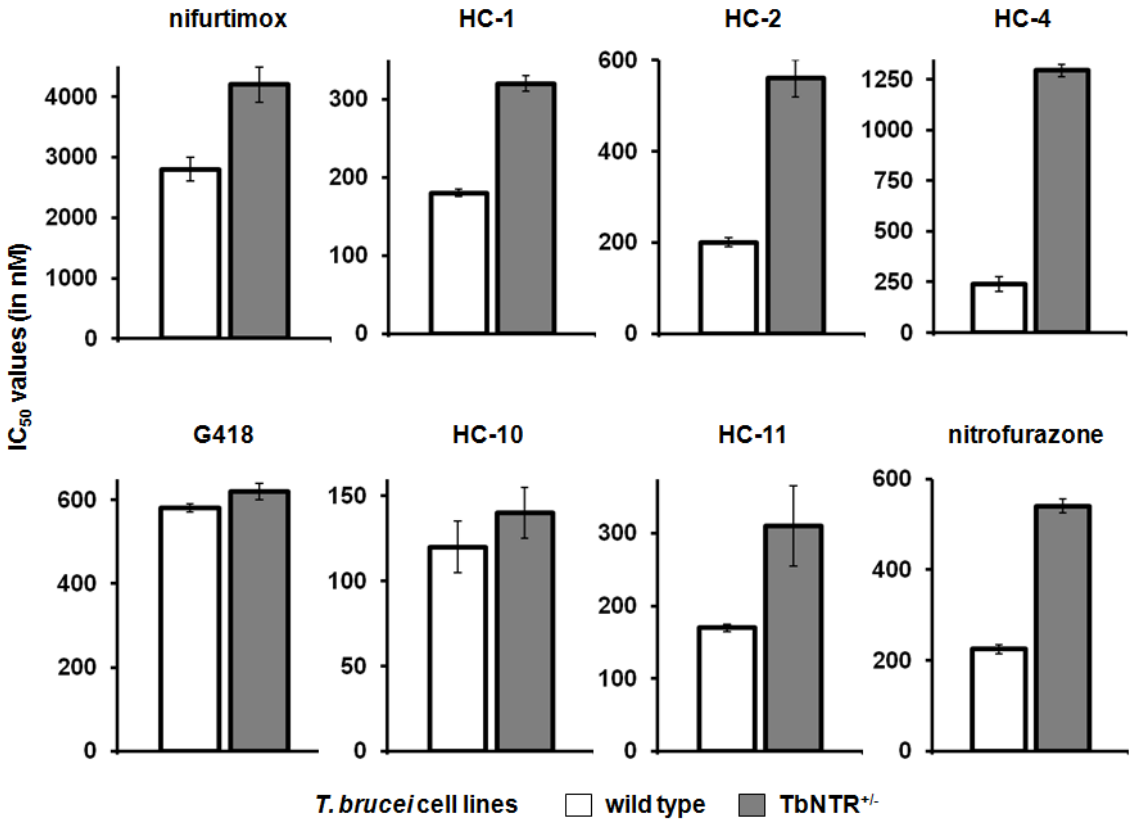

Figure 8.1.1. ***Susceptibility of bloodstream form T. brucei with reduced nitroreductase gene copy number to the 6 most potent nitrofuryls.***
Growth inhibitory effects as indicated by IC_{50} values of the six most potent nitrofuryl compounds as identified from the initial trypanocidal screen on *T. brucei* wild-type (white bars) and nitroreductase heterozygous cell ($TbNTR^{+/-}$) cells (black bars). The compounds screened are HC-1, HC-2, HC-4, HC-10, HC-11 and nitrofurazone. Data are means from four experiments ± standard deviation. G418 and nifurtimox were used as drug controls.

As the reduction of the nitroreductase gene copy number leads to resistance toward most 5' nitrofuryls, then it is implicit that elevated levels should lead to hyper-sensitivity. This hypothesis was investigated using a tetracycline based inducible cell-line that facilitates the over-expression of a tagged version of the nitroreductase (Wilkinson et al., 2008). The effect of all trypanocidal nitrofuryls on the growth of this line was monitored in the presence of tetracycline (Table 8.1.3; Figure 8.1.2). For most compounds, cells with elevated levels of nitroreductase were shown to be between 4 and 15-fold more sensitive to the nitroheterocycle, relative to control cells. These control cells consisted of the same parasite line, but grown in the absence of tetracycline. This shift in resistance was shown to be specific to the nitroheterocycles, as cells induced to express additional nitroreductase were no more susceptible to the non-nitroheterocycle G418 control drug.

Compound	***T. brucei* IC_{50} (nM)**	
	-Tet	**+Tet**
Nifurtimox	2890 ± 30	315 ± 15
G418	640 ± 10	540 ± 20
HC-1	290 ± 20	70 ± 5
HC-2	200 ± 5	35 ± 5
HC-2b	880 ± 60	65 ± 5
HC-3	500 ± 40	70 ± 5
HC-4	270 ± 15	35 ± 5
HC-4b	760 ± 45	75 ± 5
HC-5	-	-
HC-6	475 ± 40	320 ± 20
HC-7	1620 ± 15	145 ± 30
HC-8	2065 ± 225	35 ± 5
HC-9	2165 ± 140	180 ± 5
HC-10	100 ± 10	25 ± 5
HC-11	385 ± 40	50 ± 5
HC-12	2765 ± 240	835 ± 25
HC-12b	1945 ± 134	145 ± 10
Nitrofurazone	165 ± 5	40 ± 5
HC13	1165 ± 140	75 ± 5
HC14	625 ± 15	160 ± 5

Table 8.1.3. ***Susceptibility of bloodstream form T. brucei with elevated levels of nitroreductase to nitrofuryls.***
Growth-inhibitory effects as judged by IC_{50} values (in nM) of all nitrofuryl compounds on *T. brucei* control (-Tet) and nitroreductase over-expressing (+Tet) cells. Data are means from four experiments ± standard deviation. G418 and nifurtimox were used as drug controls.

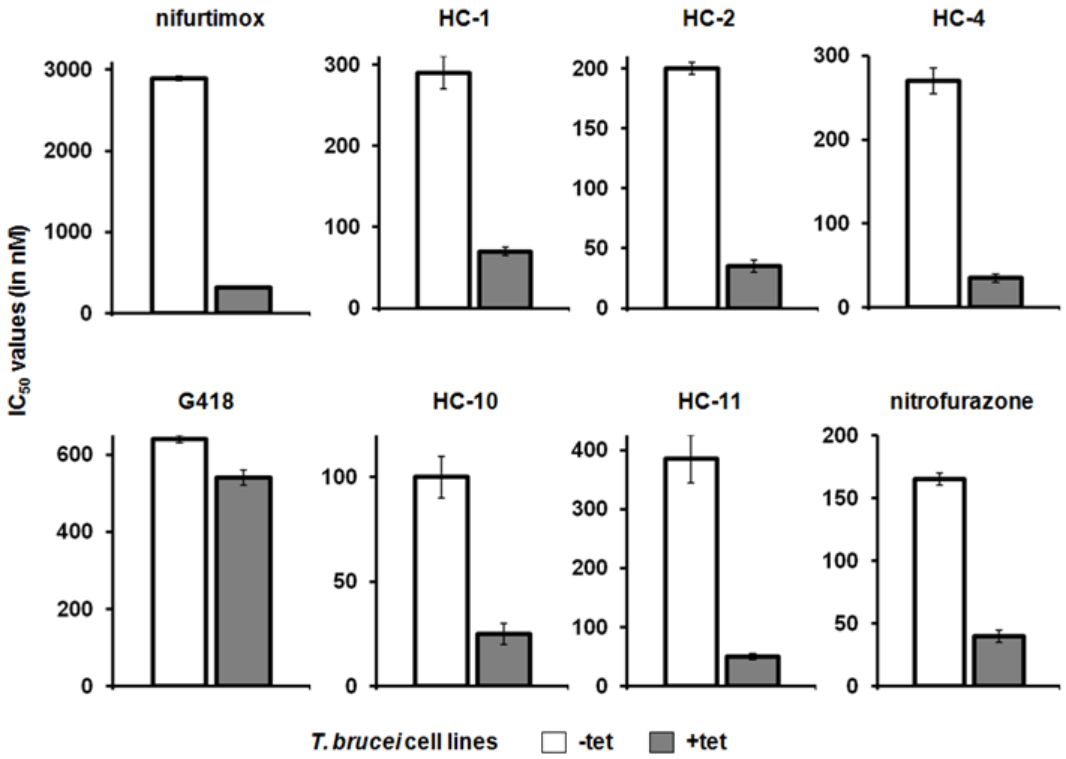

Figure 8.1.2. ***Susceptibility of bloodstream form T. brucei with elevated levels of nitroreductase to the 6 most potent nitrofuryls.***
Growth inhibitory effects as judged by IC_{50} values (in nM) of the 6 most potent nitrofuryl compounds as identified from the initial trypanocidal screen on *T. brucei* control (-tet) and nitroreductase over-expressing (+tet) cells. Data are means from four experiments ± standard deviation. G418 and nifurtimox were used as drug controls.

8.1.3 Activation of 5' nitrofuryl pro-drugs by other mechanisms

The above data strongly implies that the trypanosomal type I nitroreductase plays a key role in activation of nitrofuryl compounds within the parasite. However, other parasite enzymes have been postulated to interact with nitroheterocyclic compounds (Section 6.2) including prostaglandin F2α synthase (PGS) and cytochrome P450 reductase (CPR) (Kubata et al., 2002; Viode et al., 1999). To examine whether these enzymes activate the 6 most potent trypanocidal compounds identified through our screens, bloodstream form *T. brucei* lines expressing recombinant prostaglandin F2α synthase, cytochrome P450 reductase 2, and cytochrome P450 reductase 3 (CPR numbering accordance to Portal *et al*. 2008) were generated in a similar way to that described for nitroreductase, and the phenotype of the engineered cells to the 5' nitrofuryls evaluated.

The full length open reading frames, minus their stop codons, encoding for prostaglandin F2α synthase, cytochrome P450 reductase 2, and cytochrome P450 reductase 3, were amplified from *T. brucei* genomic DNA and the resultant fragments cloned into pRPa^{MYC}-NTR generating the expression plasmids pRPa^{MYC}-PGSF2α, pRPa^{MYC}-CPR-2, and pRPa^{MYC}-CPR-3 (Figure 8.1.3). The plasmids were digested with *Asc*I and the resultant fragments electroporated into bloodstream form *T. brucei* 2T1/TAG^{PURO} cells (Alsford and Horn, 2008). Drug selection was performed with hygromycin, and recombinant parasite clones obtained (Section 3.10.1). To demonstrate expression of recombinant protein, extracts from parasite cultures grown in the absence (no induction) or presence (induction) of tetracycline, were prepared and analysed by western blot using an antibody raised against the c-myc (9E10) epitope. For each recombinant parasite line, a band corresponding to the tagged protein was detected in tetracycline treated parasites (Figure 8.1.4).

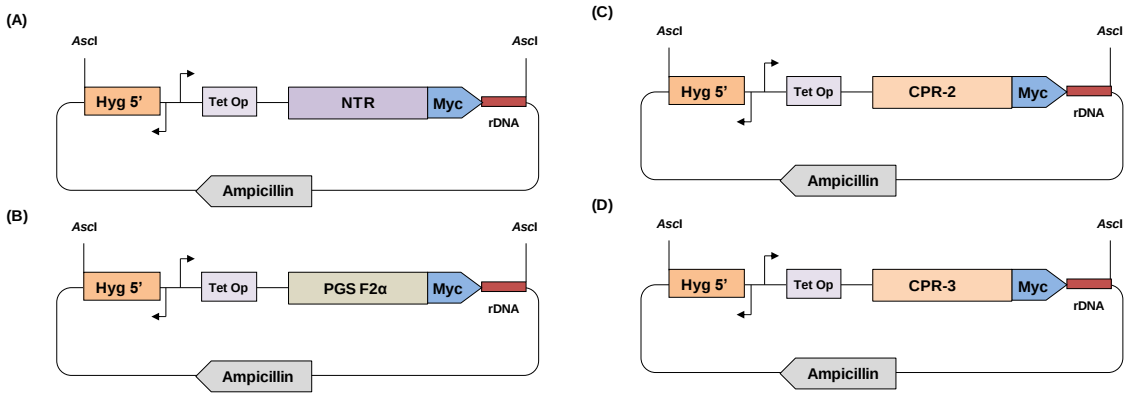

Figure 8.1.3. ***Expression plasmids used to evaluate other potential nitrofuryl activator systems.***
To examine other potential mechanisms of nitrofuryl action, the *T. brucei* genes encoding for prostaglandin F2α synthase, cytochrome P450 reductase 2, and cytochrome P450 reductase 3 were amplified from genomic DNA and cloned into the pRPa^{MYC} inducible gene expression system (Alsford and Horn, 2008). The cloning strategy involved replacing the nitroreductase gene in the plasmid pRPa^{MYC}-NTR (**A**) with appropriate DNA fragment resulting in formation of pRPa^{MYC}-PGSF2α (**B**), pRPa^{MYC}-CPR-2 (**C**), and pRPa^{MYC}-CPR-3 (**D**), respectively. All plasmids were linearized with an *Asc*I restriction digest and the resultant fragments introduced into bloodstream form *T. brucei*.

The growth inhibition properties of nifurtimox and the six most potent trypanocidal nitrofuryls (nitrofurazone, HC-1, HC-2, HC-4, HC-10, and HC-11) were then carried out on the 3 recombinant parasite lines grown in the absence (control) or presence (induced) of tetracycline (Table 8.1.4; Figure 8.1.5). In all cases, elevated levels of prostaglandin F2α synthase, cytochrome P450 reductase 2 or cytochrome P450 reductase 3 had no effect on parasite susceptibility to any of the agents screened, indicating that these enzymes, previously implicated in the activation of nifurtimox, play no observable role in metabolizing nitrofuryl compounds, including nifurtimox.

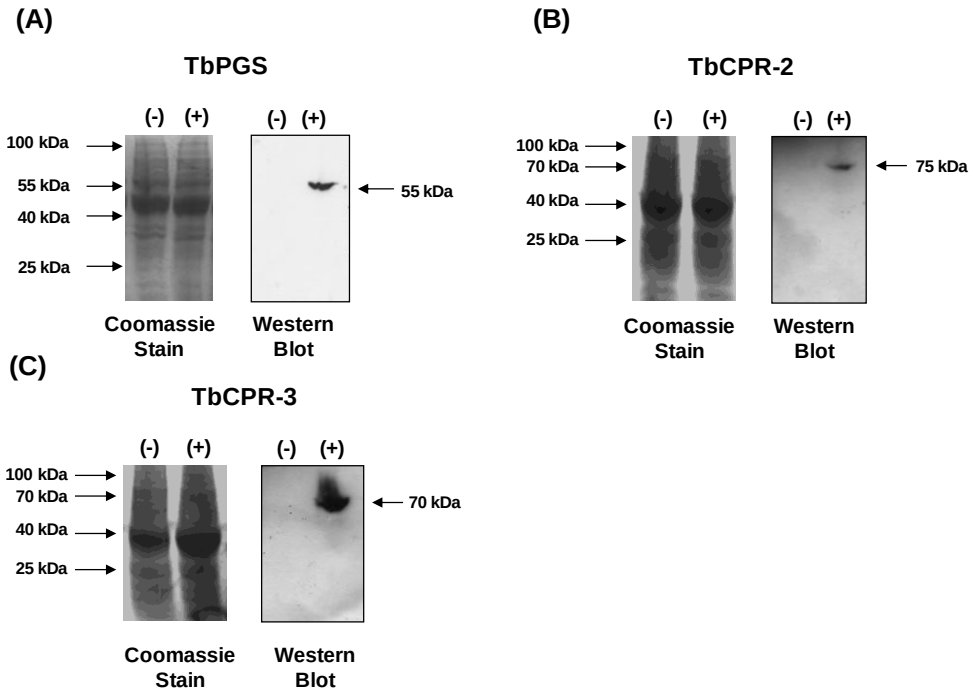

Figure 8.1.4. ***Western blots of alternative enzymes implicated in nitrofuryl activation mechanisms.***
Tetracycline inducible gene expression is demonstrated by western blot to the C-terminal myc tag of (**A**) prostaglandin F2α synthase, (**B**) cytochrome P450 reductase 2, and (**C**) cytochrome P450 reductase 3 (Section 3.9.4). In each case, a protein sample originating from a tetracycline treated culture is run parallel to an untreated control. A band of the expected size is observed for each enzyme.

Compound	TbPGS		TbCPR-2		TbCPR-3	
	-Tet	+Tet	-Tet	+Tet	-Tet	+Tet
Nifurtimox	2935 ± 100	2870 ± 20	2775 ± 100	2740 ± 90	2865 ± 25	2860 ± 95
HC-1	160 ± 5	165 ± 5	160 ± 5	175 ± 15	165 ± 10	170 ± 15
HC-2	305 ± 20	325 ± 30	190 ± 20	210 ± 25	180 ± 20	195 ± 25
HC-4	635 ± 5	640 ± 25	390 ± 15	375 ± 20	440 ± 15	495 ± 35
HC-10	95 ± 10	120 ± 20	150 ± 10	125 ± 20	250 ± 15	295 ± 10
HC-11	650 ± 45	630 ± 65	370± 20	345 ± 10	495 ± 90	465 ± 90
Nitrofurazone	360 ± 5	350 ± 5	305 ± 25	300 ± 15	345 ± 5	350 ± 5

Table 8.1.4. ***Susceptibility of bloodstream form T. brucei to nitrofuryls with elevated levels of specified activating enzymes.***
The growth inhibitory effects of select nitrofuryl compounds in terms of IC_{50} values (in nM) on the over-expressing cell-lines of prostaglandin F2α synthase (TbPGS), cytochrome P450 reductase 2 (TbCPR-2), and cytochrome P450 reductase 3 (TbCPR-3). Induction of over-expression is generated by tetracycline treatment (+Tet) and is shown next to an untreated control (-Tet). Data are means from four experiments ± standard deviation.

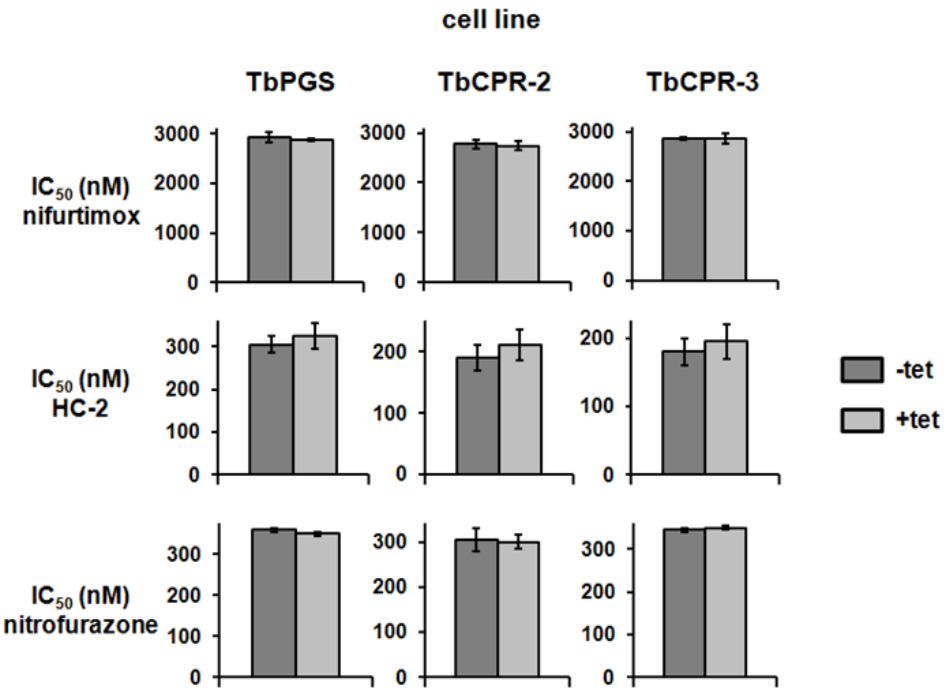

Figure 8.1.5. ***Susceptibility of bloodstream form T. brucei ectopically expressing other enzymes proposed to interact with nitrofuryls.***
Growth-inhibitory effects as judged by IC_{50}values (in nM) of nifurtimox, HC-2 and nitrofurazone on *T. brucei* cells induced to express recombinant prostaglandin F2α synthase (TbPGS), cytochrome P450 reductase 2 (TbCPR-2), or cytochrome P450 reductase 3 (TbCPR-3) (+tet), as compared to non-induced controls (-tet). The other four most potent nitrofuryls behaved similarly (see Table 8.1.4). Data are means from four experiments ± SD.

8.1.4 Investigating whether 5' nitrofuryls inhibit sterol biosynthesis

Many of the nitrofuryls used in this project were originally designed to inhibit squalene epoxidase (SQE), a key enzyme in sterol biosynthesis pathway (Petranyi et al., 1984). The core feature of these molecules consists of a 5' nitrofuran ring linked to a side chain containing derivatives of antifungal drug terbinafine (Gerpe et al., 2009). Following initial trials against *T. cruzi* it became apparent that many of the trypanocidal variants that lacked the allylamine substituent still caused the accumulation of squalene (Gerpe et al., 2009). Based on these preliminary findings it was proposed that the nitro component of the nitrofuryl undergoes an unspecified nitroreductase activation reaction generating metabolites that subsequently inhibit sterol biosynthesis. Here, we evaluated the susceptibility of bloodstream form *T. brucei* over-expressing squalene epoxidase to the 6 most potent nitrofuryl compounds. It must be noted that bloodstream form *T. brucei* are able to scavenge cholesterol from their environment (Coppens et al., 1987), thus potentially circumventing the need for a sterol biosynthetic pathway. This would suggest that in this particular parasite life-cycle stage, the nitrofuryl's trypanocidal activity may not be mediated through squalene epoxidase. Conversely, it has been noted that sterols may function in as yet unknown pathways in bloodstream form *T. brucei* and so could prove to be an important target (Zhou et al., 2007).

To assess whether the trypanocidal properties of 5' nitrofuryls (or their metabolites) target squalene epoxidase activity, the squalene epoxidase open reading frame minus its stop codon, was amplified from *T. brucei* genomic DNA and the resultant fragment used to replace the nitroreductase gene in pRPa^{MYC}-NTR (Figure 8.1.3a) to form pRPa^{MYC}-SQE (Figure 8.1.6). The plasmid was digested with *Sac*II and *Not*I, and the purified DNA fragments transfected into the bloodstream form *T. brucei* 2T1/TAG^{PURO} line (Alsford and Horn, 2008). Drug selection was performed with hygromycin and recombinant parasite clones obtained (Section 3.10.1). To demonstrate expression, extracts from parasite cultures grown in the absence (no induction) or presence (induction) of tetracycline, were prepared and analysed in western blots using an antibody raised against the c-myc (9E10) epitope (Figure 8.1.7). For the recombinant parasite line, a band of the correct size corresponding to tagged squalene epoxidase was detected in tetracycline treated parasites.

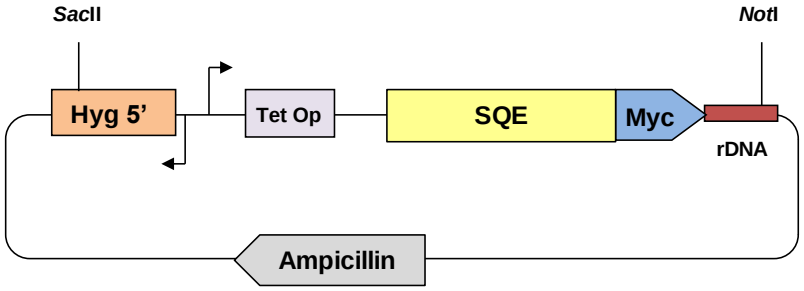

Figure 8.1.6. ***A plasmid used to over-express squalene epoxidase in T. brucei.***
The full length squalene epoxidase gene lacking its stop-codon was amplified from *T. brucei* genomic DNA and cloned into the pRPa^{MYC}-NTR plasmid (Wilkinson et al., 2008), replacing the nitroreductase gene (Section 3.6.15). The resulting plasmid pRPa^{MYC}-SQE was used in conjunction with the 2T1/TAG^{PURO} cell-line (Alsford and Horn, 2008) for tetracycline mediated inducible gene expression of squalene epoxidase.

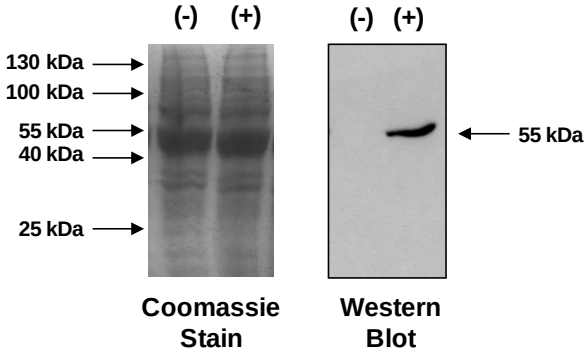

Figure 8.1.7. ***A Western blot showing the inducible expression of squalene epoxidase.***
Inducible gene expression upon tetracycline treatment is demonstrated by western blot to the C-terminal myc tag of squalene epoxidase (Section 3.9.4). Under tetracycline treatment conditions, a band of the predicted size is generated.

The growth inhibition properties of nifurtimox and the six most potent trypanocidal nitrofuryls (nitrofurazone, HC-1, HC-2, HC-4, HC-10, and HC-11) were then evaluated on trypanosomes induced to over-express squalene epoxidase (Figure 8.1.5). This group of compounds includes HC-4 which is reported to be one of the most effective agents at causing squalene accumulation in *T. cruzi* (Gerpe et al., 2008). As with the *T. brucei* over-expressing prostaglandin F2α synthase, cytochrome P450 reductase 2 or cytochrome P450 reductase 3 lines, elevated levels of squalene epoxidase had no effect on parasite susceptibility to any of the agents screened. Intriguingly, no effect on parasite growth at concentrations up to 20 μM was observed using terbinafine, suggesting that this drug does not effectively inhibit squalene epoxidase, and/or any inhibitory effect on this enzyme is not trypanocidal to bloodstream form *T. brucei*.

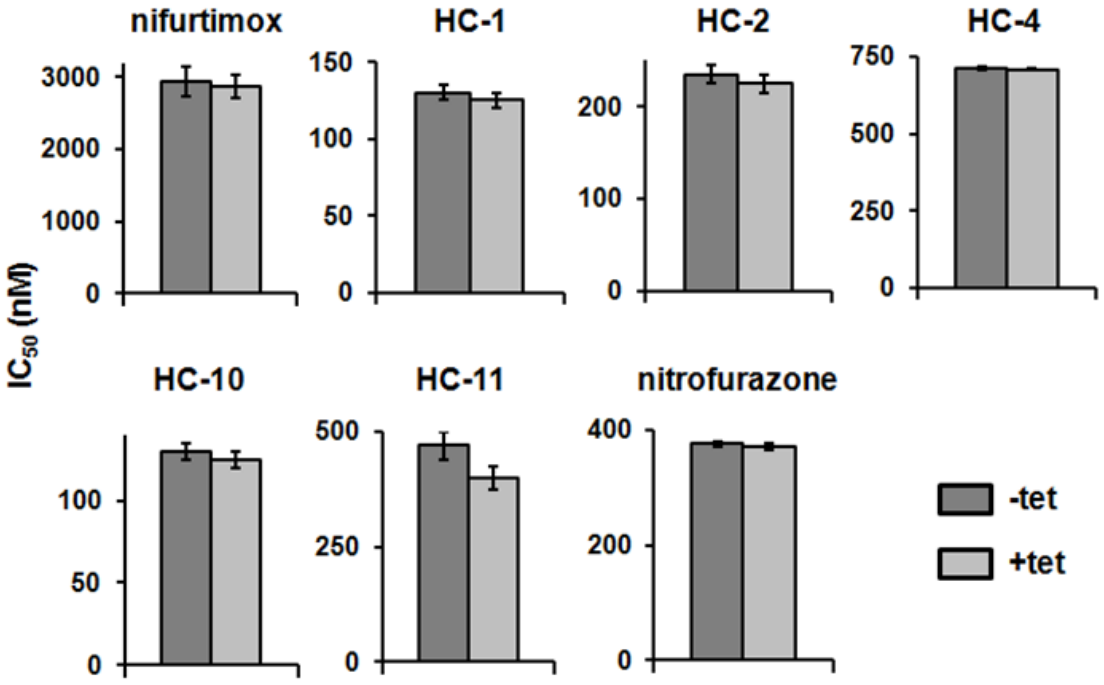

Figure 8.1.8. ***Susceptibility of bloodstream form T. brucei with elevated levels of squalene epoxidase to the 6 most potent nitrofuryls.***
Growth-inhibitory effects as judged by IC_{50} values (in nM) of the six most potent trypanocidal 5' nitrofuryls on *T. brucei* cells induced to express recombinant squalene epoxidase (+tet) in comparison to controls (-tet). Data are the means from four experiments ± SD.

8.1.5 Profiling the nitroreductase generated 5' nitrofuryl reduction products

Using a functional genomics based approach, it has now been shown that a trypanosomal type I nitroreductase plays a key step in mediating the trypanocidal activity of 5' nitrofuryl compounds, in agreement with other findings relating to other nitroaromatic agents (Bot et al., 2010; Hall et al., 2010; Wilkinson et al., 2008). Our next goal was to determine what happens following this initial activation step. Reaction of bacterial type I nitroreductases with 5' nitrofuryls can lead to the formation of various products (Figure 8.1.9). Invariably, the first step involves a series of 2 electron reduction steps resulting in conversion of the nitro group to a hydroxylamine derivative via a transient nitroso intermediate. A hydroxylamine could then be processed further to form an aminofuran (Beckett and Robinson, 1959), a saturated open chain nitrile (Gavin et al., 1966) or nitrenium ion (Streeter and Hoener, 1988).

To identify which metabolites were generated following nitroreductase reduction, the 6 most potent nitrofuryls were enzymatically reduced using recombinant nitroreductase (provided by Dr. Belinda Hall) and the resultant material analysed by tandem mass spectrometry (LC-MS/MS). For the three thiosemicarbazones HC-1, HC-2 and HC-4, LC-MS analysis identified a single analyte whose mass spectrum was compatible with the saturated open chain nitrile form of the parent compound. Unfortunately, further characterisation of the HC-1 derived product was hampered because this metabolite fragmented poorly when performing tandem-MS in either negative or positive ion modes. Therefore, this compound was not studied further. In the case of the other thiosemicarbazones, negative tandem MS unequivocally confirmed the nature of the saturated open chain nitrile structure. For HC-2, reduction leads to formation of an $[M-H]^-$ ion at 197 (Figure 8.1.10a; peak i). Secondary fragmentation of this yields 4 ions with *m/z* values of 89, 97, 107 and 124 (Figure 8.1.10b). These ions are the result of eliminative cleavage of weak N-N or N-C bonds to give thioamide (89) and truncated open chain nitrile (107 and 124) forms, with the 124 ion undergoing further fragmentation to release a nitrile moiety (97).

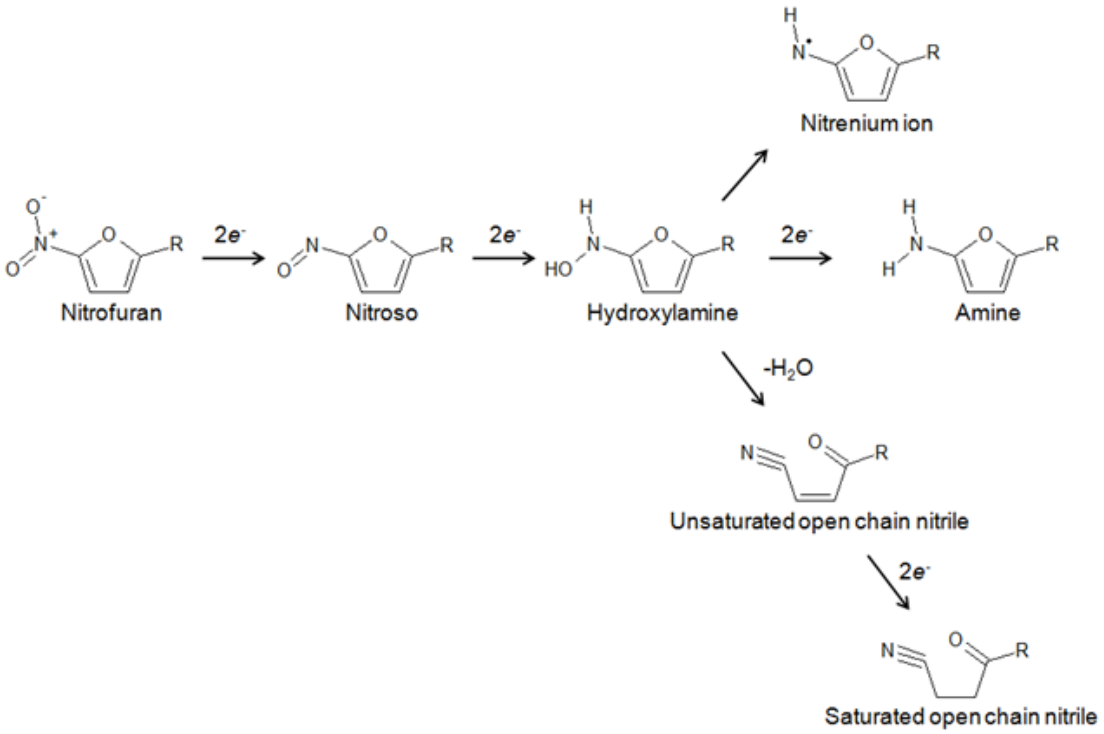

Figure 8.1.9. ***Reduction of 5' nitrofuryls by type I nitroreductases.***
In reactions mediated by type I nitroreductases, the conserved nitro group on the nitrofuryl pro-drug undergoes a series of 2-electron reductions to generate the hydroxylamine derivative via an unstable nitroso intermediate. A hydroxylamine can then be metabolised further with several pathways proposed. These include: formation of a nitrenium ion (Streeter and Hoener, 1988), reduction to the amine form (Beckett and Robinson, 1959), or cleavage of the furan ring forming unsaturated then saturated open chain nitriles (Gavin et al., 1966). Importantly for the downstream experiments reported here, the aminofuran and saturated open chain nitrile metabolites have the same molecular mass. Figure reproduced from Hall et al., 2011.

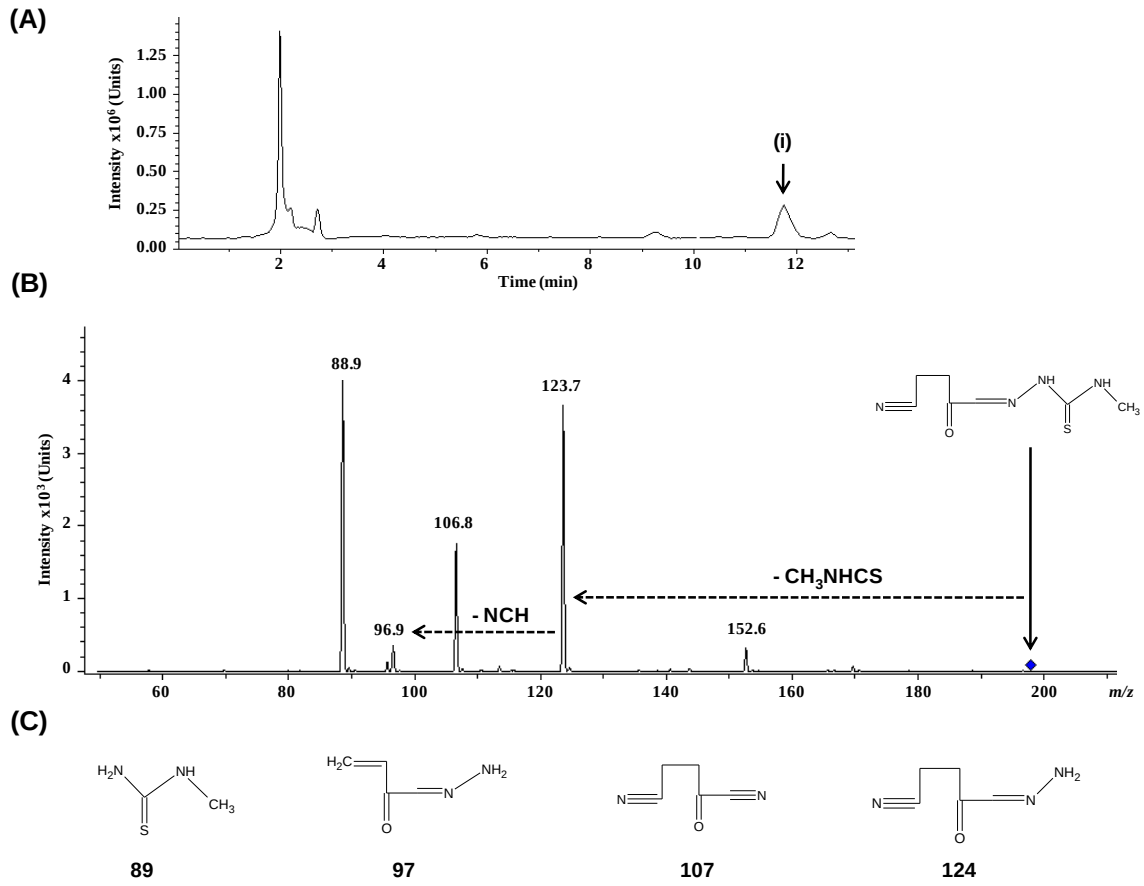

Figure 8.1.10. ***Characterizing the nitroreductase mediated HC-2 reduction products.*** Negative ESI LC-MS analysis (**A**) of the nitroreductase-mediated HC-2 reduction product identifies a single analyte (i) whose mass spectrum contained a molecular ion for $[M-H]^-$ at 197 and corresponds to a saturated open chain nitrile with a molecular weight of 198. Negative ESI MS-MS analysis (**B**) of this ion generates secondary ions with *m/z* values of 89, 97, 107 and 124 whose predicted structures are given (**C**).

The nitroreductase-mediated reduction of HC-4 generated a single metabolite with a parent ion for $[M-H]^-$ of 223. Secondary fragmentation yields five ions with *m/z* values of 91, 97, 106, 117 and 124 (Figure 8.1.11). The major ion (124) was generated by breakage of an N-C bond in the thiourea side chain that then undergoes further fragmentation to release a nitrile moiety (97). These two ions (97 and 124) have the same *m/z* values as described for HC-2, supporting the hypothesis that these fragments are derived from a common 5' nitrofuryl structure.

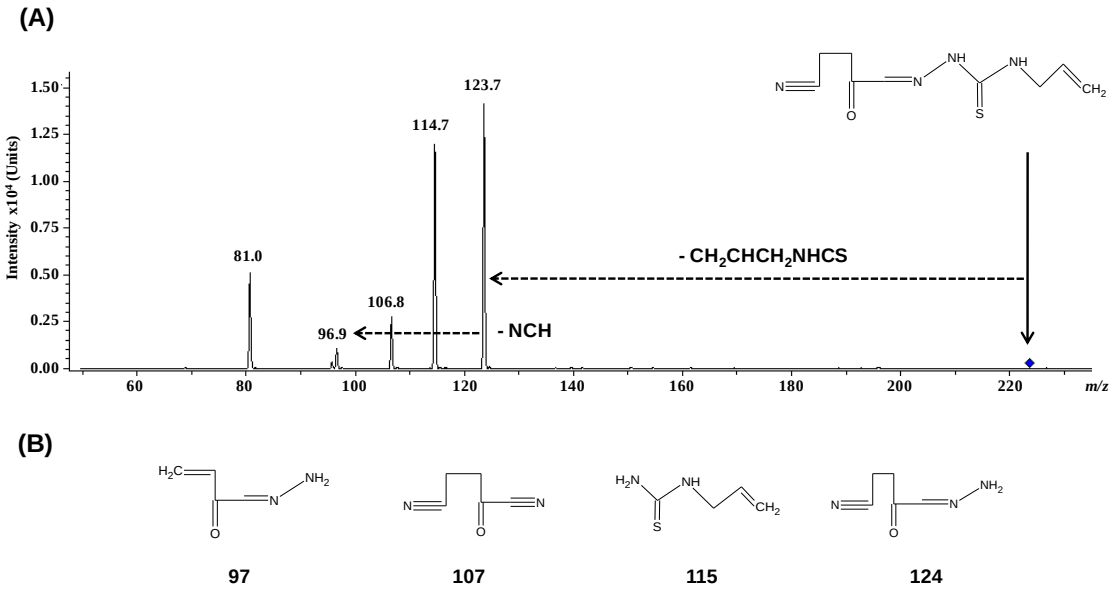

Figure 8.1.11. ***Characterizing the nitroreductase mediated HC-4 reduction products.*** Negative LC-MS analysis of the nitroreductase mediated HC-4 reduction product identifies a single analyte whose mass spectrum contained a molecular ion for $[M-H]^-$ at 223. This corresponds to a saturated open chain nitrile with a molecular weight of 224. Negative MS-MS analysis (**A**) of this ion generates secondary ions with *m/z* values of 81, 97, 107, 115 and 124, whose predicted structures are given (**B**).

In the case of the semicarbazone nitrofurazone, LC-MS analysis of the nitroreductase generated reduction products under negative ionization identified two major products with *m/z* values of 165 and 167 (Figure 8.1.12a; peaks ii and i respectively). The mass spectrum of the smaller ion corresponded to an unsaturated open chain nitrile structure with the 167 ion representing either a saturated open chain nitrile or an aminofuran form. To characterize the larger ion further, it was then subject to a second round of MS, resulting in the formation of two distinct ions with *m/z* values of 140 and 123 (Figure 8.1.12b). Fragment reconstruction analysis of these two ions indicate that the 140 ion was generated by loss of the nitrile from the nitrofurazone-derived saturated open chain nitrile structure, while the 123 ion corresponds to loss of an amide group at the opposite end of the molecule.

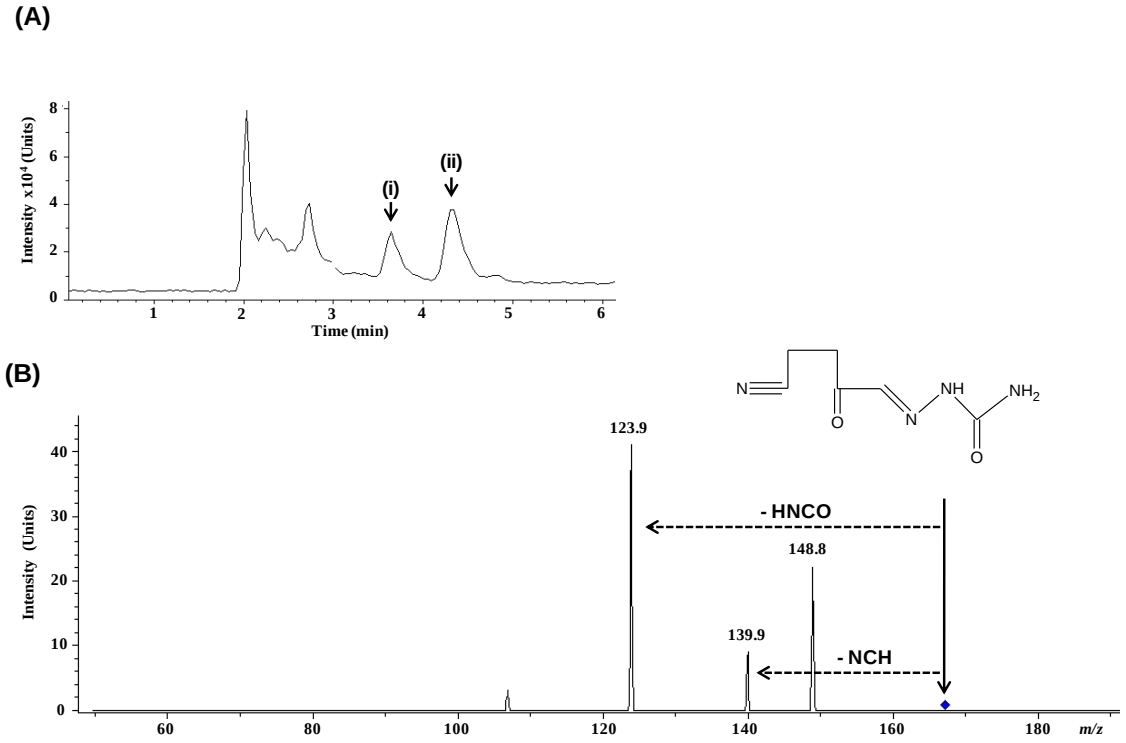

Figure 8.1.12. ***Characterizing the nitroreductase mediated nitrofurazone reduction products.***
Negative LC-MS analysis (**A**) of the nitroreductase generated nitrofurazone reduction products identifies two ions (i and ii) with *m/z* values of 167 (i) and 165 (ii). These correspond to the saturated (i) and unsaturated (ii) open chain nitrile structure, respectively. Negative MS/MS analysis (**B**) of the 167 ion (identified in **A**) generates $[M-H]^-$ ions with *m/z* values of 124 and 140. These two ions were obtained following elimination from parental saturated open chain nitrile ion of the amide (123) or nitrile (140) groups.

When the nitroreductase mediated reduction products from the two carbazonates HC-10 and HC-11 were analysed by LC-MS analysis under negative ionization, two major metabolites were detected. For HC-10, the *m/z* values were 264 and 266 while for HC-11 the values were 278 and 280. As for nitrofurazone, the mass spectrum of the smaller ions corresponded to an unsaturated open chain nitrile derivatives with the larger ions representing either the saturated open chain nitrile or aminofuran forms. For both compounds, the larger ions (266 for HC-10 and 280 for HC-11) were analysed by tandem-MS, and in both cases a major ion corresponding to elimination of a nitrile

moiety was detected (*m/z* vales of 239 for the HC-10 derived metabolite and 253 for the HC-11 derived product) (Figure 8.1.13).

Of note, the three compounds generating 2 detectable metabolites possess a urea group off the furan side-chain, whereas the compounds that produce only one metabolite contain a thiourea group. This suggests the oxygen of the urea group may have an electronic stabilising effect on the unsaturated molecule, or potentially the greater size of the sulphur atom generates a steric hindrance effect, reducing the stability of an intermediate structure.

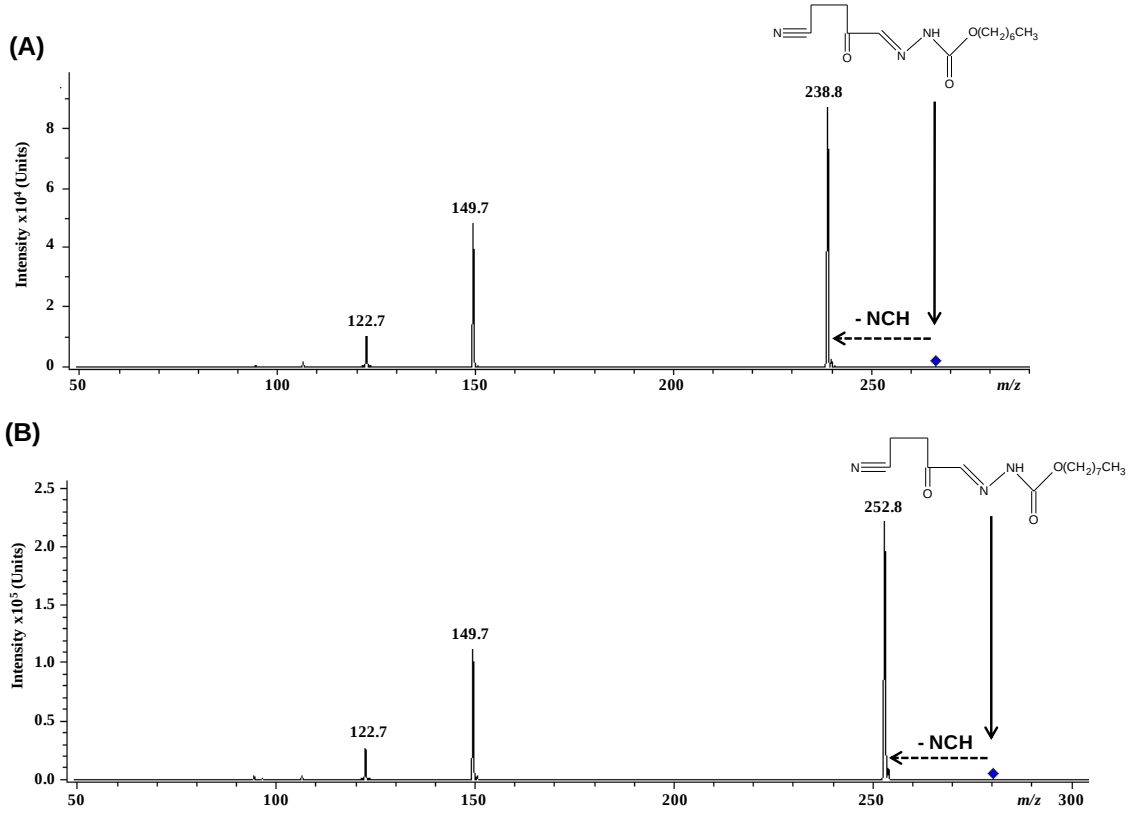

Figure 8.1.13. ***Characterizing the nitroreductase mediated HC-10 and HC-11 derived reduction products.***
Negative LC-MS analysis of the nitroreductase generated reduction products of HC-10 and HC-11 identified two ions with *m/z* values of 264 and 266 (for HC-10), and of 278 and 280 (from HC-11). In each case, the smaller ion corresponds to the unsaturated open chain nitrile form while the larger ion corresponds to the saturated form. To confirm the assignment for the larger ions, negative MS/MS analysis was performed. In both cases, secondary fragmentation resulted in a major ion whose *m/z* values correspond to the loss of a nitrile group from the parental ion. For HC-10, secondary fragmentation of the 266 parental ion generated a fragment with an *m/z* value of 239 (**A**) while secondary fragmentation of the 280 ion from HC-11 generated a fragment with an *m/z* value of 253 (**B**).

8.2 Chapter Summary

This chapter has focussed on a small series of nitrofuryl compounds and their trypanocidal effectiveness against *T. brucei*. In summary this study has revealed:

- A drug screen against wild-type *T. brucei* showed that all except one compound (HC-5), was more potent than nifurtimox (2.8 µM IC_{50}), with over half the compounds generating IC_{50} values of less than 1 µM.
- Selected 5' nitrofuryls screened against Vero cultures all demonstrated higher therapeutic index values than nifurtimox.
- Screens against *T. brucei* cell-lines with modified nitroreductase levels implicate this enzyme as the major contributor of trypanocidal activity via a pro-drug activation mechanism, as observed previously for nifurtimox (Wilkinson et al., 2008).
- Further screens against other modified *T. brucei* cell-lines designed to test alternative hypotheses of trypanocidal activity mechanisms did not support a major role for prostaglandin F2α synthase, cytochrome P450 reductase 2, or cytochrome P450 reductase 3. These alternative hypotheses were originally proposed for the activity of nifurtimox in *T. cruzi* (Docampo et al., 1981a; Portal et al., 2008).
- The nitrofuryl compounds examined here were designed as *T. cruzi* sterol biosynthesis inhibitors, potentially targeting squalene epoxidase (Gerpe et al., 2009). Using an inducible squalene epoxidase expression system no evidence of squalene epoxidase inhibition mediated trypanocidal activity was detected in *T. brucei*.
- Analysis of metabolites derived from nitroreductase mediated *in vitro* reduction of a sample of nitrofuryls show in each case a saturated open chain nitrile structure is formed. Compounds possessing a urea side group also generated a second detectable unsaturated open chain nitrile metabolite. The saturated open chain nitrile observation for nitrofurazone is in accordance with other published material (Peterson et al., 1979; Wang et al., 2010).

8.3 Discussion

The effectiveness of 5' nitrofuryl compounds against *T. brucei* was first demonstrated more than 50 years ago with nitrofurazone, and then nifurtimox emerging as potential trypanocidal therapies (Section 6.2). The experimental promise shown by both agents did not immediately translate to clinical treatments against African sleeping sickness, primarily due to unwanted side effects, although nifurtimox was made available as a monotherapy to treat Chagas disease. However, due to the toxicity, expense and resistance issues relating to other African sleeping sickness drugs, there has been renewed interest in using nitroheterocyclic drugs against *T. brucei* infections. In light of the toxicity issues relating to the use of nifurtimox, we have conducted a screening programme against *T. brucei* making use of 17 novel 5' nitrofuryl compounds originally developed against Chagas disease (Aguirre et al., 2004a; Aguirre et al., 2004b; Gerpe et al., 2008). All except 1 compound exhibited a higher potency towards the bloodstream form parasites than nifurtimox (Section 8.1.1). Unfortunately, many of the most potent compounds (IC_{50} values < 0.5 μM) showed some toxicity towards mammalian cells, despite generating better therapeutic index values than nifurtimox. Understanding how these drugs mediate their trypanocidal properties may help in designing structural modifications to these compounds to reduce their host toxicity, while maintaining their potency against the parasite.

Previous studies on both *T. brucei* and *T. cruzi* has shown that a key step in the cytotoxic and selective activities displayed by nifurtimox stems from how it is activated (Wilkinson et al., 2008). Using biochemical and genetic approaches, a type I nitroreductase has been shown to interact with this pro-drug to generate trypanocidal metabolites. All 5' nitrofuryl compounds identified as inhibitors of bloodstream form *T. b. brucei* growth from the primary screen were subject to a secondary screen using *T. brucei* cell-lines with altered expression levels of the type I nitroreductase (Section 8.1.2). For most compounds, a small increase in resistance toward the nitrofuryl was observed when using the nitroreductase heterozygous parasite line, relative to wild-type cells, although for some agents no difference in susceptibility was detected. One possible explanation for this is that a reduction in the functional gene copy number from

two to one is not necessarily accompanied by a 50% reduction in the concentration of nitroreductase enzyme within the parasite. Therefore, it would not be expected that a nitroreductase gene deletion would be directly 50% more resistant to certain nitroheterocyclics. A much better approach to studying pro-drug activation involved the implementation of the type I nitroreductase over-expressing line, where cells induced to over-express this enzyme were hypersensitive to most of the nitroheterocyclics tested, relative to non-induced controls (Section 8.1.2). This confirms that in the parasite, the type I nitroreductase plays a major role in the activation of most 5' nitrofuryls pro-drugs. Intriguingly, the susceptibility of parasites with altered levels of the type I nitroreductase towards one compound (HC-6; IC_{50} ~0.5 μM) was not greatly affected, indicating that its trypanocidal activity occurs through a mechanism distinct from all the other 5' nitrofuryls tested.

To definitively characterize any stable products arising from the *T. brucei* type I nitroreductase mediated reduction of selected 5' nitrofuryls, an analysis of the metabolites was performed using liquid chromatography coupled to tandem mass spectrometry. Using the semicarbazone nitrofurazone as a reference compound, two major end products were isolated. These were identified as open chain nitrile derivatives, with one having a saturated open-chain conformation, while the other having an unsaturated arrangement (Section 8.1.5). During nitrofuryl reduction with bacterial type I nitroreductases, the saturated form has frequently been detected whereas the unsaturated structure, although postulated as an intermediate that leads to the saturated form (Peterson et al., 1979), had not been reported. Toxicity studies have shown that the stable, saturated nitrofuryl form does not affect cell growth, resulting in the hypothesis that intermediates generated during its formation are responsible for this pro-drug's anti-microbial properties (Section 6.2). In contrast, analysis of the metabolites generated following nifurtimox reduction by the trypanosomal (*T. cruzi* and *T. brucei*) type I nitroreductase identified the unsaturated open chain nitrile as the major end product, with this then undergoing further reduction to the saturated form, albeit at a very slow rate (Hall et al., 2011). Analysis of the toxicity of the unsaturated form demonstrated that this affected *T. brucei* and mammalian cells at equivalent levels, unlike the parental pro-drug that shows selectivity toward the parasite. The data reported

here clearly shows that following the initial nitrofurazone reduction, conversion of the unsaturated to saturated form occurs more readily than for nifurtimox. Based on the above reports, it is tempting to speculate that the trypanocidal activity displayed by nitrofurazone stems from the unsaturated open chain nitrile, at least in part. However the effects of other, unstable intermediaries cannot be ruled out at this stage. When analyzing two structurally related carbazonate compounds (HC-10 and HC-11), the corresponding unsaturated and saturated end products were also observed, indicating that this reaction is common to many semicarbazone- and carbazonate-based nitrofuryl compounds, and is therefore unlikely to be an experimental artefact (Section 8.1.5).

When these studies were extended to thiosemicarbazone compounds (HC-1, HC-2 and HC-4), only the common saturated open chain nitrile end metabolite was observed (Section 8.1.5). Presumably, the unsaturated open chain nitrile metabolites resulting from the type I nitroreductase mediated reactions are too unstable to isolate with this analytical technique. The obvious difference between these compounds and those described earlier is the presence of the much bulkier sulphur containing thiourea group in place of the oxygen based urea group, which may influence the stability of any intermediates.

For all types of 5' nitrofuryls tested, the other proposed end metabolites theoretically possible following the initial 2-electron nitroreductase mediated reduction such as the aminofuran and nitrenium ion (Figure 8.1.9), were not detected. These potential metabolites have not been reported with a bacterial type I nitroreductase, although they have been observed during *in vitro* reactions using type II nitroreductases (Peterson et al., 1979; Streeter and Hoener, 1988). Therefore, the detection of the saturated (and unsaturated, where applicable) open-chain nitrile derivatives indicate that the *T. brucei* type I nitroreductase functions via a classical pathway identical to the characterized prokaryotic orthologues (Figure 6.2.2). The nature and stability of the toxic metabolite intermediates may well be the defining factors in causing their trypanocidal activity and host side-effects.

Several other parasite enzymes have been reported to interact with 5' nitrofuryls and/or any metabolites. The cytochrome P450 reductases have received considerable attention with regard to the trypanocidal activity of nifurtimox in *T. cruzi* (Section 6.2.2). To investigate whether two of these enzymes play a role in pro-drug activation in *T. brucei*, the over-expression approach that proved so effective when applied with the type I nitroreductase was used. Here, parasites induced to over-express the cytochrome P450 reductases displayed the same susceptibility to any of the tested compounds, as compared to non-induced controls (Section 8.1.3), including nifurtimox. It therefore appears that these enzymes play no major role in mediating the trypanocidal activity of 5' nitrofuryls in *T. brucei*. This, coupled to a similar finding where *T. cruzi* cells over-expressing cytochrome P450 reductase were only slightly more resistant to nifurtimox (Portal et al., 2008), indicates the same is most likely true in *T. cruzi* as well. This is not to say that 5' nitrofuryl compounds such as nifurtimox do not act as substrates for cytochrome P450 reductases in trypanosomes, or even within their human hosts, merely that any interaction is not the primary route of parasite growth inhibition.

The prostaglandin F2α synthase 'Old Yellow Enzyme' has also been implicated in nifurtimox metabolism within *T. cruzi* (Kubata et al., 2002). Again, using the over-expression system, the contribution made by this enzyme to the trypanocidal activity of this nitrofuryl in *T. brucei* was assessed by observing any alterations to drug susceptibility upon an increase in ectopic enzyme expression. This demonstrated the 'old yellow enzyme' orthologue in *T. brucei*, also called prostaglandin F2α synthase, did not noticeably contribute to the trypanocidal activity of any 5' nitrofuryl compounds tested, including nifurtimox (Section 8.1.3). Unlike for the cytochrome P450 reductases, it is difficult to extend these conclusions to the *T. cruzi* enzyme because a comparison of protein sequence between the *T. cruzi* 'Old Yellow Enzyme' and the *T. brucei* prostaglandin F2α synthase shows that although they fulfil the same function, they are remarkably different enzymes (Kubata et al., 2002).

A previous study assessing the trypanocidal properties of furyls against *T. cruzi* revealed that treatment with certain derivatives led to an intracellular build-up of squalene, a phenomenon attributed to the inhibition of squalene epoxidase (Gerpe et al., 2009). As

the accumulation of squalene was associated only with compounds possessing a nitro group on the furan ring, a possible explanation was that 5' nitrofuryl metabolites derived from nitroreductase activity acted to inhibit the squalene epoxidase enzyme. To address this hypothesis in *T. brucei*, the over-expression system featuring the native *T. brucei* squalene epoxidase was exploited. Upon induction of over-expression, the *T. brucei* line displayed no alteration in its resistance patterns as compared to controls for any of the compounds tested, suggesting that none of these agents exerted their toxic effects through squalene epoxidase inhibition (Section 8.1.4). One reason for this could be that unlike in *T. cruzi*, the bloodstream form *T. brucei* does not require a functional sterol biosynthesis pathway, as they can scavenge the end-product from their environment (Coppens et al., 1987). Another possibility is that the build-up of squalene is a consequence of nitrofuryl mediated trypanocidal activity (and its metabolites), and is not the cause of the toxicity itself. The activity of squalene epoxidase is dependent on the donation of electrons from cytochrome P450 reductase (Ono et al., 1982). If the physiological cytochrome P450 reductase activity is impeded in some way by the 5' nitrofuryls, this may reduce the rate of squalene epoxidase action, and explain the build-up of squalene in *T. cruzi*. In this setting, the observed accumulation of squalene would be coupled to 5' nitrofuryl treatment but not part of a type I nitroreductase mediated toxicity process.

Nitroheterocyclic drugs are experiencing a renaissance as treatments for African sleeping sickness. As noted, nifurtimox has been deployed against the West African form of the disease as part of a co-therapy alongside eflornithine (Priotto et al., 2009), while the nitroimidazole compound fexinidazole, is now entering phase I clinical trials (www.dndi.org). Fexinidazole activity against *T. brucei* was first discovered almost 30 years ago (Jennings and Urquhart, 1983), yet its full potential has only recently been appreciated (Torreele et al., 2010). While it has yet to be explicitly demonstrated that fexinidazole is activated by the trypanosomal type I nitroreductase, it is noteworthy that a *T. brucei* cell-line resistant to nifurtimox, benznidazole, and nitrofurazone, is also resistant to fexinidazole (Sokolova et al., 2010). Like many nitroheterocyclic drugs, fexinidazole fails the "classical" Ames test of mutagenicity, yet it is not mutagenic to type I nitroreductase deficient bacteria, or to mammalian cells (Torreele et al., 2010).

Whether the type I nitroreductase mediated activation of nitroheterocyclic drugs such as nifurtimox and fexinidazole to their toxic metabolites is the sole cause of all short- and long-term cytotoxic effects observed, remains unclear and seems unlikely, given the observation of nitroheterocyclic drug metabolites in animal tissues (Section 6.2). Therefore, perhaps the more subtle question to be addressed is: do nitroheterocyclic drugs have the potential to be designed specific enough to the trypanosomatid type I nitroreductase, so as to present only a reasonable risk for acceptable associated side-effects to human patients over both the short- and longer term? Appreciating the shared mechanism of nitroaromatic drug activation and predicting the downstream metabolites across many classes of compounds by the trypanosomal nitroreductase is a fundamental aspect in overcoming this challenge.

9 Concluding Remarks

This thesis describes two separate and distinct research projects. In the first section, the process of mitosis is addressed in the African trypanosome. Little is currently known about the mechanisms of chromosome segregation in this organism, with many of the conserved mitotic proteins found in other eukaryotes appearing absent in the *T. brucei* genome database (Berriman et al., 2005; Logan-Klumpler et al., 2012). To begin exploring the procedure of chromosome segregation, the centromeric loci of *T. brucei* megabase chromosomes were identified using topoisomerase-II mediated cleavage biochemical mapping experiments. These DNA regions each contain a period of AT-rich repeat sequence, as well as an abundance of retroelements (Obado et al., 2007). Given the variation in centromeric DNA sequence between *T. brucei* chromosomes, and also previous observations in other model systems (Section 2.2.1), it is unlikely that DNA sequence alone constitutes a centromere. However, knowledge of these chromosomal sites can in future facilitate the identification of centromere specific proteins. For example, techniques such as ChIP-Seq could be employed to detect any unusual histone modifications, or possibly a unique histone variant that may fulfil the role performed by CENP-A in other eukaryotes (Section 2.2.2). In addition, a novel strategy of using biotin labelled centromeric DNA probes could be deployed as hybridization 'bait' to isolate this region of DNA with any bound proteins, with mass spectrometry then used to identify those protein components (Dejardin and Kingston, 2009). Also, based on the observation that only the topoisomerase-IIα isoform of *T. brucei* is active at the centromere (Obado et al., 2011), the tandem affinity purification system devised as part of this thesis may be used to dissect enzyme modifications and protein associations which guide the centromere targeted activity of topoisomerase-IIα. Together, these experiments could shed light on novel proteins involved in chromosome segregation in trypanosomes, which may in turn reveal suitable drug targets to develop chemotherapies against these parasites.

The second section of this thesis explores a drug target directly, specifically a trypanosomal type I nitroreductase which catalyses the activation of nitroaromatic pro-drugs to their cytotoxic forms. The initial goal of this project was to develop a luciferase

reporter system for *T. cruzi*, which could then be adapted for drug screening in a 96-well plate format. The establishment of this system facilitated the rapid screening of novel nitroaromatic compounds against the medically relevant amastigote life-cycle stage of *T. cruzi* (Bot et al., 2010). In total, three sets of nitroaromatic compounds were screened in this way, which resulted in the identification of a selection of potential drug candidates that possessed improved potency and therapeutic index values over the current drug, nifurtimox (Bot et al., 2010; Hu et al., 2011). Given that many of these compounds are potential DNA alkylating agents, the next stage in the drug development process would be to assess these agents for host DNA mutagenicity. Firstly systems such as the Ames test, incorporating both the wild-type and nitroreductase deficient bacterial strains can be employed to perform this task. The use of either a *Drosophila* or mouse system would also be appropriate for these studies. If these compounds perform satisfactorily in mutagenicity assays, then further drug trials using a mouse model to analyse the *in vivo* drug properties appraising their suitability as safe and effective chemotherapies would be required. Experiments performed with a selection of nitrofuryl compounds, including nifurtimox, have shown that within the trypanosome, cytotoxicity appears mediated predominantly through pro-drug activation by the type I nitroreductase (Hall et al., 2011). It would be interesting to investigate how this trypanocidal activity is derived. For example observing drug metabolites such as those previously identified for the nitrofuryl series conjugated to DNA or proteins may reveal whether there are specific downstream metabolite targets, or if there is simply widespread non-specific cell damage. Overall, the second section of this thesis has demonstrated that nitroaromatic compounds can be rationally designed to be highly selective in killing trypanosomes by targeting nitroreductase. It remains to be seen whether they can also be designed to generate minimal host side-effects.

10 Appendix

10.1 Alignments

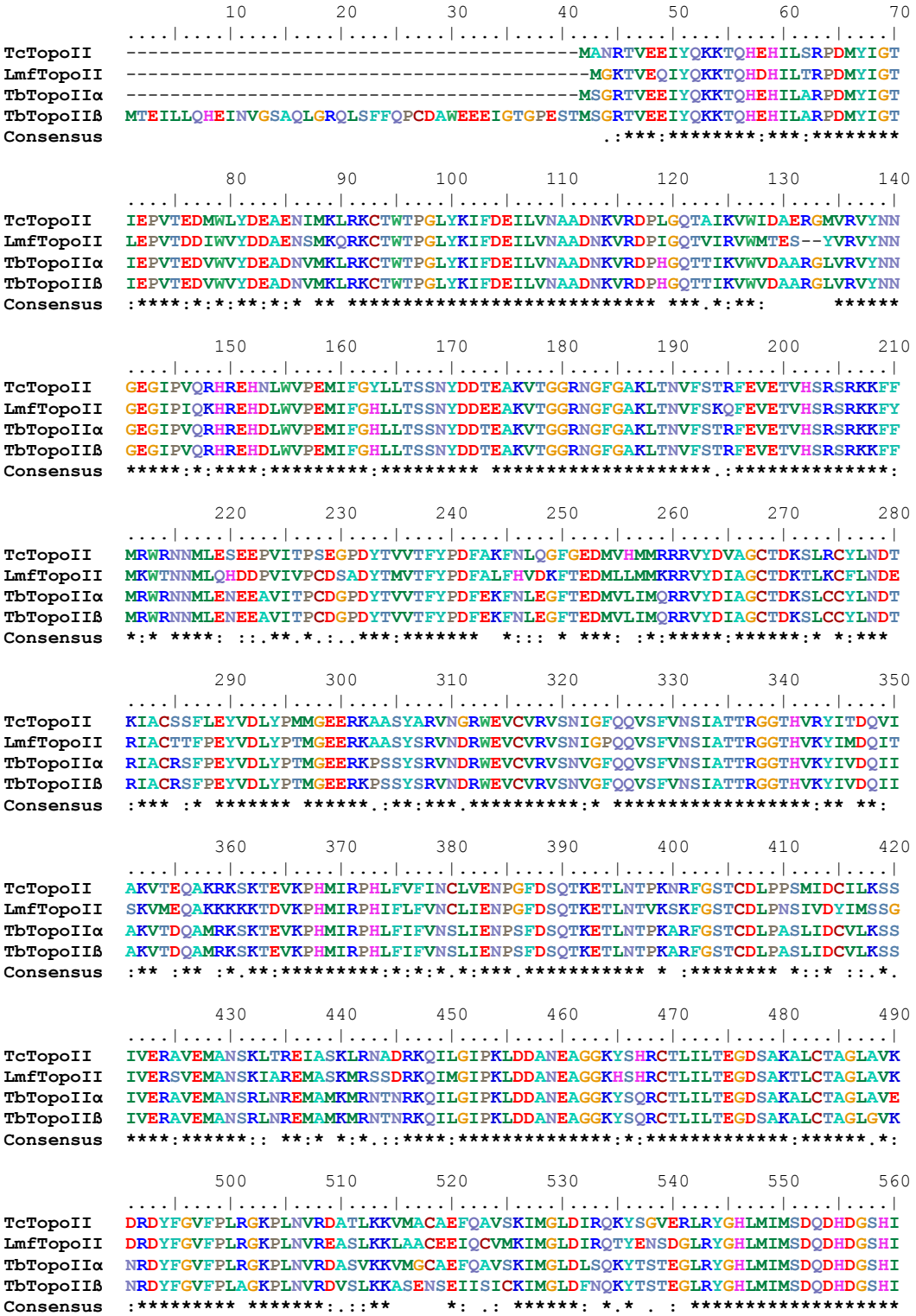

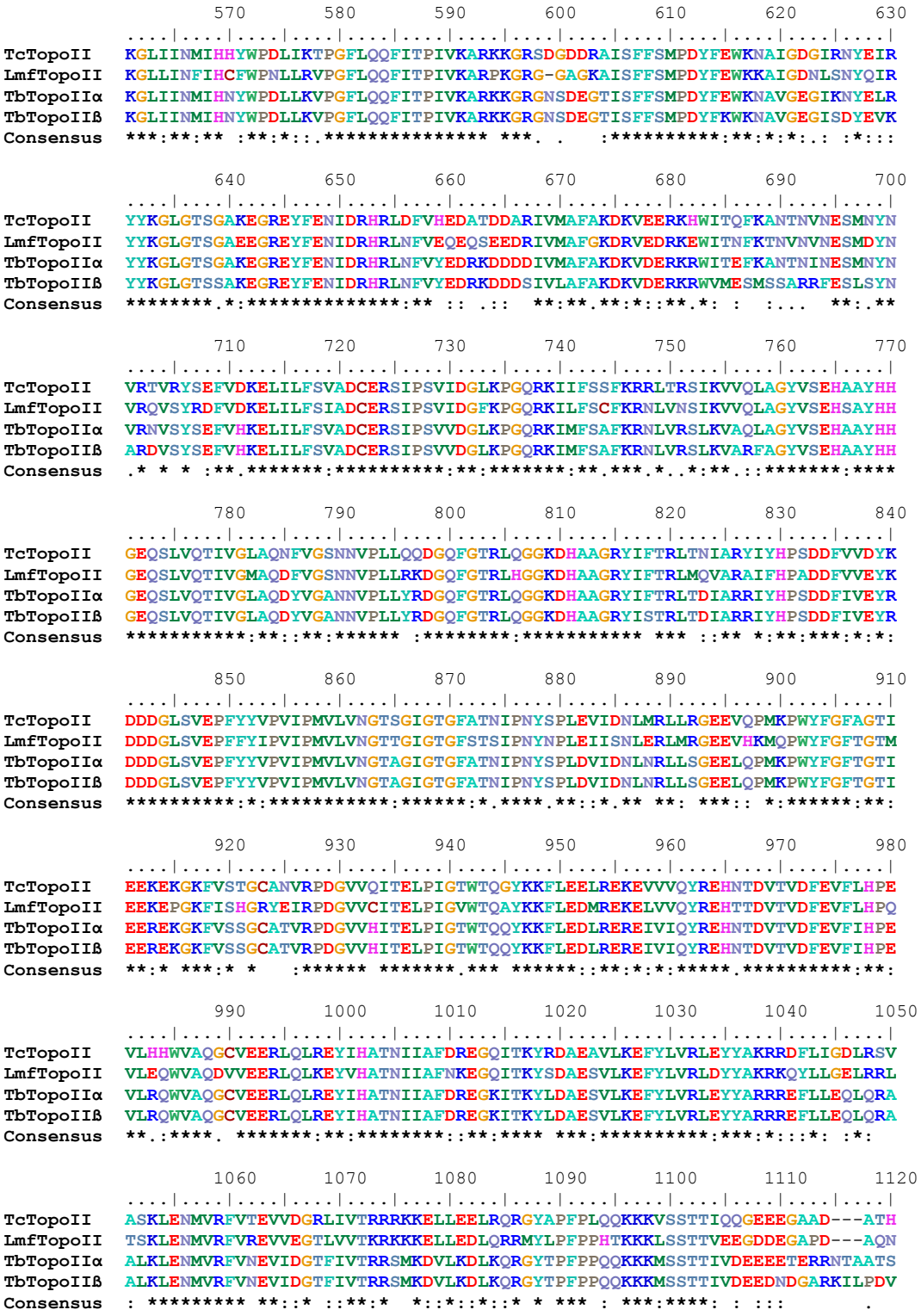
570 580 590 600 610 620 630
TcTopoII KGLIINMIHHYWPDLIKTPGFLQQFITPIVKARKKGRSDGDDRAISFFSMPDYFEWKNAIGDGIRNYEIR
LmfTopoII KGLLINFIHCFWPNLLRVPGFLQQFITPIVKARPKGRG-GAGKAISFFSMPDYFEWKKAIGDNLSNYQIR
TbTopoIIα KGLIINMIHNYWPDLLKVPGFLQQFITPIVKARKKGRGNSDEGTISFFSMPDYFEWKNAVGEGIKNYELR
TbTopoIIß KGLIINMIHNYWPDLLKVPGFLQQFITPIVKARKKGRGNSDEGTISFFSMPDYFKWKNAVGEGISDYEVK
Consensus
640 650 660 670 680 690 700
TcTopoII YYKGLGTSGAKEGREYFENIDRHRLDFVHEDATDDARIVMAFAKDKVEERKHWITQFKANTNVNESMNYN
LmfTopoII YYKGLGTSGAEEGREYFENIDRHRLNFVEQEQSEEDRIVMAFGKDRVEDRKEWITNFKTNVNVNESMDYN
TbTopoIIα YYKGLGTSGAKEGREYFENIDRHRLNFVYEDRKDDDDIVMAFAKDKVDERKRWITEFKANTNINESMNYN
TbTopoIIß YYKGLGTSSAKEGREYFENIDRHRLNFVYEDRKDDDSIVLAFAKDKVDERKRWVMESMSSARRFESLSYN
Consensus
710 720 730 740 750 760 770
TcTopoII VRTVRYSEFVDKELILFSVADCERSIPSVIDGLKPGQRKIIFSSFKRRLTRSIKVVQLAGYVSEHAAYHH
LmfTopoII VRQVSYRDFVDKELILFSIADCERSIPSVIDGFKPGQRKILFSCFKRNLVNSIKVVQLAGYVSEHSAYHH
TbTopoIIα VRNVSYSEFVHKELILFSVADCERSIPSVVDGLKPGQRKIMFSAFKRNLVRSLKVAQLAGYVSEHAAYHH
TbTopoIIß ARDVSYSEFVHKELILFSVADCERSIPSVVDGLKPGQRKIMFSAFKRNLVRSLKVARFAGYVSEHAAYHH
Consensus
780 790 800 810 820 830 840
TcTopoII GEQSLVQTIVGLAQNFVGSNNVPLLQQDGQFGTRLQGGKDHAAGRYIFTRLTNIARYIYHPSDDFVVDYK
LmfTopoII GEQSLVQTIVGMAQDFVGSNNVPLLRKDGQFGTRLHGGKDHAAGRYIFTRLMQVARAIFHPADDFVVEYK
TbTopoIIα GEQSLVQTIVGLAQDYVGANNVPLLYRDGQFGTRLQGGKDHAAGRYIFTRLTDIARRIYHPSDDFIVEYR
TbTopoIIß GEQSLVQTIVGLAQDYVGANNVPLLYRDGQFGTRLQGGKDHAAGRYISTRLTDIARRIYHPSDDFIVEYR
Consensus
850 860 870 880 890 900 910
TcTopoII DDDGLSVEPFYYVPVIPMVLVNGTSGIGTGFATNIPNYSPLEVIDNLMRLLRGEEVQPMKPWYFGFAGTI
LmfTopoII DDDGLSVEPFFYIPVIPMVLVNGTTGIGTGFSTSIPNYNPLEIISNLERLMRGEEVHKMQPWYFGFTGTM
TbTopoIIα DDDGLSVEPFYYVPVIPMVLVNGTAGIGTGFATNIPNYSPLDVIDNLNRLLSGEELQPMKPWYFGFTGTI
TbTopoIIß DDDGLSVEPFYYVPVIPMVLVNGTAGIGTGFATNIPNYSPLDVIDNLNRLLSGEELQPMKPWYFGFTGTI
Consensus
920 930 940 950 960 970 980
TcTopoII EEKEKGKFVSTGCANVRPDGVVQITELPIGTWTQGYKKFLEELREKEVVVQYREHNTDVTVDFEVFLHPE
LmfTopoII EEKEPGKFISHGRYEIRPDGVVCITELPIGVWTQAYKKFLEDMREKELVVQYREHTTDVTVDFEVFLHPQ
TbTopoIIα EEREKGKFVSSGCATVRPDGVVHITELPIGTWTQQYKKFLEDLREREIVIQYREHNTDVTVDFEVFIHPE
TbTopoIIß EEREKGKFVSSGCATVRPDGVVHITELPIGTWTQQYKKFLEDLREREIVIQYREHNTDVTVDFEVFIHPE
Consensus
990 1000 1010 1020 1030 1040 1050
TcTopoII VLHHWVAQGCVEERLQLREYIHATNIIAFDREGQITKYRDAEAVLKEFYLVRLEYYAKRRDFLIGDLRSV
LmfTopoII VLEQWVAQDVVEERLQLKEYVHATNIIAFNKEGQITKYSDAESVLKEFYLVRLDYYAKRKQYLLGELRRL
TbTopoIIα VLRQWVAQGCVEERLQLREYIHATNIIAFDREGKITKYLDAESVLKEFYLVRLEYYARRREFLLEQLQRA
TbTopoIIß VLRQWVAQGCVEERLQLREYIHATNIIAFDREGKITKYLDAESVLKEFYLVRLEYYARRREFLLEQLQRA
Consensus
1060 1070 1080 1090 1100 1110 1120
TcTopoII ASKLENMVRFVTEVVDGRLIVTRRRKKELLEELRQRGYAPFPLQQKKKVSSTTIQQGEEEGAAD---ATH
LmfTopoII TSKLENMVRFVREVVEGTLVVTKRKKKELLEDLQRRMYLPFPPHTKKKLSSTTVEEGDDEGAPD---AQN
TbTopoIIα ALKLENMVRFVNEVIDGTFIVTRRSMKDVLKDLKQRGYTPFPPQQKKKMSSTTIVDEEEETERRNTAATS
TbTopoIIß ALKLENMVRFVNEVIDGTFIVTRRSMKDVLKDLKQRGYTPFPPQQKKKMSSTTIVDEEDNDGARKILPDV
Consensus

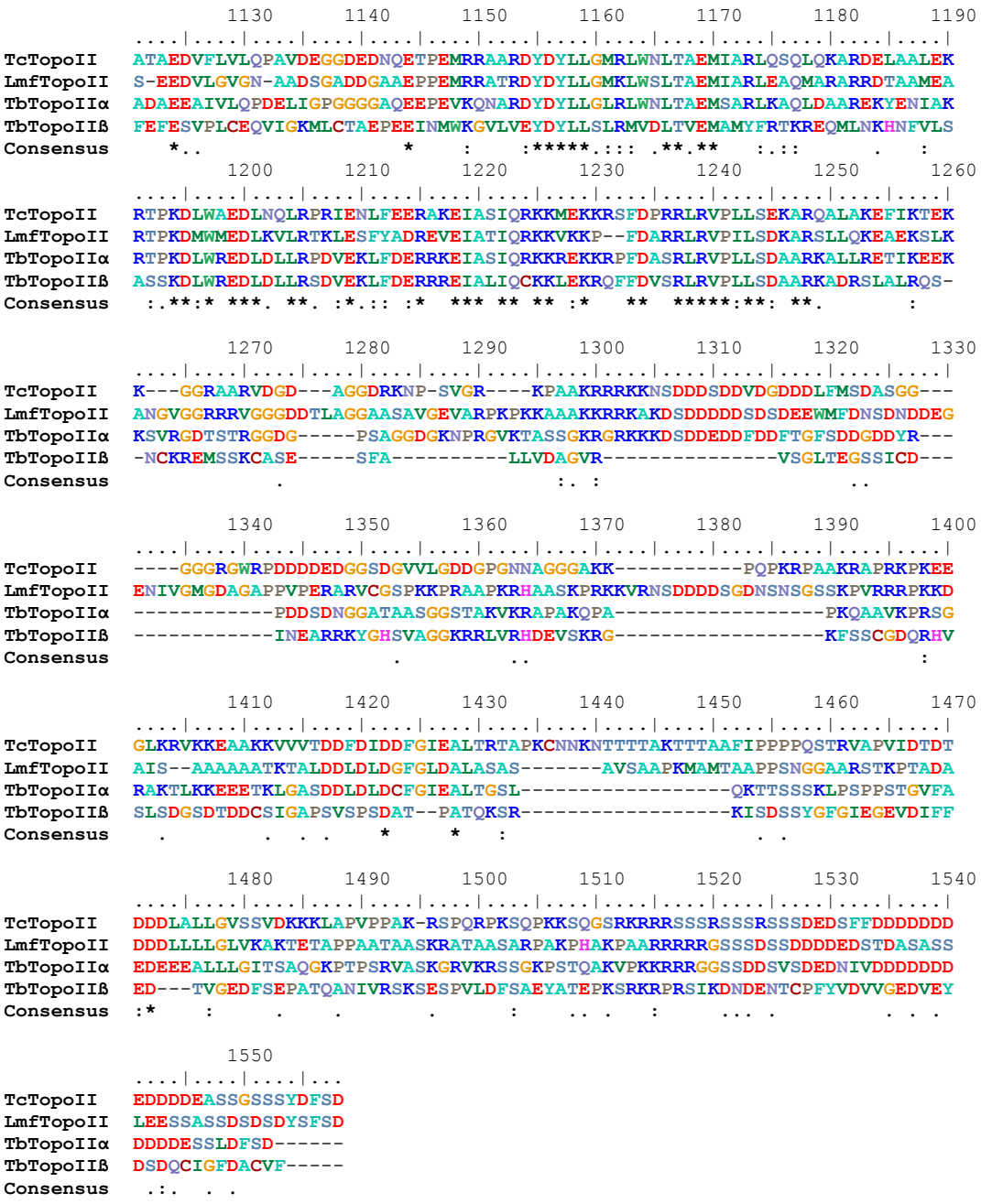

Figure 10.1.1. ***Alignment of trypanosomatid topoisomerase-II protein sequences.***
A protein alignment of the *L. major* and *T cruzi* genes from the genome database, with the published mRNA sequences of the *T. brucei* paralogues (Kulikowicz and Shapiro, 2006) generated using ClustalW (Thompson et al., 1994). The N-terminal ATPase domain (first ~500 amino acids), linker domain, and catalytic domain (amino acids ~650-1100) are highly conserved between trypanosomatids. The C-terminal domain protein sequences (residues ~ 1100 onwards) are highly variable, a feature which was exploited to facilitate differentiation between orthologues with the topoisomerase-IIα antibody (gift from the Shapiro laboratory), and with radio-labelled DNA probes at the nucleotide level.

10.2 Primer Sequences

Primer	Gene (GeneDB ID)	Sequence
Tb1 *forward*	Tb927.1.2340	*Existing α-tubulin probe used*
Tb1 *reverse*	Tb927.1.2340	
Tb2 *forward*	Tb927.1.3560	ATGTCCGTAGTTCTAGATGTTGTG
Tb2 *reverse*	Tb927.1.3560	TGGTATCTGCGTTATGGTTGCACG
Tb3 *forward*	Tb927.1.3830	ATGAGCAATTACTTGGATGATTTG
Tb3 *reverse*	Tb927.1.3830	CTCCAATTCACGACGAACCTCACT
Tb4 *forward*	Tb927.1.4720	*Existing cloned gene used*
Tb4 *reverse*	Tb927.1.4720	
Tb5 *forward*	Tb927.2.1380	GAACGTGCCAGCTTTTGACT
Tb5 *reverse*	Tb927.2.1380	CACGGTCCCATTGATATGTG
Tb6 *forward*	Tb927.2.2090	AAAGCTGGAGAGATGCCAAA
Tb6 *reverse*	Tb927.2.2090	TCTTTCGTAGGGGAGTGGTG
Tb7 *forward*	Tb927.5.570	TGACCCAGACAGTGAATGGA
Tb7 *reverse*	Tb927.5.570	TGAGGTCGCTGCTGTATCTG
Tb10 *forward*	Tb927.5.670	GCCGTTTGCGACTTTATGAT
Tb10 *reverse*	Tb927.5.670	ACGCCTGTTGGACGTTTATC
Tbmini *forward*	177 bp repeat	ATTAAACAATGCGCAGTTAACG
Tbmini *reverse*	177 bp repeat	GTGTATAATAGCGTTAACTGCG
Lmf1 *forward*	LmjF32.0120	GATCGGATCCTGCAGAAGTTTGGACCACTG
Lmf1 *reverse*	LmjF32.0120	CGATAAGCTTGCTGCATGGCTGACTTACAA
Lmf2 *forward*	LmjF12.0530	CATGGGATCCTGGAGAGCACCGAAGTCAAT
Lmf2 *reverse*	LmjF12.0530	TAGGAAGCTTGCTGGTAGAATGCGTGTTGA

Table 10.2.1. ***Primer sequences of centromere mapping probes.***

Primer	Sequence
TbTopo-IIß RNAi *forward*	CATCTCGAGGGTACCGAAAGCAGATCGTAGT TTAGCACTT
TbTopo-IIß RNAi *reverse*	TAGTCTAGAGGATCCATTGATCTGAGTCATA TTCCACGTC
TbTopoII Intergenic *forward*	ACTGGTTCGTTACAGAAG
TbTopoII Intergenic *reverse*	TTGTACGGGAATACCCTC
TbTopo-IIα 12-Myc tag *forward*	ATAGGGCCCCCGTGAGCACAATACAGATG
TbTopo-IIα 12-Myc tag *reverse*	ATATCTAGAGTCACTGAAGTCAAGAGAGGA
TbTopo-IIα 5' Disruption *forward*	ATAGCGGCCGCGTCGCACCGTTGAGGAAATA
TbTopo-IIα 5' Disruption *reverse*	CATGGATCCGTACGGGAATACCCTCACCA
TbTopo-IIα 3' Disruption *forward*	TATGGGCCCCGTCTGTGGAATCTGACTGC
TbTopo-IIα 3' Disruption *reverse*	AAAGGTACCCATCGGAAACTGAGTCGTCA
LmfTopo-II Complement *forward*	ATACCTGCAGGATGGGCAAAACCGTCGAACA
LmfTopo-II Complement *reverse*	CATGGCGCGCCCTAGTCACTGAAGCTGTAGT CGGAGT
TbTopo-IIα PTP tag *forward*	ATAGGGCCCCCGTGAGCACAATACAGATG
TbTopo-IIα PTP tag *reverse*	ATAGCGGCCGCCCGTCACTGAAGTCAAGAGA GGA
TcTopo-II PTP tag *forward*	ATAGGGCCCGCAAAGGAGATTGCATCCAT
TcTopo-II PTP tag *reverse*	ATAGCGGCCGCCCATCACTGAAGTCATATGA CGATG

Table 10.2.2. ***Primer sequences for topoisomerase-II characterization.***

Primer	Sequence
Luciferase *forward*	AAACCCGGGATCGAAGACGCCAAAAACATA
Luciferase *reverse*	GGGGGATCCTTACAATTTGGACTTTCCG
GAPDH 3' UTR *forward*	GGGCCGCGGGAACAACCTGCCGAAGGAGC
GAPDH 3' UTR *reverse*	GGGGAGCTCCACACGGCTAGCATACTCTA
3' rRNA Spacer *forward*	GGGGGTACCTATTATTACTACCACTACTGC
3' rRNA Spacer *reverse*	GGGGGACCGGCGCGCCTTGATGATCCTTTGAAATGTT

Table 10.2.3. ***Primer sequences for luciferase expression plasmids.***

Primer	Sequence
TbSQE-Full *forward*	TATAAGCTTATGGAGGCGGCCATTATT
TbSQE-Full *reverse*	ATATCTAGACAAACCAATTGGCTTCCTTT
TbSQE-Seq1	ATTATGTGTGACGGCGGTTC
TbSQE-Seq2	TTCTGCCACACGTACTTTCG
TbSQE-Seq3	CCCACGTAACCCCTGATAGA
TbSQE-Seq4	TTATCGTGGGCACTGTATGC

Table 10.2.4. ***Primer sequences for T. brucei squalene epoxidase.***

References

Aguirre, G., Boiani, L., Cerecetto, H., Fernandez, M., Gonzalez, M., Denicola, A., Otero, L., Gambino, D., Rigol, C., Olea-Azar, C., *et al.* (2004a). In vitro activity and mechanism of action against the protozoan parasite Trypanosoma cruzi of 5-nitrofuryl containing thiosemicarbazones. Bioorg Med Chem *12*, 4885-4893.

Aguirre, G., Boiani, M., Cabrera, E., Cerecetto, H., Di Maio, R., Gonzalez, M., Denicola, A., Sant'anna, C.M., and Barreiro, E.J. (2006). New potent 5-nitrofuryl derivatives as inhibitors of Trypanosoma cruzi growth. 3D-QSAR (CoMFA) studies. Eur J Med Chem *41*, 457-466.

Aguirre, G., Cabrera, E., Cerecetto, H., Di Maio, R., Gonzalez, M., Seoane, G., Duffaut, A., Denicola, A., Gil, M.J., and Martinez-Merino, V. (2004b). Design, synthesis and biological evaluation of new potent 5-nitrofuryl derivatives as anti-Trypanosoma cruzi agents. Studies of trypanothione binding site of trypanothione reductase as target for rational design. Eur J Med Chem *39*, 421-431.

Albertson, D.G., and Thomson, J.N. (1982). The kinetochores of Caenorhabditis elegans. Chromosoma *86*, 409-428.

Alejandre-Duran, E., Claramunt, R.M., Sanz, D., Vilaplana, M.J., Molina, P., and Pueyo, C. (1988). Study on the mutagenicity of nifurtimox and eight derivatives with the L-arabinose resistance test of Salmonella typhimurium. Mutat Res *206*, 193-200.

Alexander, J., Satoskar, A.R., and Russell, D.G. (1999). Leishmania species: models of intracellular parasitism. J Cell Sci *112 Pt 18*, 2993-3002.

Alsford, S., and Horn, D. (2008). Single-locus targeting constructs for reliable regulated RNAi and transgene expression in Trypanosoma brucei. Mol Biochem Parasitol *161*, 76-79.

Alsford, S., Turner, D.J., Obado, S.O., Sanchez-Flores, A., Glover, L., Berriman, M., Hertz-Fowler, C., and Horn, D. (2011). High-throughput phenotyping using parallel sequencing of RNA interference targets in the African trypanosome. Genome Res.

Alsford, S., Wickstead, B., Ersfeld, K., and Gull, K. (2001). Diversity and dynamics of the minichromosomal karyotype in Trypanosoma brucei. Mol Biochem Parasitol *113*, 79-88.

Altschul, S.F., Gish, W., Miller, W., Myers, E.W., and Lipman, D.J. (1990). Basic local alignment search tool. J Mol Biol *215*, 403-410.

Andersen, C.L., Wandall, A., Kjeldsen, E., Mielke, C., and Koch, J. (2002). Active, but not inactive, human centromeres display topoisomerase II activity in vivo. Chromosome Res *10*, 305-312.

Ando, S., Yang, H., Nozaki, N., Okazaki, T., and Yoda, K. (2002). CENP-A, -B, and -C chromatin complex that contains the I-type alpha-satellite array constitutes the prekinetochore in HeLa cells. Mol Cell Biol *22*, 2229-2241.

Andrews, N.W., Abrams, C.K., Slatin, S.L., and Griffiths, G. (1990). A T. cruzi-secreted protein immunologically related to the complement component C9: evidence for membrane pore-forming activity at low pH. Cell *61*, 1277-1287.

Anez, N., Crisante, G., da Silva, F.M., Rojas, A., Carrasco, H., Umezawa, E.S., Stolf, A.M., Ramirez, J.L., and Teixeira, M.M. (2004). Predominance of lineage I among Trypanosoma cruzi isolates from Venezuelan patients with different clinical profiles of acute Chagas' disease. Trop Med Int Health *9*, 1319-1326.

Anlezark, G.M., Melton, R.G., Sherwood, R.F., Wilson, W.R., Denny, W.A., Palmer, B.D., Knox, R.J., Friedlos, F., and Williams, A. (1995). Bioactivation of dinitrobenzamide mustards by an E. coli B nitroreductase. Biochem Pharmacol *50*, 609-618.

Aponte, J.C., Verastegui, M., Malaga, E., Zimic, M., Quiliano, M., Vaisberg, A.J., Gilman, R.H., and Hammond, G.B. (2008). Synthesis, cytotoxicity, and anti-Trypanosoma cruzi activity of new chalcones. J Med Chem *51*, 6230-6234.

Asnis, R.E. (1957). The reduction of Furacin by cell-free extracts of Furacin-resistant and parent-susceptible strains of Escherichia coli. Arch Biochem Biophys *66*, 208-216.

Atwood, J.A., 3rd, Weatherly, D.B., Minning, T.A., Bundy, B., Cavola, C., Opperdoes, F.R., Orlando, R., and Tarleton, R.L. (2005). The Trypanosoma cruzi proteome. Science *309*, 473-476.

Aufderheide, A.C., Salo, W., Madden, M., Streitz, J., Buikstra, J., Guhl, F., Arriaza, B., Renier, C., Wittmers, L.E., Jr., Fornaciari, G., *et al.* (2004). A 9,000-year record of Chagas' disease. Proc Natl Acad Sci U S A *101*, 2034-2039.

Azogue, E., La Fuente, C., and Darras, C. (1985). Congenital Chagas' disease in Bolivia: epidemiological aspects and pathological findings. Trans R Soc Trop Med Hyg *79*, 176-180.

Azuma, Y., Arnaoutov, A., Anan, T., and Dasso, M. (2005). PIASy mediates SUMO-2 conjugation of Topoisomerase-II on mitotic chromosomes. EMBO J *24*, 2172-2182.

Bachant, J., Alcasabas, A., Blat, Y., Kleckner, N., and Elledge, S.J. (2002). The SUMO-1 isopeptidase Smt4 is linked to centromeric cohesion through SUMO-1 modification of DNA topoisomerase II. Mol Cell *9*, 1169-1182.

Bahia-Oliveira, L.M., Gomes, J.A., Cancado, J.R., Ferrari, T.C., Lemos, E.M., Luz, Z.M., Moreira, M.C., Gazzinelli, G., and Correa-Oliveira, R. (2000). Immunological and clinical evaluation of chagasic patients subjected to chemotherapy during the acute phase of Trypanosoma cruzi infection 14-30 years ago. J Infect Dis *182*, 634-638.

Baker, N., Alsford, S., and Horn, D. (2010). Genome-wide RNAi screens in African trypanosomes identify the nifurtimox activator NTR and the eflornithine transporter AAT6. Mol Biochem Parasitol *176*, 55-57.

Baldi, M.I., Benedetti, P., Mattoccia, E., and Tocchini-Valentini, G.P. (1980). In vitro catenation and decatenation of DNA and a novel eucaryotic ATP-dependent topoisomerase. Cell *20*, 461-467.

Barrett, M.P., Boykin, D.W., Brun, R., and Tidwell, R.R. (2007). Human African trypanosomiasis: pharmacological re-engagement with a neglected disease. Br J Pharmacol *152*, 1155-1171.

Barrett, M.P., Burchmore, R.J., Stich, A., Lazzari, J.O., Frasch, A.C., Cazzulo, J.J., and Krishna, S. (2003). The trypanosomiases. Lancet *362*, 1469-1480.

Bastin, P., Ellis, K., Kohl, L., and Gull, K. (2000). Flagellum ontogeny in trypanosomes studied via an inherited and regulated RNA interference system. J Cell Sci *113 (Pt 18)*, 3321-3328.

Bastin, P., Matthews, K.R., and Gull, K. (1996). The paraflagellar rod of kinetoplastida: solved and unsolved questions. Parasitol Today *12*, 302-307.

Baumann, C., Korner, R., Hofmann, K., and Nigg, E.A. (2007). PICH, a centromere-associated SNF2 family ATPase, is regulated by Plk1 and required for the spindle checkpoint. Cell *128*, 101-114.

Beckett, A.H., and Robinson, A.E. (1959). The reactions of nitrofurans with bacteria. II. Reduction of a series of antibacterial nitrofurans by Aerobacter aerogenes. J Med Pharm Chem *1*, 135-154.

Benne, R., Van den Burg, J., Brakenhoff, J.P., Sloof, P., Van Boom, J.H., and Tromp, M.C. (1986). Major transcript of the frameshifted coxII gene from trypanosome mitochondria contains four nucleotides that are not encoded in the DNA. Cell *46*, 819-826.

Benson, G. (1999). Tandem repeats finder: a program to analyze DNA sequences. Nucleic Acids Res *27*, 573-580.

Bern, C., and Montgomery, S.P. (2009). An estimate of the burden of Chagas disease in the United States. Clin Infect Dis *49*, e52-54.

Bernstein, R.E. (1984). Darwin's illness: Chagas' disease resurgens. J R Soc Med *77*, 608-609.

Berriman, M., Ghedin, E., Hertz-Fowler, C., Blandin, G., Renauld, H., Bartholomeu, D.C., Lennard, N.J., Caler, E., Hamlin, N.E., Haas, B., *et al.* (2005). The genome of the African trypanosome Trypanosoma brucei. Science *309*, 416-422.

Berriman, M., and Rutherford, K. (2003). Viewing and annotating sequence data with Artemis. Brief Bioinform *4*, 124-132.

Bettiol, E., Samanovic, M., Murkin, A.S., Raper, J., Buckner, F., and Rodriguez, A. (2009). Identification of three classes of heteroaromatic compounds with activity against intracellular Trypanosoma cruzi by chemical library screening. PLoS Negl Trop Dis *3*, e384.

Bloom, K., and Yeh, E. (2010). Tension management in the kinetochore. Curr Biol *20*, R1040-1048.

Bloom, K.S., and Carbon, J. (1982). Yeast centromere DNA is in a unique and highly ordered structure in chromosomes and small circular minichromosomes. Cell *29*, 305-317.

Blumenstiel, K., Schoneck, R., Yardley, V., Croft, S.L., and Krauth-Siegel, R.L. (1999). Nitrofuran drugs as common subversive substrates of Trypanosoma cruzi lipoamide dehydrogenase and trypanothione reductase. Biochem Pharmacol *58*, 1791-1799.

Bock, M., Gonnert, R., and Haberkorn, A. (1969). Studies with Bay 2502 on animals. Bol Chil Parasitol *24*, 13-19.

Boiani, M., Piacenza, L., Hernandez, P., Boiani, L., Cerecetto, H., Gonzalez, M., and Denicola, A. (2010). Mode of action of nifurtimox and N-oxide-containing heterocycles against Trypanosoma cruzi: is oxidative stress involved? Biochem Pharmacol *79*, 1736-1745.

Bojanowski, K., Filhol, O., Cochet, C., Chambaz, E.M., and Larsen, A.K. (1993). DNA topoisomerase II and casein kinase II associate in a molecular complex that is catalytically active. J Biol Chem *268*, 22920-22926.

Boland, M.P., Knox, R.J., and Roberts, J.J. (1991). The differences in kinetics of rat and human DT diaphorase result in a differential sensitivity of derived cell lines to CB 1954 (5-(aziridin-1-yl)-2,4-dinitrobenzamide). Biochem Pharmacol *41*, 867-875.

Borch, R.F., and Millard, J.A. (1987). The mechanism of activation of 4-hydroxycyclophosphamide. J Med Chem *30*, 427-431.

Borgnetto, M.E., Tinelli, S., Carminati, L., and Capranico, G. (1999). Genomic sites of topoisomerase II activity determined by comparing DNA breakage enhanced by three distinct poisons. J Mol Biol *285*, 545-554.

Bornens, M. (2002). Centrosome composition and microtubule anchoring mechanisms. Curr Opin Cell Biol *14*, 25-34.

Bosl, W.J., and Li, R. (2005). Mitotic-exit control as an evolved complex system. Cell *121*, 325-333.

Bot, C., Hall, B.S., Bashir, N., Taylor, M.C., Helsby, N.A., and Wilkinson, S.R. (2010). Trypanocidal activity of aziridinyl nitrobenzamide prodrugs. Antimicrob Agents Chemother *54*, 4246-4252.

Boveris, A., Sies, H., Martino, E.E., Docampo, R., Turrens, J.F., and Stoppani, A.O. (1980). Deficient metabolic utilization of hydrogen peroxide in Trypanosoma cruzi. Biochem J *188*, 643-648.

Bressi, J.C., Verlinde, C.L., Aronov, A.M., Shaw, M.L., Shin, S.S., Nguyen, L.N., Suresh, S., Buckner, F.S., Van Voorhis, W.C., Kuntz, I.D., *et al.* (2001). Adenosine analogues as selective inhibitors of glyceraldehyde-3-phosphate dehydrogenase of Trypanosomatidae via structure-based drug design. J Med Chem *44*, 2080-2093.

Brooks, C.F., Francia, M.E., Gissot, M., Croken, M.M., Kim, K., and Striepen, B. (2011). Toxoplasma gondii sequesters centromeres to a specific nuclear region throughout the cell cycle. Proc Natl Acad Sci U S A *108*, 3767-3772.

Brun, R., Blum, J., Chappuis, F., and Burri, C. (2010). Human African trypanosomiasis. Lancet *375*, 148-159.

Brun, R., and Schonenberger (1979). Cultivation and in vitro cloning or procyclic culture forms of Trypanosoma brucei in a semi-defined medium. Short communication. Acta Trop *36*, 289-292.

Bryant, C., and DeLuca, M. (1991). Purification and characterization of an oxygen-insensitive NAD(P)H nitroreductase from Enterobacter cloacae. J Biol Chem *266*, 4119-4125.

Buchwitz, B.J., Ahmad, K., Moore, L.L., Roth, M.B., and Henikoff, S. (1999). A histone-H3-like protein in C. elegans. Nature *401*, 547-548.

Buckner, F., Yokoyama, K., Lockman, J., Aikenhead, K., Ohkanda, J., Sadilek, M., Sebti, S., Van Voorhis, W., Hamilton, A., and Gelb, M.H. (2003). A class of sterol 14-demethylase inhibitors as anti-Trypanosoma cruzi agents. Proc Natl Acad Sci U S A *100*, 15149-15153.

Buckner, F.S., Verlinde, C.L., La Flamme, A.C., and Van Voorhis, W.C. (1996). Efficient technique for screening drugs for activity against Trypanosoma cruzi using parasites expressing beta-galactosidase. Antimicrob Agents Chemother *40*, 2592-2597.

Burri, C., and Brun, R. (2003). Eflornithine for the treatment of human African trypanosomiasis. Parasitol Res *90 Supp 1*, S49-52.

Buschini, A., Ferrarini, L., Franzoni, S., Galati, S., Lazzaretti, M., Mussi, F., Northfleet de Albuquerque, C., Maria Araujo Domingues Zucchi, T., and Poli, P. (2009). Genotoxicity revaluation of three commercial nitroheterocyclic drugs: nifurtimox, benznidazole, and metronidazole. J Parasitol Res *2009*, 463575.

Buttrick, G.J., and Millar, J.B. (2011). Ringing the changes: emerging roles for DASH at the kinetochore-microtubule Interface. Chromosome Res *19*, 393-407.

Cabrera, E., Murguiondo, M.G., Arias, M.G., Arredondo, C., Pintos, C., Aguirre, G., Fernandez, M., Basmadjian, Y., Rosa, R., Pacheco, J.P., *et al.* (2009). 5-Nitro-2-furyl derivative actives against Trypanosoma cruzi: preliminary in vivo studies. Eur J Med Chem *44*, 3909-3914.

Callejas, S., Leech, V., Reitter, C., and Melville, S. (2006). Hemizygous subtelomeres of an African trypanosome chromosome may account for over 75% of chromosome length. Genome Res *16*, 1109-1118.

Canavaci, A.M., Bustamante, J.M., Padilla, A.M., Perez Brandan, C.M., Simpson, L.J., Xu, D., Boehlke, C.L., and Tarleton, R.L. (2010). In vitro and in vivo high-throughput assays for the testing of anti-Trypanosoma cruzi compounds. PLoS Negl Trop Dis *4*, e740.

Cancado, J.R. (2002). Long term evaluation of etiological treatment of chagas disease with benznidazole. Rev Inst Med Trop Sao Paulo *44*, 29-37.

Cardenas, M.E., Dang, Q., Glover, C.V., and Gasser, S.M. (1992). Casein kinase II phosphorylates the eukaryote-specific C-terminal domain of topoisomerase II in vivo. EMBO J *11*, 1785-1796.

Caron, P.R., Watt, P., and Wang, J.C. (1994). The C-terminal domain of Saccharomyces cerevisiae DNA topoisomerase II. Mol Cell Biol *14*, 3197-3207.

Carter, N.S., and Fairlamb, A.H. (1993). Arsenical-resistant trypanosomes lack an unusual adenosine transporter. Nature *361*, 173-176.

Casagrande, L., Ruiz, J.C., Beverley, S.M., and Cruz, A.K. (2005). Identification of a DNA fragment that increases mitotic stability of episomal linear DNAs in Leishmania major. Int J Parasitol *35*, 973-980.

Chagas, C. (1909). Nova tripanozomiaze humana: estudos sobre a morfolojia e o ciclo evolutivo do Schizotrypanum cruzi n. gen., n. sp., ajente etiolojico de nova entidade morbida do homem. Memórias do Instituto Oswaldo Cruz *1*, 159-218.

Champoux, J.J. (2001). DNA topoisomerases: structure, function, and mechanism. Annu Rev Biochem *70*, 369-413.

Chan, G.K., Liu, S.T., and Yen, T.J. (2005). Kinetochore structure and function. Trends Cell Biol *15*, 589-598.

Checchi, F., Filipe, J.A., Haydon, D.T., Chandramohan, D., and Chappuis, F. (2008). Estimates of the duration of the early and late stage of gambiense sleeping sickness. BMC Infect Dis *8*, 16.

Cheeseman, I.M., and Desai, A. (2008). Molecular architecture of the kinetochore-microtubule interface. Nat Rev Mol Cell Biol *9*, 33-46.

Chen, G.L., Yang, L., Rowe, T.C., Halligan, B.D., Tewey, K.M., and Liu, L.F. (1984). Nonintercalative antitumor drugs interfere with the breakage-reunion reaction of mammalian DNA topoisomerase II. J Biol Chem *259*, 13560-13566.

Chen, Y., Hung, C.H., Burderer, T., and Lee, G.S. (2003). Development of RNA interference revertants in Trypanosoma brucei cell lines generated with a double stranded RNA expression construct driven by two opposing promoters. Mol Biochem Parasitol *126*, 275-279.

Cheng, Z., Dong, F., Langdon, T., Ouyang, S., Buell, C.R., Gu, M., Blattner, F.R., and Jiang, J. (2002). Functional rice centromeres are marked by a satellite repeat and a centromere-specific retrotransposon. Plant Cell *14*, 1691-1704.

Chikashige, Y., Kinoshita, N., Nakaseko, Y., Matsumoto, T., Murakami, S., Niwa, O., and Yanagida, M. (1989). Composite motifs and repeat symmetry in S. pombe centromeres: direct analysis by integration of NotI restriction sites. Cell *57*, 739-751.

Choo, K.H. (2001). Domain organization at the centromere and neocentromere. Dev Cell *1*, 165-177.

Ciosk, R., Zachariae, W., Michaelis, C., Shevchenko, A., Mann, M., and Nasmyth, K. (1998). An ESP1/PDS1 complex regulates loss of sister chromatid cohesion at the metaphase to anaphase transition in yeast. Cell *93*, 1067-1076.

Claes, F., Vodnala, S.K., van Reet, N., Boucher, N., Lunden-Miguel, H., Baltz, T., Goddeeris, B.M., Buscher, P., and Rottenberg, M.E. (2009). Bioluminescent imaging of Trypanosoma brucei shows preferential testis dissemination which may hamper drug efficacy in sleeping sickness. PLoS Negl Trop Dis *3*, e486.

Clarke, L., and Carbon, J. (1980). Isolation of a yeast centromere and construction of functional small circular chromosomes. Nature *287*, 504-509.

Clayton, C.E. (2002). Life without transcriptional control? From fly to man and back again. EMBO J *21*, 1881-1888.

Cobb, L.M. (1970). Toxicity of the selective antitumor agent 5-aziridino-2,4-dinitrobenzamide in the rat. Toxicol Appl Pharmacol *17*, 231-238.

Coelho, P.A., Queiroz-Machado, J., Carmo, A.M., Moutinho-Pereira, S., Maiato, H., and Sunkel, C.E. (2008). Dual role of topoisomerase II in centromere resolution and aurora B activity. PLoS Biol *6*, e207.

Copenhaver, G.P., Nickel, K., Kuromori, T., Benito, M.I., Kaul, S., Lin, X., Bevan, M., Murphy, G., Harris, B., Parnell, L.D., *et al.* (1999). Genetic definition and sequence analysis of Arabidopsis centromeres. Science *286*, 2468-2474.

Coppens, I., Opperdoes, F.R., Courtoy, P.J., and Baudhuin, P. (1987). Receptor-mediated endocytosis in the bloodstream form of Trypanosoma brucei. J Protozool *34*, 465-473.

Corte, E.D., and Stirpe, F. (1972). The regulation of rat liver xanthine oxidase. Involvement of thiol groups in the conversion of the enzyme activity from dehydrogenase (type D) into oxidase (type O) and purification of the enzyme. Biochem J *126*, 739-745.

Cottarel, G., Shero, J.H., Hieter, P., and Hegemann, J.H. (1989). A 125-base-pair CEN6 DNA fragment is sufficient for complete meiotic and mitotic centromere functions in Saccharomyces cerevisiae. Mol Cell Biol *9*, 3342-3349.

Crenshaw, D.G., and Hsieh, T. (1993). Function of the hydrophilic carboxyl terminus of type II DNA topoisomerase from Drosophila melanogaster. I. In vitro studies. J Biol Chem *268*, 21328-21334.

Cross, G.A. (1975). Identification, purification and properties of clone-specific glycoprotein antigens constituting the surface coat of Trypanosoma brucei. Parasitology *71*, 393-417.

Cross, M., Kieft, R., Sabatini, R., Dirks-Mulder, A., Chaves, I., and Borst, P. (2002). J-binding protein increases the level and retention of the unusual base J in trypanosome DNA. Mol Microbiol *46*, 37-47.

D'Ambrosio, C., Schmidt, C.K., Katou, Y., Kelly, G., Itoh, T., Shirahige, K., and Uhlmann, F. (2008). Identification of cis-acting sites for condensin loading onto budding yeast chromosomes. Genes Dev *22*, 2215-2227.

Dachs, G.U., Tupper, J., and Tozer, G.M. (2005). From bench to bedside for gene-directed enzyme prodrug therapy of cancer. Anticancer Drugs *16*, 349-359.

Darkin, S., McQuillan, J., and Ralph, R.K. (1984). Chlorpromazine: a potential anticancer agent? Biochem Biophys Res Commun *125*, 184-191.

DaRocha, W.D., Otsu, K., Teixeira, S.M., and Donelson, J.E. (2004). Tests of cytoplasmic RNA interference (RNAi) and construction of a tetracycline-inducible T7 promoter system in Trypanosoma cruzi. Mol Biochem Parasitol *133*, 175-186.

Darwiche, N., Freeman, L.A., and Strunnikov, A. (1999). Characterization of the components of the putative mammalian sister chromatid cohesion complex. Gene *233*, 39-47.

Das, A., Dasgupta, A., Sengupta, T., and Majumder, H.K. (2004). Topoisomerases of kinetoplastid parasites as potential chemotherapeutic targets. Trends Parasitol *20*, 381-387.

Daum, J.R., and Gorbsky, G.J. (1998). Casein kinase II catalyzes a mitotic phosphorylation on threonine 1342 of human DNA topoisomerase IIalpha, which is recognized by the 3F3/2 phosphoepitope antibody. J Biol Chem *273*, 30622-30629.

Dawlaty, M.M., Malureanu, L., Jeganathan, K.B., Kao, E., Sustmann, C., Tahk, S., Shuai, K., Grosschedl, R., and van Deursen, J.M. (2008). Resolution of sister centromeres requires RanBP2-mediated SUMOylation of topoisomerase IIalpha. Cell *133*, 103-115.

De Conti, R., Oliveira, D.A., Fernandes, A.M.A.P., Melo, P.S., Rodriguez, J.A., Haun, M., De Castro, S.L., Souza-Brito, A.R.M., Duran, N. (1998). Application of a multi-endpoint cytotoxicity assay to the trypanocidal compounds 2-propen-1-amine derivatives and determination of their acute toxicity. In Vitro & Molecular Toxicology *11*, 153-160.

De Souza, C.P., and Osmani, S.A. (2007). Mitosis, not just open or closed. Eukaryot Cell *6*, 1521-1527.

de Souza, W., Attias, M., and Rodrigues, J.C. (2009). Particularities of mitochondrial structure in parasitic protists (Apicomplexa and Kinetoplastida). Int J Biochem Cell Biol *41*, 2069-2080.

de Souza, W., de Carvalho, T.M., and Barrias, E.S. (2010). Review on Trypanosoma cruzi: Host Cell Interaction. Int J Cell Biol *2010*.

Dejardin, J., and Kingston, R.E. (2009). Purification of proteins associated with specific genomic Loci. Cell *136*, 175-186.

Delgado, S., Castillo Neyra, R., Quispe Machaca, V.R., Ancca Juarez, J., Chou Chu, L., Verastegui, M.R., Moscoso Apaza, G.M., Bocangel, C.D., Tustin, A.W., Sterling, C.R., *et al.* (2011). A history of chagas disease transmission, control, and re-emergence in peri-rural La Joya, Peru. PLoS Negl Trop Dis *5*, e970.

Denny, W.A. (2003). Prodrugs for Gene-Directed Enzyme-Prodrug Therapy (Suicide Gene Therapy). J Biomed Biotechnol *2003*, 48-70.

Desjeux, P. (1996). Leishmaniasis. Public health aspects and control. Clin Dermatol *14*, 417-423.

Di Noia, J.M., Buscaglia, C.A., De Marchi, C.R., Almeida, I.C., and Frasch, A.C. (2002). A Trypanosoma cruzi small surface molecule provides the first immunological evidence that Chagas' disease is due to a single parasite lineage. J Exp Med *195*, 401-413.

Di Noia, J.M., Sanchez, D.O., and Frasch, A.C. (1995). The protozoan Trypanosoma cruzi has a family of genes resembling the mucin genes of mammalian cells. J Biol Chem *270*, 24146-24149.

Dias, J.C.P., Brener, S (1984). Chagas Disease and Blood Transfusion. Mem Inst Oswaldo Cruz *79*, 139-147.

Docampo, R., Moreno, S.N., and Stoppani, A.O. (1981a). Nitrofuran enhancement of microsomal electron transport, superoxide anion production and lipid peroxidation. Arch Biochem Biophys *207*, 316-324.

Docampo, R., Moreno, S.N., Stoppani, A.O., Leon, W., Cruz, F.S., Villalta, F., and Muniz, R.F. (1981b). Mechanism of nifurtimox toxicity in different forms of Trypanosoma cruzi. Biochem Pharmacol *30*, 1947-1951.

Docampo, R., and Stoppani, A.O. (1979). Generation of superoxide anion and hydrogen peroxide induced by nifurtimox in Trypanosoma cruzi. Arch Biochem Biophys *197*, 317-321.

Dodd, M.C. (1946). The chemotherapeutic properties of 5-nitro-2-furaldehyde semicarbazone (furacin). J Pharmacol Exp Ther *86*, 311-323.

Dodd, M.C., Stillman, W. B., Roys, M., Crosby, C. (1944). The in vitro bacteriostatic action of some simple furan derivatives. The journal of pharmacology and experimental therapeutics *82*.

Douzery, E.J., Snell, E.A., Bapteste, E., Delsuc, F., and Philippe, H. (2004). The timing of eukaryotic evolution: does a relaxed molecular clock reconcile proteins and fossils? Proc Natl Acad Sci U S A *101*, 15386-15391.

Drabek, D., Guy, J., Craig, R., and Grosveld, F. (1997). The expression of bacterial nitroreductase in transgenic mice results in specific cell killing by the prodrug CB1954. Gene Ther *4*, 93-100.

Dubessay, P., Ravel, C., Bastien, P., Crobu, L., Dedet, J.P., Pages, M., and Blaineau, C. (2002a). The switch region on Leishmania major chromosome 1 is not required for mitotic stability or gene expression, but appears to be essential. Nucleic Acids Res *30*, 3692-3697.

Dubessay, P., Ravel, C., Bastien, P., Lignon, M.F., Ullman, B., Pages, M., and Blaineau, C. (2001). Effect of large targeted deletions on the mitotic stability of an extra chromosome mediating drug resistance in Leishmania. Nucleic Acids Res *29*, 3231-3240.

Dubessay, P., Ravel, C., Bastien, P., Stuart, K., Dedet, J.P., Blaineau, C., and Pages, M. (2002b). Mitotic stability of a coding DNA sequence-free version of Leishmania major chromosome 1 generated by targeted chromosome fragmentation. Gene *289*, 151-159.

Dynek, J.N., and Smith, S. (2004). Resolution of sister telomere association is required for progression through mitosis. Science *304*, 97-100.

El-Helw, L.M., and Hancock, B.W. (2007). Treatment of metastatic gestational trophoblastic neoplasia. Lancet Oncol *8*, 715-724.

El-Sayed, N.M., Myler, P.J., Bartholomeu, D.C., Nilsson, D., Aggarwal, G., Tran, A.N., Ghedin, E., Worthey, E.A., Delcher, A.L., Blandin, G., *et al.* (2005a). The genome sequence of Trypanosoma cruzi, etiologic agent of Chagas disease. Science *309*, 409-415.

El-Sayed, N.M., Myler, P.J., Blandin, G., Berriman, M., Crabtree, J., Aggarwal, G., Caler, E., Renauld, H., Worthey, E.A., Hertz-Fowler, C., *et al.* (2005b). Comparative genomics of trypanosomatid parasitic protozoa. Science *309*, 404-409.

Ersfeld, K., and Gull, K. (1997). Partitioning of large and minichromosomes in Trypanosoma brucei. Science *276*, 611-614.

Escargueil, A.E., Plisov, S.Y., Filhol, O., Cochet, C., and Larsen, A.K. (2000). Mitotic phosphorylation of DNA topoisomerase II alpha by protein kinase CK2 creates the MPM-2 phosphoepitope on Ser-1469. J Biol Chem *275*, 34710-34718.

Evens, F., Niemegeers, K., and Packchanian, A. (1957). Nitrofurazone therapy of Trypanosoma gambiense sleeping sickness in man. Am J Trop Med Hyg *6*, 665-678.

Fenn, K., and Matthews, K.R. (2007). The cell biology of Trypanosoma brucei differentiation. Curr Opin Microbiol *10*, 539-546.

Ferreira, R.C., Schwarz, U., and Ferreira, L.C. (1988). Activation of anti-Trypanosoma cruzi drugs to genotoxic metabolites promoted by mammalian microsomal enzymes. Mutat Res *204*, 577-583.

Field, M.C., and Carrington, M. (2009). The trypanosome flagellar pocket. Nat Rev Microbiol *7*, 775-786.

Fishel, B., Amstutz, H., Baum, M., Carbon, J., and Clarke, L. (1988). Structural organization and functional analysis of centromeric DNA in the fission yeast Schizosaccharomyces pombe. Mol Cell Biol *8*, 754-763.

Fitzgerald-Hayes, M., Clarke, L., and Carbon, J. (1982). Nucleotide sequence comparisons and functional analysis of yeast centromere DNAs. Cell *29*, 235-244.

Floeter-Winter, L.M., Souto, R.P., Stolf, B.S., Zingales, B., and Buck, G.A. (1997). Trypanosoma cruzi: can activity of the rRNA gene promoter be used as a marker for speciation? Exp Parasitol *86*, 232-234.

Floridia, G., Zatterale, A., Zuffardi, O., and Tyler-Smith, C. (2000). Mapping of a human centromere onto the DNA by topoisomerase II cleavage. EMBO Rep *1*, 489-493.

Fragoso, S.P., Mattei, D., Hines, J.C., Ray, D., and Goldenberg, S. (1998). Expression and cellular localization of Trypanosoma cruzi type II DNA topoisomerase. Mol Biochem Parasitol *94*, 197-204.

Franzen, O., Ochaya, S., Sherwood, E., Lewis, M.D., Llewellyn, M.S., Miles, M.A., and Andersson, B. (2011). Shotgun sequencing analysis of Trypanosoma cruzi I Sylvio X10/1 and comparison with T. cruzi VI CL Brener. PLoS Negl Trop Dis *5*, e984.

Freitas, J.M., Lages-Silva, E., Crema, E., Pena, S.D., and Macedo, A.M. (2005). Real time PCR strategy for the identification of major lineages of Trypanosoma cruzi directly in chronically infected human tissues. Int J Parasitol *35*, 411-417.

Funabiki, H., Yamano, H., Kumada, K., Nagao, K., Hunt, T., and Yanagida, M. (1996). Cut2 proteolysis required for sister-chromatid seperation in fission yeast. Nature *381*, 438-441.

Gajewska, J., Szczypka, M., Tudek, B., and Szymczyk, T. (1990). Studies on the effect of ascorbic acid and selenium on the genotoxicity of nitrofurans: nitrofurazone and furazolidone. Mutat Res *232*, 191-197.

Galanti, N., Galindo, M., Sabaj, V., Espinoza, I., and Toro, G.C. (1998). Histone genes in trypanosomatids. Parasitol Today *14*, 64-70.

Gaunt, M.W., Yeo, M., Frame, I.A., Stothard, J.R., Carrasco, H.J., Taylor, M.C., Mena, S.S., Veazey, P., Miles, G.A., Acosta, N., *et al.* (2003). Mechanism of genetic exchange in American trypanosomes. Nature *421*, 936-939.

Gavin, J.J., Ebetino, F.F., Freedman, R., and Waterbury, W.E. (1966). The aerobic degradation of 1-(5-nitrofurfurylideneamino)-2-imidazolidinone (NF-246) by Escherichia coli. Arch Biochem Biophys *113*, 399-404.

Gellert, M., Mizuuchi, K., O'Dea, M.H., and Nash, H.A. (1976). DNA gyrase: an enzyme that introduces superhelical turns into DNA. Proc Natl Acad Sci U S A *73*, 3872-3876.

Gerpe, A., Alvarez, G., Benitez, D., Boiani, L., Quiroga, M., Hernandez, P., Sortino, M., Zacchino, S., Gonzalez, M., and Cerecetto, H. (2009). 5-Nitrofuranes and 5-nitrothiophenes with anti-Trypanosoma cruzi activity and ability to accumulate squalene. Bioorg Med Chem *17*, 7500-7509.

Gerpe, A., Odreman-Nunez, I., Draper, P., Boiani, L., Urbina, J.A., Gonzalez, M., and Cerecetto, H. (2008). Heteroallyl-containing 5-nitrofuranes as new anti-Trypanosoma cruzi agents with a dual mechanism of action. Bioorg Med Chem *16*, 569-577.

Gluenz, E., Sharma, R., Carrington, M., and Gull, K. (2008). Functional characterization of cohesin subunit SCC1 in Trypanosoma brucei and dissection of mutant phenotypes in two life cycle stages. Mol Microbiol *69*, 666-680.

Gomes, Y.M., Lorena, V.M., and Luquetti, A.O. (2009). Diagnosis of Chagas disease: what has been achieved? What remains to be done with regard to diagnosis and follow up studies? Mem Inst Oswaldo Cruz *104 Suppl 1*, 115-121.

Green, D.E. (1934). Studies of reversible dehydrogenase systems: The reversibility of the xanthine oxidase system. Biochem J *28*, 1550-1560.

Grozav, A.G., Chikamori, K., Kozuki, T., Grabowski, D.R., Bukowski, R.M., Willard, B., Kinter, M., Andersen, A.H., Ganapathi, R., and Ganapathi, M.K. (2009). Casein kinase I delta/epsilon phosphorylates topoisomerase IIalpha at serine-1106 and modulates DNA cleavage activity. Nucleic Acids Res *37*, 382-392.

Grunberg, E., and Titsworth, E.H. (1973). Chemotherapeutic properties of heterocyclic compounds: monocyclic compounds with five-membered rings. Annu Rev Microbiol *27*, 317-346.

Gull, K., Alsford, S., and Ersfeld, K. (1998). Segregation of minichromosomes in trypanosomes: implications for mitotic mechanisms. Trends Microbiol *6*, 319-323.

Haering, C.H., Farcas, A.M., Arumugam, P., Metson, J., and Nasmyth, K. (2008). The cohesin ring concatenates sister DNA molecules. Nature *454*, 297-301.

Haering, C.H., and Nasmyth, K. (2003). Building and breaking bridges between sister chromatids. Bioessays *25*, 1178-1191.

Hager, K.M., and Hajduk, S.L. (1997). Mechanism of resistance of African trypanosomes to cytotoxic human HDL. Nature *385*, 823-826.

Hall, B.S., Bot, C., and Wilkinson, S.R. (2011). Nifurtimox activation by trypanosomal type I nitroreductases generates cytotoxic nitrile metabolites. J Biol Chem.

Hall, B.S., Wu, X., Hu, L., and Wilkinson, S.R. (2010). Exploiting the drug-activating properties of a novel trypanosomal nitroreductase. Antimicrob Agents Chemother *54*, 1193-1199.

Hall, N., Berriman, M., Lennard, N.J., Harris, B.R., Hertz-Fowler, C., Bart-Delabesse, E.N., Gerrard, C.S., Atkin, R.J., Barron, A.J., Bowman, S., *et al.* (2003). The DNA sequence of chromosome I of an African trypanosome: gene content, chromosome organisation, recombination and polymorphism. Nucleic Acids Res *31*, 4864-4873.

Hammarton, T.C. (2007). Cell cycle regulation in Trypanosoma brucei. Mol Biochem Parasitol *153*, 1-8.

Hammarton, T.C., Clark, J., Douglas, F., Boshart, M., and Mottram, J.C. (2003). Stage-specific differences in cell cycle control in Trypanosoma brucei revealed by RNA interference of a mitotic cyclin. J Biol Chem *278*, 22877-22886.

Hande, K.R. (1998). Etoposide: four decades of development of a topoisomerase II inhibitor. Eur J Cancer *34*, 1514-1521.

Handman, E. (2001). Leishmaniasis: current status of vaccine development. Clin Microbiol Rev *14*, 229-243.

Haupt, W., Fischer, T.C., Winderl, S., Fransz, P., and Torres-Ruiz, R.A. (2001). The centromere1 (CEN1) region of Arabidopsis thaliana: architecture and functional impact of chromatin. Plant J *27*, 285-296.

Heller, R., Brown, K.E., Burgtorf, C., and Brown, W.R. (1996). Mini-chromosomes derived from the human Y chromosome by telomere directed chromosome breakage. Proc Natl Acad Sci U S A *93*, 7125-7130.

Helsby, N.A., Atwell, G.J., Yang, S., Palmer, B.D., Anderson, R.F., Pullen, S.M., Ferry, D.M., Hogg, A., Wilson, W.R., and Denny, W.A. (2004a). Aziridinyldinitrobenzamides: synthesis and structure-activity relationships for activation by E. coli nitroreductase. J Med Chem *47*, 3295-3307.

Helsby, N.A., Ferry, D.M., Patterson, A.V., Pullen, S.M., and Wilson, W.R. (2004b). 2-Amino metabolites are key mediators of CB 1954 and SN 23862 bystander effects in nitroreductase GDEPT. Br J Cancer *90*, 1084-1092.

Helsby, N.A., Wheeler, S.J., Pruijn, F.B., Palmer, B.D., Yang, S., Denny, W.A., and Wilson, W.R. (2003). Effect of nitroreduction on the alkylating reactivity and cytotoxicity of the 2,4-dinitrobenzamide-5-aziridine CB 1954 and the corresponding nitrogen mustard SN 23862: distinct mechanisms of bioreductive activation. Chem Res Toxicol *16*, 469-478.

Hemmerich, P., Weidtkamp-Peters, S., Hoischen, C., Schmiedeberg, L., Erliandri, I., and Diekmann, S. (2008). Dynamics of inner kinetochore assembly and maintenance in living cells. J Cell Biol *180*, 1101-1114.

Henderson, G.B., Ulrich, P., Fairlamb, A.H., Rosenberg, I., Pereira, M., Sela, M., and Cerami, A. (1988). "Subversive" substrates for the enzyme trypanothione disulfide reductase: alternative approach to chemotherapy of Chagas disease. Proc Natl Acad Sci U S A *85*, 5374-5378.

Hendriks, E., van Deursen, F.J., Wilson, J., Sarkar, M., Timms, M., and Matthews, K.R. (2000). Life-cycle differentiation in Trypanosoma brucei: molecules and mutants. Biochem Soc Trans *28*, 531-536.

Henikoff, S., Ahmad, K., Platero, J.S., and van Steensel, B. (2000). Heterochromatic deposition of centromeric histone H3-like proteins. Proc Natl Acad Sci U S A *97*, 716-721.

Hertz-Fowler, C., Figueiredo, L.M., Quail, M.A., Becker, M., Jackson, A., Bason, N., Brooks, K., Churcher, C., Fahkro, S., Goodhead, I., *et al.* (2008). Telomeric expression sites are highly conserved in Trypanosoma brucei. PLoS One *3*, e3527.

Hertz-Fowler, C., Peacock, C.S., Wood, V., Aslett, M., Kerhornou, A., Mooney, P., Tivey, A., Berriman, M., Hall, N., Rutherford, K., *et al.* (2004). GeneDB: a resource for prokaryotic and eukaryotic organisms. Nucleic Acids Res *32*, D339-343.

Herwaldt, B.L. (1999). Leishmaniasis. Lancet *354*, 1191-1199.

Hiraku, Y., Sekine, A., Nabeshi, H., Midorikawa, K., Murata, M., Kumagai, Y., and Kawanishi, S. (2004). Mechanism of carcinogenesis induced by a veterinary antimicrobial drug, nitrofurazone, via oxidative DNA damage and cell proliferation. Cancer Lett *215*, 141-150.

Hirumi, H., and Hirumi, K. (1989). Continuous cultivation of Trypanosoma brucei blood stream forms in a medium containing a low concentration of serum protein without feeder cell layers. J Parasitol *75*, 985-989.

Horowitz, D.S., and Wang, J.C. (1987). Mapping the active site tyrosine of Escherichia coli DNA gyrase. J Biol Chem *262*, 5339-5344.

Hoyt, M.A., Totis, L., and Roberts, B.T. (1991). S. cerevisiae genes required for cell cycle arrest in response to loss of microtubule function. Cell *66*, 507-517.

Hu, L., Wu, X., Han, J., Chen, L., Vass, S.O., Browne, P., Hall, B.S., Bot, C., Gobalakrishnapillai, V., Searle, P.F., *et al.* (2011). Synthesis and structure-activity relationships of nitrobenzyl phosphoramide mustards as nitroreductase-activated prodrugs. Bioorg Med Chem Lett *21*, 3986-3991.

Hu, L., Yu, C., Jiang, Y., Han, J., Li, Z., Browne, P., Race, P.R., Knox, R.J., Searle, P.F., and Hyde, E.I. (2003). Nitroaryl phosphoramides as novel prodrugs for E. coli nitroreductase activation in enzyme prodrug therapy. J Med Chem *46*, 4818-4821.

Hudson, D.F., Fowler, K.J., Earle, E., Saffery, R., Kalitsis, P., Trowell, H., Hill, J., Wreford, N.G., de Kretser, D.M., Cancilla, M.R., *et al.* (1998). Centromere protein B null mice are mitotically and meiotically normal but have lower body and testis weights. J Cell Biol *141*, 309-319.

Hudson, D.F., Marshall, K.M., and Earnshaw, W.C. (2009). Condensin: Architect of mitotic chromosomes. Chromosome Res *17*, 131-144.

Hwang, L.H., Lau, L.F., Smith, D.L., Mistrot, C.A., Hardwick, K.G., Hwang, E.S., Amon, A., and Murray, A.W. (1998). Budding yeast Cdc20: a target of the spindle checkpoint. Science *279*, 1041-1044.

Iatropoulos, M.J., Wang, C.X., von Keutz, E., and Williams, G.M. (2006). Assessment of chronic toxicity and carcinogenicity in an accelerated cancer bioassay in rats of Nifurtimox, an antitrypanosomiasis drug. Exp Toxicol Pathol *57*, 397-404.

Ivens, A.C., Lewis, S.M., Bagherzadeh, A., Zhang, L., Chan, H.M., and Smith, D.F. (1998). A physical map of the Leishmania major Friedlin genome. Genome Res *8*, 135-145.

Ivens, A.C., Peacock, C.S., Worthey, E.A., Murphy, L., Aggarwal, G., Berriman, M., Sisk, E., Rajandream, M.A., Adlem, E., Aert, R., *et al.* (2005). The genome of the kinetoplastid parasite, Leishmania major. Science *309*, 436-442.

Iyanagi, T., and Mason, H.S. (1973). Some properties of hepatic reduced nicotinamide adenine dinucleotide phosphate-cytochrome c reductase. Biochemistry *12*, 2297-2308.

Jackson, Y., Alirol, E., Getaz, L., Wolff, H., Combescure, C., and Chappuis, F. (2010). Tolerance and safety of nifurtimox in patients with chronic chagas disease. Clin Infect Dis *51*, e69-75.

Jacobs, W.R., Jr., Barletta, R.G., Udani, R., Chan, J., Kalkut, G., Sosne, G., Kieser, T., Sarkis, G.J., Hatfull, G.F., and Bloom, B.R. (1993). Rapid assessment of drug susceptibilities of Mycobacterium tuberculosis by means of luciferase reporter phages. Science *260*, 819-822.

Jallepalli, P.V., and Lengauer, C. (2001). Chromosome segregation and cancer: cutting through the mystery. Nat Rev Cancer *1*, 109-117.

Jennings, F.W., and Urquhart, G.M. (1983). The use of the 2 substituted 5-nitroimidazole, Fexinidazole (Hoe 239) in the treatment of chronic T. brucei infections in mice. Z Parasitenkd *69*, 577-581.

Jiang, Y., Han, J., Yu, C., Vass, S.O., Searle, P.F., Browne, P., Knox, R.J., and Hu, L. (2006). Design, synthesis, and biological evaluation of cyclic and acyclic nitrobenzylphosphoramide mustards for E. coli nitroreductase activation. J Med Chem *49*, 4333-4343.

Jiang, Y., and Hu, L. (2008). N-(2,2-Dimethyl-2-(2-nitrophenyl)acetyl)-4-aminocyclophosphamide as a potential bioreductively activated prodrug of phosphoramide mustard. Bioorg Med Chem Lett *18*, 4059-4063.

Kallio, M., and Lahdetie, J. (1996). Fragmentation of centromeric DNA and prevention of homologous chromosome separation in male mouse meiosis in vivo by the topoisomerase II inhibitor etoposide. Mutagenesis *11*, 435-443.

Kamhawi, S. (2006). Phlebotomine sand flies and Leishmania parasites: friends or foes? Trends Parasitol *22*, 439-445.

Kazibwe, A.J., Nerima, B., de Koning, H.P., Maser, P., Barrett, M.P., and Matovu, E. (2009). Genotypic status of the TbAT1/P2 adenosine transporter of Trypanosoma brucei gambiense isolates from Northwestern Uganda following melarsoprol withdrawal. PLoS Negl Trop Dis *3*, e523.

Kelly, J.M., McRobert, L., and Baker, D.A. (2006). Evidence on the chromosomal location of centromeric DNA in Plasmodium falciparum from etoposide-mediated topoisomerase-II cleavage. Proc Natl Acad Sci U S A *103*, 6706-6711.

Kelly, J.M., Ward, H.M., Miles, M.A., and Kendall, G. (1992). A shuttle vector which facilitates the expression of transfected genes in Trypanosoma cruzi and Leishmania. Nucleic Acids Res *20*, 3963-3969.

Kendall, G., Wilderspin, A.F., Ashall, F., Miles, M.A., and Kelly, J.M. (1990). Trypanosoma cruzi glycosomal glyceraldehyde-3-phosphate dehydrogenase does not conform to the 'hotspot' topogenic signal model. EMBO J *9*, 2751-2758.

Kieft, R., Capewell, P., Turner, C.M., Veitch, N.J., MacLeod, A., and Hajduk, S. (2010). Mechanism of Trypanosoma brucei gambiense (group 1) resistance to human trypanosome lytic factor. Proc Natl Acad Sci U S A *107*, 16137-16141.

King, R.W., Peters, J.M., Tugendreich, S., Rolfe, M., Hieter, P., and Kirschner, M.W. (1995). A 20S complex containing CDC27 and CDC16 catalyzes the mitosis-specific conjugation of ubiquitin to cyclin B. Cell *81*, 279-288.

Kniola, B., O'Toole, E., McIntosh, J.R., Mellone, B., Allshire, R., Mengarelli, S., Hultenby, K., and Ekwall, K. (2001). The domain structure of centromeres is conserved from fission yeast to humans. Mol Biol Cell *12*, 2767-2775.

Knox, R.J., Boland, M.P., Friedlos, F., Coles, B., Southan, C., and Roberts, J.J. (1988). The nitroreductase enzyme in Walker cells that activates 5-(aziridin-1-yl)-2,4-dinitrobenzamide (CB 1954) to 5-(aziridin-1-yl)-4-hydroxylamino-2-nitrobenzamide is a form of NAD(P)H dehydrogenase (quinone) (EC 1.6.99.2). Biochem Pharmacol *37*, 4671-4677.

Knox, R.J., Burke, P.J., Chen, S., and Kerr, D.J. (2003). CB 1954: from the Walker tumor to NQO2 and VDEPT. Curr Pharm Des *9*, 2091-2104.

Knox, R.J., Friedlos, F., Marchbank, T., and Roberts, J.J. (1991). Bioactivation of CB 1954: reaction of the active 4-hydroxylamino derivative with thioesters to form the ultimate DNA-DNA interstrand crosslinking species. Biochem Pharmacol *42*, 1691-1697.

Koch, J.E., Kolvraa, S., Petersen, K.B., Gregersen, N., and Bolund, L. (1989). Oligonucleotide-priming methods for the chromosome-specific labelling of alpha satellite DNA in situ. Chromosoma *98*, 259-265.

Kohn, D.B., Sadelain, M., and Glorioso, J.C. (2003). Occurrence of leukaemia following gene therapy of X-linked SCID. Nat Rev Cancer *3*, 477-488.

Kollien, A.H., and Schaub, G.A. (2000). The development of Trypanosoma cruzi in triatominae. Parasitol Today *16*, 381-387.

Kooter, J.M., and Borst, P. (1984). Alpha-amanitin-insensitive transcription of variant surface glycoprotein genes provides further evidence for discontinuous transcription in trypanosomes. Nucleic Acids Res *12*, 9457-9472.

Kops, G.J., Weaver, B.A., and Cleveland, D.W. (2005). On the road to cancer: aneuploidy and the mitotic checkpoint. Nat Rev Cancer *5*, 773-785.

Kubata, B.K., Kabututu, Z., Nozaki, T., Munday, C.J., Fukuzumi, S., Ohkubo, K., Lazarus, M., Maruyama, T., Martin, S.K., Duszenko, M., *et al.* (2002). A key role for old yellow enzyme in the metabolism of drugs by Trypanosoma cruzi. J Exp Med *196*, 1241-1251.

Kulikowicz, T., and Shapiro, T.A. (2006). Distinct genes encode type II Topoisomerases for the nucleus and mitochondrion in the protozoan parasite Trypanosoma brucei. J Biol Chem *281*, 3048-3056.

Kun, H., Moore, A., Mascola, L., Steurer, F., Lawrence, G., Kubak, B., Radhakrishna, S., Leiby, D., Herron, R., Mone, T., *et al.* (2009). Transmission of Trypanosoma cruzi by heart transplantation. Clin Infect Dis *48*, 1534-1540.

Lang, T., Goyard, S., Lebastard, M., and Milon, G. (2005). Bioluminescent Leishmania expressing luciferase for rapid and high throughput screening of drugs acting on amastigote-harbouring macrophages and for quantitative real-time monitoring of parasitism features in living mice. Cell Microbiol *7*, 383-392.

LeBlanc, H.N., Tang, T.T., Wu, J.S., and Orr-Weaver, T.L. (1999). The mitotic centromeric protein MEI-S332 and its role in sister-chromatid cohesion. Chromosoma *108*, 401-411.

Lehrman, S. (1999). Virus treatment questioned after gene therapy death. Nature *401*, 517-518.

Leitsch, D., Kolarich, D., Wilson, I.B., Altmann, F., and Duchene, M. (2007). Nitroimidazole action in Entamoeba histolytica: a central role for thioredoxin reductase. PLoS Biol *5*, e211.

Lenardo, M.J., Rice-Ficht, A.C., Kelly, G., Esser, K.M., and Donelson, J.E. (1984). Characterization of the genes specifying two metacyclic variable antigen types in Trypanosoma brucei rhodesiense. Proc Natl Acad Sci U S A *81*, 6642-6646.

Li, H., Wang, Y., and Liu, X. (2008). Plk1-dependent phosphorylation regulates functions of DNA topoisomerase IIalpha in cell cycle progression. J Biol Chem *283*, 6209-6221.

Li, Z., Han, J., Jiang, Y., Browne, P., Knox, R.J., and Hu, L. (2003). Nitrobenzocyclophosphamides as potential prodrugs for bioreductive activation: synthesis, stability, enzymatic reduction, and antiproliferative activity in cell culture. Bioorg Med Chem *11*, 4171-4178.

Liao, H., Winkfein, R.J., Mack, G., Rattner, J.B., and Yen, T.J. (1995). CENP-F is a protein of the nuclear matrix that assembles onto kinetochores at late G2 and is rapidly degraded after mitosis. J Cell Biol *130*, 507-518.

Lim, H.H., Zhang, T., and Surana, U. (2009). Regulation of centrosome separation in yeast and vertebrates: common threads. Trends Cell Biol *19*, 325-333.

Liu, L.F., Rowe, T.C., Yang, L., Tewey, K.M., and Chen, G.L. (1983). Cleavage of DNA by mammalian DNA topoisomerase II. J Biol Chem *258*, 15365-15370.

Logan-Klumpler, F.J., De Silva, N., Boehme, U., Rogers, M.B., Velarde, G., McQuillan, J.A., Carver, T., Aslett, M., Olsen, C., Subramanian, S., *et al.* (2012). GeneDB--an annotation database for pathogens. Nucleic Acids Res *40*, D98-D108.

Lorenzi, H.A., Vazquez, M.P., and Levin, M.J. (2003). Integration of expression vectors into the ribosomal locus of Trypanosoma cruzi. Gene *310*, 91-99.

Losada, A., and Hirano, T. (2001). Shaping the metaphase chromosome: coordination of cohesion and condensation. Bioessays *23*, 924-935.

Lucumi, E., Darling, C., Jo, H., Napper, A.D., Chandramohanadas, R., Fisher, N., Shone, A.E., Jing, H., Ward, S.A., Biagini, G.A., *et al.* (2010). Discovery of potent small-molecule inhibitors of multidrug-resistant Plasmodium falciparum using a novel miniaturized high-throughput luciferase-based assay. Antimicrob Agents Chemother *54*, 3597-3604.

Lukes, J., Hashimi, H., and Zikova, A. (2005). Unexplained complexity of the mitochondrial genome and transcriptome in kinetoplastid flagellates. Curr Genet *48*, 277-299.

Lundkvist, G.B., Kristensson, K., and Bentivoglio, M. (2004). Why trypanosomes cause sleeping sickness. Physiology (Bethesda) *19*, 198-206.

Lutumba, P., Robays, J., Miaka, C., Kande, V., Simarro, P.P., Shaw, A.P., Dujardin, B., and Boelaert, M. (2005). [The efficiency of different detection strategies of human African trypanosomiasis by T. b. gambiense]. Trop Med Int Health *10*, 347-356.

Machado, C.A., and Ayala, F.J. (2001). Nucleotide sequences provide evidence of genetic exchange among distantly related lineages of Trypanosoma cruzi. Proc Natl Acad Sci U S A *98*, 7396-7401.

Maggert, K.A., and Karpen, G.H. (2001). The activation of a neocentromere in Drosophila requires proximity to an endogenous centromere. Genetics *158*, 1615-1628.

Mair, G., Shi, H., Li, H., Djikeng, A., Aviles, H.O., Bishop, J.R., Falcone, F.H., Gavrilescu, C., Montgomery, J.L., Santori, M.I., *et al.* (2000). A new twist in trypanosome RNA metabolism: cis-splicing of pre-mRNA. RNA *6*, 163-169.

Marschall, L.G., and Clarke, L. (1995). A novel cis-acting centromeric DNA element affects S. pombe centromeric chromatin structure at a distance. J Cell Biol *128*, 445-454.

Martinez-Calvillo, S., and Hernandez, R. (1994). Trypanosoma cruzi ribosomal DNA: mapping of a putative distal promoter. Gene *142*, 243-247.

Martinez-Calvillo, S., Lopez, I., and Hernandez, R. (1997). pRIBOTEX expression vector: a pTEX derivative for a rapid selection of Trypanosoma cruzi transfectants. Gene *199*, 71-76.

Maser, P., Sutterlin, C., Kralli, A., and Kaminsky, R. (1999). A nucleoside transporter from Trypanosoma brucei involved in drug resistance. Science *285*, 242-244.

Masocha, W., Rottenberg, M.E., and Kristensson, K. (2007). Migration of African trypanosomes across the blood-brain barrier. Physiol Behav *92*, 110-114.

Mason, R.P., and Holtzman, J.L. (1975). The mechanism of microsomal and mitochondrial nitroreductase. Electron spin resonance evidence for nitroaromatic free radical intermediates. Biochemistry *14*, 1626-1632.

Masumoto, H., Masukata, H., Muro, Y., Nozaki, N., and Okazaki, T. (1989). A human centromere antigen (CENP-B) interacts with a short specific sequence in alphoid DNA, a human centromeric satellite. J Cell Biol *109*, 1963-1973.

Matovu, E., Geiser, F., Schneider, V., Maser, P., Enyaru, J.C., Kaminsky, R., Gallati, S., and Seebeck, T. (2001). Genetic variants of the TbAT1 adenosine transporter from African trypanosomes in relapse infections following melarsoprol therapy. Mol Biochem Parasitol *117*, 73-81.

Matthews, K.R., Ellis, J.R., and Paterou, A. (2004). Molecular regulation of the life cycle of African trypanosomes. Trends Parasitol *20*, 40-47.

Matthews, K.R., and Gull, K. (1994). Evidence for an interplay between cell cycle progression and the initiation of differentiation between life cycle forms of African trypanosomes. J Cell Biol *125*, 1147-1156.

Matthews, K.R., Tschudi, C., and Ullu, E. (1994). A common pyrimidine-rich motif governs trans-splicing and polyadenylation of tubulin polycistronic pre-mRNA in trypanosomes. Genes Dev *8*, 491-501.

Maya, J.D., Bollo, S., Nunez-Vergara, L.J., Squella, J.A., Repetto, Y., Morello, A., Perie, J., and Chauviere, G. (2003). Trypanosoma cruzi: effect and mode of action of nitroimidazole and nitrofuran derivatives. Biochem Pharmacol *65*, 999-1006.

Maya, J.D., Repetto, Y., Agosin, M., Ojeda, J.M., Tellez, R., Gaule, C., and Morello, A. (1997). Effects of nifurtimox and benznidazole upon glutathione and trypanothione content in epimastigote, trypomastigote and amastigote forms of Trypanosoma cruzi. Mol Biochem Parasitol *86*, 101-106.

McCalla, D.R. (1983). Mutagenicity of nitrofuran derivatives: review. Environ Mutagen *5*, 745-765.

McCalla, D.R., Kaiser, C., and Green, M.H. (1978). Genetics of nitrofurazone resistance in Escherichia coli. J Bacteriol *133*, 10-16.

McCalla, D.R., Reuvers, A., and Kaiser, C. (1970). Mode of action of nitrofurazone. J Bacteriol *104*, 1126-1134.

McCalla, D.R., and Voutsinos, D. (1974). On the mutagenicity of nitrofurans. Mutat Res *26*, 3-16.

McCleland, M.L., Kallio, M.J., Barrett-Wilt, G.A., Kestner, C.A., Shabanowitz, J., Hunt, D.F., Gorbsky, G.J., and Stukenberg, P.T. (2004). The vertebrate Ndc80 complex contains Spc24 and Spc25 homologs, which are required to establish and maintain kinetochore-microtubule attachment. Curr Biol *14*, 131-137.

McCulloch, R. (2004). Antigenic variation in African trypanosomes: monitoring progress. Trends Parasitol *20*, 117-121.

McKean, P.G., Baines, A., Vaughan, S., and Gull, K. (2003). Gamma-tubulin functions in the nucleation of a discrete subset of microtubules in the eukaryotic flagellum. Curr Biol *13*, 598-602.

McNeish, I.A., Green, N.K., Gilligan, M.G., Ford, M.J., Mautner, V., Young, L.S., Kerr, D.J., and Searle, P.F. (1998). Virus directed enzyme prodrug therapy for ovarian and pancreatic cancer using retrovirally delivered E. coli nitroreductase and CB1954. Gene Ther *5*, 1061-1069.

Mellone, B.G., Zhang, W., and Karpen, G.H. (2009). Frodos found: Behold the CENP-a "Ring" bearers. Cell *137*, 409-412.

Meluh, P.B., Yang, P., Glowczewski, L., Koshland, D., and Smith, M.M. (1998). Cse4p is a component of the core centromere of Saccharomyces cerevisiae. Cell *94*, 607-613.

Melville, S.E., Leech, V., Gerrard, C.S., Tait, A., and Blackwell, J.M. (1998). The molecular karyotype of the megabase chromosomes of Trypanosoma brucei and the assignment of chromosome markers. Mol Biochem Parasitol *94*, 155-173.

Melville, S.E., Leech, V., Navarro, M., and Cross, G.A. (2000). The molecular karyotype of the megabase chromosomes of Trypanosoma brucei stock 427. Mol Biochem Parasitol *111*, 261-273.

Michels, P.A., Bringaud, F., Herman, M., and Hannaert, V. (2006). Metabolic functions of glycosomes in trypanosomatids. Biochim Biophys Acta *1763*, 1463-1477.

Miles, M.A., Feliciangeli, M.D., and de Arias, A.R. (2003). American trypanosomiasis (Chagas' disease) and the role of molecular epidemiology in guiding control strategies. BMJ *326*, 1444-1448.

Miranda, J.J., De Wulf, P., Sorger, P.K., and Harrison, S.C. (2005). The yeast DASH complex forms closed rings on microtubules. Nat Struct Mol Biol *12*, 138-143.

Mittra, B., Saha, A., Chowdhury, A.R., Pal, C., Mandal, S., Mukhopadhyay, S., Bandyopadhyay, S., and Majumder, H.K. (2000). Luteolin, an abundant dietary component is a potent anti-leishmanial agent that acts by inducing topoisomerase II-mediated kinetoplast DNA cleavage leading to apoptosis. Mol Med *6*, 527-541.

Mizushima, T., Natori, S., and Sekimizu, K. (1992). Inhibition of Escherichia coli DNA topoisomerase I activity by phospholipids. Biochem J *285 (Pt 2)*, 503-506.

Moncada, C., Repetto, Y., Aldunate, J., Letelier, M.E., and Morello, A. (1989). Role of glutathione in the susceptibility of Trypanosoma cruzi to drugs. Comp Biochem Physiol C *94*, 87-91.

Moncayo, A. (1999). Progress towards interruption of transmission of Chagas disease. Mem Inst Oswaldo Cruz *94 Suppl 1*, 401-404.

Moncayo, A., and Silveira, A.C. (2009). Current epidemiological trends for Chagas disease in Latin America and future challenges in epidemiology, surveillance and health policy. Mem Inst Oswaldo Cruz *104 Suppl 1*, 17-30.

Moraga, A.A., and Graf, U. (1989). Genotoxicity testing of antiparasitic nitrofurans in the Drosophila wing somatic mutation and recombination test. Mutagenesis *4*, 105-110.

Moran, M., Guzman, J., Ropars, A.L., McDonald, A., Jameson, N., Omune, B., Ryan, S., and Wu, L. (2009). Neglected disease research and development: how much are we really spending? PLoS Med *6*, e30.

Morris, C.A., and Moazed, D. (2007). Centromere assembly and propagation. Cell *128*, 647-650.

Morrison, A., and Cozzarelli, N.R. (1979). Site-specific cleavage of DNA by E. coli DNA gyrase. Cell *17*, 175-184.

Mortara, R.A., da Silva, S., Araguth, M.F., Blanco, S.A., and Yoshida, N. (1992). Polymorphism of the 35- and 50-kilodalton surface glycoconjugates of Trypanosoma cruzi metacyclic trypomastigotes. Infect Immun *60*, 4673-4678.

MSF (2010). Médecins Sans Frontières Clinical Guidelines: Diagnosis and Treatment Manual.

Muelas-Serrano, S., Nogal-Ruiz, J.J., and Gomez-Barrio, A. (2000). Setting of a colorimetric method to determine the viability of Trypanosoma cruzi epimastigotes. Parasitol Res *86*, 999-1002.

Murataliev, M.B., Feyereisen, R., and Walker, F.A. (2004). Electron transfer by diflavin reductases. Biochim Biophys Acta *1698*, 1-26.

Murphy, T.D., and Karpen, G.H. (1995). Localization of centromere function in a Drosophila minichromosome. Cell *82*, 599-609.

Murphy, T.D., and Karpen, G.H. (1998). Centromeres take flight: alpha satellite and the quest for the human centromere. Cell *93*, 317-320.

Murray, H.W., Berman, J.D., Davies, C.R., and Saravia, N.G. (2005). Advances in leishmaniasis. Lancet *366*, 1561-1577.

Musacchio, A., and Salmon, E.D. (2007). The spindle-assembly checkpoint in space and time. Nat Rev Mol Cell Biol *8*, 379-393.

Nagel, R., and Nepomnaschy, I. (1983). Mutagenicity of 2 anti-chagasic drugs and their metabolic deactivation. Mutat Res *117*, 237-242.

Nelson, E.M., Tewey, K.M., and Liu, L.F. (1984). Mechanism of antitumor drug action: poisoning of mammalian DNA topoisomerase II on DNA by 4'-(9-acridinylamino)-methanesulfon-m-anisidide. Proc Natl Acad Sci U S A *81*, 1361-1365.

Ngan, V.K., and Clarke, L. (1997). The centromere enhancer mediates centromere activation in Schizosaccharomyces pombe. Mol Cell Biol *17*, 3305-3314.

Ngo, H., Tschudi, C., Gull, K., and Ullu, E. (1998). Double-stranded RNA induces mRNA degradation in Trypanosoma brucei. Proc Natl Acad Sci U S A *95*, 14687-14692.

Nikolskaia, O.V., de, A.L.A.P., Kim, Y.V., Lonsdale-Eccles, J.D., Fukuma, T., Scharfstein, J., and Grab, D.J. (2006). Blood-brain barrier traversal by African trypanosomes requires calcium signaling induced by parasite cysteine protease. J Clin Invest *116*, 2739-2747.

Nishino, T., Okamoto, K., Eger, B.T., and Pai, E.F. (2008). Mammalian xanthine oxidoreductase - mechanism of transition from xanthine dehydrogenase to xanthine oxidase. FEBS J *275*, 3278-3289.

Nixon, J.E., Wang, A., Field, J., Morrison, H.G., McArthur, A.G., Sogin, M.L., Loftus, B.J., and Samuelson, J. (2002). Evidence for lateral transfer of genes encoding ferredoxins, nitroreductases, NADH

oxidase, and alcohol dehydrogenase 3 from anaerobic prokaryotes to Giardia lamblia and Entamoeba histolytica. Eukaryot Cell *1*, 181-190.

Nozaki, T., and Cross, G.A. (1995). Effects of 3' untranslated and intergenic regions on gene expression in Trypanosoma cruzi. Mol Biochem Parasitol *75*, 55-67.

Nunes, L.R., de Carvalho, M.R., and Buck, G.A. (1997). Trypanosoma cruzi strains partition into two groups based on the structure and function of the spliced leader RNA and rRNA gene promoters. Mol Biochem Parasitol *86*, 211-224.

Obado, S.O., Bot, C., Echeverry, M.C., Bayona, J.C., Alvarez, V.E., Taylor, M.C., and Kelly, J.M. (2011). Centromere-associated topoisomerase activity in bloodstream form Trypanosoma brucei. Nucleic Acids Res.

Obado, S.O., Bot, C., Nilsson, D., Andersson, B., and Kelly, J.M. (2007). Repetitive DNA is associated with centromeric domains in Trypanosoma brucei but not Trypanosoma cruzi. Genome Biol *8*, R37.

Obado, S.O., Taylor, M.C., Wilkinson, S.R., Bromley, E.V., and Kelly, J.M. (2005). Functional mapping of a trypanosome centromere by chromosome fragmentation identifies a 16-kb GC-rich transcriptional "strand-switch" domain as a major feature. Genome Res *15*, 36-43.

Ocana-Mayorga, S., Llewellyn, M.S., Costales, J.A., Miles, M.A., and Grijalva, M.J. (2010). Sex, subdivision, and domestic dispersal of Trypanosoma cruzi lineage I in southern Ecuador. PLoS Negl Trop Dis *4*, e915.

Oegema, K., Desai, A., Rybina, S., Kirkham, M., and Hyman, A.A. (2001). Functional analysis of kinetochore assembly in Caenorhabditis elegans. J Cell Biol *153*, 1209-1226.

Ogbadoyi, E., Ersfeld, K., Robinson, D., Sherwin, T., and Gull, K. (2000). Architecture of the Trypanosoma brucei nucleus during interphase and mitosis. Chromosoma *108*, 501-513.

Ohnishi, T., Ohashi, Y., Nozu, K., and Inoki, S. (1980). Mutagenicity of nifurtimox in Escherichia coli. Mutat Res *77*, 241-244.

Oli, M.W., Cotlin, L.F., Shiflett, A.M., and Hajduk, S.L. (2006). Serum resistance-associated protein blocks lysosomal targeting of trypanosome lytic factor in Trypanosoma brucei. Eukaryot Cell *5*, 132-139.

Olive, P.L. (1978). Nitrofurazone-induced DNA damage to tissues of mice. Chem Biol Interact *20*, 323-331.

Ono, T., Nakazono, K., and Kosaka, H. (1982). Purification and partial characterization of squalene epoxidase from rat liver microsomes. Biochim Biophys Acta *709*, 84-90.

Orna, M.V., and Mason, R.P. (1989). Correlation of kinetic parameters of nitroreductase enzymes with redox properties of nitroaromatic compounds. J Biol Chem *264*, 12379-12384.

Osorio, Y., Travi, B.L., Renslo, A.R., Peniche, A.G., and Melby, P.C. (2011). Identification of small molecule lead compounds for visceral leishmaniasis using a novel ex vivo splenic explant model system. PLoS Negl Trop Dis *5*, e962.

Packchanian, A. (1955). Chemotherapy of African sleeping sickness. I. Chemotherapy of experimental Trypanosoma gambiense infection in mice (Mus musculus) with nitrofurazone. Am J Trop Med Hyg *4*, 705-711.

PAHO/WHO (2007). Estimación cuantitativa de la enfermedad de Chagas en les Américas. Organizacion Panamericana de la Salud.

Palmer, D.K., O'Day, K., Wener, M.H., Andrews, B.S., and Margolis, R.L. (1987). A 17-kD centromere protein (CENP-A) copurifies with nucleosome core particles and with histones. J Cell Biol *104*, 805-815.

Partridge, J.F., Borgstrom, B., and Allshire, R.C. (2000). Distinct protein interaction domains and protein spreading in a complex centromere. Genes Dev *14*, 783-791.

Patel, P., Young, J.G., Mautner, V., Ashdown, D., Bonney, S., Pineda, R.G., Collins, S.I., Searle, P.F., Hull, D., Peers, E., *et al.* (2009). A phase I/II clinical trial in localized prostate cancer of an adenovirus expressing nitroreductase with CB1954 [correction of CB1984]. Mol Ther *17*, 1292-1299.

Pays, E., Vanhamme, L., and Perez-Morga, D. (2004). Antigenic variation in Trypanosoma brucei: facts, challenges and mysteries. Curr Opin Microbiol *7*, 369-374.

Peacock, L., Ferris, V., Sharma, R., Sunter, J., Bailey, M., Carrington, M., and Gibson, W. (2011). Identification of the meiotic life cycle stage of Trypanosoma brucei in the tsetse fly. Proc Natl Acad Sci U S A *108*, 3671-3676.

Perez-Morga, D., Vanhollebeke, B., Paturiaux-Hanocq, F., Nolan, D.P., Lins, L., Homble, F., Vanhamme, L., Tebabi, P., Pays, A., Poelvoorde, P., *et al.* (2005). Apolipoprotein L-I promotes trypanosome lysis by forming pores in lysosomal membranes. Science *309*, 469-472.

Peters, J.M. (1999). Subunits and substrates of the anaphase-promoting complex. Exp Cell Res *248*, 339-349.

Peterson, F.J., Mason, R.P., Hovsepian, J., and Holtzman, J.L. (1979). Oxygen-sensitive and -insensitive nitroreduction by Escherichia coli and rat hepatic microsomes. J Biol Chem *254*, 4009-4014.

Petranyi, G., Ryder, N.S., and Stutz, A. (1984). Allylamine derivatives: new class of synthetic antifungal agents inhibiting fungal squalene epoxidase. Science *224*, 1239-1241.

Picozzi, K., Fevre, E.M., Odiit, M., Carrington, M., Eisler, M.C., Maudlin, I., and Welburn, S.C. (2005). Sleeping sickness in Uganda: a thin line between two fatal diseases. BMJ *331*, 1238-1241.

Pimenta, P.F., Modi, G.B., Pereira, S.T., Shahabuddin, M., and Sacks, D.L. (1997). A novel role for the peritrophic matrix in protecting Leishmania from the hydrolytic activities of the sand fly midgut. Parasitology *115 (Pt 4)*, 359-369.

Pinazo, M.J., Munoz, J., Posada, E., Lopez-Chejade, P., Gallego, M., Ayala, E., del Cacho, E., Soy, D., and Gascon, J. (2010). Tolerance of benznidazole in treatment of Chagas' disease in adults. Antimicrob Agents Chemother *54*, 4896-4899.

Polnaszek, C.F., Peterson, F.J., Holtzman, J.L., and Mason, R.P. (1984). No detectable reaction of the anion radical metabolite of nitrofurans with reduced glutathione or macro-molecules. Chem Biol Interact *51*, 263-271.

Portal, P., Villamil, S.F., Alonso, G.D., De Vas, M.G., Flawia, M.M., Torres, H.N., and Paveto, C. (2008). Multiple NADPH-cytochrome P450 reductases from Trypanosoma cruzi suggested role on drug resistance. Mol Biochem Parasitol *160*, 42-51.

Portman, N., and Gull, K. (2010). The paraflagellar rod of kinetoplastid parasites: from structure to components and function. Int J Parasitol *40*, 135-148.

Prathalingham, S.R., Wilkinson, S.R., Horn, D., and Kelly, J.M. (2007). Deletion of the Trypanosoma brucei superoxide dismutase gene sodb1 increases sensitivity to nifurtimox and benznidazole. Antimicrob Agents Chemother *51*, 755-758.

Prieto-Alamo, M.J., Abril, N., and Pueyo, C. (1993). Mutagenesis in Escherichia coli K-12 mutants defective in superoxide dismutase or catalase. Carcinogenesis *14*, 237-244.

Priotto, G., Kasparian, S., Mutombo, W., Ngouama, D., Ghorashian, S., Arnold, U., Ghabri, S., Baudin, E., Buard, V., Kazadi-Kyanza, S., *et al.* (2009). Nifurtimox-eflornithine combination therapy for second-stage African Trypanosoma brucei gambiense trypanosomiasis: a multicentre, randomised, phase III, non-inferiority trial. Lancet *374*, 56-64.

Prosser, G.A., Copp, J.N., Syddall, S.P., Williams, E.M., Smaill, J.B., Wilson, W.R., Patterson, A.V., and Ackerley, D.F. (2010). Discovery and evaluation of Escherichia coli nitroreductases that activate the anti-cancer prodrug CB1954. Biochem Pharmacol *79*, 678-687.

Race, P.R., Lovering, A.L., Green, R.M., Ossor, A., White, S.A., Searle, P.F., Wrighton, C.J., and Hyde, E.I. (2005). Structural and mechanistic studies of Escherichia coli nitroreductase with the antibiotic nitrofurazone. Reversed binding orientations in different redox states of the enzyme. J Biol Chem *280*, 13256-13264.

Raether, W., and Hanel, H. (2003). Nitroheterocyclic drugs with broad spectrum activity. Parasitol Res *90 Supp 1*, S19-39.

Rassi, A., Jr., Rassi, A., and Marin-Neto, J.A. (2010). Chagas disease. Lancet *375*, 1388-1402.

Rattner, J.B., Hendzel, M.J., Furbee, C.S., Muller, M.T., and Bazett-Jones, D.P. (1996). Topoisomerase II alpha is associated with the mammalian centromere in a cell cycle- and species-specific manner and is required for proper centromere/kinetochore structure. J Cell Biol *134*, 1097-1107.

Repetto, Y., Opazo, E., Maya, J.D., Agosin, M., and Morello, A. (1996). Glutathione and trypanothione in several strains of Trypanosoma cruzi: effect of drugs. Comp Biochem Physiol B Biochem Mol Biol *115*, 281-285.

Rieger, P.G., Meier, H.M., Gerle, M., Vogt, U., Groth, T., and Knackmuss, H.J. (2002). Xenobiotics in the environment: present and future strategies to obviate the problem of biological persistence. J Biotechnol *94*, 101-123.

Rifkin, M.R. (1978). Identification of the trypanocidal factor in normal human serum: high density lipoprotein. Proc Natl Acad Sci U S A *75*, 3450-3454.

Rigaut, G., Shevchenko, A., Rutz, B., Wilm, M., Mann, M., and Seraphin, B. (1999). A generic protein purification method for protein complex characterization and proteome exploration. Nat Biotechnol *17*, 1030-1032.

Robinson, D.R., and Gull, K. (1991). Basal body movements as a mechanism for mitochondrial genome segregation in the trypanosome cell cycle. Nature *352*, 731-733.

Robinson, K.A., and Beverley, S.M. (2003). Improvements in transfection efficiency and tests of RNA interference (RNAi) approaches in the protozoan parasite Leishmania. Mol Biochem Parasitol *128*, 217-228.

Rochette, A., Raymond, F., Ubeda, J.M., Smith, M., Messier, N., Boisvert, S., Rigault, P., Corbeil, J., Ouellette, M., and Papadopoulou, B. (2008). Genome-wide gene expression profiling analysis of Leishmania major and Leishmania infantum developmental stages reveals substantial differences between the two species. BMC Genomics *9*, 255.

Roditi, I., Carrington, M., and Turner, M. (1987). Expression of a polypeptide containing a dipeptide repeat is confined to the insect stage of Trypanosoma brucei. Nature *325*, 272-274.

Rodriguez, A., Webster, P., Ortego, J., and Andrews, N.W. (1997). Lysosomes behave as Ca2+-regulated exocytic vesicles in fibroblasts and epithelial cells. J Cell Biol *137*, 93-104.

Rodriques Coura, J., and de Castro, S.L. (2002). A critical review on Chagas disease chemotherapy. Mem Inst Oswaldo Cruz *97*, 3-24.

Rogers, M.E., Ilg, T., Nikolaev, A.V., Ferguson, M.A., and Bates, P.A. (2004). Transmission of cutaneous leishmaniasis by sand flies is enhanced by regurgitation of fPPG. Nature *430*, 463-467.

Rogojina, A.T., and Nitiss, J.L. (2008). Isolation and characterization of mAMSA-hypersensitive mutants. Cytotoxicity of Top2 covalent complexes containing DNA single strand breaks. J Biol Chem *283*, 29239-29250.

Roldan, M.D., Perez-Reinado, E., Castillo, F., and Moreno-Vivian, C. (2008). Reduction of polynitroaromatic compounds: the bacterial nitroreductases. FEMS Microbiol Rev *32*, 474-500.

Rolon, M., Vega, C., Escario, J.A., and Gomez-Barrio, A. (2006). Development of resazurin microtiter assay for drug sensibility testing of Trypanosoma cruzi epimastigotes. Parasitol Res *99*, 103-107.

Roy, G., Dumas, C., Sereno, D., Wu, Y., Singh, A.K., Tremblay, M.J., Ouellette, M., Olivier, M., and Papadopoulou, B. (2000). Episomal and stable expression of the luciferase reporter gene for quantifying Leishmania spp. infections in macrophages and in animal models. Mol Biochem Parasitol *110*, 195-206.

Rudenko, G., Blundell, P.A., Taylor, M.C., Kieft, R., and Borst, P. (1994). VSG gene expression site control in insect form Trypanosoma brucei. EMBO J *13*, 5470-5482.

Ruiz, C., Rigoni, V.L., Gonzalez, J., and Yoshida, N. (1993). The 35/50 kDa surface antigen of Trypanosoma cruzi metacyclic trypomastigotes, an adhesion molecule involved in host cell invasion. Parasite Immunol *15*, 121-125.

Ruiz, R.C., Favoreto, S., Jr., Dorta, M.L., Oshiro, M.E., Ferreira, A.T., Manque, P.M., and Yoshida, N. (1998). Infectivity of Trypanosoma cruzi strains is associated with differential expression of surface glycoproteins with differential Ca2+ signalling activity. Biochem J *330 (Pt 1)*, 505-511.

Sacks, D., and Kamhawi, S. (2001). Molecular aspects of parasite-vector and vector-host interactions in leishmaniasis. Annu Rev Microbiol *55*, 453-483.

Sacks, D., and Sher, A. (2002). Evasion of innate immunity by parasitic protozoa. Nat Immunol *3*, 1041-1047.

Saffery, R., Irvine, D.V., Griffiths, B., Kalitsis, P., Wordeman, L., and Choo, K.H. (2000). Human centromeres and neocentromeres show identical distribution patterns of >20 functionally important kinetochore-associated proteins. Hum Mol Genet *9*, 175-185.

Samsonova, J.V., Douglas, A.J., Cooper, K.M., Kennedy, D.G., and Elliott, C.T. (2008). The identification of potential alternative biomarkers of nitrofurazone abuse in animal derived food products. Food Chem Toxicol *46*, 1548-1554.

Sander, M., and Hsieh, T. (1983). Double strand DNA cleavage by type II DNA topoisomerase from Drosophila melanogaster. J Biol Chem *258*, 8421-8428.

Schimanski, B., Nguyen, T.N., and Gunzl, A. (2005). Highly efficient tandem affinity purification of trypanosome protein complexes based on a novel epitope combination. Eukaryot Cell *4*, 1942-1950.

Schueler, M.G., Higgins, A.W., Rudd, M.K., Gustashaw, K., and Willard, H.F. (2001). Genomic and genetic definition of a functional human centromere. Science *294*, 109-115.

Seed, J.R., and Wenck, M.A. (2003). Role of the long slender to short stumpy transition in the life cycle of the african trypanosomes. Kinetoplastid Biol Dis *2*, 3.

Sengupta, T., Mukherjee, M., Das, A., Mandal, C., Das, R., Mukherjee, T., and Majumder, H.K. (2005a). Characterization of the ATPase activity of topoisomerase II from Leishmania donovani and identification of residues conferring resistance to etoposide. Biochem J *390*, 419-426.

Sengupta, T., Mukherjee, M., Das, R., Das, A., and Majumder, H.K. (2005b). Characterization of the DNA-binding domain and identification of the active site residue in the 'Gyr A' half of Leishmania donovani topoisomerase II. Nucleic Acids Res *33*, 2364-2373.

Sengupta, T., Mukherjee, M., Mandal, C., Das, A., and Majumder, H.K. (2003). Functional dissection of the C-terminal domain of type II DNA topoisomerase from the kinetoplastid hemoflagellate Leishmania donovani. Nucleic Acids Res *31*, 5305-5316.

Shi, H., Djikeng, A., Tschudi, C., and Ullu, E. (2004). Argonaute protein in the early divergent eukaryote Trypanosoma brucei: control of small interfering RNA accumulation and retroposon transcript abundance. Mol Cell Biol *24*, 420-427.

Shi, H., Tschudi, C., and Ullu, E. (2006). An unusual Dicer-like1 protein fuels the RNA interference pathway in Trypanosoma brucei. RNA *12*, 2063-2072.

Shiflett, A.M., Faulkner, S.D., Cotlin, L.F., Widener, J., Stephens, N., and Hajduk, S.L. (2007). African trypanosomes: intracellular trafficking of host defense molecules. J Eukaryot Microbiol *54*, 18-21.

Siegel, T.N., Hekstra, D.R., and Cross, G.A. (2008). Analysis of the Trypanosoma brucei cell cycle by quantitative DAPI imaging. Mol Biochem Parasitol *160*, 171-174.

Siegel, T.N., Hekstra, D.R., Kemp, L.E., Figueiredo, L.M., Lowell, J.E., Fenyo, D., Wang, X., Dewell, S., and Cross, G.A. (2009). Four histone variants mark the boundaries of polycistronic transcription units in Trypanosoma brucei. Genes Dev *23*, 1063-1076.

Siegel, T.N., Hekstra, D.R., Wang, X., Dewell, S., and Cross, G.A. (2010). Genome-wide analysis of mRNA abundance in two life-cycle stages of Trypanosoma brucei and identification of splicing and polyadenylation sites. Nucleic Acids Res *38*, 4946-4957.

Siim, B.G., Denny, W.A., and Wilson, W.R. (1997). Nitro reduction as an electronic switch for bioreductive drug activation. Oncol Res *9*, 357-369.

Simarro, P.P., Diarra, A., Ruiz Postigo, J.A., Franco, J.R., and Jannin, J.G. (2011). The human African trypanosomiasis control and surveillance programme of the World Health Organization 2000-2009: the way forward. PLoS Negl Trop Dis *5*, e1007.

Simpson, L., Sbicego, S., and Aphasizhev, R. (2003). Uridine insertion/deletion RNA editing in trypanosome mitochondria: a complex business. RNA *9*, 265-276.

Sloof, P., Bos, J.L., Konings, A.F., Menke, H.H., Borst, P., Gutteridge, W.E., and Leon, W. (1983). Characterization of satellite DNA in Trypanosoma brucei and Trypanosoma cruzi. J Mol Biol *167*, 1-21.

Sokolova, A.Y., Wyllie, S., Patterson, S., Oza, S.L., Read, K.D., and Fairlamb, A.H. (2010). Cross-resistance to nitro drugs and implications for treatment of human African trypanosomiasis. Antimicrob Agents Chemother *54*, 2893-2900.

Solari, A.J. (1980). Function of the dense plaques during mitosis in Trypanosoma cruzi. Exp Cell Res *127*, 457-460.

Southern, E.M. (1975). Detection of specific sequences among DNA fragments separated by gel electrophoresis. J Mol Biol *98*, 503-517.

Spence, J.M., Critcher, R., Ebersole, T.A., Valdivia, M.M., Earnshaw, W.C., Fukagawa, T., and Farr, C.J. (2002). Co-localization of centromere activity, proteins and topoisomerase II within a subdomain of the major human X alpha-satellite array. EMBO J *21*, 5269-5280.

Spence, J.M., Fournier, R.E., Oshimura, M., Regnier, V., and Farr, C.J. (2005). Topoisomerase II cleavage activity within the human D11Z1 and DXZ1 alpha-satellite arrays. Chromosome Res *13*, 637-648.

Spence, J.M., Phua, H.H., Mills, W., Carpenter, A.J., Porter, A.C., and Farr, C.J. (2007). Depletion of topoisomerase IIalpha leads to shortening of the metaphase interkinetochore distance and abnormal persistence of PICH-coated anaphase threads. J Cell Sci *120*, 3952-3964.

Spencer, F., and Hieter, P. (1992). Centromere DNA mutations induce a mitotic delay in Saccharomyces cerevisiae. Proc Natl Acad Sci U S A *89*, 8908-8912.

Steverding, D. (2008). The history of African trypanosomiasis. Parasit Vectors *1*, 3.

Stockdale, C., Swiderski, M.R., Barry, J.D., and McCulloch, R. (2008). Antigenic variation in Trypanosoma brucei: joining the DOTs. PLoS Biol *6*, e185.

Stover, C.K., Warrener, P., VanDevanter, D.R., Sherman, D.R., Arain, T.M., Langhorne, M.H., Anderson, S.W., Towell, J.A., Yuan, Y., McMurray, D.N., *et al.* (2000). A small-molecule nitroimidazopyran drug candidate for the treatment of tuberculosis. Nature *405*, 962-966.

Streeter, A.J., and Hoener, B.A. (1988). Evidence for the involvement of a nitrenium ion in the covalent binding of nitrofurazone to DNA. Pharm Res *5*, 434-436.

Stuart, K. (1979). Kinetoplast DNA Of Trypanosoma brucei: physical map of the maxicircle. Plasmid *2*, 520-528.

Stuart, K.D., Schnaufer, A., Ernst, N.L., and Panigrahi, A.K. (2005). Complex management: RNA editing in trypanosomes. Trends Biochem Sci *30*, 97-105.

Sudakin, V., Ganoth, D., Dahan, A., Heller, H., Hershko, J., Luca, F.C., Ruderman, J.V., and Hershko, A. (1995). The cyclosome, a large complex containing cyclin-selective ubiquitin ligase activity, targets cyclins for destruction at the end of mitosis. Mol Biol Cell *6*, 185-197.

Sugimoto, K., Yata, H., Muro, Y., and Himeno, M. (1994). Human centromere protein C (CENP-C) is a DNA-binding protein which possesses a novel DNA-binding motif. J Biochem *116*, 877-881.

Sun, X., Le, H.D., Wahlstrom, J.M., and Karpen, G.H. (2003). Sequence analysis of a functional Drosophila centromere. Genome Res *13*, 182-194.

Sun, X., Wahlstrom, J., and Karpen, G. (1997). Molecular structure of a functional Drosophila centromere. Cell *91*, 1007-1019.

Swaminathan, S., Lower, G.M., Jr., and Bryan, G.T. (1982). Nitroreductase-mediated metabolic activation of 2-amino-4-(5-nitro-2-furyl)thiazole and binding to nucleic acids and proteins. Cancer Res *42*, 4479-4484.

Takahashi, K., Chen, E.S., and Yanagida, M. (2000). Requirement of Mis6 centromere connector for localizing a CENP-A-like protein in fission yeast. Science *288*, 2215-2219.

Takahashi, K., Yamada, H., and Yanagida, M. (1994). Fission yeast minichromosome loss mutants mis cause lethal aneuploidy and replication abnormality. Mol Biol Cell *5*, 1145-1158.

Talbert, P.B., Masuelli, R., Tyagi, A.P., Comai, L., and Henikoff, S. (2002). Centromeric localization and adaptive evolution of an Arabidopsis histone H3 variant. Plant Cell *14*, 1053-1066.

Tamar, S., and Papadopoulou, B. (2001). A telomere-mediated chromosome fragmentation approach to assess mitotic stability and ploidy alterations of Leishmania chromosomes. J Biol Chem *276*, 11662-11673.

Tanaka, K., Mukae, N., Dewar, H., van Breugel, M., James, E.K., Prescott, A.R., Antony, C., and Tanaka, T.U. (2005). Molecular mechanisms of kinetochore capture by spindle microtubules. Nature *434*, 987-994.

Tang, M.H., Helsby, N.A., Wilson, W.R., and Tingle, M.D. (2005). Aerobic 2- and 4-nitroreduction of CB 1954 by human liver. Toxicology *216*, 129-139.

Tang, Z., Sun, Y., Harley, S.E., Zou, H., and Yu, H. (2004). Human Bub1 protects centromeric sister-chromatid cohesion through Shugoshin during mitosis. Proc Natl Acad Sci U S A *101*, 18012-18017.

Tatsumi, K., Nakabeppu, H., Takahashi, Y., and Kitamura, S. (1984). Metabolism in vivo of furazolidone: evidence for formation of an open-chain carboxylic acid and alpha-ketoglutaric acid from the nitrofuran in rats. Arch Biochem Biophys *234*, 112-116.

Taylor, M.C., and Kelly, J.M. (2006). pTcINDEX: a stable tetracycline-regulated expression vector for Trypanosoma cruzi. BMC Biotechnol *6*, 32.

Thompson, J.D., Higgins, D.G., and Gibson, T.J. (1994). CLUSTAL W: improving the sensitivity of progressive multiple sequence alignment through sequence weighting, position-specific gap penalties and weight matrix choice. Nucleic Acids Res *22*, 4673-4680.

Tibayrenc, M. (1998). Genetic epidemiology of parasitic protozoa and other infectious agents: the need for an integrated approach. Int J Parasitol *28*, 85-104.

Tibbetts, R.S., Klein, K.G., and Engman, D.M. (1995). A rapid method for protein localization in trypanosomes. Exp Parasitol *80*, 572-574.

Tielens, A.G., and Van Hellemond, J.J. (1998). Differences in energy metabolism between trypanosomatidae. Parasitol Today *14*, 265-272.

Torreele, E., Bourdin Trunz, B., Tweats, D., Kaiser, M., Brun, R., Mazue, G., Bray, M.A., and Pecoul, B. (2010). Fexinidazole--a new oral nitroimidazole drug candidate entering clinical development for the treatment of sleeping sickness. PLoS Negl Trop Dis *4*, e923.

Truc, P., Lejon, V., Magnus, E., Jamonneau, V., Nangouma, A., Verloo, D., Penchenier, L., and Buscher, P. (2002). Evaluation of the micro-CATT, CATT/Trypanosoma brucei gambiense, and LATEX/T b gambiense methods for serodiagnosis and surveillance of human African trypanosomiasis in West and Central Africa. Bull World Health Organ *80*, 882-886.

Trunz, B.B., Jedrysiak, R., Tweats, D., Brun, R., Kaiser, M., Suwinski, J., and Torreele, E. (2011). 1-Aryl-4-nitro-1H-imidazoles, a new promising series for the treatment of human African trypanosomiasis. Eur J Med Chem *46*, 1524-1535.

Tyler, K.M., and Engman, D.M. (2001). The life cycle of Trypanosoma cruzi revisited. Int J Parasitol *31*, 472-481.

Uhlmann, F., Lottspeich, F., and Nasmyth, K. (1999). Sister-chromatid separation at anaphase onset is promoted by cleavage of the cohesin subunit Scc1. Nature *400*, 37-42.

Urbina, J.A., Concepcion, J.L., Rangel, S., Visbal, G., and Lira, R. (2002). Squalene synthase as a chemotherapeutic target in Trypanosoma cruzi and Leishmania mexicana. Mol Biochem Parasitol *125*, 35-45.

Urena, F. (1988). Ultrastructure of the mitotic nuclei in Leishmania mexicana ssp. Tridimensional reconstruction of the mitotic spindle and dense plaques. Rev Biol Trop *36*, 129-137.

Van der Ploeg, L.H., Schwartz, D.C., Cantor, C.R., and Borst, P. (1984). Antigenic variation in Trypanosoma brucei analyzed by electrophoretic separation of chromosome-sized DNA molecules. Cell *37*, 77-84.

van Deursen, F.J., Shahi, S.K., Turner, C.M., Hartmann, C., Guerra-Giraldez, C., Matthews, K.R., and Clayton, C.E. (2001). Characterisation of the growth and differentiation in vivo and in vitro-of bloodstream-form Trypanosoma brucei strain TREU 927. Mol Biochem Parasitol *112*, 163-171.

Van Nieuwenhove, S., Schechter, P.J., Declercq, J., Bone, G., Burke, J., and Sjoerdsma, A. (1985). Treatment of gambiense sleeping sickness in the Sudan with oral DFMO (DL-alpha-difluoromethylornithine), an inhibitor of ornithine decarboxylase; first field trial. Trans R Soc Trop Med Hyg *79*, 692-698.

Vanhamme, L., Paturiaux-Hanocq, F., Poelvoorde, P., Nolan, D.P., Lins, L., Van Den Abbeele, J., Pays, A., Tebabi, P., Van Xong, H., Jacquet, A., *et al.* (2003). Apolipoprotein L-I is the trypanosome lytic factor of human serum. Nature *422*, 83-87.

Vega-Lopez, F. (2003). Diagnosis of cutaneous leishmaniasis. Curr Opin Infect Dis *16*, 97-101.

Venitt, S., and Crofton-Sleigh, C. (1987). The toxicity and mutagenicity of the anti-tumour drug 5-aziridino-2,4-dinitrobenzamide (CB1954) is greatly reduced in a nitroreductase-deficient strain of E. coli. Mutagenesis *2*, 375-381.

Vickerman, K., and Preston, T.M. (1970). Spindle microtubules in the dividing nuclei of trypanosomes. J Cell Sci *6*, 365-383.

Vincent, I.M., Creek, D., Watson, D.G., Kamleh, M.A., Woods, D.J., Wong, P.E., Burchmore, R.J., and Barrett, M.P. (2010). A molecular mechanism for eflornithine resistance in African trypanosomes. PLoS Pathog *6*, e1001204.

Viode, C., Bettache, N., Cenas, N., Krauth-Siegel, R.L., Chauviere, G., Bakalara, N., and Perie, J. (1999). Enzymatic reduction studies of nitroheterocycles. Biochem Pharmacol *57*, 549-557.

Voullaire, L.E., Slater, H.R., Petrovic, V., and Choo, K.H. (1993). A functional marker centromere with no detectable alpha-satellite, satellite III, or CENP-B protein: activation of a latent centromere? Am J Hum Genet *52*, 1153-1163.

Waizenegger, I.C., Hauf, S., Meinke, A., and Peters, J.M. (2000). Two distinct pathways remove mammalian cohesin from chromosome arms in prophase and from centromeres in anaphase. Cell *103*, 399-410.

Walczak, C.E., Cai, S., and Khodjakov, A. (2010). Mechanisms of chromosome behaviour during mitosis. Nat Rev Mol Cell Biol *11*, 91-102.

Wang, L.H., Schwarzbraun, T., Speicher, M.R., and Nigg, E.A. (2008). Persistence of DNA threads in human anaphase cells suggests late completion of sister chromatid decatenation. Chromosoma *117*, 123-135.

Wang, Y., Jester, E.L., El Said, K.R., Abraham, A., Hooe-Rollman, J., and Plakas, S.M. (2010). Cyano metabolite as a biomarker of nitrofurazone in channel catfish. J Agric Food Chem *58*, 313-316.

Wang, Z., Morris, J.C., Drew, M.E., and Englund, P.T. (2000). Inhibition of Trypanosoma brucei gene expression by RNA interference using an integratable vector with opposing T7 promoters. J Biol Chem *275*, 40174-40179.

Warburton, P.E., Cooke, C.A., Bourassa, S., Vafa, O., Sullivan, B.A., Stetten, G., Gimelli, G., Warburton, D., Tyler-Smith, C., Sullivan, K.F., *et al.* (1997). Immunolocalization of CENP-A suggests a distinct nucleosome structure at the inner kinetochore plate of active centromeres. Curr Biol *7*, 901-904.

Weaver, B.A., and Cleveland, D.W. (2005). Decoding the links between mitosis, cancer, and chemotherapy: The mitotic checkpoint, adaptation, and cell death. Cancer Cell *8*, 7-12.

Wells, N.J., and Hickson, I.D. (1995). Human topoisomerase II alpha is phosphorylated in a cell-cycle phase-dependent manner by a proline-directed kinase. Eur J Biochem *231*, 491-497.

Wen, L.M., Xu, P., Benegal, G., Carvaho, M.R., Butler, D.R., and Buck, G.A. (2001). Trypanosoma cruzi: exogenously regulated gene expression. Exp Parasitol *97*, 196-204.

Wen, Y.Z., Zheng, L.L., Liao, J.Y., Wang, M.H., Wei, Y., Guo, X.M., Qu, L.H., Ayala, F.J., and Lun, Z.R. (2011). Pseudogene-derived small interference RNAs regulate gene expression in African Trypanosoma brucei. Proc Natl Acad Sci U S A *108*, 8345-8350.

Werbovetz, K.A., Lehnert, E.K., Macdonald, T.L., and Pearson, R.D. (1992). Cytotoxicity of acridine compounds for Leishmania promastigotes in vitro. Antimicrob Agents Chemother *36*, 495-497.

WHO (1990). IARC Monographs on the Evaluation of Carcinogenic Risks to Humans. International agency for research on cancer *50*.

WHO (2000). African trypanosomiasis
WHO report on global surveillance of epidemic-prone infectious diseases *Chapter 8*.

WHO (2002). Control of Chagas Disease. WHO Technical Report Series *905*.

WHO (2004). The global burden of disease: 2004 update

WHO (2006). Human African trypanosomiasis (sleeping sickness): epidemiological update. Weekly epidemiological record *81*, 69-80.

WHO (2010). Control of Leishmaniasis. WHO Technical Report Series *949*.

Wickstead, B., Ersfeld, K., and Gull, K. (2004). The small chromosomes of Trypanosoma brucei involved in antigenic variation are constructed around repetitive palindromes. Genome Res *14*, 1014-1024.

Wilkinson, S.R., Bot, C., Kelly, J.M., and Hall, B.S. (2011). Trypanocidal Activity of Nitroaromatic Prodrugs: Current Treatments and Future Perspectives. Curr Top Med Chem.

Wilkinson, S.R., and Kelly, J.M. (2009). Trypanocidal drugs: mechanisms, resistance and new targets. Expert Rev Mol Med *11*, e31.

Wilkinson, S.R., Meyer, D.J., Taylor, M.C., Bromley, E.V., Miles, M.A., and Kelly, J.M. (2002). The Trypanosoma cruzi enzyme TcGPXI is a glycosomal peroxidase and can be linked to trypanothione reduction by glutathione or tryparedoxin. J Biol Chem *277*, 17062-17071.

Wilkinson, S.R., Prathalingam, S.R., Taylor, M.C., Horn, D., and Kelly, J.M. (2005). Vitamin C biosynthesis in trypanosomes: a role for the glycosome. Proc Natl Acad Sci U S A *102*, 11645-11650.

Wilkinson, S.R., Taylor, M.C., Horn, D., Kelly, J.M., and Cheeseman, I. (2008). A mechanism for cross-resistance to nifurtimox and benznidazole in trypanosomes. Proc Natl Acad Sci U S A *105*, 5022-5027.

Wirtz, E., and Clayton, C. (1995). Inducible gene expression in trypanosomes mediated by a prokaryotic repressor. Science *268*, 1179-1183.

Wood, A.J., Severson, A.F., and Meyer, B.J. (2010). Condensin and cohesin complexity: the expanding repertoire of functions. Nat Rev Genet *11*, 391-404.

Wood, K.W., Sakowicz, R., Goldstein, L.S., and Cleveland, D.W. (1997). CENP-E is a plus end-directed kinetochore motor required for metaphase chromosome alignment. Cell *91*, 357-366.

Wood, V., Gwilliam, R., Rajandream, M.A., Lyne, M., Lyne, R., Stewart, A., Sgouros, J., Peat, N., Hayles, J., Baker, S., *et al.* (2002). The genome sequence of Schizosaccharomyces pombe. Nature *415*, 871-880.

Woodward, R., and Gull, K. (1990). Timing of nuclear and kinetoplast DNA replication and early morphological events in the cell cycle of Trypanosoma brucei. J Cell Sci *95 (Pt 1)*, 49-57.

Yamada, M., Espinosa-Aguirre, J.J., Watanabe, M., Matsui, K., Sofuni, T., and Nohmi, T. (1997). Targeted disruption of the gene encoding the classical nitroreductase enzyme in Salmonella typhimurium Ames test strains TA1535 and TA1538. Mutat Res *375*, 9-17.

Yamamoto, A., Guacci, V., and Koshland, D. (1996). Pds1p, an inhibitor of anaphase in budding yeast, plays a critical role in the APC and checkpoint pathway(s). J Cell Biol *133*, 99-110.

Yoshida, N., Mortara, R.A., Araguth, M.F., Gonzalez, J.C., and Russo, M. (1989). Metacyclic neutralizing effect of monoclonal antibody 10D8 directed to the 35- and 50-kilodalton surface glycoconjugates of Trypanosoma cruzi. Infect Immun *57*, 1663-1667.

Yu, H. (2002). Regulation of APC-Cdc20 by the spindle checkpoint. Curr Opin Cell Biol *14*, 706-714.

Yun, O., Priotto, G., Tong, J., Flevaud, L., and Chappuis, F. (2010). NECT is next: implementing the new drug combination therapy for Trypanosoma brucei gambiense sleeping sickness. PLoS Negl Trop Dis *4*, e720.

Zacks, M.A. (2007). Impairment of cell division of Trypanosoma cruzi epimastigotes. Mem Inst Oswaldo Cruz *102*, 111-115.

Zenno, S., Koike, H., Kumar, A.N., Jayaraman, R., Tanokura, M., and Saigo, K. (1996a). Biochemical characterization of NfsA, the Escherichia coli major nitroreductase exhibiting a high amino acid sequence homology to Frp, a Vibrio harveyi flavin oxidoreductase. J Bacteriol *178*, 4508-4514.

Zenno, S., Koike, H., Tanokura, M., and Saigo, K. (1996b). Gene cloning, purification, and characterization of NfsB, a minor oxygen-insensitive nitroreductase from Escherichia coli, similar in biochemical properties to FRase I, the major flavin reductase in Vibrio fischeri. J Biochem *120*, 736-744.

Zhou, W., Cross, G.A., and Nes, W.D. (2007). Cholesterol import fails to prevent catalyst-based inhibition of ergosterol synthesis and cell proliferation of Trypanosoma brucei. J Lipid Res *48*, 665-673.

Zingales, B., Andrade, S.G., Briones, M.R., Campbell, D.A., Chiari, E., Fernandes, O., Guhl, F., Lages-Silva, E., Macedo, A.M., Machado, C.R., *et al.* (2009). A new consensus for Trypanosoma cruzi intraspecific nomenclature: second revision meeting recommends TcI to TcVI. Mem Inst Oswaldo Cruz *104*, 1051-1054.

Zingales, B., Pereira, M.E., Oliveira, R.P., Almeida, K.A., Umezawa, E.S., Souto, R.P., Vargas, N., Cano, M.I., da Silveira, J.F., Nehme, N.S., *et al.* (1997). Trypanosoma cruzi genome project: biological characteristics and molecular typing of clone CL Brener. Acta Trop *68*, 159-173.

Zomerdijk, J.C., Kieft, R., and Borst, P. (1992). A ribosomal RNA gene promoter at the telomere of a mini-chromosome in Trypanosoma brucei. Nucleic Acids Res *20*, 2725-2734.

Zwelling, L.A., Kerrigan, D., and Marton, L.J. (1985). Effect of difluoromethylornithine, an inhibitor of polyamine biosynthesis, on the topoisomerase II-mediated DNA scission produced by 4'-(9-acridinylamino)methanesulfon-m-anisidide in L1210 murine leukemia cells. Cancer Res *45*, 1122-1126.